Study of Milky Way Halo stars and connection to globular clusters

A thesis

submitted for the degree of

Doctor of Philosophy

in

The Department of Physics,

Pondicherry University,

Puducherry - 605 014, India

by

Avrajit Bandyopadhyay

Indian Institute of Astrophysics,

Bangalore - 560 034, India

April 2019

Study of Milky Way Halo stars and connection to globular clusters

Avrajit Bandyopadhyay
Indian Institute of Astrophysics

Indian Institute of Astrophysics
Bangalore - 560 034, India

Title of the thesis	:	**Study of Milky Way Halo stars and connection to globular clusters**
Name of the author	:	**Avrajit Bandyopadhyay**
Address	:	Indian Institute of Astrophysics II Block, Koramangala Bangalore - 560 034, India
Email	:	avrajit@iiap.res.in
Name of the supervisor	:	**Prof. Sivarani Thirupathi**
Address	:	Indian Institute of Astrophysics II Block, Koramangala Bangalore - 560 034, India
Email	:	sivarani@iiap.res.in

Declaration of Authorship

I hereby declare that the matter contained in this thesis is the result of the investigations carried out by me at the Indian Institute of Astrophysics, Bangalore, under the supervision of Prof. Sivarani Thirupathi. This work has not been submitted for the award of any other degree, diploma, associateship, fellowship, etc. of any other university or institute.

Signed: _____

Date: _____

Certificate

This is to certify that the thesis titled **'Study of Milky Way halo stars and connection to globular clusters'** submitted to the Pondicherry University by Mr. Avrajit Bandyopadhyay for the award of the degree of Doctor of Philosophy, is based on the results of the investigations carried out by him under my supervision and guidance, at the Indian Institute of Astrophysics. This thesis has not been submitted for the award of any other degree, diploma, associateship, fellowship, etc. of any other university or institute.

Signed:

Date:

List of Publications

1. **Bandyopadhyay, Avrajit**, Sivarani, Thirupathi; Susmitha, Antony; Beers, Timothy C.; Giridhar, Sunetra; Surya, Arun; Masseron, Thomas 2018, "Chemical composition of two bright Extremely Metal Poor stars from SDSS MARVELS Pre-survey", *The Astrophysical Journal*, 859:114, https://doi.org/10.3847/1538-4357/aabe80 [arXiv:1805.02280v1]

2. **Discovery of globular escapees in the Halo**

   Bandyopadhyay, Avrajit, Thirupathi Sivarani, in preparation

3. **Abundance analysis of new thorium rich star and other r-process rich stars in the halo**

   Bandyopadhyay, Avrajit, Thirupathi Sivarani, in preparation

4. **New CEMP stars in the halo**

   Bandyopadhyay, Avrajit, Thirupathi Sivarani, in preparation

5. **Li distribution in the Halo and new VMP stars**

   Bandyopadhyay, Avrajit, Thirupathi Sivarani, in preparation

Presentations

1. Poster presentation in the *Astronomical Society of India meeting 2016 (ASI:2016)* held at the University of Kashmir, Srinagar,Jammu and Kashmir, India, during 10-13 May 2016.

2. Oral presentation in the international conference *TMT Science Forum* held at Infosys Mysore campus, during 7-9 November 2017.

3. Oral presentation in the conference *Astronomical Society of India meeting 2018 (ASI:2018)* held at the Osmania University, Hyderabad during 5-9 February 2018.

4. Oral presentation in the international conference *Exploring the Universe: Near earth Space Science to Extra-Galactic Astronomy* held at SN Nose National Centre for Basic Sciences, Kolkata, West Bengal, during 14-17 November 2018.

5. Oral presentation in the international conference *Chemical Evolution and nucleosynthesis across the Galaxy* held at Max-Planck House, Heidelberg, Germany, during 26-29 November 2018.

6. Poster presentation in the *Astronomical Society of India meeting 2019 (ASI:2019)* held at Christ University,Bangalore, Karnataka, India, during 18-22 February 2019. Received best poster presentation award of ASI.

Acknowledgements

It would have been extremely difficult to carry out the work for my PhD without the active support and help of several individuals. I would like to extend my deepest gratitude to all of them.

I am very grateful to my supervisor, Prof Sivarani Thirupathi. She have been immensely supportive of my work and the continuous encouragement and scientific discussions over the course of last 5 years have helped me a lot to gain deep insights in my field of study. I also thank her for providing a lot of freedom to pursue my hobbies and develop interest in reading academic journals during the stint of my PhD.

I would also like thank Susmitha di for all the academic and non-academic help.I would also like to thank her for helping me to learn IRAF, IDL and turbospectrum code, three of the most important tools I used for my thesis. I thank Athira for being such a nice junior. I really enjoyed those healthy discussions during the observation nights at CREST. I also thank Devika, Drisya di and Arun for all the help and support.

I would also extend my most sincere gratitude to Prof. Sunetra Giridhar for teaching me high resolution spectroscopy and providing an opportunity to work ttogether for preparation of the first wavelength calibration chart for HESP.

I would also like to thank Prof. Timothy C Beers, Prof Wako Aoki, and Prof Piercarlo Bonifacio for their help and valuable suggestions.

I would also take this opportunity to thank my doctoral committee members Prof. G.C.Anupama, Prof. Aruna Goswami and Prof. Bharathi Mohan for their help and suggestions.

I feel obliged to the Director, the Dean and the Board of Graduate Studies (BGS) for giving me the opportunity to work in this institute and providing all the facilities required for my research work. I thank to the librarian for helping me to access necessary books and journals. I would like to thank Dr. Baba Varghese, Ashok, Fayaz, Anish and other staffs of 'Data Center' for their help in computer and internet related issues. Many thanks to Administrative Officer, Personnel Officer, Accounts Officers and all other administrative staff for their timely help in the administrative related work. I thank the supervisors, cooks and other staff members of Bhaskara for taking care during my stay.

I express my gratitude to the course work instructors Prof. Joseph Samuel, Prof. Seetha, Prof. Prabhavati Chingangbam, Prof Tarundeep Saini, Prof. U. S. Kamath, Prof. S. P. Rajaguru, Prof. Prateek Sharma, Prof. Avinash Despande, Prof. Biswajit Paul, Prof. Shreedhar, Prof. Shiv Shethi and Prof. H. C. Bhatt for teaching me the basics of astrophysics. I thank Sourav, Prasun, Varun and Harsha for their help during course work. I also thank Prof. Ram Sagar for taking special classes at IIA and Kavalur, which played an indispensable role in understanding the basics as well as nuances of optical astronomy.

I am fortunate to have friends like Prasanta, Rubinur, Priyanka, Suman Bala and Seniors like Samyaday, Sajal and Susmitha who are always there to stand by with me. I am happy to thank my seniors Tanmoy, Sudip, Nancy, Susmitha, Honey, Abhijit, Vaibhav, Shubham, Joice, Mayuresh, Prasanna S and Prasanna D for helping me in administrative as well as thesis related work.

I wish to express my thanks to my colleagues and juniors Dipanweeta, Sneha, Tridib, Amit, Anirban, Samrat, Chayan, Megha, Bhoomika, Deepak, Panini, Priya, Raghubar, Ramya, Ritesh, Sandeep, Annu, Ambily, Anshu, Anwesh, Aritra, Hemanth, Joby, Jyothi, Mageshwaran, Prerna, Nirmal, Partha, Pavana, Mayuresh, Satabdwa, Sreekanth, Varun, Deshmukh, Phanindra, Subhamay, Suman Saha,

Tanya, Kshama, Shejeela, Meenakshi, Keyuri, Abha, Brajesh, Kanhaiya, Asish Raj, Arun Surya, Avinash Surendran.

I would like to thank Prof. Somnath Bharadwaj, Prof. A.K. Singh, Prof. Krishna Kumar. Prof. S.P. Khastagir and Prof. Sonjoy Majumder for their excellent teaching during my M.Sc at IIT Kharagpur. I thank Ramchandra, Srimanta, Prasanta, Sayan, Suvrakanti, Sushil, Pralay, Arkadeb, Jagannath, Bappa, Krishna, Arpita, Arindam, Kousik, Alapan, Soumalya, Aritra, Prasun,, Sourav, Prantika, Nabhanila, Sudeshna, Ghanashyam for the amazing time I spent with them.

I thank Prof. Saugata Bhattacharya, Prof. Sukanya Dasgupta, Prof. Sushil Kumar Sarkar, Prof Archan De, and Prof. Sankari Roychowdhuri who taught physics in a lively and exciting manner during my B.Sc. in Vidyasagar College. I wish to convey my gratitude to Prof Dipak Nath for teaching me the experiments. I also wish to thank the laboratory assistant Rajen Da for helping me to learn the experiments. I would like to extend thank my B.Sc. friends Rajesh, Ramchandra, Anindita, Bikramjit, Ipshita, Piyali, Antara, Julius Swarup, Subhasish, Sunil Bhuja, Soumen for their invaluable friendship.

I like to thank my school teachers Mr. S. Bhaduri, Dr Sudip Chatterjee, Mr. S. P. Mukherjee, Mrs. Chandrima Nayak, Mrs Parvin Imam, Mrs. Rinki Ghosh, Mrs. C. Banerjee, Mr. Avijit Mukherjee, Mr. Gayen, Mr. Rana Sarkar, Mr. Kevin David, Mrs Ruplekha Chatterjee, Mrs Gomes, Mrs Moumita Bhattacharya, Mrs S Buxy, Mrs T. Basu, Mr Anamitra Saha . I would have been nowhere near without their classes. I also specially thank my teacher Mr. Sourav Mitra for motivating me to take up Hons. in physics as my stream of study after schooling. I also thank my school friends Seemon, Indrajit, Abhishek Ghosh, Abhishek Gupta, Arnab Ghosh, Rupen, Mayurakshi, Samrat, Amrin, Arijit, Sohom, Debarati, Priyadarshi, Sourav De, Sahana, Abir, Sayan Banerjee, Lakshmipriya, Debojyoti, Javed Omar and many others.

I also specially thank Rakesh, Avinash and Prasanta for helping me in learning programming languages. I would also take this opportunity to thank Rubi, Prasanta, Tanve and Rubel for being like a family to me in Bangalore.

I also extend my gratitude to Rajesh for being the constant source of motivation and words of wisdom which has been integral to my development as a human being.

I have been extremely fortunate to have been taught by a few extremely inspirational teachers. I would specially like to thank Mr. Manab Mukherjee, Shreyan da, Mumi didi, Dr. Pratip K Chaudhury, Dr Saugata Bhattacharyya and Dr. Somnath Bharadwaj. Without them I would have been nowhere close.

I would like to thank to my parents, grand parents and my aunt Dalia Mukherjee, uncle Ashok Ganguly and cousin Devapriya Banerjee for everything. Everything I could achieve in life is only because of their unconditional support, love and dedication.

Data usage

The study presented in the thesis has used data from various ground based facilities. I would like to thank the respective instrument teams for providing the data in public domain and I duly acknowledge the usage of the data for this work.

We have extensively acquired and used data from the 2m Himalayan Chandra Telescope (HCT) maintained by Indian Institute of Astrophysics, Bangalore. Hanle Echelle SPectrograph (HESP) was used for acquiring the spectrum of several objects.

Archival data was used from European Southern Observatory. The spectroscopic data was obtained for NGC 1851 under the program ID 084.D-0470(A). The GIRAFFE spectrograph in Fibre Large Array Multi Element Spectrograph (FLAMES) was used for the observation. I thank ESO for releasing the data in the public domain.

Archival data from Sloan Digital Sky Survey (SDSS) was also used. We thank the team for providing access to the data.

Dedicated to my parents

Mrs. Siuli Banerjee

and

Mr. Partha Pratim Banerjee

for their love and sacrifices

to impart the best possible quality of education to me

Abstract

The thesis aims to study the chemical abundances of very metal poor Milky Way halo stars and Globular cluster stars, to understand their possible common origin. Halo stars and globular clusters belong to the oldest stellar population of the Galaxy and detailed Chemical tagging of these populations can addresses several intriguing problems in the area of galaxy formation and globular cluster formation and evolution. In this study we have used low and high resolution spectroscopic abundance analysis to address possible connection between halo stars and globular clusters. In order to achieve this, We carried out high resolution spectroscopic survey using the Hanle echelle spectrograph at 2m Himalayan Chandra telescope. We also use low resolution spectra of Halo stars and globular clusters from Sloan Digital Sky Survey (SDSS). The thesis describes detailed abundances analysis of about 50 stars, in the metallicity range of halo and Globular clusters. These are selected from bright SDSS-MARVELS pre-survey data. All these objects are newly discovered VMP or EMP stars and their detailed chemical abundances are studied for the first time in the this work. These results are presented in detail in individual chapters.

The results include two stars (EMP & CEMP-no) in the metallicity range $<$ -3.0 has already been published in ApJ. The other interesting results of the study are three globular cluster escapees that show the typical light-element anomalies (CH-CN, Na-O, Mg-Al anti-correlations) associated with second generation GC stars. Two of them are RGBs and one is a blue straggler star, which is a rare class of object among halo stars. It is also the most metal poor Gc escapee discovered till date. The blue straggler shows strong overabundances of Na([Na/Fe]=+1.50) along with a very depleted Mg and Ca([Mg/Fe]=-0.30; [Ca/Fe]=-0.50). Lithium is also be detected in two of these GC escapees which is very important to constrain the nature of the original polluters of the GC. These objects are bright for detailed isotopic abundances studies with 8-10

class telescopes, which will provide insights to the origin of globular cluster abundance anomaly and efforts are underway.

Additional interesting objects include discovery of an $r-$process rich star with [Eu/Fe]=+0.9 and [Th/Fe]=1.28 and other R-I and R-II stars with +0.30<[Eu/Fe]<+1.2. We also identified two CEMP-no stars and two CEMP-s stars. One of the CEMP-s star ([Fe/H]=-2.3,[C/Fe]=0.87) shows a rather unusually high abundance of n-capture like [Ba/Fe]=1.67 and [Eu/Fe]=0.78 and uniform enhancement in all heavy elements. This could be a signature of NS-NS merger events that produce a blue Kilo-Novae and synthesis light r-process elements or i-process. We have also conducted a comparative study of CEMP-no and EMP stars using their heavy element enrichment and Lithium. Lithium was detected in CEMP giants and dwarfs and they exhibit the expected depletion from Spite plateau as they ascend the giant branch. We found Lithium to have a similar distribution among CEMP-no and EMP stars. Lithium was also detected (A(Li)=1.60) in one of the r-I stars which a rare occurrence. We also present heavy element abundance among GC stars using low resolution SDSS data and compare them with Halo stars to understand the common origin.

We have used the archival data of ESO and SDSS to study the key neutron capture elements like Sr and Ba for globular cluster stars. A spectral grid was developed over wide ranges of temperature,log(g),]Fe/H],[Sr/Fe] and [Ba/Fe]. We tried to explore the common origin for the Halo stars and individual clusters. Neutron star mergers were found to the chief contributor for globular clusters whereas Halo stars showed both NS-NS mergers and supernovae to play a key role in different paradigms.

Contents

List of Figures

List of Tables

Abbreviations

NASA	**N**ational **A**eronautics and **S**pace **A**dministration
SDSS	**S**loan **D**igital **S**ky **S**urvey
VLT	**V**ery **L**arge **T**elescope
ESO	**E**uropean **S**outhern **O**bservatory
FLAMES	**F**ibre **L**arge and **A**rray **M**ulti **E**lement **S**pectrograph
UFD	**U**ltra faint **D**warf **G**alaxies
HCT	**H**imalayan **C**handra **T**elescope
HESP	**H**anle **E**chelle **SP**ectrograph
IAO	**I**ndian **A**stronomical **O**bservatory
GC	**G**lobular and **C**luster
MW	**M**ilky **W**ay
CCD	**C**harge **C**oupled **D**evice

Chapter 1

Introduction

1.1 Near Field Cosmology

The idea that even the stars in the Milky Way galaxy could reveal significant clues about the conditions that existed in the early universe, a few billion years following the Big Bang as described by Freeman and Bland-Hawthorn (2002) is summarily known as near field cosmology. It had taken several decades to become an important realm of investigation for scientists probing the earliest epochs of the universe.

The long-lived metal poor stars in the Galactic halo provides invaluable information regarding several intriguing questions. Some of the main aspects of such studies are given below

- The abundance pattern in the metal poor star are used as inputs for determining the first mass function (FMF) which is believed to be largely different

from the typical power law initial mass function (IMF) that holds true for the current epoch. It is also essential to determine the nature of the first stars.

- The chemical yields in the metal poor stars provide key information towards the nature of supernova and the production of elements (sequence of nucleosynthesis events) during the explosion. These low mass long-lived stars are least likely to be polluted by several events and hence, retain the signatures to this day.

- The derivation of metallicity distribution function (MDF) for the Halo requires study of a large sample of halo stars. This would help us to answer the question if we have reached the limits of the lowest metallicity in the Galaxy.

- Detailed abundance analysis of the heavy elements for a large number of halo stars, satellite galaxies and globular clusters provide us relevant information about the production sites for neutron capture elements. Neutron star-neutron star mergers and supernovae with jets are the most likely astrophysical sites known till date.

1.2 The Milky Way system

The Milky Way is a spiral galaxy which contains billions of stars and gas. It consists of a flat disc-like structure in the central region called the disc which contains the spiral arms, a spheroidal distribution of luminous matter about the centre called bulge and a halo extending to several kpc. Before discussing the substructures of Milky Way galaxy, let us discuss the formation of the galaxies in the universe.

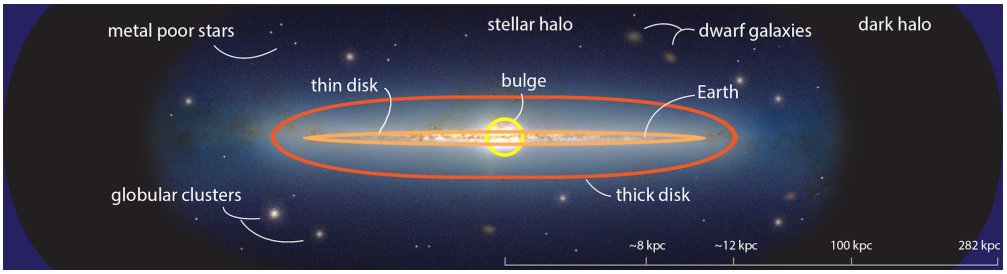

FIGURE 1.1: Structure of the Milky Way galaxy. The different parts of the Galaxy are marked in the cartoon diagram. The image is taken from Frebel (2018)

1.2.1 Formation models

The understanding of the formation of galaxies and larger structures in the universe involves two different approaches - a top-down approach which states that the huge clouds fragmented to form protogalactic clouds whereas the other paradigm takes a bottom-up approach which states that smaller structures combined to form larger structures.

The top-down approach is also known as the theory of monolithic collapse, came into existence following the work of Eggen, Lynden and Sandage (ELS theory; Eggen *et al.* 1962) who conducted the study on the formation of a single galaxy which in their case was Milky Way. The ELS theory predicts that the giant cloud collapses and reaches an equilibrium when the inward gravitational force is balanced by the outward centrifugal force which develops to conserve the angular momentum. In this model rapid star formation took place in the halo which was formed of the protogalactic gas. The process of star formation in the halo lasted for a time scale comparable to the free fall time. The galactic disc was formed later out of the leftover gas which fragmented after sufficient cooling to initiate another episode of star formation. Although this theory successfully explains several features of the galaxy, it fails to explain a number of observed phenomena like the retrograde motion of a significant number of stars in the Halo, age spread in globular clusters and few others.

The hierarchical clustering or merging follows the bottom-up approach which states that smaller systems combined over significantly large time scales to form large structures (Searle and Zinn 1978). The lack of correlations of characteristics of galactic globular clusters (e.g metallicity, stellar mass functions etc) and halo stars with galactocentric distance points towards a picture where these subsystems merged over a large time scale to form the galaxy. It also explains the formation of elliptical galaxies which could be shown to be a merger of disc galaxies. Toomre and Toomre (1972a,b) stated that all galaxies started as disc galaxies, some of which later merged to form elliptical galaxies. Two of the Toomre objects NGC 3921 and NGC 7252 were discovered to be post starburst objects which led to the understanding that these mergers lead to a burst of star formation which exhausts the available gas in these systems resulting into a merger with primarily old stellar systems and very little star formation activity. The spiral galaxies like the Milky Way are the ones which have not undergone any strong interactions or mergers and thus star formation could still take place in the disk.

ΛCDM model is the most widely accepted theory to successfully explain the observed properties of the cosmos like the large scale structure formation and the rate of expansion of the universe (Madriz Aguilar *et al.* 2017). In this framework, Λ denotes the cosmological constant whereas CDM denoted the cold dark matter. In the ΛCDM model also known as the standard model of the big bang, the universe comprises of the Λ which is related to dark energy, the cold dark matter and the visible matter (Solà and Gómez-Valent 2015). The theory postulates that as the universe began to cool after the big bang, the dark matter clumps started to condense. The gravitational attraction of the gas molecules inside these clumps accelerated the clumping. This gave rise to regions of higher density. These went on to become the minihalos which contained the seeds of the first galaxies. As the subhalos became more massive, the gravitational collapse started and the protogalaxies were formed. The process of merging continued to form larger systems and is known as hierarchical merging.

1.2.2 Galactic populations

1.2.3 Disk and Bulge

The bulge is the spheroidal distribution of stars as seen in Figure 1.1. It mainly contains old stars and also a significant amount of gas and dust. The obscuration by dust makes the observation of the bulge stars a difficult process and large uncertainties hover over the determination of the age of the bulge population. Baade's window is a small region with a diameter of 2 degree which has a relatively sparse distribution of dust and thus provides an opportunity to observe and study the bulge population (e.g. Fulbright *et al.* 2006).

The disk of the Galaxy is a flattened distribution of stars, surrounding the bulge in the plane about the galactic centre. It primarily contains the young and intermediate stellar populations which move in a coherent orbit about the galactic centre. The density of the stars decreases both radially and vertically from the centre in the disk. It also contains the spiral arms where star formation takes place at a higher rate than the rest of the galaxy. The disk could be categorized into two sub-categories - the thick disk which contains the old stars formed at earlier epochs and thin disk which contains the new stars.

1.2.4 Halo

The Galactic halo is a two component spheroidal system - the extended dark halo following an NFW profile (Navarro-Frenk-White profile; Dalal *et al.* 2010) which forms 90% of its mass and the luminous matter which is comprised of the oldest stars and globular clusters. In terms of the ΛCDM model, tidal stripping

and accretion from smaller sub-halos played the key roles in the formation of the Galactic halo. The chemo-dynamical studies have also led to the separation of the halo population into two groups -

- The inner halo population have a higher metallicity distribution which peaks at [Fe/H] = -1.6 and extends to 10-15 kpc. They show a net prograde motion with highly eccentric orbits (Carollo *et al.* 2007). Jofré and Weiss (2011) studied the age distribution of the halo population. No gradient of age was obtained with metallicity for the stellar halo. This indicates a very rapid formation of the halo during the collapse of the protogalactic gas. They also found a number of stars younger than the dominant population which must have migrated from external galaxies. More recently, Helmi *et al.* (2018) have described inner halo to be dominated by net debris from the infall of Gaia-Enceladus.

- The outer halo population is much older with a lower metallicity distribution peaking at [Fe/H] = -2.2. They exhibit a net retrograde motion about the Galactic centre. They provide the most valuable insights into the accretion and merging history of the Milky Way. Battaglia *et al.* (2017) have found the outer halo population to be originating from regions of high initial star formation rates with large contributions from the asymptotic giant branch (AGB) stars with respect to the inner halo populations.

1.2.5 Globular Clusters

"Perhaps the most wonderful of all the star clusters are those in which hundreds upon hundreds of faint stars are all gathered together in the shape of a globe." Although numerically flawed, Reverend James Baikie beautifully describes the striking visual appeal of globular clusters. Apart from the magnificent appearance,

they also play a key role in astronomy. They are isolated systems comprising of millions of stars located at virtually the same distance which provides us an excellent opportunity to study various aspects of stellar structure and evolution. These rich ensembles of stars with a significant population at all evolutionary stages are considered as natural stellar laboratories for extensive studies. The image of the globular cluster M55 along with its Hertzsprung-Russell (H-R) diagram showing the rich stellar system with a large number of stars in all evolutionary phases is shown in Figure 1.2.

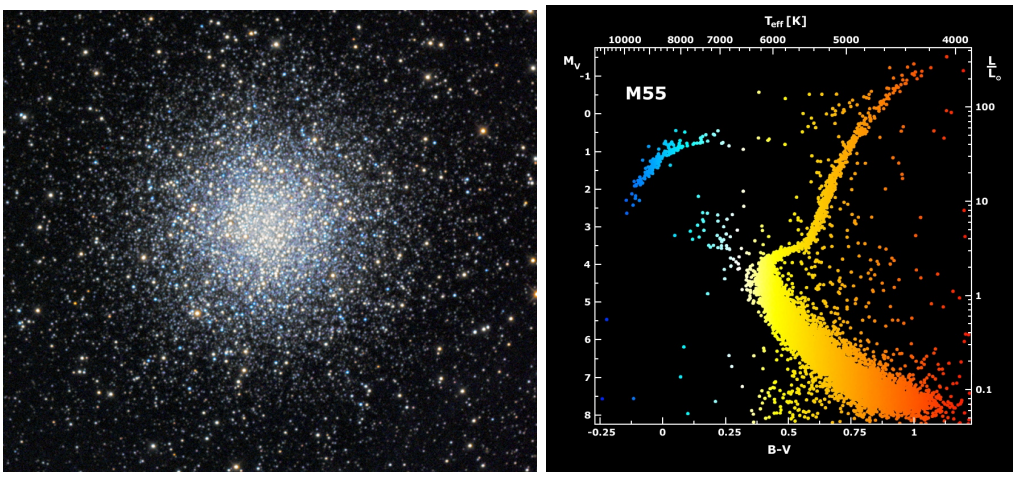

FIGURE 1.2: The photometric image of the metal poor Globular Cluster M55 is shown in the left. The HR diagram for the same cluster is given in the right.

The investigations over several decades have led to several striking discoveries about globular clusters. They are found to be among the oldest structures to still exist with estimated ages similar to that of the known universe. They provide precious information regarding the astrophysical conditions of the early universe and are of immense importance as fossils of that epoch. They are also found to host several generations of stars instead of a simple stellar population. Certain discrepancies have also evolved regarding star-to-star abundance variations, the peculiar evolution of the cluster stars, chemical enrichment during their formation, etc which we shall discuss later. The Galactic globular clusters are found to populate in the Halo.

1.2.6 Satellite galaxies

There exist more than 50 dwarf galaxies in the vicinity of the Milky Way covering a wide range of luminosity. Most of them were discovered and could be studied after the emergence of large sky surveys. The stars in these dwarf spheroidal systems resemble the abundance pattern of the halo population. This indicates that both the population were born at similar epochs and have undergone similar chemical enrichment history. These studies also provide shreds of evidence for the theory of hierarchical merging.

1.3 Stellar Archaeology: Tracing the path towards early universe

Stellar archaeology is the field of study that is dedicated to the investigation of the astrophysical conditions in the early universe. It probes into the astrophysical sites, the physical processes governing star formation at the earliest epochs. The subject has developed on the results obtained from the chemical abundances of the older population of stars. The results primarily focus on the patterns of the distribution of the elements in the periodic table in these metal poor Halo stars. These observed abundances along with the theoretical models provide detailed insights into the conditions that prevailed during their formation epochs and the nature of their predecessors which are believed to be the first generation stars in the universe (Sneden *et al.* 2000; Frebel and Norris 2015a; Beers and Christlieb 2005; Frebel and Norris 2015b; Frebel 2018).

1.3.1 Exploring the earliest times

The first stars were supposed to be formed in metal free environments. The interstellar matter contained H, He and small amounts of Li. All the heavier elements (known as metals in astronomy) were synthesized in stellar interiors and supernova explosions and the ejecta from these stars introduced metals in the otherwise pristine interstellar matter. As the universe got older, the proportion of metals in the ISM kept increasing. Thus metallicity could be treated as a proxy for the age of the universe. Lower the metallicity of an object, earlier was the epoch of its formation.

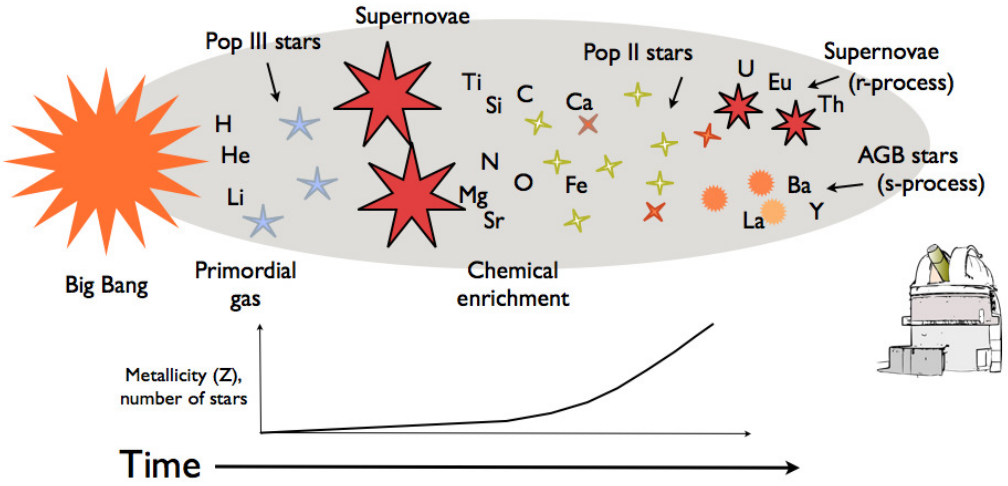

FIGURE 1.3: The schematic diagram representing the evolution of elements in the universe from the big bang to the present epoch. The diagram is adopted from Frebel (2018).

Star formation began within the first few hundred million years of the big bang as depicted in Figure 1.3 (taken from Frebel (2018)). The first generation of stars are believed to be massive (known as population III stars due to historical reasons) and they enriched the ISM by introducing the seeds of heavy elements for subsequent star formation. The same process got repeated and the cycles of star formation and death went on with each generation enriching the ISM with more amount of metals. The primary contributors were the more massive stars which exploded as

supernovae of type II resulting in their ejecta getting mixed with the ISM and the mass loss in the form of winds over long time scales from the relatively lower mass stars. Both played significant roles to alter the metallicity content of the gas.

With the advent of modern scientific tools like high resolution spectroscopy, several stars with extremely poor metallicity could be detected with the lowest being [Fe/H] = -7.3 (Keller *et al.* 2014). The low mass stars formed in the early epochs could still be observed today. These are believed to be the direct successors of the first stars. The ultra faint dwarf spheroidal satellite galaxies of the Milky Way are also found to host a large fraction of the extremely metal poor stars. On the contrary, globular clusters which are also one of the oldest stellar systems to still exist, do not host any star with a metallicity lower than [Fe/H] = -2.5. Another interesting problem is the estimated over-abundance of carbon in the lowest metallicity.

Hence, chemical enrichment of the early galaxy is an intriguing problem and demands special attention. The first step towards a deeper understanding of the problems at hand is to focus on the origin of elements which we shall try to discuss in the next section.

1.3.2 Nucleosynthesis: Origin of elements

There are several mechanisms by which elements could be produced in the universe. The lightest elements are believed to have been produced immediately following the big bang. Most of the elements in the periodic table (barring ^{1}H) up to Fe are cooked up in the stellar interiors whereas the elements heavier than Fe require exotic conditions (e.g. high energy, high neutron flux, a certain degree of entropy and few others) and are synthesized by neutron capture methods. Let us discuss the details of these mechanisms of how the elements are formed in the universe.

1.3.2.1 Big Bang Nucleosynthesis

Big bang nucleosynthesis or BBN, also known as primordial nucleosynthesis is an event which refers to the production of the very light elements for the first time in the nascent stage of the universe. It was proposed by Ralph Alpher (Alpher-Bethe-Gamow; Alpher *et al.* (1948)) who for the first time did the detailed calculations for production of light elements in the early universe. BBN is supposed to have taken place in the interval between 10 seconds to 20 minutes from the big bang. The standard scenario of BBN explains the formation of the elements like ^{1}H, ^{2}H, ^{3}H, ^{3}He, ^{4}He, ^{7}Li and ^{7}Be. Out of these nuclei, ^{3}H and ^{7}Be were unstable and they subsequently decayed into ^{3}He and ^{7}Li respectively. All other elements heavier than ^{7}Li were produced in stellar interiors or explosive stars as we shall discuss below.

1.3.2.2 Stellar Interiors

The temperature starts rising in the core as the protostellar cloud collapses under its own gravity. When the core reaches sufficient temperature, the core starts getting hotter. Once sufficient temperature has reached the hydrogen in the core starts fusing to form helium. The energy generated from this process of nuclear fusion halts the further gravitational collapse and the star attains the state of hydrostatic equilibrium where the radiation pressure balances gravity. This stage is called the main sequence (MS) and is the most long-lived phase in the journey of a star. For a solar or sub-solar star, proton-proton (pp) chain is the dominant source of nuclear energy whereas for a star massive than 1.3 $M_{\odot}$ the fusion reactions occur via the CNO (Carbon-Nitrogen-Oxygen) cycle. In both the modes of reactions, hydrogen get converted to He but different sets of chain reactions are involved. Temperature for pp chain to be ignited is around 4×10^{6} whereas CNO cycle operates at a temperature of 10×10^{6} and higher.

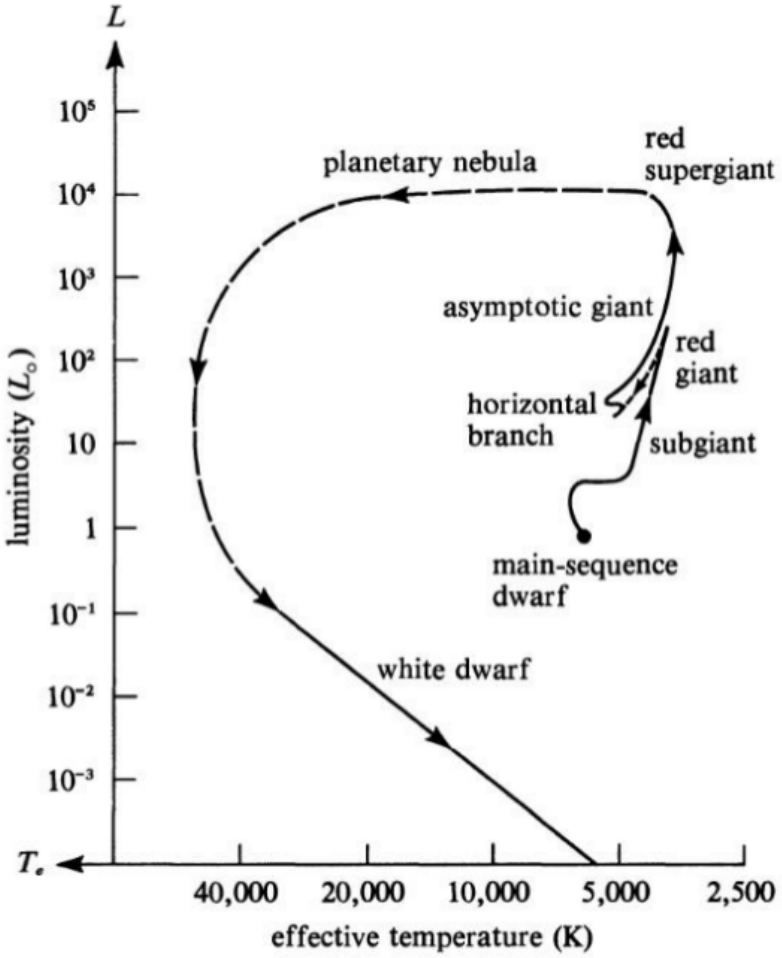

FIGURE 1.4: Evolutionary sequences of a low mass star in its journey from main sequence to white dwarf. The image is taken from "The physical universe, An Introduction to Astronomy" by Frank Shu.

After spending a long time in this stable hydrostatic equilibrium, the core slowly gets exhausted and gradually stops burning. Despite having more fuel, the more massive stars burn it at a faster rate than the low mass stars and move out of the MS earlier. Then begins the giant phases.

Once the burning hydrogen core is extinguished, gravity again takes over and the temperature of the core starts rising. This leads to begin the phase of shell H-burning around the He core. At this stage the star expands, luminosity increases and the surface temperature falls. This is due to proton diffusion which does not

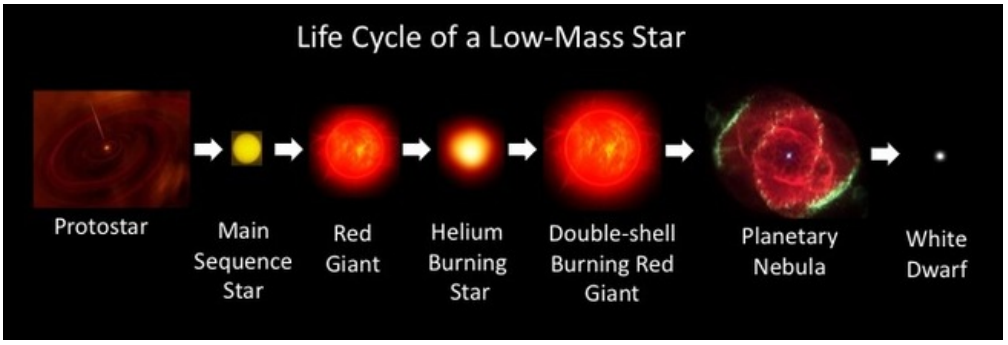

FIGURE 1.5: The different stages in the evolution of a low mass star. Image credits : https://nate-thegreat.weebly.com/blog/the-life-cycle-of-low-mass-stars

allow the entire radiation generated by the burning H-shell to reach the surface resulting it to blot up. As a result, the star takes a sharp right turn as shown in Figure 1.4. However, at the same time, the core keeps contracting under gravity and the ash from H-burning shell keeps adding more He to the core. However, it takes some time for the core to reach He-burning temperature. At this stage, a convective zone is developed near the surface which transports the products of H-burning to the surface and is known as "first dredge-up" or FDU. This significantly alters the surface composition (e.g. 12c/13c ratio, Li depletion, etc) and increases efficiency in energy transport to the surface. This results in the rapid upward rise and the phase of the star is known as "Red Giant Branch" (RGB). This continues until the core attains sufficient temperature (10^8 K) and pressure to trigger the fusion of He into C known as the triple alpha reaction. For low mass stars, it is known as "Helium Flash" where He ignition occurs in the "degenerate core" and is a violent mechanism which lifts the degeneracy. The point where He fusion starts is known as the tip of the RGB.

Then follows the downward and leftward movement in which the star shrinks in size, the temperature starts rising and the luminosity becomes constant after a sudden drop. This is the second hydrostatic equilibrium phase and is known as the Horizontal Branch (HB) where the burning He core is surrounded by a burning H shell. The mass, metallicity and the initial composition of the star play the key

roles in determining the position of a star in HB. After spending certain time in HB, the He core gets exhausted and the chain of events get repeated as the star takes an upward turning ascending into the phase known as "Asymptotic Giant Branch" or AGB. It is approximately parallel to the RGB. It is usually characterised by an inert C-O core, an inner He burning shell and an outer H burning shell which again becomes convective initiating the "Second Dredge Up" or SDU. Any event of the envelope becoming convective after this point are termed as "Third Dredge Up". The surface abundance of the star gets significantly altered by the SDU and FDU. For massive stars, several chain reactions like Ne-Na cycle and Mg-Al cycle takes place. Hot bottom burning and Thermally Pulsating AGB (TP-AGB) are the phases in which different nucleosynthesis events take place (Iben and Renzini 1982; Lattanzio and Forestini 1999; Langer *et al.* 1999; Herwig 2005). Several elements of higher atomic numbers like Si, Ne, Al, Na is synthesized in the stellar interior. Depending upon mass, such chain of nucleosynthesis events can proceed until the core ash is iron. At the end of this stage, the star is comprised of different layers which contain ashes from different burning sequences. Figure 1.6 shows the internal structure of a massive star towards the end of the AGB phase. At this stage, the stars undergo substantial mass loss and finally it sheds the entire envelope as a planetary nebula which in turn enriches the ISM with the products of different burning stages. The schematic diagram of the evolution of a low mass star is displayed in Figure 1.5

1.3.2.3 Explosive stars

The elements in the periodic table till Fe can be synthesized in the stellar interior. Nucleosynthesis cannot proceed further in the usual manner as Fe has the highest binding energy per nucleon. The two primary methods by which elements beyond Fe can be produced are by slow neutron capture (s-process) or rapid neutron capture (r-process). The s-process can occur with relatively low neutron flux

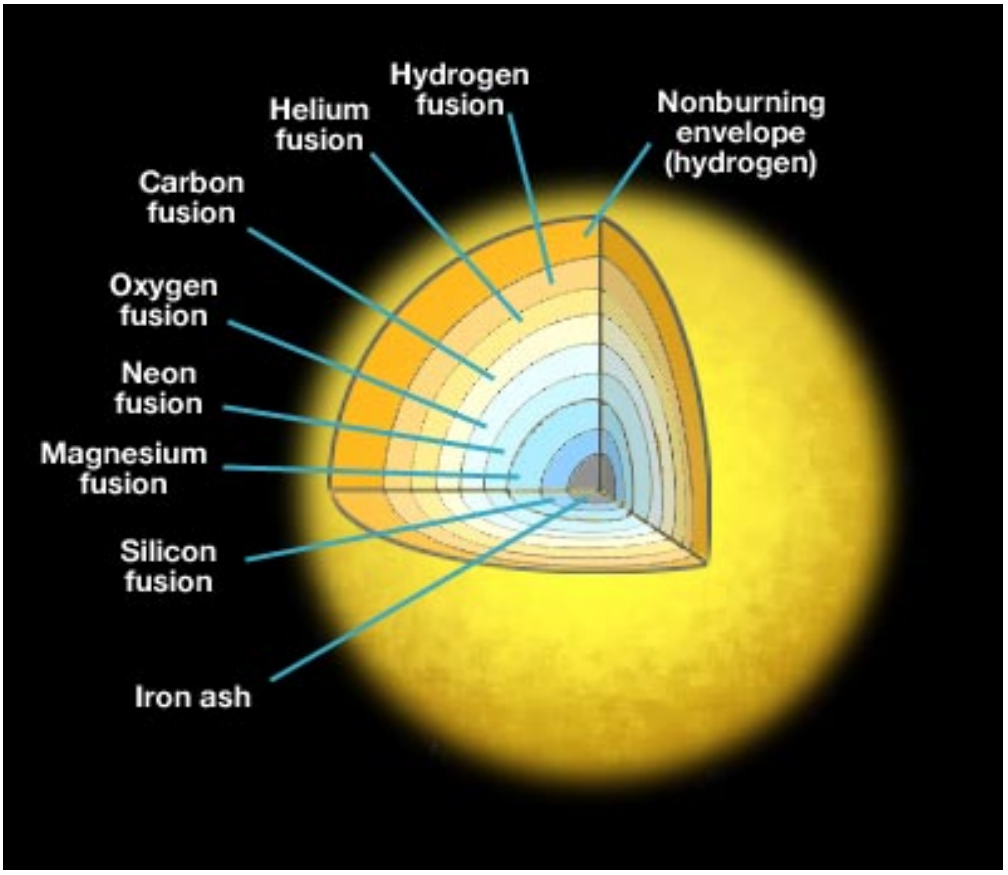

FIGURE 1.6: The internal structure of a massive star towards the end of its AGB phase. Image credits: https://www.e-education.psu.edu/astro801/book/export/html/1824

and is known to take place inside AGB stars whereas the extremely high neutron flux to produce r-process cannot be attained inside AGB stars. The primary site for r-process nucleosynthesis are supernovae, neutron star-neutron star (NS-NS) merger and neutron star-black hole (NS-BH) merger. Several Fe-peak elements like Ti, Co, Cr, Ni and Zn are also synthesized during the explosive stages of the supernovae via the complete and incomplete Si burning in its outer layers. The α rich freeze out in the supernovae is the primary source for α elements in the universe.

The burning phase during the explosion of a typical core-collapse supernova is shown in Figure 1.7. As the shock wave propagates, explosive burning takes place outside the core and the layers nearest to the centre contain only free neutrons.

The adjacent layers contain α particles while the heavier nuclei are found furthest from the core. These heavier nuclei act as the seeds for r-process nucleosynthesis. In case of NS-NS merger or NS-BH merger, the nucleosynthesis reactions proceed along the neutron drip line and due to much higher energy being produced in these mergers, elements much higher in the periodic table like U could be synthesized.

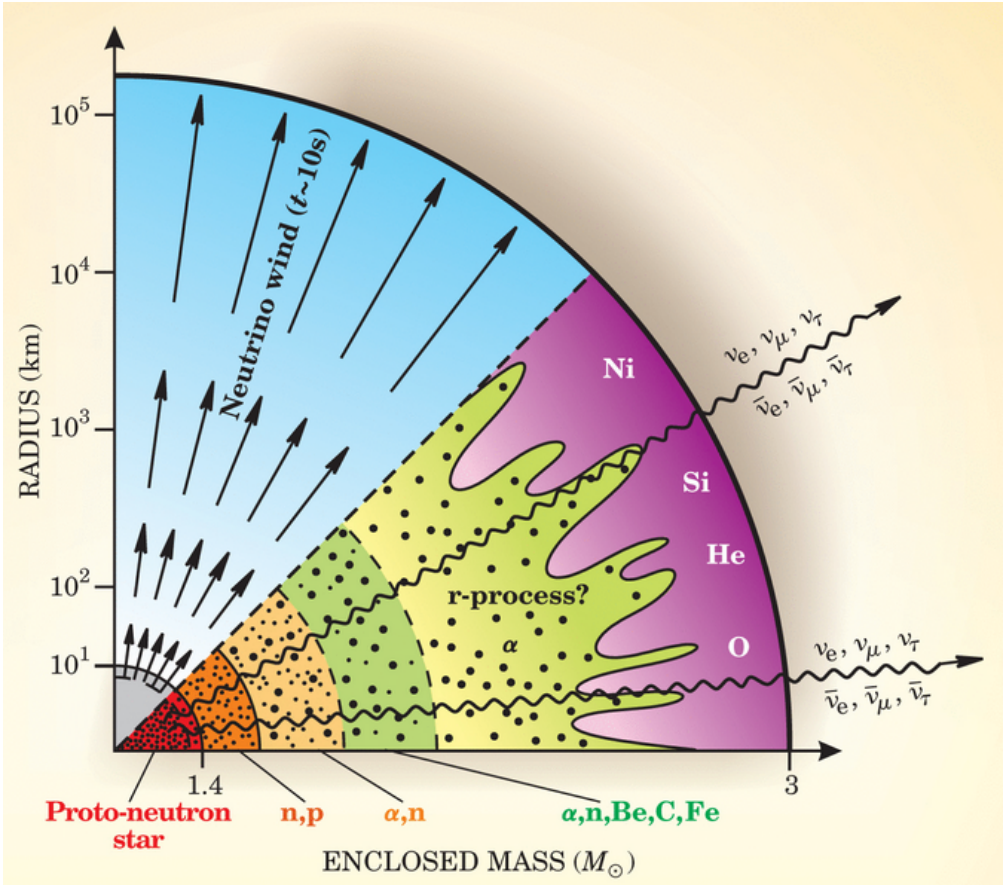

FIGURE 1.7: The explosive burning and production of elements in the different regions of a core collapse supernova. Image credits : https://physicstoday.scitation.org/doi/full/10.1063/1.1825268

1.4 Metal poor Halo stars: Relics of the early age

In the previous sections, we have discussed the chemical evolution of the universe from the early stages to the current epoch. It is extremely important to categorize and classify these early generations of stars as discussed in the previous section. Frebel (2018) provided a detailed scheme of classification based on the paucity of Fe content in the stars as given in table 1.1.

It is essential to note that in astronomy the abundance of an element with respect to another is usually quoted in comparison to their ratios in the sun which can be mathematically represented as

$$[A/B] = log_{10}(N_A/N_B)_* - log_{10}(N_A/N_B)_\odot$$

where N_A and N_B denotes the number of atoms of the elements A and B respectively. Apart from the classification based on metallicity as shown in table 1.1, the metal poor stars can be categorized based on certain abnormalities in their abundances. Some show overabundance in carbon, some have excess nitrogen, some are discovered with a large excess of heavy elements and so on. Discussing each of such scenarios is beyond the scope of the thesis and so let us briefly discuss a few of the important classes of stars relevant to this study.

1.4.1 CEMP and EMP stars

Extremely Metal Poor or EMP stars play an important role in understanding the first stars. As we have discussed already, lower the content of metals in a star, earlier is the epoch of its formation. The discovery of more number of stars in

TABLE 1.1: Classes and Signatures of Metal-Poor Stars

Description	Definition	Abbreviation
Population III stars	Postulated first stars, formed from metal-free gas	Pop III
Population II stars	Old (halo) stars formed from low-metallicity gas	Pop II
Population I stars	Young (disk) metal-rich stars	Pop I
Super metal-rich	[Fe/H] > 0.0	MR
Solar	[Fe/H] $= 0.0$	
Metal-poor	[Fe/H] < -1.0	MP
Very metal-poor	[Fe/H] < -2.0	VMP
Extremely metal-poor	[Fe/H] < -3.0	EMP
Ultra metal-poor	[Fe/H] < -4.0	UMP
Hyper metal-poor	[Fe/H] < -5.0	HMP
Mega metal-poor	[Fe/H] < -6.0	MMP
Septa metal-poor	[Fe/H] < -7.0	SMP
Octa metal-poor	[Fe/H] < -8.0	OMP
Giga metal-poor	[Fe/H] < -9.0	GMP
Ridiculously metal-poor	[Fe/H] < -10.0	RMP
Signature	Metal-poor stars with neutron-capture element patterns	Abbreviation
Main r-process	$0.3 \leq$ [Eu/Fe] $\leq +1.0$ and [Ba/Eu] < 0.0	r-I
	[Eu/Fe] $> +1.0$ and [Ba/Eu] < 0.0	r-II
Limited r-process	[Eu/Fe] < 0.3, [Sr/Ba] > 0.5, and [Sr/Eu] > 0.0	r_{lim}
s-process:	[Ba/Fe] $> +1.0$, [Ba/Eu] $> +0.5$; also [Ba/Pb] > -1.5	s
r- and s-process	$0.0 <$ [Ba/Eu] $< +0.5$ and $-1.0 <$ [Ba/Pb] < -0.5	$r + s$
i-process	$0.0 <$ [La/Eu] $< +0.6$ and [Hf/Ir] ~ 1.0	i
Signature	Metal-poor stars with other element characteristics	Abbreviation
Neutron-capture-*normal*	[Ba/Fe] < 0	no
Carbon-enhancement	[C/Fe] $> +0.7$, for $\log(L/L_{\odot}) \leq 2.3$	CEMP
	[C/Fe] $\geq (+3.0 - \log(L/L_{\odot}))$, for $\log(L/L_{\odot}) > 2.3$[e]	
α-element enhancement	[Mg, Si, Ca, Ti/Fe] $\sim +0.4$	α-enhanced

this class enhances the likelihood of observing undiluted signatures of population III stars and imprints of the first supernova. With an increase in the number of studied EMP stars, a curious feature has emerged. As the metallicity decreases, [C/Fe] starts increasing. Such stars with [C/Fe] $> +0.7$ are termed as CEMP or Carbon Enhanced Metal Poor stars.

The CEMP stars have been categorised into several sub-classes based on abundances of neutron-capture elements as follows

- CEMP-s stars: They show an enhancement in *s*-process elements. Such enhancements are attributed to mass transfer scenarios in which it receives contributions from its binary component during its AGB phase. Binarity studies also tend to confirm the same.
- CEMP-r stars: They show an excess in *r*-process elements and are extremely rare to find in the halo. The progenitor of these stars could be faint supernovae but the exact source or *r*-process remains unclear. More discoveries of such objects could greatly help the cause.
- CEMP-r/s stars: These stars are found to have excess abundances for both *s*-process and *r*-process elements. The source of *s*-process are AGB stars or Fast Rotating Massive Stars (FRMS) but the origin of *r*-process is not very clear.
- CEMP-no stars: These are discovered with no excess of n-capture elements. The source of this class of stars are believed to be mixing and fallback supernovae (e.g Nomoto *et al.* 2013; Tominaga *et al.* 2014) or spinstars (e.g., Meynet *et al.* 2006; Chiappini 2013). Their frequency goes up as metallicity decreases and tends to dominate at lowest metallicities.

Apart from the standard [C/Fe] ratios, CEMP stars could also be classified using the absolute C abundances as described by Yoon *et al.* (2016). The Yoon-Beers

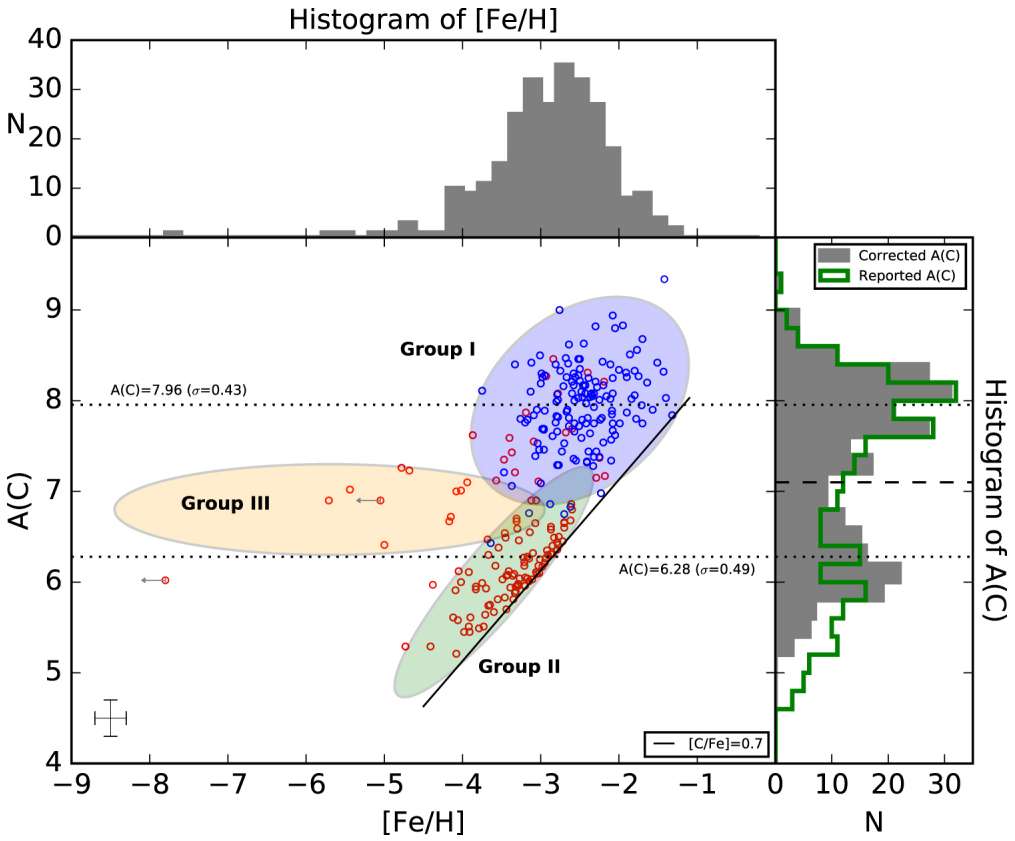

FIGURE 1.8: The Yoon-Beers diagram presenting an alternate classification of CEMP stars based on the absolute carbon abundances. Group I stars with higher C abundances are all CEMP-s stars whereas CEMP-no stars occupy the lower C band. The CEMP-no stars are also divided into two groups which could be lightly associated with the different progenitors.

diagram is shown in Figure 1.8. All the CEMP-s stars occupy the higher band whereas the CEMP-no stars occupy the lower band. The CEMP-no stars could be further divided into two classes based upon the trends with metallicity which could roughly be associated with the two different modes of their formation.

1.4.2 *R*-process rich stars

The *r*-process rich stars are those which show enhancements in *r*-process elements. They are a rare class of objects formed out of material that underwent mixing with the ejecta of NS-NS merger, NS-BH merger or core-collapse supernova. The

r-process pattern (after the first peak) found in these stars is identical to the solar r-process. Such discoveries indicate the universality of the event and it seems, there was only one class of progenitor for this population of stars. The Ultra Faint Dwarf Spheroidal galaxies are the potential sites for their origin which later migrated to the halo. With the onset of r-process Alliance, there has been a surge in the discoveries of r-process rich stars. It is very essential to identify more of these stars to investigate the astrophysical production sites and conditions of the progenitor population.

1.4.2.1 The Li distribution

The Li problem has been troubling the astronomers for a long time. Li is an element which is produced after the big bang and not in stellar interiors. However, the measurement of abundances of Li in the oldest low mass stars shows a constant value (known as the Spite plateau) at A(Li) = 2.19 which is significantly lower than the predictions of the BBN model. This reflects on the poor understanding of the modes of Li depletion in the MSTO stars (Korn *et al.* 2006) and events that deplete Li in the early universe (Piau *et al.* 2006). Li being a fragile element tends to get destroyed at higher temperatures and thus serves as an excellent tool for stellar studies.

1.5 Globular clusters: Fossils from the primordial population

1.5.1 Formation and evolution

Following Fall and Rees (1988), models and mechanisms for the formation of globular clusters could be categorized into three classes - primary, secondary and tertiary.

- In the primary formation models, globular clusters are formed prior to the galaxies. According to Peebles and Dicke (1968), the Jeans mass following recombination for the hierarchically clustering models is around 10^6 $M_\odot$ which is similar to the mass of a globular cluster. Although, it was later shown that both astrophysical, as well as cosmological factors play significant roles in the determination of the mass-scale (e.g. Gunn 1980; Carr and Rees 1984; Ashman and Carr 1988; Ashman and Zepf 1992) but the values are still comparable.

- Secondary formation models assume that formation of the host galaxy and globular clusters took place at the same epoch. This is the most attractive among the different models as they could justify for the strong correlations between some of the globular cluster properties like metallicity gradients (Searle and Zinn 1978; Zinn 1985; Armandroff *et al.* 1992), stellar radii distributions (van den Bergh 1994), stellar mass function (Piotto 1991; Capaccioli *et al.* 1991, 1993; Djorgovski *et al.* 1993) etc with the galactocentric distance. Fall and Rees (1985) showed that thermal instabilities in the protogalaxy could give rise to pockets of cool clouds. For such clouds at low metallicity, the cooling becomes inefficient for a significantly large timescale. These cool clouds were thought to be the progenitors of globular clusters.

The model had several drawbacks (King *et al.* 1990) like the cooling time was required to be longer than the dynamical time of the clouds (Gunn 1982) and several improvements on the model gradually came along (e.g. Murray and Lin 1992; Richtler and Fichtner 1993, and many more). The secondary formation scenario could successfully explain many of the observed properties of globular clusters but also fails to explain.

- The tertiary models are those in which globular clusters are formed after the host galaxy. However, as a word of caution, there is an overlap between these formation models due to the hierarchical clustering of the galaxy which itself takes a long time to assemble and thus in many scenarios the distinction becomes largely semantic. The globular clusters residing in the galactic disc carry substantial evidence for the tertiary models (Burkert *et al.* 1992; Ashman and Zepf 1992).

Based on these fundamental paradigms several advances have taken place in the last decade. These include cosmological galaxy merging theories (Kruijssen 2014b; Forbes *et al.* 2018) which takes a fresh approach to solve the problem.

1.5.2 Abundances

More than a few decades ago, star-to-star variations exceeding an order of magnitude in the abundances of the elements like Na and Al were discovered for some globular clusters like M3, M13 and NGC6752 (Cohen 1978; Peterson 1980; Norris *et al.* 1981). The scatter largely exceeded the observational errors. CN band strength was also found to be anti-correlated with the CH band for the stars at same evolutionary stage (i.e with the same temperature and gravity) 47 Tuc (Harbeck *et al.* 2003) and similar traits were also found for many other clusters later on (Ramirez and Cohen 2001; Ramírez *et al.* 2001 and many more). The higher

abundances of N leads to the formation of the stronger CN band while CH band is weaker due to relatively lower C. O abundances were also found to be inconsistent in many of the studied clusters and those were in turn found to be anti-correlated with Na abundances.

With the advent of high resolution spectroscopic survey in the 1990s, abundances for the light elements like C, N, O, Al, Na and Mg could be measured in a statistically significant number of stars in the clusters (e.g. the Lick-Texas survey). Abundances could also be derived for a large number of α and Fe-peak elements which provided very valuable insights into the chemical abundances in GC stars. We are going to discuss the results from these surveys and implications for nucleosynthesis events inside GCs in the next section.

1.5.3 Nucleosynthesis and Recycling of products

The discovery of the anti-correlations as discussed in the previous section ensued a long series of debate among the astronomers. Initially, it was thought that variable amounts of Na and O could be produced in massive stars but then it must be accompanied by a scatter in n-capture elements which was again not seen in GCs (Armosky *et al.* 1994; Ivans *et al.* 2001). This puzzle was apparently solved when it was found that Na could be produced by proton capture reactions in the same region near the H-burning shell of the giant stars where oxygen begins to deplete via the incomplete ON cycle (Langer *et al.* 1993; Salaris *et al.* 2002; Gratton *et al.* 2004). At even hotter temperatures($T > 70 \times 10^6$ K), ^{27}Al could be produced by subsequent proton capture reactions on ^{24}Mg. The most likely stars to produce these elements in their interiors were thought to be either low mass RGB stars ascending the giant branch and intermediate mass AGB (IM-AGB) stars. However, if RGB stars were the true sites of production then a non-standard dredge up to bring the processed material from the stellar interior to the surface

has to be incorporated in order to explain the observed chemical signatures in the GC stars. The idea of evolutionary mixing was kept alive by incorporating rotation induced differential mixing in GC stars to produce the observed abundances (e.g. Denissenkov and VandenBerg 2003a,b; Denissenkov and Herwig 2003 among many others).

The paradigm of evolutionary mixing in GC stars to show the observed abundances were also useful to explain several observed phenomena like a steady decline in [C/Fe] as the stars move towards the tip of the RGB, constancy in the sum of C, N, O as well as Mg, Al for individual GC stars (Briley *et al.* 1996). However, the big hurdle of the scenario of evolutionary mixing came with the discovery of dwarf stars by Gratton *et al.* (2001) using high resolution UVES/VLT spectra which yielded similar abundance ratios and same anti-correlations as in giant stars. Early sub-giants and turn off stars also showed similar traits. Thus, deep mixing was ruled out as the primary phenomenon driving the abundances as such high temperatures for advanced p-capture reactions could not be attained in these stars.

In the current picture, primordial variations are believed to have played the key role. The intra-cluster material was polluted by a significant number of IM-AGB stars which could produce an enhanced fraction of Na and Al in the inter-shell region which is rich in neutrons during the thermal pulses (Iben 1976; Forestini and Charbonnel 1997; Marigo *et al.* 1998; Ventura *et al.* 2002; Karakas and Lattanzio 2003). AGB stars with hot bottom burning (HBB) are also known as excellent candidates to have polluted the intracluster gas (Denissenkov *et al.* 1997; Ventura *et al.* 2002; García-Hernández *et al.* 2013; Cristallo *et al.* 2015). The winds from these AGB stars have mixed with the proto-cluster gas and raised the floor of the abundances for these elements. The AGB stars begin to loose mass only after the very massive stars in the cluster have exploded as core collapse supernovae which disperse the cluster ISM and the slow winds of the AGB stars allow the processed gas to be retained by the cluster and get mixed with proto-cluster gas. Thus the

subsequent generations of stars that were formed from the mixed clouds which we observe today have higher abundances of Na, Al and a re-distribution of C-N-O abundances.

Thus, the primordial variations provide the floor of the abundances upon which the evolutionary mixing could play a role in case of giant GC stars. So, the first generation of stars in the cluster would still show normal abundances like field stars whereas the second and subsequent generation of stars would show the light element anomalies. This brings us to the question of multiple populations in GCs which we will discuss in the next section.

1.5.4 Multiple population

Instantaneous star formation and homogenization of chemical abundances of the molecular clouds would be expected to give rise to a single stellar population. However, such a scenario would not be pragmatic for a large ensemble of stars like globular clusters. In the last section, we have discussed that the spread in the chemical abundances is much larger than the expected original inhomogeneities and this gives rise to the idea of multiple populations of stars. The multiple generations of stars include a primordial population, first generation stars and second generation of stars which itself may have several distinct sub-classes. The second generation of stars were born out of the material mixed with the ejecta of a few of the first generation of stars (e.g. Gratton *et al.* 2001; Ramírez and Cohen 2002; Gratton *et al.* 2004; Carretta *et al.* 2009a,b; Gratton *et al.* 2012a) which could be seen from the study of the abundances of the light elements. Majority of the stars found in a GC belong to the second generation. Only the low mass stars of the first generation still survive in the GCs and are very similar to the Halo stars. They constitute roughly one-third of total cluster stars and show the composition of the ejecta of a core collapse supernovae.

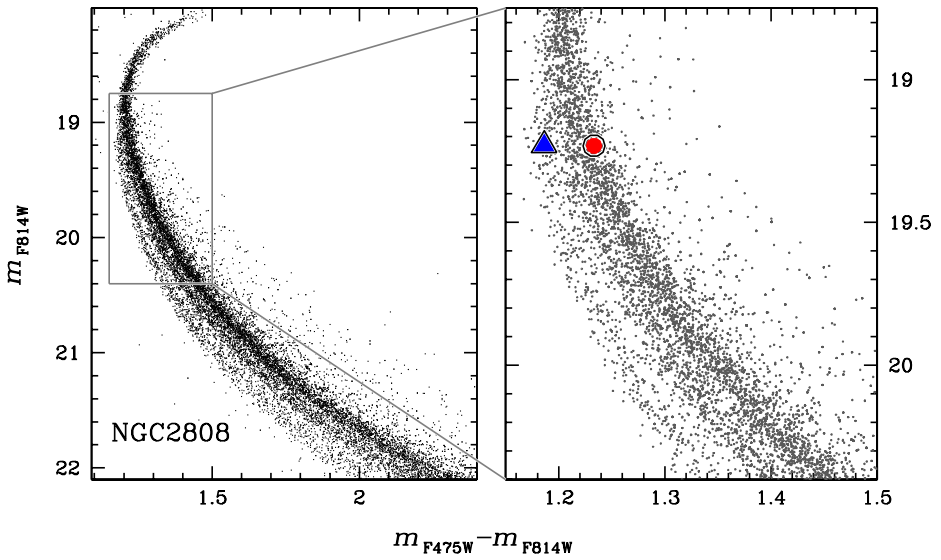

FIGURE 1.9: The discovery of two dwarf stars on the red and blue main sequence of NGC 2808 by Bragaglia *et al.* (2010). The triple main sequence for the same GC was obtained by Piotto *et al.* (2007). Image taken from Gratton *et al.* (2012a)

High quality photometric data displayed multiple sequences in the colour-magnitude diagram in the main sequence and sub-giant phases for a large number of clusters which could be studied in great detail (Piotto 2009). Multiple sequences could be observed photometrically even in the case of NGC 6397 which has an extremely narrow main sequence in the CMD (Milone *et al.* 2012).

The era of high quality photometric observations of GCs started with the advent of the Hubble Space Telescope (HST) which led to a dramatic reduction of the photometric errors and thus finer details in the Color-Magnitude Diagrams (CMD) of individual clusters could be discovered. Two or more splits in the main sequence of several clusters like ω-centauri (Bedin *et al.* 2004; Villanova *et al.* 2007) and NGC 2808 (Piotto *et al.* 2007) were discovered soon. Spectroscopic observations were also not to be left behind. In 2007, the highly sensitive X-SHOOTER at the Very Large Telescope (VLT) could record the spectrum of two faint main sequence

stars in NGC 2808. One of them was on the blue MS and the other on the red MS in the CMD as showing in Figure 1.9. The result of the chemical tagging was extremely interesting. The one on the red MS showed normal abundances while the one on the blue MS showed the typical abundances expected in a second generation GC star with elevated levels of Na, Al, and N, and depleted levels of C and Mg (Bragaglia *et al.* 2010). Thus multiple generations in GCs were confirmed with a combination of photometry and spectroscopic data. The observational data for correlation between photometry and spectroscopy is robust and the same could be affirmed for many clusters thereafter.

1.5.5 Nature of primary polluters

In the previous sections, we have discussed the light element abundances which could be significantly altered in the stellar interiors during different phases across the evolutionary sequence of a star. However, the heavy elements are immune to such alterations. Here, we mainly discuss the abundances of neutron-capture elements which would help us to shed light on the pre-enrichment in GCs. The elements higher than Fe in the periodic table could only be produced by n-capture reactions. In the early galaxy, $r-$process is the chief mode for the production of these elements as it requires significant time to elapse for the $s-$process to set in. The signature of these r-process events are retained in the GC stars and can be studied with powerful telescopes. This provides a great opportunity to study the primordial population that polluted the GC clouds during its formation.

1.6 Globular clusters and Halo connection

1.6.1 Formation

Following the theory of hierarchical merging, the globular clusters and halo stars were formed in mini-halos which later migrated to the Milky Way halo. Both the populations are believed to be ancient and were formed at similar epochs in the nascent stages of the universe. However, self enrichment in globular clusters took place as the gas could not escape the cluster potential resulting in an evolved population. The detailed abundance study of the GCs and halo stars could shed light on the chemical enrichment during their formation epochs and provide valuable information about the astrophysical sites and conditions that prevailed in the early galaxy.

1.6.2 Population

Globular clusters must be formed during massive episodes of star formation (for the second generation of stars to be formed out of the ejecta of a fraction of the first generation of stars) and thus they are expected to loose a large number of their original population of stars.

Evaporation is the primary mode for the loss of stars from the cluster. The frequent two body encounters in a GC leads to the velocity distribution being a Maxwellian. Since the globular clusters are old (age) they are also supposed to have undergone mass segregation following equipartition of energy. Thus, the low mass stars with higher velocity occupy the outer layers of the clusters while the more massive stars sink towards the centre. These low mass stars at the high velocity end of the Maxwellian tend to move out of the cluster potential. A substantial fraction

of the Halo is believed to be composed of such GC escapees as we shall discuss in great detail in Chapter 4.

1.7 Scope of the thesis

The thesis work focuses on the chemical abundances of bright (Vmag < 13.0) metal poor stars in the metallicity range $-3.5 < [Fe/H] < -1.0$. This metallicity range covers major milestones of the formation history of Milky Way. It also covers the metallicity range of the metal poor Globular clusters. Targets were selected from the SDSS-MARVELS pre-survey (discussed in Chapter 2), which has maximum overlapping sky with the 2m Himalayan Chandra Telescope (HCT), in India that is equipped with a high resolution optical spectrograph.

The work involves observations of high resolution spectra presented in the thesis and the detailed analysis and the interpretation of the results. The metal poor sample studied here span a wide range of chemical abundance pattern. In this work, we present the abundance trends in CEMP-no and EMP stars, r-process rich stars and possible and stars that have similar light element anomaly as seen in Globular clusters. We study the commonality among EMP and CEMP-no stars. We also compare the abundance pattern in the light and heavy r-process elements among different types of Halo stars and Globular clusters and try to infer the nature of possible first generation massive stars and the role of environment. Lithium abundance among in the different Halo stars is also presented. Halo stars among different groups (VMP, EMP, CEMP-no, r-I stars, GC escapees) show similar Lithium abundances.

1.8 Plan of the thesis

1.8.1 Chapter 1 : Introduction

This chapter contains a brief introduction about the Milky Way halo stars, globular clusters and their relevance in the context of this thesis work. It also gives a brief account of the previous studies and survey that have been carried out with a similar goal. described in short in the above two sections.

1.8.2 Chapter 2: Data, sample selection and methodology

The observations and data used in this study are presented in this chapter. High-resolution ($R \sim 30,000$) spectroscopic observations of about 50 stars were carried out as a part of the HESP-GOMPA (Galactic survey Of bright Metal Poor stArs) survey using the Hanle Echelle Spectrograph on the 2.3-m Himalayan Chandra telescope (HCT) at the Indian Astronomical Observatory (IAO). The targets were selected from the sub survey MARVELS which was carried out as a part of SDSS-III. It offers the chance to identify bright Halo stars which could be studied in high resolution using moderate class telescopes. The potential selection biases could also be reduced due to the simple magnitude and color cuts ($B - V > 0.6$ and $8 < V < 13$) of the MARVELS survey. We have used synthetic spectral fitting of the pre-survey data to identify new metal-poor candidates(in the domain of globular cluster metallicity; [Fe/H] > -2.50) with a weak G-band which is a well known feature of globular cluster stars and could be studied from low resolution data (e.g. SDSS). We have also identified several other classes of stars like EMP, CEMP-s, CEMP-no, r-process rich stars. We have also been able to detect Li over different evolutionary phases of several metal poor stars.

1.8.3 Chapter 3: Abundance analysis of new bright EMP and CEMP stars

In this chapter, we discuss the study on several new CEMP and EMP stars discovered in the survey. The origin of carbon in CEMP-s stars is mostly due to mass transfer from a binary component like AGB stars and thus it does not provide much insights into the early generations of stars. On the other hand, CEMP-no and EMP stars have a primordial origin and are supposed to be direct descendants of pop III stars. A comparative study using elemental abundances of Fe peak elements and heavy elements has been conducted to find the differences (and similarities) between these two channels of star formation following the early supernovae. We have also tried to find the progenitor type for each CEMP-no stars in the survey using the individual abundances.

1.8.4 Chapter 4: Discovery of a blue straggler and other GC escapees in the Halo

Globular clusters are supposed to have lost a large number of stars during their migration to the Halo. In this chapter, we discuss three such stars found in the Halo with light element anomalies typically expected to be observed in second generation stars of globular clusters. One of these stars was found to be a blue straggler which is a rare object to be studied in detail. We have carried out the detailed abundance analysis for these objects and the findings are consistent with previous studies of globular cluster escapees in the Halo.

1.8.5 Chapter 5: R-process rich stars from the HESP Gompa Survey

The Halo contains a very small population of stars which are rich in r-process elements. It is valuable to find more of these stars as they could possibly be formed in dwarf spheroidal galaxies where they experienced one or more strong r-process events. They provide key information to the formation of a wide range of heavy elements in the early phases of the universe. A complete understanding still eludes the scientific community. In this chapter, we discuss the new r-I and r-II stars emanating from the survey. We have carried out a detailed abundance analysis of each star and compared to the existing literature. Th could also be detected in one of the targets. We have also used the archival data of SDSS and ESO to study the key neutron capture elements like Sr and Ba for several globular cluster stars. A spectral grid was developed over wide ranges of temperature, log(g), [Fe/H], [Sr/Fe] and [Ba/Fe]. We tried to explore the common origin for the Halo stars and individual clusters. Neutron star mergers were found to the chief contributor for globular clusters whereas Halo stars showed both NS-NS mergers and supernovae to play a key role in different paradigms. The results from SDSS were only indicative due to the low resolution of the available data and thus are included in the future plan

1.8.6 Chapter 6: Li distribution and new VMP stars from HESP-GOMPA survey

Li is a fragile element which is likely to be destroyed as a star ascends the giant branch. In this chapter, we discuss the Li abundances detected for several stars in the survey which include main sequence stars, subgiants and red giants. They showed the expected behaviour of Li depletion. Li was also found not to correlate

with any other elemental abundances and stellar parameters like temperature and gravity which is consistent with previous studies. Different classes of stars were found to have a very similar distribution of Li which points towards a common origin.

1.8.7 Chapter 7: Conclusion and future work

This chapter summarizes all the results and findings of the thesis. It also describes the future plans following thesis submission.

Chapter 2

Observations, sample selection and methodology

2.1 Introduction

The advances in the field of spectroscopy over the last few decades have revolutionized the human ability to study the laws of nature and unravel the secrets of the universe. Prior to the advent of spectroscopy, the entire subject of astronomy was limited to mapping the positions of stars and other luminous objects in the sky, estimating their brightness and in certain cases, marking the trajectory of few of these heavenly bodies. The long standing questions like what are stars, what are stars made up of, exactly how far away are these objects from us remained unanswered. The emergence of spectroscopy, the ability to split starlight to study the spectrum in detail marked a new dawn in the subject of astronomy. This tool that could help scientists unravel the secrets about the composition of a star, the

processes which led to the formation of elements in the periodic table and speculate the driving forces and events that shaped the evolution of the universe to its currently known form.

Stellar spectroscopy is primarily the study of absorption and emission lines in the spectrum of a star. The absorption lines are formed when the photons coming from inside the star get absorbed by the surface of last scattering. These lines could be detected and measured by splitting the starlight using a prism, grating, grism or their combinations. The element causing an absorption line could be uniquely identified since the discrete energy levels of the transitions for the atoms of a particular element are unique. Fraunhofer, Kirchhoff and other notable scientists of the 19th century demonstrated that such atomic transitions could be identified and used as fingerprint of a particular element in the periodic table. The depth of the absorption feature is indicative of the relative proportion of that element in the stellar surface.

2.2 Sample selection

Most of the work presented in the thesis is based upon detailed study of the spectra of Galactic halo stars in high resolution. The sample of stars have been selected from the MARVELS (Multi-object APO Radial Velocity Exoplanet Large-area Survey) pre-survey which is a constituent of SDSS (Sloan Digital Sky Survey) III by using certain selection criteria. Let us discuss SDSS, MARVELS and the selection criteria employed to shortlist the targets in the sections below.

2.2.1 SDSS

Sloan Digital Sky Survey (abbreviated as SDSS) is an imaging and spectroscopic survey with the 2.5m class telescope (Gunn *et al.* 2006) located at Apache Point Observatory (APO). It has been observing the celestial sphere since the year 2000 and has till now acquired spectra for more than 4 million objects. SDSS is composed of several stages as briefly discussed below.

- SDSS I - It was the first phase of its operations between 2000 and 2005 which conducted the 'legacy survey' (imaging in all the five bands u, g, r, i and z) and spectroscopy of galaxies and quasars (York *et al.* 2000; Gunn *et al.* 1998; Eisenstein *et al.* 2001; Strauss *et al.* 2002; Richards *et al.* 2002).

- SDSS II - The second phase of its operations was conducted in the period 2005-2008. It completed the legacy survey and carried out spectroscopic observations of the Galactic stars (Yanny *et al.* 2009). These spectroscopic observations were a part of Sloan Extension for Galactic Understanding and Exploration (SEGUE) which was conducted to obtain a three dimensional structure of the Milky Way.

- SDSS III - It was carried out in the period 2008-2014 and comprised of four different surveys (Eisenstein *et al.* 2011); (i) The APOGEE (APO Galactic Evolution Experiment) which primarily used infrared high resolution spectroscopy to observe the Galactic stars in great detail (Majewski *et al.* 2017), (ii) BOSS (Baryon Oscillation Spectroscopic Survey) to study the rate of expansion of the universe by detecting the baryon oscillations in the galaxy clusters (Dawson *et al.* 2013; Anderson *et al.* 2014), (iii) SEGUE-2 which was completed in this period and (iv) MARVELS to measure the radial velocities of the bright stars for exoplanet studies (Ge *et al.* 2015).

- SDSS IV - It is the fourth phase and is being presently carried out from 2014 to 2020. It is comprised of APOGEE-2, eBOSS (extended BOSS) and MaNGA (Mapping Nearby Galaxies)

2.2.2 MARVELS

MARVELS (Paegert *et al.* 2015), a multi-object radial-velocity survey designed for efficient exoplanet searches, was one of the four sub-surveys carried out as part of SDSS-III (Eisenstein *et al.* 2011) as discussed above. The targets for the first two years of MARVELS were selected based on a lower-resolution (R $\sim$ 1800) spectroscopic pre-survey using the SDSS spectrographs. Most of the pre-survey observations were carried out during twilight when the fields were at low elevation. Targets were selected from these pre-survey fields for the MARVELS main radial velocity (RV) survey, which were later observed at higher elevations. There were about 30,000 stars observed as part of the spectroscopic pre-survey of stars with $B - V > 0.6$ and $8 < V < 13$. The distribution of the number of observed stars in terms of their V magnitudes is shown in Figure 2.1 (taken from Paegert *et al.* (2015). Target fields for the first two years of the MARVELS survey were around known RV standards and about 75% of the target fields were in the Galactic latitude (b) range $2^\circ < |b| < 30^\circ$. The distribution of the fields in the galactic coordinates are shown in Figure 2.2 (taken from Paegert *et al.* (2015). Although not the ideal location to find metal-poor stars, it does offer the chance to identify a small number of bright halo targets, suitable for high-resolution spectroscopic follow-up with moderate-aperture telescopes, that happen to fall into the MARVELS pre-survey footprint during their orbits about the Galactic center. The pre-survey also has simple magnitude and color cuts, which reduces potential selection biases. The metallicity distribution for the targets is being shown in Figure 2.3. The left panel represents the compilation of entire MARVELS spectra whereas in the right the metallicity distribution of a single field is shown.

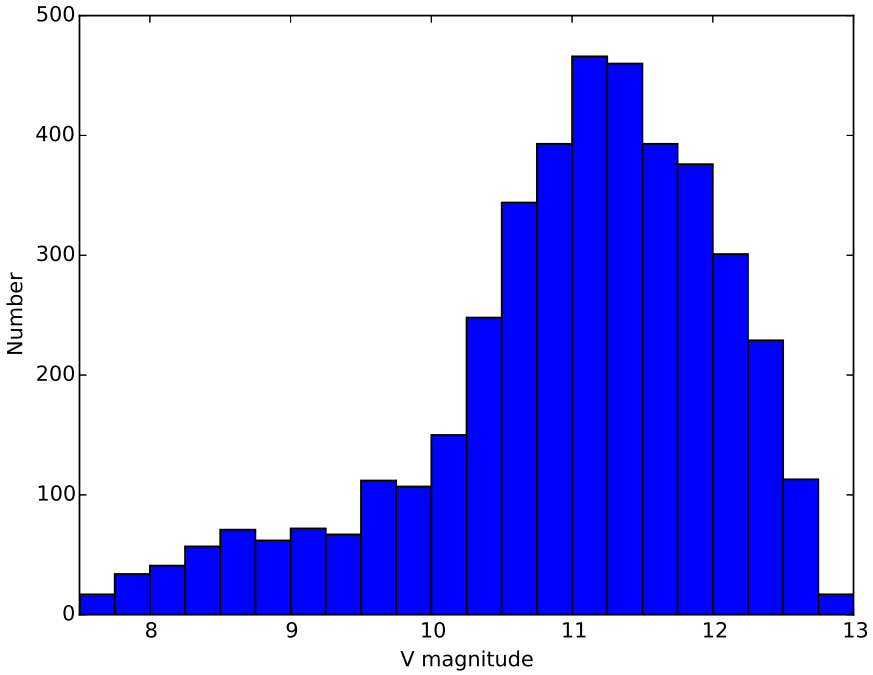

FIGURE 2.1: The distribution of V-magnitudes in the observed data for MARVELS taken from Paegert *et al.* (2015)

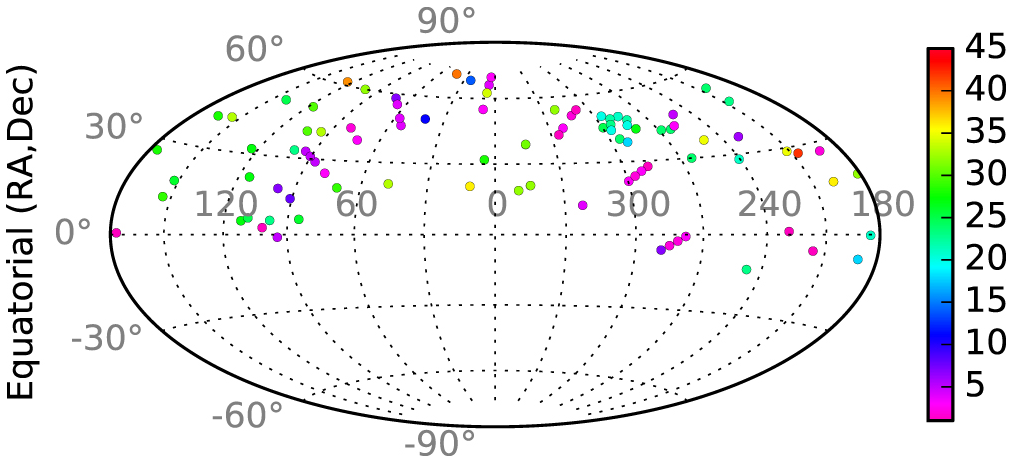

FIGURE 2.2: The distribution of the observed fields in MARVELS in galactic coordinates taken from Paegert *et al.* (2015).

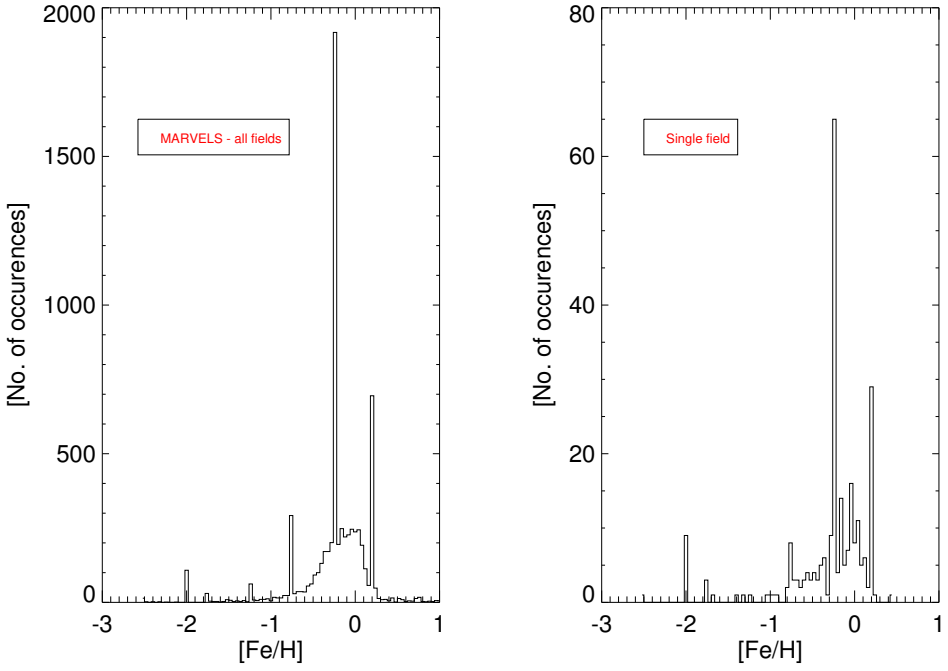

FIGURE 2.3: The metallicity distribution for the MARVELS pre survey data. The spread of the entire compilation of MARVELS spectra over all fields is shown in the left panel while the distribution of a single field is shown in the right panel.

2.2.3 Parameters for target selection

As in our previously published work (Bandyopadhyay *et al.* 2018), we used synthetic spectral fitting of the pre-survey data to identify new metal-poor candidates. The main criteria used for short selecting the stars for follow up observation in high resolution using HESP are the following:

- The stars with a good quality of spectral fit with higher values of signal-to-noise ratios were considered for selection. This was done to eliminate those with grossly wrong estimates for stellar parameters.
- The stars that lie in the domain of globular cluster metallicity were short-listed for further observation. We wanted to tag the escapees from the metal poor globular cluster escapees in the Halo. So we selected only those stars

which had [Fe/H] < -1.0. As seen in Figure 2.3, the number of stars in this regime was relatively lower and thus imposition of these criteria reduced the number of selections drastically.

- Globular cluster stars show a typical anomaly in light element abundances like a weak C molecular g-band which could be measured from the low resolution spectra of the MARVELS data. Thus, we used this additional criterion to further to refine the selection in order to enhance the probability of finding the true GC escapees.

- Apart from GC escapees, we were also interested in doing a detailed abundance analysis of the early generations of stars or the extremely metal poor stars. Hence, we also selected those stars which had a good fit and were found to be very metal poor from the low resolution data with/without weak g-band.

The stars were selected for follow up, as they were found to be very metal poor from the spectral fitting of the pre-survey data and were also very bright. Results from the spectral fitting used to identify metal-poor candidates from the MARVELS pre-survey will be discussed in a separate paper.

2.3 Observation

2.3.1 Himalayan Chandra Telescope

The Himalayan Chandra Telescope (HCT) is a 2m class telescope installed in the Indian Astronomical Observatory (IAO), on Mt Saraswati, Hanle in the eastern part of the Indian state of Jammu and Kashmir and is operated by Indian Institute

of Astrophysics. The site is located at a relatively high altitude of 4500 metres above the mean sea level. It boasts of good seeing conditions all around the year mainly due to high altitude and lower levels of humidity, dust and aerosols. In order to withstand the extremely low temperatures, the primary mirror is made up of corning ultra low ceramic. The telescope is set up in an alt-azimuth mount and a modified form of Ritchey-Chretein configuration has been used. The main instruments of the telescope are the following

- Hanle Faint Object Spectrograph and Camera (HFOSC)
- TIFR Near Infrared Spectrometer and Imager (TIRSPEC)
- Hanle Echelle Spectrograph (HESP)

If needed, all the instrument could be accessed during the same night. This is made possible by mounting them at the Cassegrain focus on an instrument mount cube which has four ports on the four sides and one on the axis. It is remotely operated from Centre for Research in Education, Science and Technology (CREST), Hoskote which is just 35 km away from Bengaluru.

2.3.2 HESP

The design of HESP was based on the concept of white pupil permitting continuous spectral coverage from 350 nm to 1000 nm in a 4K $\times$ 4K detector (single CCD - Charge Coupled Device). It can operate in two resolution modes - R = 30,000 and R = 60,000 using the image slicer. HESP has a dual fiber mode available, one fiber for the target star and another, which can be fed with a calibration source for precise RV measurements, or by the night sky through a pinhole that has a separation of about 13$''$ from the target. The sky fiber is used for background subtraction. The spectrograph layout for HESP is shown in Figure 2.4.

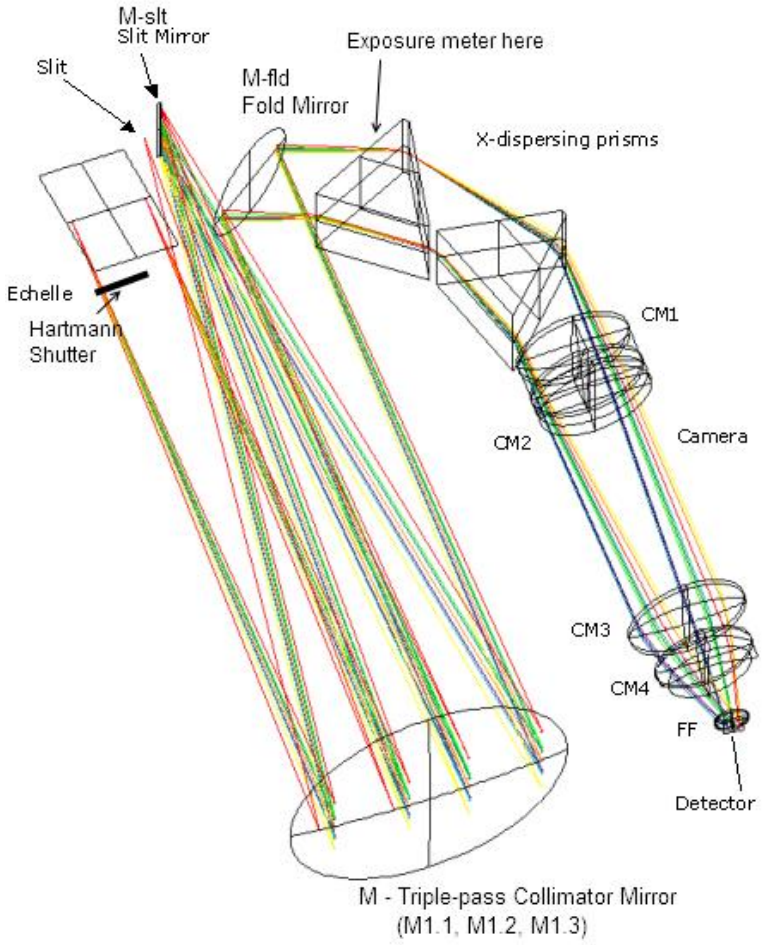

FIGURE 2.4: Spectrograph layout for the Hanle Echelle SPectrograph (HESP).

The HESP instrument is thermally controlled to $\Delta T = \pm\ 0.1^{\circ}$ C at a set point of 16° C over the entire year, which is expected to provide long term stability of $\sim$ 200 m s^{-1} (Sivarani et al. in preparation), substantially lowering systematic errors with respect to a spectrograph that does not have such control.

2.4 HESP-GOMPA survey

The HESP-GOMPA or Galactic survey of Metal Poor stArs with HESP is the high resolution survey carried out as a part of this thesis. Detailed observations of

more than 50 metal poor stars were carried out in this survey at resolutions of R = 30000 and R = 60000 depending upon the brightness and S/N ratio of the target star. The target stars were selected from the SDSS MARVELS pre-survey based on the criteria as discussed above. The aim of the survey was to detect stars of GC origin in the halo and study the ancient population of stars at low metallicities to find the signatures of the first stars and first supernova. We have been able to detect several interesting objects which include GC escapees, r-process rich, CEMP, EMP and VMP stars. Li could also be detected in a few of these stars. The metallicity spreads from [Fe/H] = −1.20 to [Fe/H] = −3.20 with the peak at [Fe/H] = −2.50. The distribution in [Fe/H] is shown in Figure 2.5. The details of observation for many of the objects from HESP-GOMPA survey is given in Table 2.1. It would be beyond the scope of the thesis to discuss all the objects studied in this survey and in the forthcoming chapters we shall discuss the interesting results obtained so far.

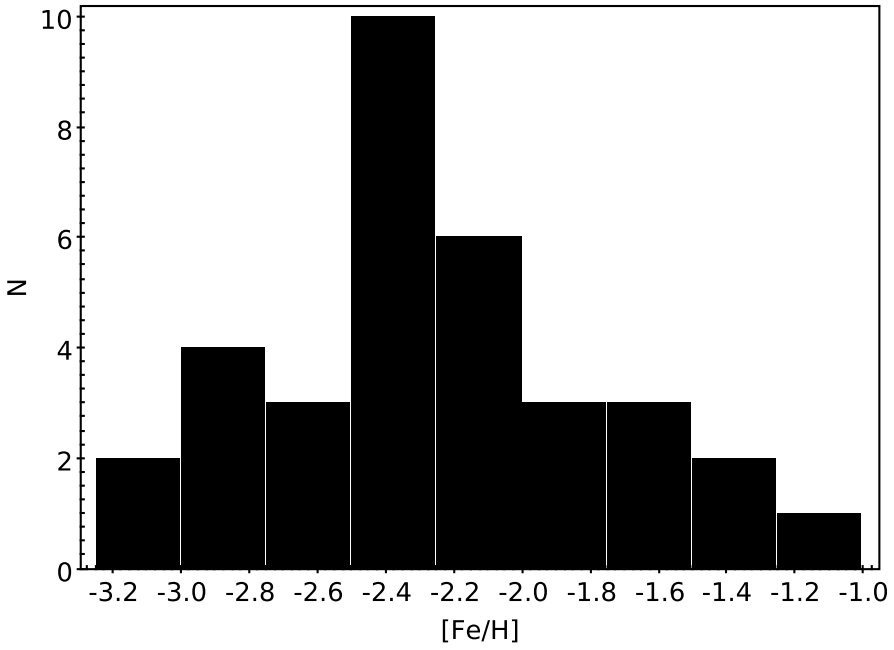

FIGURE 2.5: The distribution of the metallicity of the stars studied as a part of HESP-GOMPA survey. [Fe/H] varies between −1.0 to −3.2 for the studied samples.

TABLE 2.1: Observation details for the reported objects observed through HESP at R $\sim$ 30000.

Object	obs.time	frames	SNR	Vmag	Rad.vel
SDSS J1937+5024	2400s	3	130	10.44	−184.0
SDSS J0210+3220	2400s	6	61.5	11.54	34.5
SDSS J0753+4908	2400s	3	46.0	11.28	3.0
SDSS J0646+4116	2400s	6	43.1	11.14	−285.0
SDSS J1521+3647	2400s	9	40.4	11.58	−73.5
SDSS J1725+4202	2700s	3	53.0	11.66	−266.5
SDSS J1350+4819	2400s	11	54.8	11.65	−109.0
SDSS J1146+2343	2700s	3	49.1	11.51	−9.5
SDSS J0315+2123	2400s	3	55.4	11.35	−49.0
SDSS J0216+3310	2400s	6	41.1	11.68	−40.0
SDSS J1938+4515	2400s	3	67.2	10.80	2.20
SDSS J0043+1948	1800s	6	130.2	9.90	−196.5
SDSS J0648+3231	2400s	3	117.8	9.92	135.5
SDSS J0652+4105	2700s	3	68.0	11.36	98.5
SDSS J0921+5034	2400s	7	50.9	11.75	−130.5
SDSS J1730+4143	2400s	3	58.7	12.03	−133.0
SDSS J1930+6926	2400s	3	40.4	12.33	126.0
SDSS J2319+1917	2700s	3	77.0	11.60	−250.5
SDSS J1953+4222	2400s	3	245.0	9.23	−308.1
SDSS J0643+5934	2700s	3	71.6	11.44	52.2
SDSS J2320+1742	2400s	3	35.7	11.56	289.0
SDSS J0447+5434	2700s	3	50.2	12.11	−293.7
SDSS J1024+4151	2400s	3	49.5	11.83	194.0
SDSS J0024+3203	2400s	3	70.3	11.58	−434.0
SDSS J1933+4524	2700s	3	65.50	11.48	157
SDSS J2256+3951	2400s	6	41.4	11.56	−22.0
SDSS J0022+3212	2400s	3	51.3	12.0	−77.0
SDSS J0646+4127	2400s	3	53.3	11.48	279.0
SDSS J1143+2740	2400s	3	36.8	11.1	52.9
SDSS J1144+2651	2400s	3	40.4	11.3	2.90
SDSS J1608+2811	2700s	3	57.2	10.86	−35.0
SDSS J0013+3141	7200s	3	148.4	11.32	22.0
SDSS J0826+6125	2400s	15	49.0	11.44	−95.6
SDSS J1341+4741	2400s	9	47.0	12.38	−190.5

2.5 Analysis of stellar spectrum/stellar spectroscopy

2.5.1 Stellar atmosphere

It is the outermost layer of a star through which the photons escape into free space. The spectral lines are formed in this region and are of utmost importance for spectroscopy. All the information about the nature and properties of a star could be revealed from a detailed study of the stellar atmospheres.

2.5.1.1 Effective temperature

It is defined as the temperature of a black body emitting an identical amount of radiation as measured for the star. Albeit a close approximation, it helps us to measure the temperature via the well known Stefan-Boltzmann law

$$L = 4\pi R^2 \sigma T_{eff}^4$$

where L is the luminosity of the star, R is radius, σ is the Stefan-Boltzmann constant = 5.6705×10^{-5} erg cm^{-2} K^{-4} s^{-1} and T_{eff} is the effective temperature. Here T_{eff} is the only unknown parameter which can be deduced by measuring radius and luminosity of any star.

The effective temperatures could also be measured using photometric colors and spectroscopic methods as described with examples in the next section.

2.5.1.2 Surface gravity

Surface gravity is analogous to the acceleration encountered by a particle of test mass on the stellar surface. It is usually expressed in a logarithmic scale. It starts decreasing for a star as it moves out of the main sequence to enter the sub-giant and then on to the red giant branch. Higher values of surface gravity indicate the compact nature of the star and higher collision rate in the surface which leads to broadening of the spectral lines. This provides an opportunity to astronomers to measure the surface gravity of a star using the spectrum and measuring the broadening in certain lines which are more sensitive to changes in gravity (e.g. Mg triplet in 5172 Å region). Evolutionary tracks could also be used to measure gravity by determining the position of a star in the HR diagram.

2.5.1.3 Metallicity

Astronomers refer to all elements heavier than H and He as metals. Despite O being the most common element in the universe after H and He, the abundance of Fe is used to determine metallicty of a star. This is because Fe lines are most frequently found in the optical domain and hence could be easily measured to determine the metal abundance with highest degree of precision and accuracy. It is represented by [Fe/H]

2.5.1.4 Micro-turbulent velocity

It is defined as the non-thermal component of velocity of an individual particle on the stellar surface which can cause broadening in the spectral lines. It primarily arises from convection currents close to the surface. Micro-turbulent velocity is usually denoted by the symbol as ξ.

2.5.2 Boltzmann and Saha equations

Radiative and collisional excitations and de-excitations is a regular phenomena in the stellar atmosphere. Thermodynamic equilibrium is said to be attained when the net excitation and de-excitations are in balance, In thermodynamic equilibrium, the no. of atoms in the lower energy level determines the strength of an absorption line. The distribution of the relative no. of atoms in each energy level can be obtained by the well known Boltzmann equation which is given by

$$\frac{n_u}{n_l} = \frac{g_u e^{-\frac{E_u}{kT}}}{g_l e^{-\frac{E_l}{kT}}} = \frac{g_u}{g_l} e^{-\frac{(E_u - E_l)}{kT}}$$

where n_u is the number of atoms per unit volume in a state u
n_l is the number of atoms per unit volume in a state l
E_u is the energy of the level u
E_l is the energy of the level l
k is the Boltzmann constant
T is the gas temperature
g_i is the statistical weight of the energy level i

So, the Boltzmann equation can be employed for a given state of ionization to determine the relative number of atoms in various excitation states as a function of temperature. This can be employed to determine the temperature of stars as the information about the population in different atomic states can be obtained via knowledge from spectral features.

As the frequency of collisions increases in a star more number of atoms tend to get ionized. Equilibrium is attained when the ionization rate is balanced by the rate of recombination, The celebrated Saha's ionization equation governs the relative population of a species in different ionization state under thermodynamic

equilibrium. It is given as

$$\frac{n_{i+1}}{n_i} = \frac{2Z_{i+1}}{n_e Z_i}(\frac{2\pi m_e kT}{h^2})^{\frac{3}{2}} e^{-\frac{\chi_i}{kT}}$$

where χ_i is the ionization energy required for removing the electron from the state i to $i+1$

n_e is the number density of free electrons

Z is the partition function which is the weighted sum of the different ways that an atom or ion distribute its electron among the energy levels. It can be expressed as:

$$Z = \sum_{j=1}^{\infty} g_j e^{-\frac{E_j - E_1}{kT}}$$

Pressure and temperature of an ideal gas can be related as

$$P_e = n_e kT$$

, P_e being the electron pressure. Substituting n_e by P_e in the Saha equation

$$\frac{n_{i+1}}{n_i} P_e = \frac{2Z_{i+1}}{Z_i}(\frac{2\pi m_e}{h^2})^{\frac{3}{2}} (kT)^{\frac{5}{2}} e^{-\frac{\chi_i}{kT}}$$

This could also be expressed in the form

$$log_{10}\frac{n_{i+1}}{n_i} = -0.1761 - log_{10}P_e + log_{10}\frac{Z_{i+1}}{Z_i} + 2.5log_{10}T - \frac{5040}{T}\chi_i$$

T being the ionization temperature, χ_i is the ionization energy and P_e is the electron pressure which is proportional to the gravity ($g^{1/3}$). Thus Saha's ionization equation can be used to measure the surface gravity of a star.

2.5.3 Equivalent width

Equivalent width is the standard term used to indicate the strength of a spectral feature. It represents the width of a box of the same height as the depth of the spectral line and having the same area as that of the spectral line

Mathematically *equivalent width* can be expressed as

$$W_\lambda = \int_{\lambda_1}^{\lambda_2} \frac{F_{\lambda c} - F_\lambda}{F_{\lambda c}}\, d\lambda$$

where $F_{\lambda c}$ represents the flux at the level of continuum and F_λ denotes the flux at the wavelength λ. Depth of a spectral line is given by the quantity $(F_{\lambda c} - F_\lambda)/F_{\lambda c}$

Measurement of the equivalent width of a line leads to the determination of the abundance of the corresponding element using the Curve Of Growth(COG) technique. It is a mathematical relation between equivalent width (W_λ) and abundance which is linear for lower values of equivalent width, Thus weaker lines provide the best estimates of the abundance for a species.

The COG is related to excitation temperature by the formula -

$$log\frac{W_\lambda}{\lambda} = logC + log(gf\lambda) - \frac{5040}{T_{ex}}\chi + log(N) - log(\kappa_c)$$

C is constant for given star and ion, N is the abundance, gf is the statistical weight times the oscillator strength, T_{ex} is the excitation temperature, χ is the excitation potential for the lower level in eV, λ is the wavelength position of the line, κ_c is the continuum opacity at the line position.

2.6 Methodology

The standard methodology for spectroscopy of stars includes reduction of the data, a compilation of line lists, choosing the correct model for stellar atmosphere and then derive the stellar parameters. Describing the reduction of data is beyond the scope of the thesis. In this section, we shall discuss compilation of line lists, stellar modelling and spectrum synthesis. The next section is entirely dedicated to the determination of stellar parameters.

2.6.1 Linelist

Each transition of an atom in the stellar surface corresponds to a line in the spectrum of the star. The probability of formation of a line depends upon the conditions of the star. Thus detecting a line in the spectrum provides a wealth of information about the physical conditions and chemical nature of the photosphere where the transition has taken place. Wavelength, details of the energies of different atomic states and the transition probabilities (also known as oscillator strengths) are the basic parameters to characterize a spectral feature. A line list is the compilation of the precise measurements of these parameters corresponding to every possible transition for all the atoms and molecules present in the stellar spectra. NIST, VALD and KURUCZ database with the updated *gf* values are used in this study.

2.6.2 Modeling stellar atmosphere

For modelling of stellar atmosphere, the assumptions used are -

- Plane parallel geometry holds good as the thickness of the photosphere is usually very small ($\Delta R/R << 1$). However, spherical geometry becomes considerably important for the cool giant stars (Heiter and Eriksson 2006).
- The steady state approximation holds true for the stellar atmospheres.
- It is supposed to be homogeneous as granules, magnetic fields, spots, etc are ignored.
- The energy generated deep below is entirely transferred through the atmospheric layers keeping the energy flux constant at any depth. This could be quantified by,

$$flux = \sigma T_{eff}^4$$

where $\sigma = 5.6704 \times 10^{-5}$ erg cm$^{-2}s^{-1}K^{-4}$.

- There is no relative motion between the layers of the atmosphere in the normal direction. This is important to consider as pressure is entirely assumed to balance the gravity.

2.6.3 Model atmosphere- ATLAS9 models

The tabulated set of data for opacity known Opacity Distribution Functions are employed in the ATLAS9 program (Kurucz 1993) to develop a grid of stellar atmospheric models (Castelli and Kurucz 2004). These models contain 72 These ATLAS9 models have 72 plane parallel layers from $\log\tau_{Ross} = -6.875$ to $+2.00$ at steps of $\Delta\log\tau_{Ross} = 0.125$. Mixing-length convection with l/H_p =1.25 is incorporated for all the models.

2.6.4 Turbospectrum

TURBOSPECTRUM (Plez 2012) is the code used to synthesize stellar spectra (Plez *et al.* 1992, 1993; Alvarez and Plez 1998a). It works by evaluating the continuous opacities and solves for the radiative transfer equations via opacity sampling technique. It can handle the formation of a large number of lines (millions) to determine the spectrum corresponding to the desired model. The calculations for radiative transfer are done based on the input parameters of the model (e.g. temperature, gravity, metallicity and micro-turbulent velocity).

2.7 Derivation of the stellar parameters

Data reduction of the spectrum of individual stars was carried out using the IRAF* echelle package. Recently, a custom data reduction pipeline has been developed by A. Surya (available publicly†) that is more suitable for the crowded and curved orders of the stellar spectra observed with HESP. However, for the study, we use IRAF, and proper care was taken to avoid drift of the spectral tracings blending into adjacent orders.

Radial velocity shifts have been taken into account after the continuum normalization by using the idl routine crosscor.pro where the radial velocity is calculated by cross-correlating the observed spectra with the template synthetic spectra. The template spectrum for an individual star is generated from the approximate stellar parameters from the low resolution fitting of the MARVELS presurvey data using the turbospectrum code for spectral synthesis. The IRAF task **rvcorrect** is also

*IRAF is distributed by the National Optical Astronomy Observatory, which is operated by the Association of Universities for Research in Astronomy (AURA) under cooperative agreement with the National Science Foundation.

†*https* : *//www.iiap.res.in/hesp/*

employed for the heliocentric corrections after measuring the radial velocity shifts in velocity units.

We have measured the equivalent widths of the clean absorption lines present in the spectra and considered only those lines for abundance analysis whose equivalent width is less than 120 mÅ, since they are on the linear part of the curve of growth and are sensitive to the choice of micro-turbulence. Equivalent widths for each spectral line is measured multiple times and the median is adopted to minimize the error in measurement. The adopted equivalent widths for the measured lines are used as the input to the spectral generation codes to determine the abundances corresponding to each line.

Both photometric and spectroscopic data were used to derive estimates of the stellar parameters for the program stars. The effective temperatures were determined using various photometric observations in the literature and the $T_{\rm eff}$-color relations derived by Ramírez and Meléndez (2005). They were found to be in close proximity (a difference of less than 60 K was found) to values obtained using Alonso *et al.* (1996) and Alonso *et al.* (1999). The $V-K$ temperature estimate is expected to be superior, as it is least affected by metallicity and the possible presence of molecular carbon bands. We also employed VOSA (http://svo2.cab.inta-csic.es/), the online SED fitter (Bayo *et al.* 2008), to derive the temperatures using all of the available photometry (optical, 2MASS, and WISE). A Bayesian fit using the Kurucz ODFNEW/NOVER model was used to obtain the SED temperature. Examples for two of the stars are shown in Figure 2.9

Fe lines have been used to determine the ionization balance because of their presence in a large number in the optical domain. The equivalent widths of the Fe lines serve as the input to determine the abundance corresponding to each line depending upon the model. The models are generated large ranges of $T_{\rm eff}$, $log(g)$, [Fe/H] and microturbulent velocity. All the possible combinations of these four

TABLE 2.2: Estimates of Effective Temperature

Method	$T_{\rm eff}$ (K)	
	SDSS J0826+6125	SDSS J1341+4741
$J-K$	4565	5779
$J-H$	4494	5503
$V-K$	4427	5916
SED	4500	5500
Hα	4400	5450
Fe I/Fe II	4300	5400

free parameters are fitted iteratively to obtain the best fit which is adopted as the stellar parameters as described below.

$T_{\rm eff}$ estimates have also been derived spectroscopically, by demanding that there be no trend of Fe I line abundances with excitation potential (shown in the upper panels of Figures 2.6 and 2.7), as well by fitting the H_α profiles as shown for two stars in Figure 2.8. Examples for estimates for the effective temperatures of the two of our target stars are listed in Table 2.2. For most of the stars, we have verified by independently measuring the temperature obtained from fitting of the H_α wings, as it is highly sensitive to small variations in temperature. In cases of asymmetric the H_α profile observed in few stars (e.g. SDSS J0826+6125), it could not be used for accurate measurement of temperature. So, the temperature obtained from Fe I line abundances was adopted.

Surface gravity, $\log(g)$, estimates for the stars have been determined by the usual technique that demands equality of the iron abundances derived for the neutral (Fe I) lines and singly ionized (Fe II) lines. We used as many clean Fe II lines and Fe I lines for each spectrum (e.g. 7 Fe II lines and 82 Fe I lines for SDSS J0826+6125 , and 5 Fe II lines and 49 Fe I lines for SDSS J1341+4741);

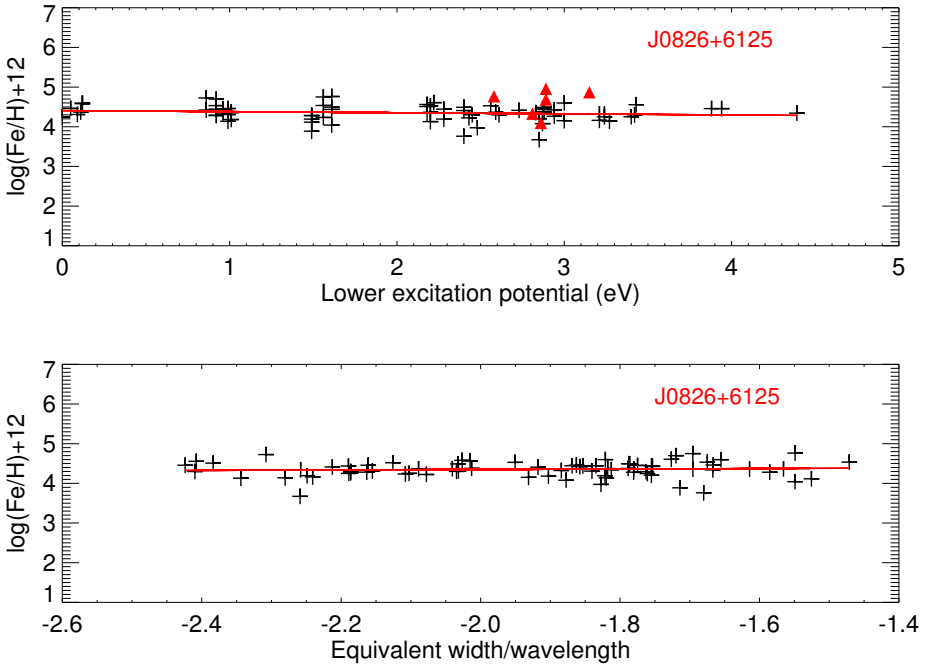

FIGURE 2.6: Top panel: Fe abundances derived from all lines, as a function of the lower excitation potential, for the adopted model for SDSS J0826+6125. Lower panel: Fe abundances, as a function of reduced equivalent widths, for the measured lines.

best-fit models for two of our target stars are shown in the upper panels of Figures 2.6 and 2.7. The wings of the Mg I lines have also been fitted to obtain estimates for log(g) as they are highly sensitive to differences of log(g); best-fit models are shown in Figure 2.10.

The micro-turbulent velocity (ξ) estimates for each star have been derived iteratively in this process, by demanding no trend of Fe I abundances with the reduced equivalent widths, and are plotted in the lower panels of Figures 2.6 and 2.7. The final adopted stellar atmospheric parameters are listed in Table 4.

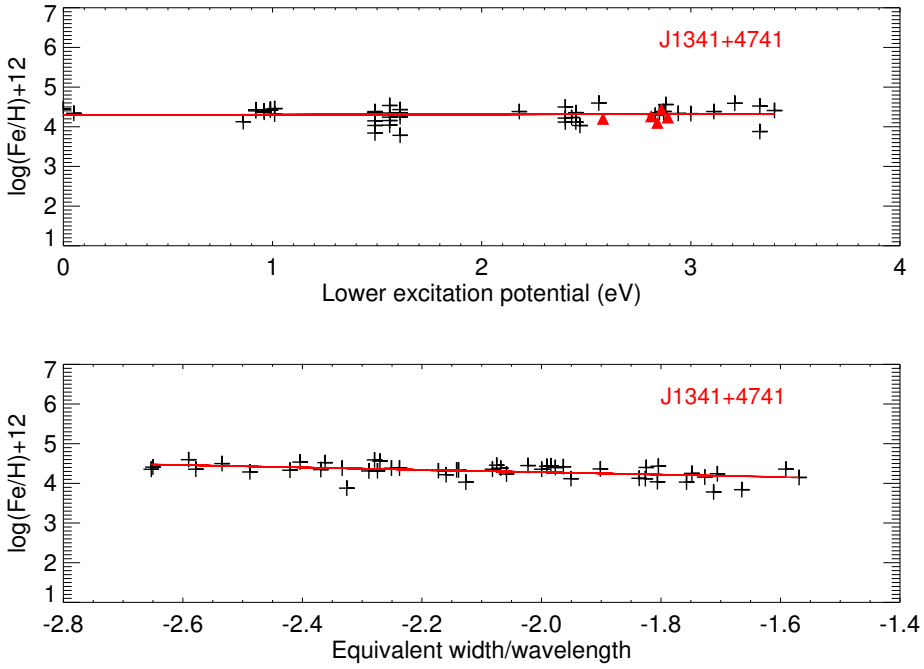

FIGURE 2.7: Top panel: Fe abundances derived from all lines, as a function of the lower excitation potential, for the adopted model for SDSS J1341+4741. Lower panel: Fe abundances, as a function of reduced equivalent widths, for the measured lines.

2.8 Archival data for globular clusters

2.8.1 ESO

Reduced spectroscopic data were obtained from the archives of European Southern Observatory. The observations were carried out through UVES and GIRRAFFE. The spectra were individually normalized using IDL package. We have also generated the model spectra for each star and calculated the abundances of key neutron capture elements like strontium and barium as described in the next paragraph.

The photometric data for NGC 1851 was obtained from ACS survey of globular clusters. The color indices and magnitude were obtained by comparing coordinates of the spectra obtained from ESO with those in the catalogue from ACS

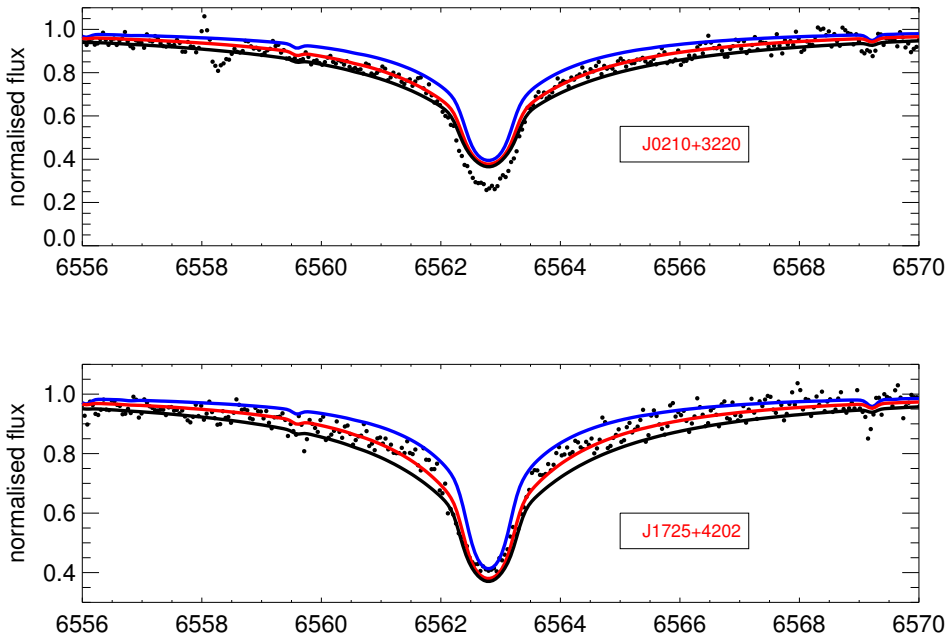

FIGURE 2.8: Estimates of effective temperature for metal poor stars using Hα wings. Example of fitting for two stars are shown here. Red denotes the best fit.

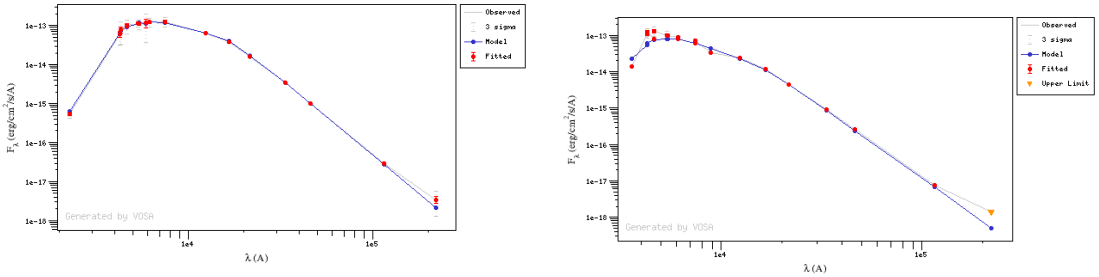

FIGURE 2.9: The SED obtained from VOSA for SDSS J0826+6125 in the left shows the temperature to be ∼4500 K. The SED obtained from VOSA for SDSS J1341+4741 in the right shows the temperature to be ∼5500 K.

survey (Anderson *et al.* 2008). The spectroscopic data (red dots) is over plotted on the photometric data (black dots) for NGC 1851 as shown in the left panel of Figure 2.11. Then, an isochrone with the given cluster age and cluster metallicity is fitted with the data to obtain effective temperature and log g corresponding to each star. For this process the isochrones given by Marigo *et al.* (2008) and Girardi *et al.* (2000) were used. The fit of the data with the isochrone is demonstrated in the right panel of Figure 2.11. The blue dots mark the data set while the green

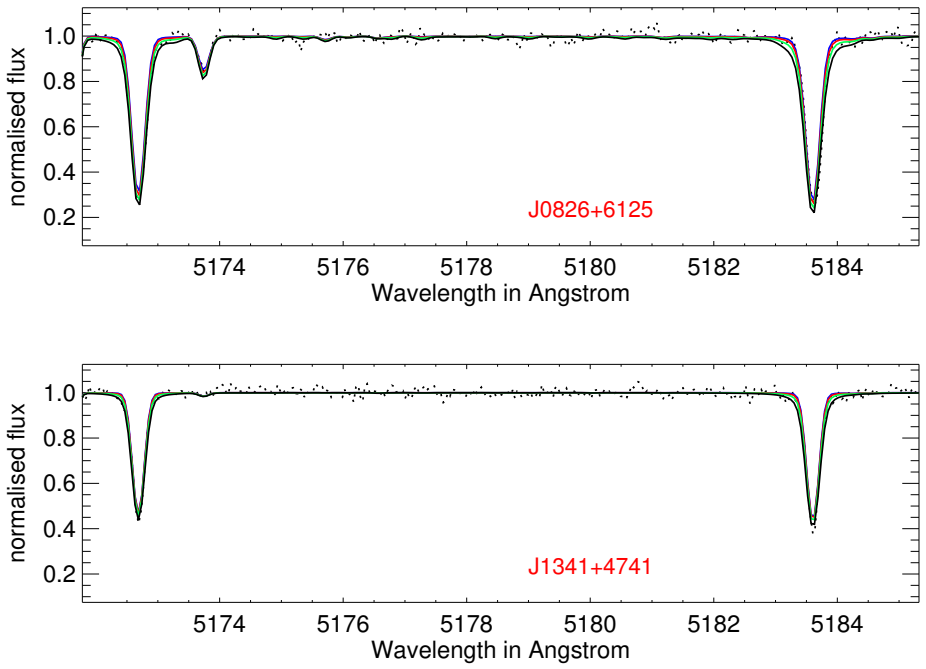

FIGURE 2.10: High-resolution HESP spectra of SDSS J0826+6125 (upper panel) and SDSS J1341+4741 (lower panel) in the region of the Mg I triplet for different values of $\log(g)$, in steps of 0.25 dex. The red solid line indicates the best-fit synthetic spectrum.

dots are the isochrones. These stellar parameters are the free parameters required to generate the model spectra.

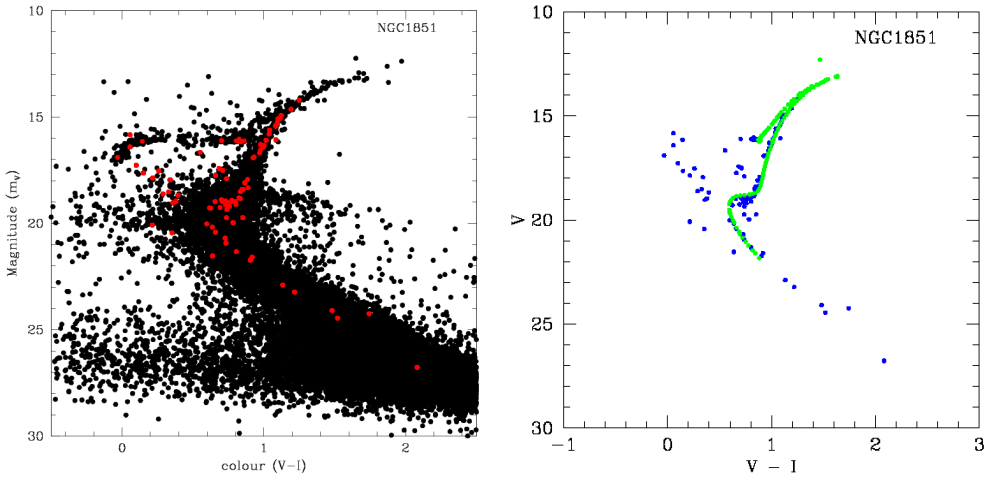

FIGURE 2.11: The spectroscopic data for NGC 1851 from GIRAFFE marked in red overlaid on the data from ACS survey marked in black dots is shown in the left. The isochrone fitting to derive the temperature and gravity is shown in the right

We have used the models based on ATLAS-9 opacity distribution functions given by kurucz. It is a computer program to calculate model stellar atmospheres in radiative and convective equilibrium for the complete range of stellar temperatures with the plane parallel and horizontally homogeneous approximations. The codes are written in Fortran IV. So, after obtaining the stellar parameters, we generated a model spectra corresponding to each star covering the wavelength region as in the UVES/GIRAFFE spectrum. We ran the process iteratively with different abundance values of the different lines of Sr and Ba until the best fit is obtained. Some of the examples of best fit spectra will be discussed in Chapter 5.

2.8.2 SDSS

Spectroscopic data obtained from the Sloan Digital Sky Survey (SDSS) has been used. The stellar parameters have been derived using the color indices and magnitudes from SDSS. A grid for working with the SDSS data and finding abundances of key elements is also generated. The grid generated models for temperatures from 4000k to 7000k in steps of 200k, log g from 0 to 5.0 in steps of 0.50, [Fe/H] from 0.0 to -2.50 in steps of 0.50 and [Ba,Sr/Fe] from -4.0 to 4.0 in steps of 0.50 so as to span the entire globular cluster range for all given parameters. We have used the models based on ATLAS-9 opacity distribution functions given by kurucz. So, after obtaining the stellar parameters, a template spectrum was used to cross-correlate with the observed spectrum to find the radial velocity which is re-checked for accuracy. Method of interpolation is used to produce the model for each input stellar parameter from SDSS data and a chi-square fit was carried out to obtain the minima of [Ba,Sr/Fe] fits and is adopted as the abundance corresponding to the star. This grid was run for four globular clusters in the domain of lower metallicity and the relevant abundances were obtained.

Chapter 3

Abundance analysis of new bright EMP and CEMP stars[†]

3.1 Introduction

After the Big Bang, cosmic primordial gas consisted mostly of H, He, and a small proportion of the very light element Li. The heavier elements were synthesized during the evolution and explosion of the first (likely very massive) stars, which were free of heavy metals. These first supernovae had a considerable dynamical, thermal, and chemical impact on the evolution of the surrounding interstellar medium, including mini-halos that can be some distance away from the location of the first star explosion (Cooke and Madau 2014; Smith *et al.* 2015). Stars (and the galaxies to which they belong) that formed thereafter are expected to carry the imprints of the nucleosynthesis events from these Population III stars (Beers and Christlieb 2005; Frebel and Norris 2015a; Sharma *et al.* 2017). Hence, identifying

[†]Results of this chapter are published in Bandyopadhyay *et al.* (2018)

and analyzing early generations of stars is of crucial importance to advance our understanding of this epoch.

Extremely metal-poor (EMP; [Fe/H] < -3.0) stars of the Galactic halo are thought to be the immediate successors of the first stars, and were likely to have formed when the Universe was only a few hundred million years old (see, e.g. Bromm *et al.* 2009). Studies of such stars, sometimes referred to as "near-field cosmology" have greatly benefited from the large spectroscopic surveys that were carried out in the past in order to identify them in significant numbers, such as the HK survey of Beers and collaborators (Beers *et al.* 1985, 1992) and the Hamburg/ESO Survey of Christlieb and colleagues (Christlieb 2003). More recent surveys, such as SDSS, RAVE, APOGEE and LAMOST continue to expand the known members of this rare class of stars (e.g., Fulbright *et al.* 2010; Ivezić *et al.* 2012; Aoki *et al.* 2013; Zhao *et al.* 2012; García Pérez *et al.* 2013; Anders *et al.* 2014; Li *et al.* 2015).

High-resolution spectroscopic studies of metal-poor Galactic halo stars have demonstrated diversity in their chemical compositions. For example, on the order of 15-20% of stars with [Fe/H] < -2.0 exhibit large enhancements in their carbon-to-iron ratios ([C/Fe] $> +0.7$; Aoki *et al.* 2007; Lee *et al.* 2013, 2017). As shown by numerous studies, the frequency of carbon-enhanced metal-poor (CEMP) stars continues to increase with decreasing [Fe/H]. The fractions of CEMP stars also increase with distance from the Galactic plane (Frebel *et al.* 2006; Beers *et al.* 2017), and also between the inner-halo and the outer-halo regions (Lee *et al.* 2017).

CEMP stars can be separated into four sub-classes (Beers and Christlieb 2005): i) CEMP-s stars, which show enhancements of s-process elements, ii) CEMP-r stars, which exhibit enhancements of r-process elements, iii) CEMP-r/s stars,

which show enhancements in both r- and s-process elements*, and iv) CEMP-no stars, which exhibit no neutron-capture element enhancements. Long-term radial-velocity monitoring studies have shown that most (>80 %, possibly all) CEMP-s stars are members of binary systems involving a (now extinct) asymptotic giant branch (AGB) star that transferred carbon and s-process rich material to the presently observed (lower-mass) star (Lucatello *et al.* 2005; Starkenburg *et al.* 2014; Hansen *et al.* 2016a), while CEMP-no stars exhibit observed binary frequencies typical of non-carbon-enhanced halo giants, $\sim$ 18% (Starkenburg *et al.* 2014; Hansen *et al.* 2016b).

Yoon *et al.* (2016) have considered the rich morphology of the absolute abundance of carbon A(C)= $log(C)$ as a function of [Fe/H], based on high-resolution analyses of a large sample of CEMP stars (their Figure 1, the Yoon-Beers diagram). In addition to their Group I stars, which are dominated by CEMP-s stars, they demonstrate that the CEMP-no stars not only exhibit substantially lower A(C), but bifurcate into two apparently different regions of the diagram, which they refer to as Group II and Group III stars. This behaviour immediately suggests that these groups might be associated with different progenitors responsible for the carbon production, a suggestion borne out by the modelling carried out by Placco *et al.* (2016), and/or on the nature of the mini-halo environment in which these stars formed. Multiple models for the production of CEMP-no stars have been considered in the literature, such as the "spinstar" models (e.g., Meynet *et al.* 2006, 2010; Chiappini 2013), and the "mixing and fallback" models for faint SNe (e.g., Umeda and Nomoto 2003, 2005; Nomoto *et al.* 2013; Tominaga *et al.* 2014). Both processes may well play a role (Maeder and Meynet 2015; Choplin *et al.* 2016).

Regardless of the complexity of the situation, additional detailed observations of

*Hampel *et al.* (2016) suggest that the observed heavy element patterns of these stars are well accounted for by an "intermediate neutron-capture process," (as first suggested by Cowan and Rose (1977)) and should be referred to henceforth as CEMP-i stars.

EMP stars with and without clear carbon enhancement, such as those carried out here, are required for progress in understanding.

In this chapter, we discuss the detailed analysis of one EMP, two CEMP-no and two CEMP-s stars from the HESP-GOMPA survey. The chapter is outlined as follows. In Section 2 we describe our high-resolution observations. Consideration of possible radial-velocity variations for the two targets which could be observed over several epochs is presented in Section 2. Section 3 summarizes our estimates of stellar atmospheric parameters and describes our abundance analyses. Results of the abundance analysis are reported in Section 4. We present a discussion of our results with a comparative study of CEMP-no and EMP stars in Section 5, along with a brief conclusion in Section 6.

3.2 RADIAL VELOCITIES

Radial velocities (RVs) were calculated for SDSS J0826+6125 based on six epochs of observations spread over a period of 12 months. For SDSS J1341+4741 , we obtained five observations spread over six months. A cross-correlation the analysis was performed with a synthetic template spectrum suitable for each star to obtain the RV measurement for each spectrum. We made use of the software package RVLIN provided by Wright and Howard (2009), which is a set of IDL routines used to fit Keplerian orbits to derive the orbital parameters from the RV data. The RV measurements exhibit peak-to-peak variations of $\sim$ 60 km s^{-1}, with a period of 180 days for SDSS J0826+6125 , and $\sim$ 110 km s^{-1}, with a period of 116 days for SDSS J1341+4741 . The best-fit orbits for these stars, based on the data in hand, are shown in Figure 3.1. Although the existence of RV variations is secure, with such sparse coverage of the proposed orbits more data are required to confirm the periods.

TABLE 3.1: Observation log and radial velocities for SDSS J0826+6125

Date	MJD	λ Coverage (Å)	SNR	Radial Velocity (km sec^{-1})
2015-11-03	57330.20903	3600-10800	51	−110.4
2015-11-29	57356.36042	3600-10800	49	−95.6
2015-12-22	57379.10417	3600-10800	47	−80.3
2016-01-27	57415.09792	3600-10800	47	−52.3
2016-10-20	57682.21667	3600-10800	50	−108.9
2016-11-16	57709.13542	3600-10800	51	−104.1

TABLE 3.2: Observation log and radial velocities for SDSS J1341+4741

Date	MJD	λ Coverage (Å)	SNR	Radial Velocity (km sec^{-1})
2016-27-01	57415.24722	3600-10800	43	−240.1
2016-24-04	57503.18819	3600-1080	49	−190.5
2016-26-04	57505.06458	3600-1080	47	−192.1
2016-24-06	57564.02361	3600-1080	48	−176.2
2016-25-06	57565.20139	3600-1080	47	−174.5

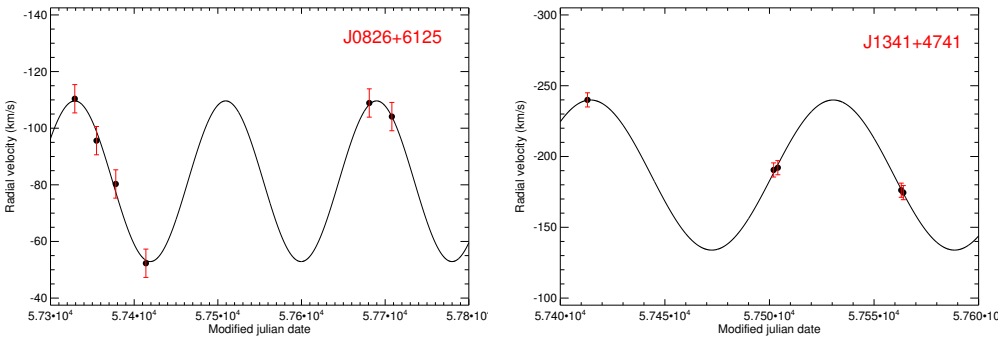

FIGURE 3.1: Variation of radial velocity for SDSS J0826+6125 is shown on the left. The derived period is of 180.4 days. Variation of radial velocity for SDSS J1341+4741 is shown on the right. The derived period is 116.0 days.

TABLE 3.3: Adopted Stellar Parameters

Object	T_{eff} (K)	log(g)	ξ	[Fe/H]
SDSS J0826+6125	4300	0.40	1.80	−3.10
SDSS J1341+4741	5450	2.50	1.80	−3.20
SDSS J0013+3141	4400	1.00	1.90	−2.30
SDSS J1953+4222	6000	4.00	1.75	−2.25
SDSS J1350+4819	5100	2.50	1.20	−3.00

3.3 STELLAR PARAMETERS

The adopted stellar parameters are tabulated in table 3.3.

3.3.1 Abundance Analysis

To determine the abundance estimates for the various elements present in our target stars we have employed one dimensional LTE stellar atmospheric models (ATLAS9; Castelli and Kurucz 2004) and the spectral synthesis code turbo-spectrum (Alvarez and Plez 1998b). We measured the equivalent widths of the absorption lines present in the spectra and considered only those lines for abundance analysis whose equivalent width is less than 120 mÅ, since they are on the linear part of the curve of growth, and are relatively sensitive to the choice of microturbulence. We have adopted the solar abundances for each element from Asplund *et al.* (2009); Scott *et al.* (2015a,b); Grevesse *et al.* (2015); solar isotopic fractions were used for all the elements. Version 12 of the turbo-spectrum code for spectrum synthesis and abundance estimates have been used for the analysis. We have adopted the hyperfine splitting provided by McWilliam (1998) and solar isotopic ratios. The total broadening including instrumental broadening was estimated by convolving with a Gaussian for the resolution(R 30000 and R=60000) of HESP. We have

measured FWHM of telluric and Th-Ar lines to broaden the synthetic spectra using Gaussian profile. We have also used 2D MARCS models (Gustafsson *et al.* 2008) to derive the abundances, but no significant deviations were obtained. The abundances differed by values ranging from 0.01 to 0.02 dex for individual species.

We have used the Chi-square minimization technique and taken the fit with the minimum residue as the best. The sum over the line width was taken as the error in the theoretical the equivalent widths. The error in abundance was calculated using this error in equivalent width.

3.4 Abundances

3.4.1 Carbon, Nitrogen, and Oxygen

Carbon-abundance estimates for our stars were derived by iteratively fitting the CH bandhead region with synthetic spectra, and adopting the value that yields the best match. We have used the CH molecular line list compiled by Bertrand Plez (Plez and Cohen 2005). The CN and CH molecular linelists are taken from the Kurucz database.

For the EMP star SDSS J0826+6125 , fits to the CH *G*-band yielded a value of [C/Fe] = −0.82 The oxygen line at 630 nm is too weak to be detected, hence meaningful O abundance could be derived only for SDSS J0826+6125 and SDSS J001331.76+314144.10 . We could, however, detect the bandhead in the region of the CN band at 3884, Å, and obtain an enhancement in nitrogen corresponding to a value of [N/Fe] = +1.27 for SDSS J0826+6125 .

TABLE 3.4: Elemental Abundance Determinations for SDSS J0826+6125 .

Elements	Species	N_{lines}	A(X)	Solar	[X/H]	[X/Fe]	σ
C	CH	...	4.60	8.43	−3.92	−0.82	synth
N	CN	...	6.00	7.83	−1.83	1.27	synth
O	O I	...	6.50	8.69	−2.19	0.91	synth
Na	Na I	2	3.30	6.24	−2.94	0.16	synth
Mg	Mg I	4	5.05	7.60	−2.53	0.57	synth
Al	Al I	1	3.40	6.45	−3.05	0.05	synth
Ca	Ca I	8	3.68	6.34	−2.66	0.44	0.06
Sc	Sc II	5	−0.06	3.15	−3.21	−0.11	synth
Ti	Ti I	7	1.96	4.95	−2.99	0.11	0.03
	Ti II	6	2.06	4.95	−2.89	0.21	0.04
Cr	Cr I	3	2.10	5.64	−3.54	−0.44	0.05
	Cr II	2	2.35	5.64	−3.29	−0.19	0.05
Mn	Mn I	4	1.60	5.43	−3.83	−0.73	synth
Co	Co I	2	2.00	4.99	−2.99	0.11	synth
Ni	Ni I	3	3.00	6.22	−3.22	−0.12	0.04
Zn	Zn I	2	1.50	4.56	−2.96	0.14	0.05
Sr	Sr II	2	−0.90	2.87	−3.77	−0.67	synth
Y	Y II	1	−1.47	2.21	−3.68	−0.58	synth
Zr	Zr II	2	−0.75	2.58	−3.33	−0.23	synth
Ba	Ba II	2	−1.80	2.18	−3.98	−0.88	synth

σ indicates the random error.

TABLE 3.5: Elemental Abundance Determinations for SDSS J1341+4741 .

Elements	Species	N_{lines}	A(X)	Solar	[X/H]	[X/Fe]	σ
Li	Li I	1	1.95	...	...	...	synth
C	CH	...	6.22	8.43	−2.21	0.99	synth
Na	Na I	2	2.80	6.24	−3.44	−0.24	synth
Mg	Mg I	5	5.10	7.60	−2.50	0.70	synth
Al	Al I	1	3.2	6.45	−3.25	−0.05	synth
Si	Si I	1	5.33	7.51	−2.18	1.02	0.07
Ca	Ca I	11	3.60	6.34	−2.74	0.46	0.05
Sc	Sc II	3	−0.1	3.15	−3.25	−0.05	synth
Ti	Ti I	4	2.23	4.95	−2.72	0.48	0.05
	Ti II	13	1.89	4.95	−3.06	0.19	0.04
Cr	Cr I	6	2.31	5.64	−3.33	−0.13	0.04
	Cr II	1	2.77	5.64	−2.87	0.33	0.06
Mn	Mn I	5	1.89	5.43	−3.54	−0.34	0.05
Co	Co I	2	1.99	4.99	−3.00	0.20	0.05
Ni	Ni I	4	3.35	6.22	−2.87	0.33	0.04
Sr	Sr II	2	−0.88	2.87	−3.75	−0.55	synth
Ba	Ba II	2	−1.68	2.18	−3.86	−0.66	synth

σ indicates the random error. Values obtained after applying NLTE corrections.

For all the CEMP stars, the derived fit to the CH *G*-band yielded [C/Fe] > 0.65 showing the enhancement in C. The signal-to-noise ratio at the region of CN band at 3884 AA is too low to confirm enhancement in nitrogen for most of the stars; so we could only obtain an upper limit of [N/Fe] < +2.37 for SDSS J1341+4741 and no meaningful values could be derived for SDSS J1953+4722 and SDSS J1350+4819 . However, SDSS J001331.76+314144.10 was found to be deficient in N abundances with [N/Fe]= -1.53. O abundances for SDSS J001331.76+314144.10 could also be measured from the lines at 6300,Å and 6363,Å after the telluric corrections and was obtained to be [O/Fe]=0.61.

TABLE 3.6: Elemental Abundance Determinations for SDSS J001331.76+314144.10 .

Elements	Species	N_{lines}	A(X)	Solar	[X/H]	[X/Fe]	σ
C	CH		7.0	8.43	−1.43	0.87	synth
N	CN		4.0	7.83	−3.83	−1.53	synth
O	OI	1	7.0	8.69	−1.69	0.61	synth
Na	Na I	2	4.5	6.24	−1.72	0.58	synth
Mg	Mg I	5	5.40	7.60	−2.20	0.10	synth
Al	Al I	1	2.7	6.45	−3.35	−1.05	
Si	Si I	2	5.50	7.51	−2.01	0.29	synth
Ca	Ca I	11	4.40	6.34	−1.94	0.36	
Sc	Sc II	3	0.95	3.15	−2.20	0.10	
Ti	Ti I	4	3.3	4.95	−1.65	0.65	
	Ti II	13	3.15	4.95	−1.80	0.50	
V	V I	2	1.50	3.93	−2.43	−0.13	synth
Cr	Cr I	6	3.10	5.64	−2.54	−0.24	
	Cr II	1	3.5	5.64	−2.14	0.16	
Mn	Mn I	5	2.80	5.43	−2.63	−0.33	
Co	Co I	2	2.70	4.99	−2.29	0.01	
Ni	Ni I	4	3.9	6.22	−2.32	0.02	synth
Cu	Cu I	2	1.25	4.19	−2.94	−0.64	synth
Zn	Zn I	1	2.50	4.56	−2.06	0.24	synth
Sr	Sr II	2	1.75	2.87	−1.12	1.18	synth
Y	Y II	2	−0.25	2.21	−2.46	−0.16	synth
Zr	Zr II	3	0.50	2.58	−2.08	0.22	synth
Ba	Ba II	2	1.5	2.18	−-0.68	1.62	synth
Ce	Ce II	3	−0.50	1.58	−2.08	0.22	synth
Nd	Nd II	2	−0.50	1.42	−1.92	0.38	synth
Sm	Sm II	2	−0.75	0.96	−1.71	0.59	synth
Eu	Eu II	1	−1.0	0.52	−1.52	0.78	synth
Dy	Dy II	2	−0.50	1.10	−1.60	0.70	synth

σ indicates random error.

TABLE 3.7: Elemental Abundance Determinations for SDSS J1953+4722 .

Elements	Species	N_{lines}	A(X)	Solar	[X/H]	[X/Fe]	σ
Li	Li I	1	2.00	...	...	...	synth
C	CH	...	7.00	8.43	−1.43	0.82	synth
Na	Na I	2	4.50	6.24	−1.74	0.51	synth
Mg	Mg I	5	5.80	7.60	−1.80	0.45	synth
Al	Al I	1	3.12	6.45	−3.33	−1.08	synth
Ca	Ca I	11	4.60	6.34	−1.74	0.51	0.07
Sc	Sc II	3	1.30	3.15	−1.85	0.40	synth
Ti	Ti I	4	3.00	4.95	−1.95	0.30	0.12
	Ti II	13	2.93	4.95	−2.02	0.23	0.08
Cr	Cr I	6	3.50	5.64	−2.14	0.11	0.08
	Cr II	1	3.67	5.64	−1.97	0.28	0.09
Mn	Mn I	5	3.05	5.43	−2.38	−0.13	0.05
Co	Co I	2	2.90	4.99	−2.09	0.16	0.07
Ni	Ni I	4	4.25	6.22	−1.97	0.28	0.12
Sr	Sr II	2	1.00	2.87	−1.87	0.38	synth
Zr	Zr II	2	1.07	2.58	−1.51	0.74	synth
Ba	Ba II	2	0.55	2.18	−1.63	0.62	synth

σ indicates the random error.

Fits for in the region of the CH G-band are shown for two of the stars, SDSS J0826+6125 and SDSS J1341+4741 in Figure 3.2

3.4.2 The α-Elements

Several magnesium lines were detected in the spectra of our target stars. Two of the lines in the Mg triplet at 5172 Å, and three other lines at 4167 Å, 4702 Å, and 5528 Å were used to obtain the abundances. The derived [Mg/Fe] ratios

TABLE 3.8: Elemental Abundance Determinations for SDSS J1350+4819 .

Elements	Species	N_{lines}	A(X)	Solar	[X/H]	[X/Fe]	σ
C	CH	...	6.10	8.43	−2.33	0.67	synth
Na	Na I	2	3.75	6.24	−2.49	0.51	synth
Mg	Mg I	5	5.17	7.60	−2.43	0.57	synth
Ca	Ca I	11	3.70	6.34	−2.64	0.36	0.05
Sc	Sc II	3	0.25	3.15	−2.90	−0.10	synth
Ti	Ti I	4	2.23	4.95	−2.72	0.28	0.09
	Ti II	13	2.00	4.95	−2.95	0.05	0.07
Cr	Cr I	6	2.18	5.64	−3.46	−0.46	0.10
Mn	Mn I	5	2.07	5.43	−3.36	−0.36	0.13
Co	Co I	2	2.37	4.99	−2.62	0.38	0.07
Ni	Ni I	4	3.45	6.22	−2.77	0.23	0.09
Sr	Sr II	2	0.00	2.87	−2.87	0.13	synth
Ba	Ba II	2	−0.50	2.18	−2.68	0.32	synth

σ indicates the random error.

were enhanced and consistent with the values often found among halo stars. The silicon lines at 5268 Å and 6237 Å were too weak to be used for abundance estimates of SDSS J0826+6125 , SDSS J1350+4819 and SDSS J1953+4722 but for SDSS J1341+4741 and SDSS J001331.76+314144.10 , we obtain [Si/Fe] = +1.0 and [Si/Fe]=0.29. It should be noted that Si may appear over-abundant for metal-poor stars because LTE results are known to overestimate the true value (Shi *et al.* 2012).

Several clean Ca I lines were detected in the spectra of all the stars were used to measure the abundance which includes the prominent lines at 4226.73 Å, 4302.53 Å, and 4454.78 Å. The measurements indicate slightly enhanced [Ca/Fe] ratios as given in the respective abundance table for each star. The overall abundance of the α-elements are consistent with the typical halo enhancement of $[\alpha/\mathrm{Fe}] = +0.4$.

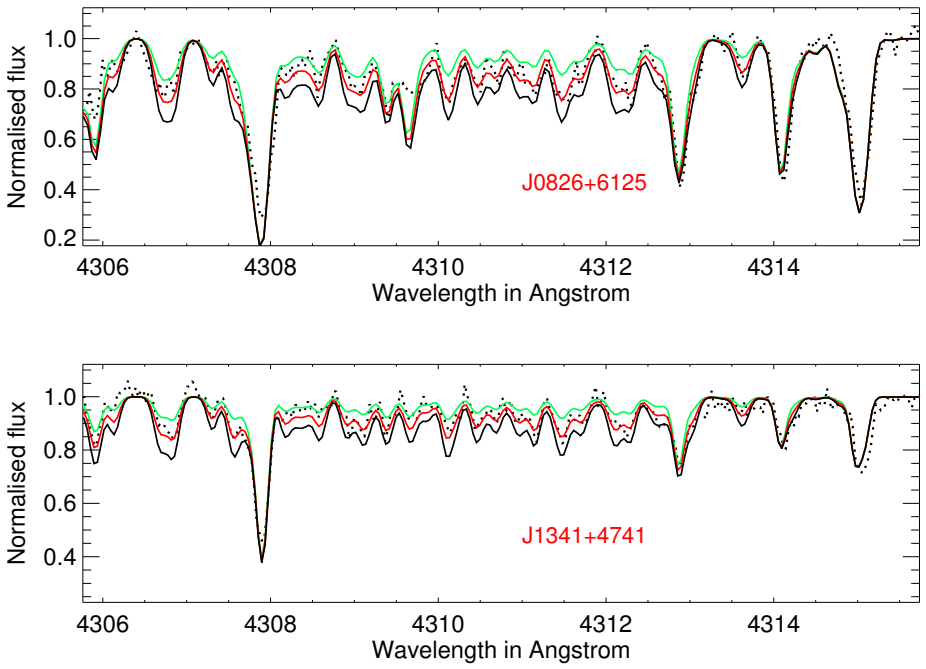

FIGURE 3.2: High-resolution HESP spectra in the CH $G-$band region for SDSS J0826+6125 (upper panel) and SDSS J1341+4741 (lower panel). The red solid line indicates the synthetic spectrum corresponding to the best fit, overplotted with two synthetic spectra with carbon 0.20 dex higher and lower than the adopted value.

3.4.3 The Odd-Z Elements

The sodium abundance is determined from the Na D_1 and D_2 resonance lines at 5890 Å and 5896 Å. The aluminium abundance is obtained from one of the resonance lines at 3961.5 Å. This line is not the ideal indicator, as it can have large departures from LTE, as discussed by Baumueller and Gehren (1997), who found it to be as large as +0.6 dex. Gratton *et al.* (2001) showed that incorporation of these corrections improves the agreement between the values of aluminium abundances obtained from this line and the high-excitation infrared doublet at 8773 Å in the case of globular cluster dwarfs. Hence, we have applied this non-LTE correction to Al in our abundance table. Aluminium is slightly enhanced for some of the stars SDSS J0826+6125 , while Na tracks the iron content of the stars. The scandanium content is also very similar to iron. Na and Al are produced by the Ne-Na and

Mg-Al cycles in intermediate and massive stars during H-shell burning. Sodium and aluminium in the two stars could be due to a well-mixed ISM, and unlikely to have received a direct contribution from intermediate-mass or massive-star winds.

3.4.4 The Iron-Peak Elements

Iron abundances for SDSS J0826+6125 were calculated using clean Fe I lines and Fe II lines found in the spectra; a maximum difference of 0.40 dex was noted between the derived abundances. This difference between Fe I and Fe II is in agreement with the NLTE effects explored by Asplund (2005).

We also detected the iron-peak elements Mn, Cr, Co, Ni, and Zn in our target stars. Mn and Cr are products of incomplete explosive silicon burning, and their abundances decrease with decreasing metallicity (McWilliam *et al.* 1995; Ryan *et al.* 1996; Carretta *et al.* 2002). The abundance of Mn was derived from the resonance Mn triplet at 4030 Å, 3823 Å and three weaker lines near 4780 Å. Cr lines are measured from 4 lines, including the stronger ones at 4646 Å and 5206 Å. Products of complete silicon burning such as Co, Ni, and Zn have also been detected in most of the stars and all of these elements are found to track the iron content. The observed abundances of Mn and Cr are similar to other stars of similar metallicity.

For SDSS J1341+4741 , the abundance of Mn was derived from the resonance Mn triplet at 4030 Å and an additional line at 3823 Å. The abundance derived for Ni using the 4 lines of this element present in the spectrum of SDSS J1341+4741 is clearly higher relative to iron, [Ni/Fe] = +0.33.

3.4.5 The Neutron-Capture Elements

Strontium and barium are the two neutron-capture elements detected in all the stars. Resonance lines of Sr II at 4077 Å and 4215 Å were used to measure the Sr abundance. Ba II resonance lines at 4554 Å and 4937 Å were used to determine the Ba abundances. The EMP star SDSS J0826+6125 is found to be under-abundant in both strontium and barium, with abundances of [Sr/Fe] = −0.67 and [Ba/Fe] = −0.88, respectively. The other neutron-capture elements found in this star are Y and Zr, which are under-abundant as well. The stars SDSS J1341+4741 and SDSS J1350+4819 are also found to be under-abundant in both strontium and barium with enhanced abundances for carbon. Based on the clear under-abundance of the neutron-capture elements, along with the elevated carbon abundance, these stars can be classified as a CEMP-no star following Beers and Christlieb (2005).

Best-fit spectra of the Sr and Ba syntheses for two of the stars are shown in Figures 3.3 and 3.4 with (SDSS J082625.70+612515.10) at the upper panel and (SDSS J134144.60+474128.90) at the lower panel.

3.4.6 Lithium

A strong feature of Li could be obtained in SDSS J1953+4722 and SDSS J1341+4741 at 6707 Å, the Li doublet, from which we obtain an abundance A(Li) = 2.00 and A(Li) = 1.95 respectively. The measurement of Li in SDSS J1341+4741 is similar to some other CEMP-no stars (e.g , Sivarani *et al.* 2006; Matsuno *et al.* 2017) but the Li abundance of SDSS J1953+4722 is comparatively higher than a typical CEMP-s star. The synthesis for this element is shown in Figure 3.5.

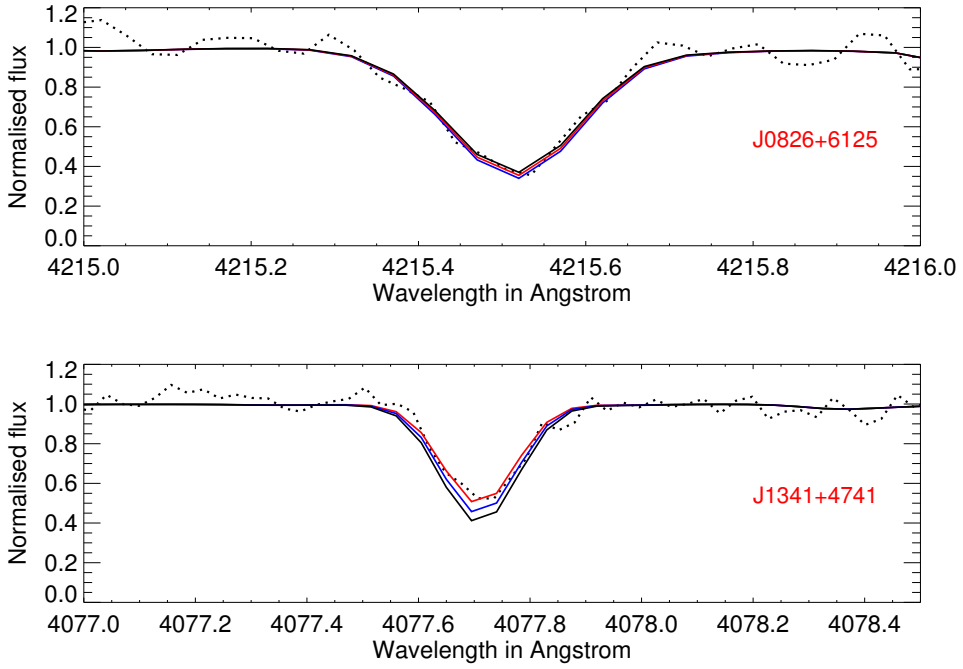

FIGURE 3.3: Synthesis in the Sr II region for SDSS J0826+6125(upper panel) and SDSS J1341+4741(lower panel). The red line indicates the best-fit, over-plotted with two synthetic spectra with Sr abundance 0.20 dex higher and lower than the adopted value.

3.5 Discussion

3.5.1 EMP stars

3.5.1.1 Carbon, Nitrogen, and the Non-detection of Lithium

In the *First Stars VI* paper, Spite *et al.* (2005) carbon and nitrogen was found to be anti-correlated, and the faint halo stars could be classified into two groups – "unmixed" stars, which exhibited C enhancement with N depletion, having A(Li) between 0.2 and 1.2, and "mixed" stars, which showed [C/Fe] < 0.0, [N/Fe] $> +0.5$, and Li below the detection threshold. SDSS J0826+6125 clearly falls into the second group. Li is a very fragile element which is destroyed at temperatures in

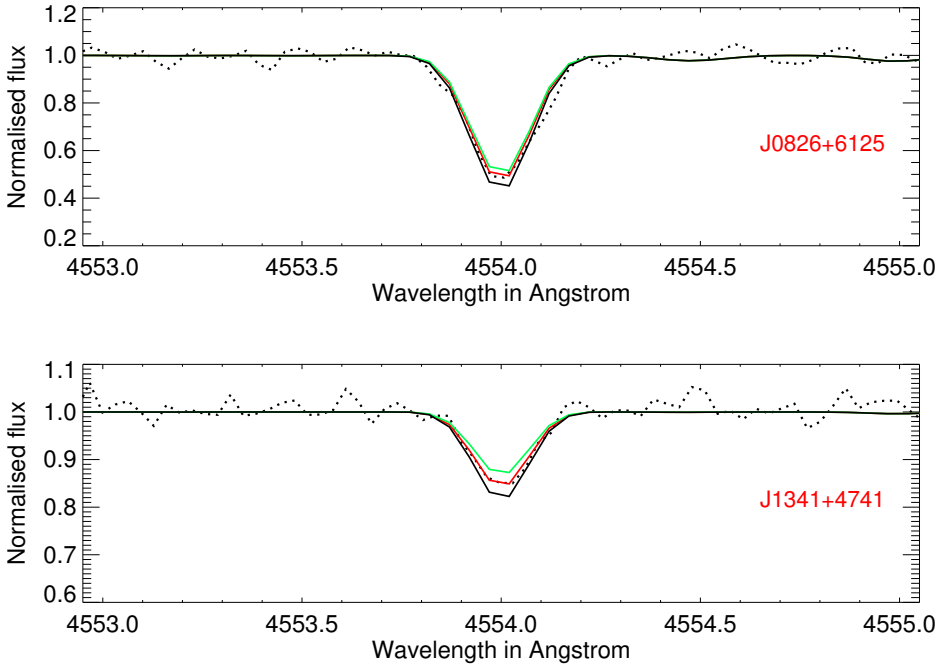

FIGURE 3.4: Synthesis in the Ba II region for SDSS J0826+6125 (upper panel) and SDSS J1341+4741(lower panel). The red line indicates the best-fit, over-plotted with two synthetic spectra with Ba abundance 0.20 dex higher and lower than the adopted value.

excess of 2.5 million Kelvin. Evidence for this can be seen in previous samples of metal-poor stars; the $A(\mathrm{Li}) = 2.3$ observed for metal-poor dwarfs starts decreasing as the star ascends the giant branch, to $A(\mathrm{Li}) < 1.2$ for giants (*First Stars VII*; Bonifacio *et al.* 2007b). The non-detection of lithium for this star could be understood in this way.

In *First Stars IX*, Spite *et al.* (2006) argued that such destruction could be taken as a signature of mixing, and placed this mixed group of stars higher up in the giant branch stage of evolution. Other scenarios for the depletion of lithium, such as binary mass transfer, can be eliminated for SDSS J0826+6125 , as no such peculiar chemical imprints have been found. During mixing, material from deeper layers where carbon is converted to nitrogen is brought to the stellar surface. Figure 4 of Cayrel *et al.* (2004) shows the decline in the value of [C/Fe] for temperatures below 4800 K in metal-poor stars, which is again attributed to deep mixing at lower

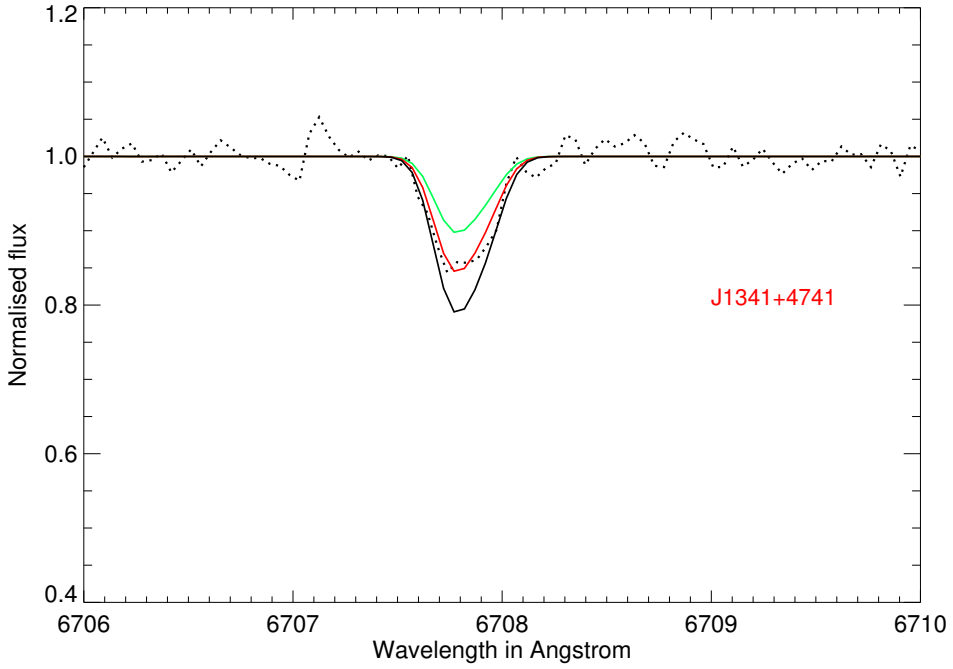

FIGURE 3.5: Synthesis of Lithium for SDSS J1341+4741 at 6707 Å. The red line indicates the best-fit, overplotted with two synthetic spectra with Li abundance 0.20 dex higher and lower than the adopted value of A(Li)=1.95.

temperatures. With a $T_{\rm eff}$ of 4300 K and a low $\log(g) = 0.4$, SDSS J0826+6125 can be placed in the mixed group of stars close to the tip of the red giant branch (RGB).The left panel of Figure 3.6 shows the position of the star in $\log(g)$-$T_{\rm eff}$ plane compared with other metal-poor halo stars compiled in the SAGA database (Suda *et al.* 2008). The right panel in Figure 3.6 compares the [C/N] ratio with metallicity of the halo stars having carbon deficiency (for which both estimates of carbon and nitrogen are available).

3.5.1.2 The Light Elements

SDSS J0826+6125 exhibits a low Na, high Mg, and low Al content, consistent with the odd-even pattern expected to occur during massive-star nucleosynthesis at low metallicities. A slight enhancement of Na is observed, which could be an imprint

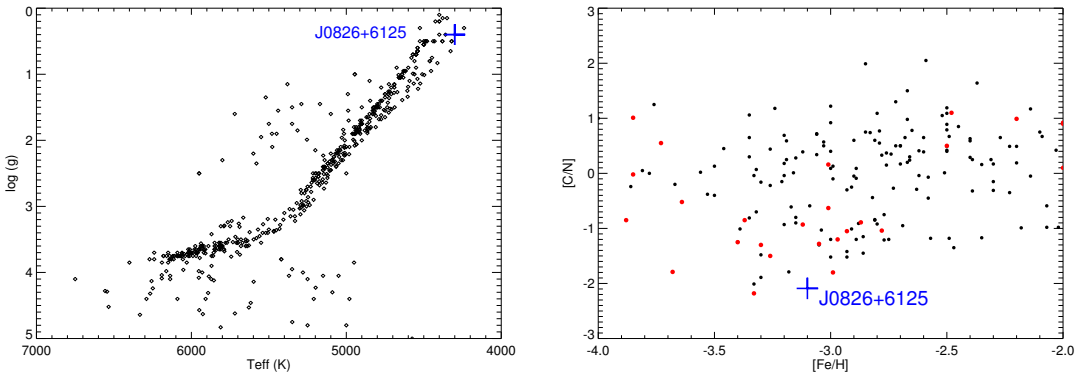

FIGURE 3.6: Left: The position of SDSS J0826+6125 among other EMP halo stars. Right: The very low [C/N] ratio for other low-metallicity halo stars with carbon deficiency. SDSS J0826+6125 is marked by the blue cross. The red dots mark the stars at the tip of the RGB with log(g) less than 1.

of the previous generations of stars which underwent the Ne-Na cycle, as it is not possible to produce these elements in the RGB phase. Such an anomaly could be similar to that seen in globular cluster stars (Gratton *et al.* 2001, 2004), which have undergone the AGB phase and passed on processed material to a subsequent generation of star formation in a closed system. Unfortunately, other signatures seen in globular cluster stars, such as the C-N-O and O-Na-Mg-Al correlations and anti-correlations (Shetrone 1996; Gratton *et al.* 2004; Carretta *et al.* 2010a; Coelho *et al.* 2011; Mészáros *et al.* 2015) were not observed in this star.

3.5.1.3 The Iron-Peak Elements

Abundances of Fe-peak elements (Cr, Mn, Co, and Ni) for metal-poor stars from the SAGA database are plotted, as a function of metallicity, in Figure 7, along with the position of SDSS J0826+6125 . This star appears is relatively rich in Co, but poor in Cr, Mn, and Ni, consistent with McWilliam *et al.* (1995) and Audouze and Silk (1995), who showed the same trends for several stars with metallicity below [Fe/H] $= -2.4$. The relative abundances of the Fe-peak nuclei could be well-explained by their dependence on the mass cut of the progenitor supernova

with temperature, which gives rise to a photo-disintegration process (Woosley and Weaver 1986).

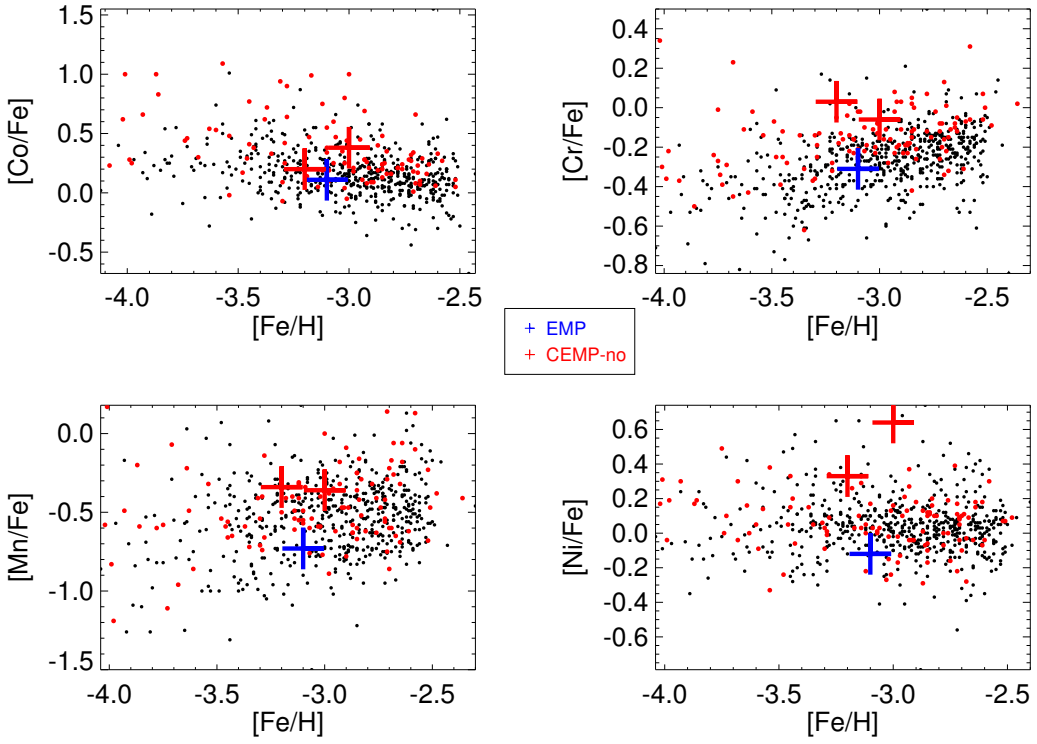

FIGURE 3.7: Distribution of Fe-peak elements for Galactic halo stars. The red dots represent the CEMP-no stars, while black dots represent C-normal halo stars. The program CEMP-no and EMP stars are indicated by blue and red crosses, respectively.

3.5.1.4 The Neutron-Capture Elements

Abundances of both the heavy and light *s*-process elements found in SDSS J0826+6125 are low, which is again consistent with the lack of available neutron flux (Audouze and Silk 1995). The abundance values are very similar to other EMP giants.

3.5.1.5 The Asymmetric Hα Profile of SDSS J0826+6125

SDSS J0826+6125 was observed several times, and an asymmetry in the Hα profile was noted for all of the spectra. The profile also could not be well-fit with synthetic spectra. The Hα profile and its fit with the model spectrum is shown in Figure 3.8. This could be due to the inadequacy of the 1D stellar models, or it may be due to an extended atmosphere present in the star. The Hα profile was also found to be not varying over several observation epochs indicating no ongoing mass transfer. The extended atmosphere could be the result of past mass transfer from an intermediate-mass AGB companion or mixing due to first dredge up of the star in the RGB phase. It is also possible that the star itself is an AGB star (e.g., Masseron *et al.* 2006).

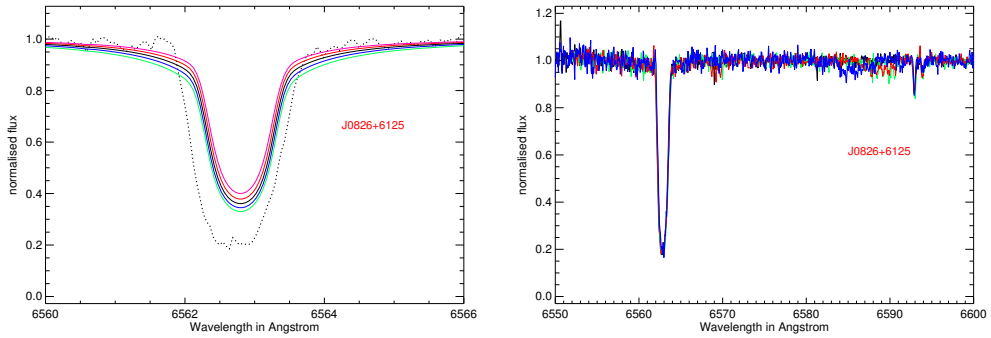

FIGURE 3.8: The strange Hα profile of SDSS J0826+6125 for different values of temperature from 4200k to 4600k in steps of 100k shown in the left. The lack of variability of the Hα profile of SDSS J0826+6125 for four epochs of observation are shown in the right.

3.5.2 CEMP stars

3.5.2.1 Lithium

We have obtained a measurement of A(Li) = 1.95 for SDSS J1341+4741 , which is lower than the Spite Plateau (Spite and Spite 1982) value of A(Li) = 2.2±

0.1 (Pinsonneault *et al.* 1999), and much lower than the predicted amount of Li from Big Bang nucleosynthesis (A(Li) = 2.75; Steigman 2005). Our limited RV information for this star indicates clear variation, from which we derive a possible period of 116 days. However, we have no other evidence that a mass-transfer event may have occurred. A slight depletion from the Spite Plateau value (A(Li) = 2.19) could be attributed to internal mixing of the star, or the observed value of lithium for SDSS J1341+4741 and SDSS J1953+4722 may be the result of several concurrent phenomena as discussed in details later in Chapter 6.

3.5.2.2 Carbon

According to Spite *et al.* (2013) and Bonifacio *et al.* (2015), CEMP stars are distributed along two bands in the A(C) vs. [Fe/H] plane. The upper band is centred around A(C)$\sim$ 8.25, and comprises relatively more metal-rich CEMP-s stars, while the lower band centred around A(C) $\sim$ 6.50 comprises more metal-poor, and primarily CEMP-no, stars. Further investigation by Hansen *et al.* (2016b) also led the result that the majority of the stars that are known binaries lie close to the upper band.

By expanding the list of CEMP stars with available high-resolution spectroscopic analyses to include more evolved sub-giants and giants (with the later giants having C abundances corrected for evolutionary mixing effects; Placco et al. 2014), Yoon *et al.* (2016) demonstrated that the morphology of this abundance space is more complex, with three prominent groups identified in the so-called Yoon-Beers diagram (their Figure 1). They argued that a separation between CEMP-s stars and CEMP-no stars in their sample could be reasonably achieved by splitting the sample at A(C) = 7.1, with the Group I CEMP-s stars lying above this level and the Group II and III CEMP-no stars lying below this level. In this classification scheme, SDSS J1341+4741 , with A(C) $\sim$6.22) can be comfortably identified as a

Group II CEMP-no star. Hence, the enhancement of carbon in this star is most likely to be intrinsic to the star (i.e., the C was present in its natal gas), and not the result of mass transfer from an extinct AGB companion. Thus, the elemental-abundance pattern observed from this star is associated with nucleosynthesis from a core collapse SN at early times, perhaps with additional contributions from stars that formed and evolved within its natal gas cloud.

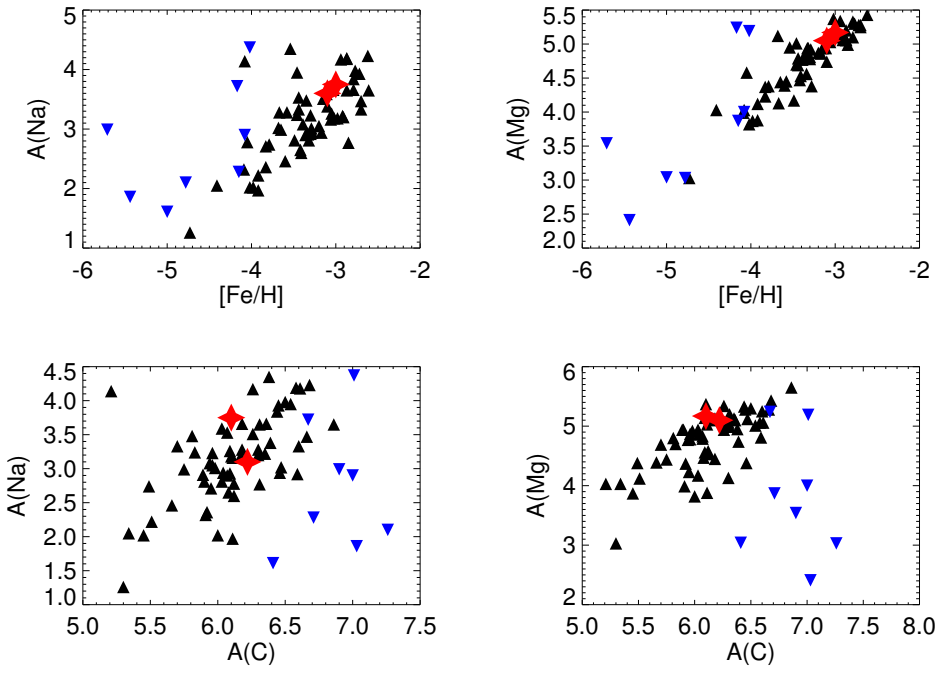

FIGURE 3.9: Top: Variation of A(Na) and A(Mg) with metallicity for the two groups of CEMP-no stars. The Group II and Group III stars are shown as black and blue colored points, respectively. The program star CEMP-no stars, shown in red diamonds, again falls within the Group II sub-class. Bottom: Variation of A(Na) and A(Mg) with A(C) for the two groups of CEMP-no stars, following the classification of Yoon *et al.* (2016). The program CEMP-no stars, shown as a red cross, is clearly a member of Group II.

3.5.2.3 The Light Elements

The program CEMP-no stars exhibit the low [Na/Fe], high [Mg/Fe], and low [Al/Fe] ratios expected from the odd-even pattern in massive-star nucleosynthesis yields at low metallicities (e.g., Arnett 1971; Truran and Arnett 1971; Peterson

1976; Umeda *et al.* 2000; Heger and Woosley 2002). The light elements closely follow the overall halo population observed in the Galaxy as well (Cayrel *et al.* 2004). Following Yoon *et al.* (2016), both SDSS J1341+4741 and SDSS J1350+4819 are clearly members of the Group II stars as shown in Figure 11, and supports a possible mixing and fallback SN as a likely progenitor.

3.5.2.4 The Iron-Peak Elements

Abundances of Fe-peak elements for CEMP-no stars (Cr, Mn, Co, and Ni) are shown in Figure 3.7, as a function of [Fe/H], compared with other CEMP-no and C-normal EMP stars compiled from the SAGA database (Suda *et al.* 2008). One feature that clearly stands out is the over-abundance of Cr and Ni, and to some extent Mn. In the low-metallicity regime, the stars are expected to show signatures of Type II SNe nucleosynthesis. All three elements play key roles in determining the progenitor population in the halo and the subsequent SNe yields. A decrease in [Cr/Fe] and [Mn/Fe] with decreasing [Fe/H] should be accompanied with enhancement in [Co/Fe] as a function of deeper mass cuts in the progenitor SNe (refer to Figure 9 of Nakamura *et al.* 1999). However, enhancement in both [Cr/Fe] and [Mn/Fe] can be explained by an excess of neutrons as well. Since neutron excess is a function of metallicity, we have plotted [Cr/Fe] vs. [Mn/Fe] in Figure 22 to eliminate the trend with Fe abundance (following, e.g., Carretta *et al.* 2002). In this plot, SDSS J1341+4741 occupies a relatively higher position amidst the population of CEMP-no stars. From Heger and Woosley (2002), Heger and Woosley (2010) and Qian and Wasserburg (2002), it is known that very massive stars ($80 < M/M_{\odot} < 240$) belonging to population III explode as pair-instability SNe, which should not produce a correlation between [Cr/Fe] and [Mn/Fe]. Thus, the presence of this correlation points us towards Type II SNe associated with a relatively high-mass ($M/M_{\odot} < 80$), but not extremely high-mass, progenitor.

Nickel is an extremely important element to gain further insight into the nature of the progenitor of SDSS J1341+4741 . The depth of the gravitational potential and amount of neutrino absorbing material in the models are the two factors that compete for the production of Ni in Type II SNe. In very massive ($M/M_{\odot} > 30$) stars the deeper gravitational potential restricts nickel from being ejected due to fallback, while intermediate-mass ($10 < M/M_{\odot} < 20$) stars eject large amounts of Ni because of a large neutrino-absorbing region (Nakamura *et al.* 1999). Thus, enhancement of Ni also points in the same direction, that the progenitor is likely to be a massive ($20 < M/M_{\odot} < 30$) star exploding as a Type II SNe in the early Galaxy. The observations support the hypothesis of a mixing and fallback model (Nomoto *et al.* 2013) with a lower degree of fallback, so as to eject a larger mass of ^{56}Ni.

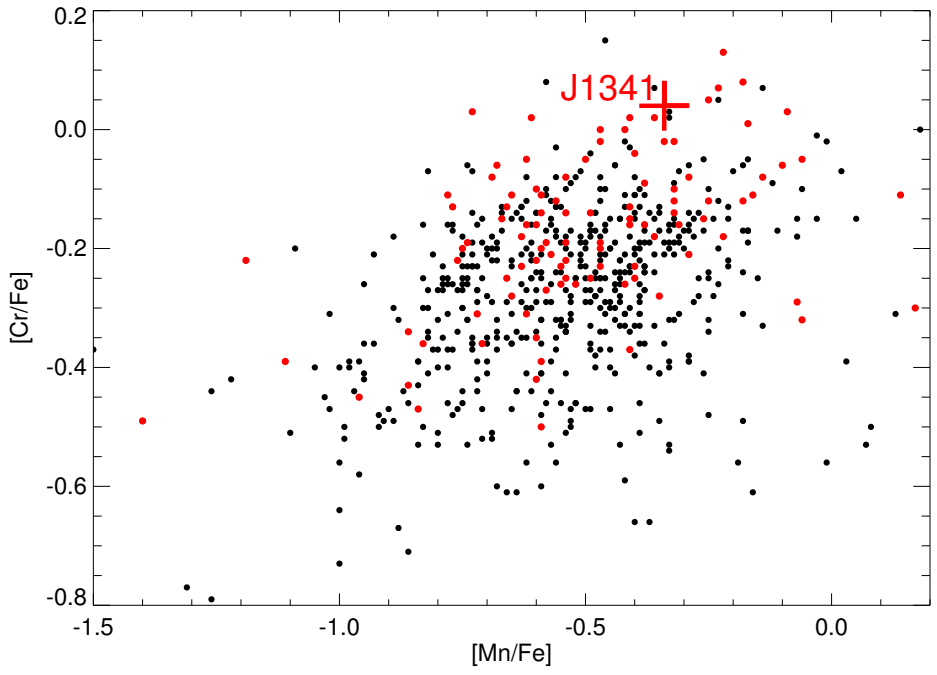

FIGURE 3.10: The relative enhancement of Cr and Mn for SDSS SDSS J1341+4741 , shown as a red cross, in the [Cr/Fe] vs. [Mn/Fe] space. Red dots mark the CEMP-no stars while the black dots mark the EMP stars.

3.5.2.5 The Neutron-Capture Elements

The first *s*-process peak element Sr and the second *s*-process peak element Ba have been detected in both the CEMP-no stars, and they exhibit under-abundances. The ratio of light to heavier neutron-capture elements are sensitive to the nature of the progenitors. Neutron star mergers are expected to produce heavy neutron-capture elements (e.g., Argast *et al.* 2004) and have been observed to do so in the kilonova SSS17a associated with GW170817 (Kilpatrick *et al.* 2017), which exhibited clear evidence for the presence of unstable isotopes created by the *r*-process (Drout *et al.* 2017; Shappee *et al.* 2017a). SNe with jets (e.g., Winteler *et al.* 2012; Nishimura *et al.* 2015) may also produce heavy neutron-capture elements. Formation of these systems may depend on the environment as well.

3.5.2.6 Nature of the Binary Companions of SDSS J0826+6125 and SDSS J1341+4741

Both of our program stars exhibit clear radial-velocity variations, indicating the likely presence of a binary companion. In the case of SDSS J0826+6125 , the enhanced abundances of N and under-abundance of C indicates the possible mixing of the atmosphere with CN-cycle products. This can result from first dredge-up mixing in the star, which is currently in the RGB, from mass transfer from an intermediate-mass AGB star that might have gone through hot bottom burning (Lau *et al.* 2007; Suda *et al.* 2012). The low $\log(g)$ value of the star supports RGB mixing, although AGB mass transfer cannot be ruled out. The non-detection of Li and peculiar Hα profiles could indicate either internal mixing or binary mass transfer as well. The O abundance can help to differentiate between the RGB and AGB scenarios. In the case of an intermediate-mass AGB that goes through hot bottom burning, the temperatures are sufficiently high for the star to operate the CNO cycle, which will result in a depleted O abundance. In that

case, SDSS J0826+6125 may be a true nitrogen-enhanced metal-poor (NEMP; see Johnson *et al.* 2007, Pols *et al.* 2009, Pols *et al.* 2012) star, which are known to exist, but are relatively rare.

In the case of SDSS J1341+4741 , the binary companion did not likely contribute through a mass-transfer event, since the Li abundance in the star is similar to other EMP stars, although it is lower than the Spite Plateau value. The mild depletion of Li could be due to binary-induced mixing or internal mixing of the star during its sub-giant phase. It may well be worthwhile to mount an RV-monitoring campaign for this and other Li-depleted EMP stars to test for a possible binary-star origin to the declining lithium abundance problem for stars with [Fe/H] < -3.0.

3.5.3 SDSS J001331.76+314144.10

SDSS J001331.76+314144.10 is a CEMP-s star discovered in this study along with SDSS J1953+4722 . SDSS J001331.76+314144.10 shows an elevated [C/Fe]=0.87, a low [N/Fe]-1.53 and [O/Fe]=0.61. It also shows a slightly lower [Mg/Fe]=0.10 but [Ca/Fe]=0.36 consistent with the α enrichment of the Halo stars. The Fe-peak elements track the Fe abundances but [Cu/Fe]-0.64 deviates from the expected abundance pattern.

The abundances of n-capture elements show a peculiar distribution. The light n-capture elements have values close to solar abundances with the exception of Sr which exhibits a very strong enhancement of [Sr/Fe]= +1.18. Among the heavier n-capture elements, Ba abundance is also very high with [Ba/Fe]=+1.62. The other heavy n-capture elements show a moderate enhancement of [n/Fe]=0.65.

The abundances are not typical of a halo star. It is very likely that SDSS J001331.76+314144.10 has undergone a chemical enrichment history completely

different from the usual metal poor stars. The paper is in progress and it might be of considerable interest for stellar modelling.

3.5.4 CEMP-no and EMP Stars

From the above discussion, and based on previous studies, it is evident that CEMP-no and C-normal EMP stars have very different origins. Even within the sub-class of CEMP-no stars, there may well be different types of progenitors. As discussed by Yoon *et al.* (2016), the Group II CEMP-no stars could be associated with the faint mixing and fallback SNe, whereas the Group III CEMP-no stars can be attributed to the spinstar models, with a number of exceptions for both the classes (Meynet *et al.* 2006; Nomoto *et al.* 2013). See also the discussion of the progenitors for CEMP-no stars by Placco *et al.* (2016). Some of the CEMP-no stars lying in the low A(C) region may have a binary component, but no mass transfer is supposed to have taken place (Starkenburg *et al.* 2014; Bonifacio *et al.* 2015; Yoon *et al.* 2016), which is further strengthened by the only "slight" depletion of Li in SDSS J1341+4741 , as described in the previous section. Iron-peak elements can provide valuable insights regarding the nucleosynthetic yields of their progenitor supernovae, as these elements cannot be produced or modified during the post main-sequence evolutionary stages of the star. Figure 3.7 shows the distribution of some key Fe-peak elements for both CEMP-no and C-normal EMP stars. Visual inspection suggests that Cr and Co are enhanced for the CEMP-no population. We have compiled data from SAGA database to see if there is an enhancement of Cr in CEMP-no stars. The fit is given in Figure 18 for [Cr/Fe]. There is a slight offset between the EMP and CEMP-no stars, but they exhibit similar increasing trends of [Cr/Fe] with [Fe/H]. We have checked, and these behaviours apply to both dwarfs and giants. The similar offset could also be noted for Co. Lai *et al.* (2008) and Bonifacio *et al.* (2009) have considered the discrepancies in the behaviour of Cr between giants and dwarfs, since Cr II could be measured only in

giants, while Cr I is a resonance line, and could suffer substantial NLTE effects. However, such issues are not expected to play a substantial role when we compare only giants with giants or dwarfs. Temperature and gravity do not play a major role in deviations from LTE abundances (Bergemann and Cescutti 2010), so we have not used them to further refine our sample from the archival data. Enhancement in [Cr/Fe] for CEMP-no stars with respect to C-normal EMP stars can play a key role in the understanding of SNe ejecta and relevant mass cuts. It would be very interesting to investigate the origin of this discrepancy.

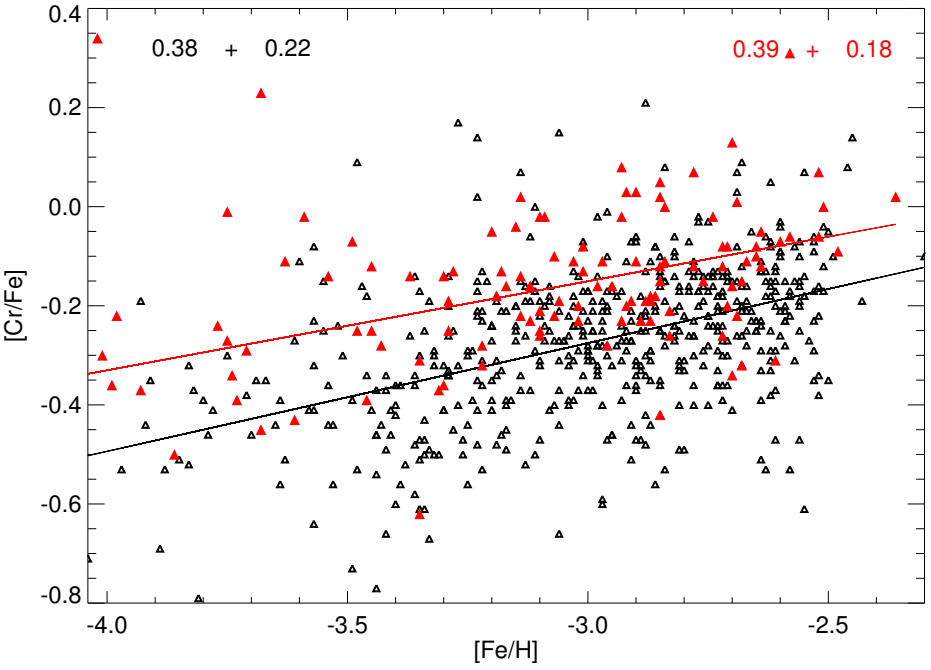

FIGURE 3.11: Linear fit for CEMP-no and C-normal EMP stars. Red is used for CEMP-no stars while black is used for EMP stars. The slope and σ are shown for each fit in the corresponding color.

3.6 Conclusion

We have derived LTE abundances for the EMP star SDSS J082625.70+612515.10 ; it is mostly consistent with the behaviour of other halo stars. The depletion in carbon and enhancement in nitrogen could be due to internal mixing within the

star. It is unlikely that self enrichment similar to that is seen in globular clusters has occurred, due to the overabundance in oxygen. The peculiar Hα profiles of SDSS J0826+6125 also supports the possibility of mixing that might occur in an extended atmosphere. The radial-velocity variation strongly suggests this star is a member of a binary system, but it is likely there is no ongoing mass transfer, due to non-variable peculiar Hα profile over a period of a year.

SDSS J134144.60+474128.90 and SDSS J1350+4819 are CEMP-no type stars with SDSS J1341+4741 likely being a member of a binary system. The lithium is detected in SDSS J1341+4741 and mildly depleted, similar to other EMP stars. Lithium in EMP dwarfs and CEMP-no stars exhibit similar trends at different metallicities. SDSS J001331.76+314144.10 and SDSS J1953+4722 are found to be CEMP-s stars with SDSS J001331.76+314144.10 showing a very peculiar nucleosynthesis pattern which might be very interesting for stellar modellers.

Below [Fe/H] < -3.0, EMP and CEMP-no stars often have lithium abundance below the Spite Plateau. We also studied the trends of heavy elements among EMP and CEMP stars. At a given metallicity, CEMP-no stars appear to have larger abundances of Cr. This might provide important clues to the nature of the progenitors that contributed to the origin of carbon.

Chapter 4

Discovery of a blue straggler and other GC escapees in the Halo

4.1 Introduction

Globular clusters are expected to loose a large amount of stellar mass during their migration and evolution in the Halo (e.g. Martell 2018 and references therein; Kruijssen 2014a). There are several processes by which stars can escape from the globular clusters. The most important of them is evaporation. The clusters owing to their large age are dynamically relaxed systems which allow mass segregation to have already taken place. Thus the stars with the highest velocity are pushed towards the least bound or outer parts of the cluster making it very easy for them to escape (Balbinot and Gieles 2018) from the cluster potential. Another important process resulting in mass loss from the clusters is tidal interactions with the Galaxy as observed in the case in the well studied GC Palomar 5 (Odenkirchen *et al.* 2001). Other processes like disc shocking and dynamical friction also contribute towards loss of stars from globular clusters. The importance of each mass-loss process

depends upon the properties of the cluster as shown in the "vital diagram" by Gnedin and Ostriker (1997). On average, each globular cluster is expected to have lost half its mass over a span of 12 Gyr (Fall and Zhang 2001).

Chemical tagging is one of the important tools to identify stars of globular cluster origin among the field stars (Freeman and Bland-Hawthorn 2002). Both the populations display a similar elemental abundances for alpha, Fe-peak and n-capture elements (Gratton *et al.* 2004; Pritzl *et al.* 2005; Lind *et al.* 2015). However, globular clusters show certain unique trends for light elements like C, N, O, Na, Mg, Al which is uncharacteristic of halo stars (e.g. Kraft *et al.* 1979; Kraft 1979; Norris and Freeman 1979 and many references since). These traits emerge as a result of self evolution where the gas from the first generation of stars does not escape from the cluster but instead pollutes the second generation stars with the products of evolved hydrogen burning (Kraft *et al.* 1997; Carretta *et al.* 2009a,b). In hotter regions (T $>$ 40 million K) Ne-Na chain starts converting ^{20}Ne to ^{23}Na while at the same region O starts depleting via the ON cycle (Gratton *et al.* 2012a). In even hotter temperatures (T $>$ 70 million K) Mg-Al cycle is ignited which steadily depletes ^{24}Mg and then ^{25}Mg to ^{27}Al (Denissenkov and Weiss 1996; Salaris and Weiss 2002). The true sites where C-N-O, Ne-Na, and Mg-Al cycles occur are the H-burning shells of low mass ($<$1 M$_{\odot}$) RGB stars, and in the Hot Bottom Burning (HBB) regions (Bloecker and Schoenberner 1991; Boothroyd and Sackmann 1992) of the outer convective envelope of intermediate mass (38 M$_{\odot}$) AGB stars. The fast rotating massive stars (FRMS) is also a probable site for similar nucleosynthesis reactions to take place (Decressin and Charbonnel 2007). The winds from these early generations of IM-AGB stars and FRMS alters the chemical composition of the birth cloud of subsequent generations of stars. Consequently, a large fraction of present-day GC stars is enhanced in Na and Al along with depleted levels of C, O and Mg. Spectroscopically almost all the studied Galactic globular clusters are found to host multiple generations of stars (Bragaglia *et al.* 2017) and can be traced by the C-N-O anomaly (Kayser *et al.* 2008; Smolinski *et al.* 2011) and the

anticorrelations of Na and O, Mg and Al (e.g. Carretta *et al.* 2009a,b; Martell and Grebel 2010; Martell 2011; Lee 2010; Bragaglia *et al.* 2015; Carretta *et al.* 2017).

Martell and Grebel (2010) demonstrated that 2.5% of the 2000 low metallicity Halo giants studied from the SEGUE survey had and enhanced N and depleted C relative to the field stars. A similar result was obtained by Martell *et al.* (2011) from SEGUE-II. Ramírez *et al.* (2012) discovered two field dwarfs showing the Na-O anti-correlations which could be attributed to globular cluster origin. Lind *et al.* (2015) found one star from the GAIA-ESO survey with the Mg and Al abundances largely different from the Halo population but consistent with globular cluster abundances. Halo giants with globular cluster abundances of N and Al were also obtained by Martell *et al.* (2016) using the SDSS-IV APOGEE survey.

The studies have estimated a substantial part of the Halo to be contributed by globular cluster stars(e.g. Carretta *et al.* 2010b; Ramírez *et al.* 2012;Lind *et al.* 2015) but the scientific community is still in pursuit of a consensus regarding the precise number. Martell and Grebel (2010), Martell (2011) have estimated 3% of the Halo to be contributed by globular clusters. This number is consistent with the high resolution studies conducted by Carretta *et al.* (2010b) which suggested 3% while Ramírez *et al.* (2012) found it to be 3±2 %. Martell *et al.* (2016) have found 2% of their sample of halo stars to have the chemical signatures of second generation GC stars which accounts for a much larger amount of mass loss from globular clusters. Following Martell *et al.* (2011) the original contribution from GCs amounts to 13% of the Halo stars in order to account for the 2% being chemically taggable.

Here we discuss the first discovery of three second generation globular cluster escapees with enhanced Na, Al and depleted C, O and Mg. One of them is a blue straggler which is a rare discovery and also the most metal poor globular escapee discovered to date.

TABLE 4.1: Observation details for the reported objects observed through HESP at R 30000.

Object	obs.time	frames	SNR	Vmag	Rad.vel
SDSS J1937+5024	2400s	3	130	10.44	−184.0
SDSS J0646+4116	2400s	6	43.1	11.14	−285.0
SDSS J2256+3951	2400s	6	41.4	11.56	−22.0

4.2 Observations and analysis

High-resolution ($R \sim 30,000$) spectroscopic observations of the three stars were carried out as a part of the HESP-GOMPA (Galactic survey Of bright Metal Poor stArs) survey using the Hanle Echelle Spectrograph on the 2.3-m Himalayan Chandra Telescope (HCT) at the Indian Astronomical Observatory (IAO). The target selection was done as explained in Chapter 2. We have used synthetic spectral fitting of the pre-survey data to identify new metal-poor candidates(in the domain of globular cluster metallicity; [Fe/H] > -2.50) with a weak G-band which is a well known feature of globular cluster stars and could be studied from low resolution data(e.g. SDSS). We identified 3 globular cluster escapees showing the expected chemical signatures out of 55 metal poor stars with weak G-band from low resolution data. The epoch of observation, radial velocities, signal-to-noise ratio are listed in Table 4.1.

The stellar parameters were derived following the same technique as described in Chapter 2. The adopted values for the three stars are given in Table 4.2.

TABLE 4.2: Adopted stellar parameters for the stars

Object	Eff.temp(K)	log(g)	ξ	[Fe/H]
SDSS J1937+5024	4800	1.50	1.50	−2.20
SDSS J0646+4116	5150	2.25	1.50	−1.90
SDSS J2256+3951	7000	5.00	1.80	−2.40

4.3 Abundances

4.3.1 Light elements

Lithium could be detected in SDSS J193712.01+502455.50 and SDSS J064655.6+411620.5 . The strong Li doublet at 6707 Å, was used from which we obtain an abundance $A(\mathrm{Li}) = 1.05$ and 0.95 respectively, which is similar to some other giants observed in the field. Li could not be measured for SDSS J225641.25+395145.9 which is expected as it is a very fragile element and likely to be destroyed at higher temperatures.

Carbon abundances are measured by performing a spectral synthesis around the CH G bandhead region around 4313 Å. The bandhead could be detected and measured in SDSS J193712.01+502455.50 and SDSS J064655.6+411620.5 which yielded the best fit values of [C/Fe] = 0.02 and [C/Fe] = −0.53 respectively. However, the G band could not be detected in case of SDSS J225641.25+395145.9 which is understandable because of its relatively high temperature of 6800 K. N abundances were obtained by measuring the CN molecular band at 3883 Å. The C abundances obtained from the G band was used with a wide range of N abundances and the best fit in the spectral bandhead was taken as the value of the N abundance. However, being close to the extreme blue end of the spectrum the signal-to-noise in the region is poor. N could be measured only in case of SDSS

J193712.01+502455.50 owing to its brightness and high SNR and it is found to be slightly enhanced with a value of [N/Fe] = +0.37. O abundances are measured from the weak lines at 6300 Åand 6363 Ålines which are the regions heavily populated by atmospheric lines and thus telluric correction is vital for obtaining the correct values of oxygen. O could be measured for SDSS J193712.01+502455.50 and SDSS J064655.6+411620.5 and both are found to be enhanced with abundances of [O/Fe] = +0.61 and [O/Fe] = +0.51 respectively.

Among the α elements, Mg and Ca could be studied in the stars. The Si lines were too weak to derive any meaningful abundances. Several lines for Mg and Ca could be obtained throughout the spectra of which only the clean lines were used to derive the abundances. The very strong lines like the strongest among the Mg triplet around 5172 Åwere ignored in the computation of the abundances. For SDSS J193712.01+502455.50 [Ca/Fe] = +0.21 is slightly enhanced but lower than the typical Halo α enhancement of +0.4 whereas [Mg/Fe]= −0.13 is depleted. SDSS J064655.6+411620.5 is also found to have [Ca/Fe] = 0.23 and [Mg/Fe] = 0.21 which are lower than typical Halo stars. Ca could be taken as the true representative of α elements as the other elements like O, Si and Mg are mostly altered due to the recycling of the products of an earlier generation of stars during subsequent star formation inside globular clusters (Kraft *et al.* 1997; Gratton *et al.* 2004; Carretta *et al.* 2010b; Gratton *et al.* 2012a). SDSS J225641.25+395145.9 shows a depleted value of both the α elements [Ca/Fe] = −0.63 and [Mg/Fe]= −0.40.

Na and Al are the most important among the odd Z elements to tag a star of globular cluster origin(ref). Both of them could be detected for all the three stars. Al abundances have been derived by spectral fitting of the strong resonance line at 3961 Åwhile the D1 and D2 lines at 5890 Åand 5896 Åwere used for deriving abundances of Na. The spectral fit for Al have been shown in Figure 1. The NLTE corrections for this line could rather high upto 0.75 dex as discussed by Baumueller and Gehren (1997); Andrievsky *et al.* (2008); Nordlander and Lind (2017). The

NLTE corrections for Na (Andrievsky *et al.* 2007) has also been taken into account which is incorporated in the final values.

4.3.2 Fe-peak elements

Abundances of Cr, Co, Mn, Ni and Zn could be measured by the usual equivalent width analysis of the clean lines. The non LTE correction for each species (e.g. Bergemann and Gehren 2008; Bergemann *et al.* 2010; Bergemann and Cescutti 2010; Sitnova *et al.* 2016) have been incorporated in the final abundances.

The two odd Z elements Mn and Cu show the usual deficiency with respect to Fe in the metal poor domain as found in previous studies for halo as well as GC stars. However, Ni is found to be high for SDSS J225641.25+395145.9 and SDSS J193712.01+502455.50 which could be explained by invoking mass cuts (Woosley and Weaver 1986) or a progenitor which is likely to be a massive ($20 < M/M_{\odot} < 30$) star exploding as a Type II SNe in the early Galaxy. The over-abundance of [Co/Fe] in the case of SDSS J225641.25+395145.9 could also be explained by deeper mass cuts, as Co is formed in the innermost layers whereas Fe can be synthesized in deeper layers as well as outer layers during Si burning (Maeda and Nomoto 2003; Nomoto *et al.* 2013). The identical trends for Fe-peak elements in GCs and halo stars indicate that they had a similar pre-enrichment history during the epoch of formation at the early phases of galactic evolution.

4.3.3 Neutron capture elements

Neutron capture elements like Sr and Ba could be measured in all the three stars and they are found to have normal abundances without notable irregularities. The

resonance lines of Sr II at 4077 Åand 4215 Åwere used to derive the Sr abundances while resonance lines at 4554 Åand 4934 Åwere measured to determine the Ba abundances. Method of spectral synthesis was employed to derive the abundances which took care of the hyperfine transitions.

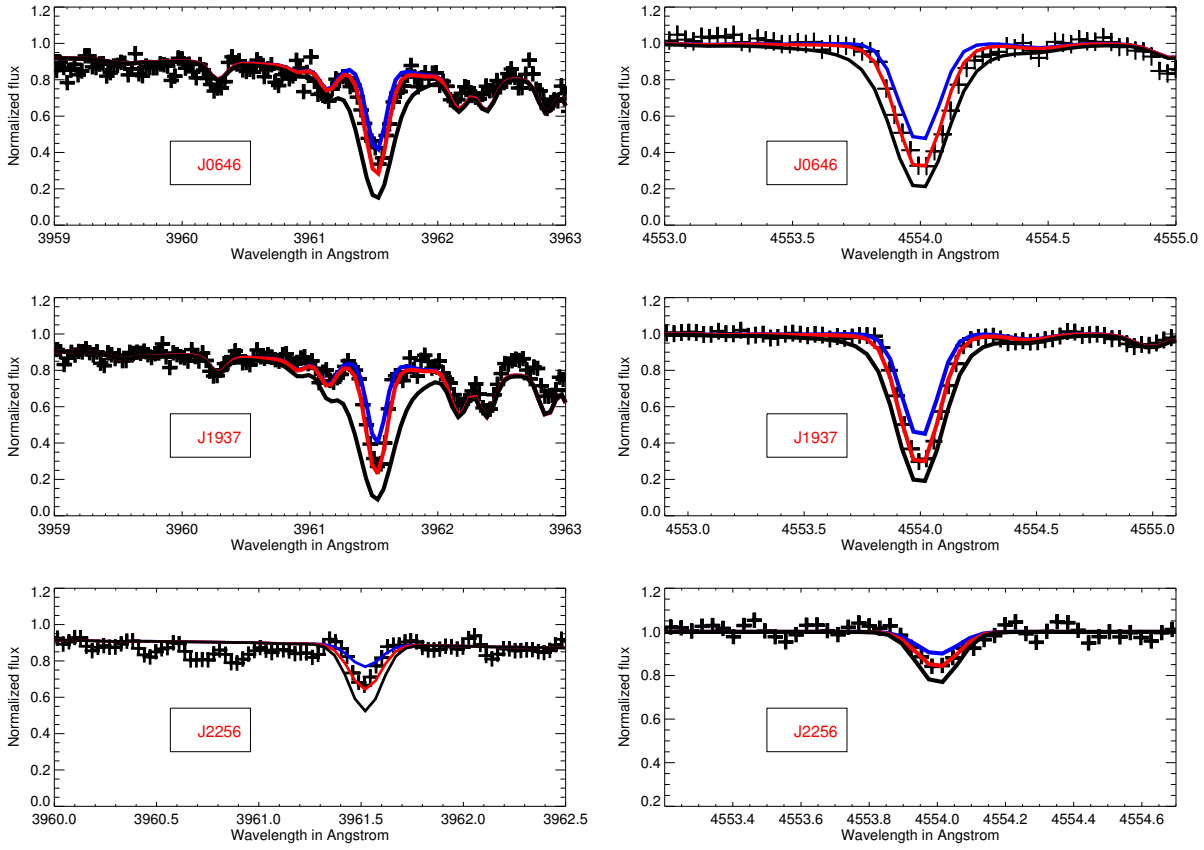

FIGURE 4.1: Spectral fitting for the key elements The left panels show the fits for Al while the right panels show the fits for Ba

TABLE 4.3: Elemental Abundance Determinations for SDSS J193712.01+502455.50 .

Elements	Species	N_{lines}	A(X)	Solar	[X/H]	[X/Fe]	σ
Li	LiI	1	1.05				
C	CH	...	6.25	8.43	−2.18	−0.02	synth
N	CN	...	6.05	7.83	−1.78	0.42	synth
O	O I	...	7.10	8.69	−1.59	0.61	synth
Na	Na I	2	4.50	6.24	−1.74	0.46	synth
Mg	Mg I	4	5.17	7.60	−2.43	−0.23	synth
Al	Al I	1	4.70	6.45	−1.75	0.45	synth
Ca	Ca I	8	4.35	6.34	−1.99	0.21	0.06
Sc	Sc II	5	0.95	3.15	−2.20	0.00	synth
Ti	Ti I	7	3.14	4.95	−1.81	0.39	0.03
	Ti II	6	2.86	4.95	−2.09	0.11	0.04
Cr	Cr I	3	3.33	5.64	−2.31	−0.11	0.05
	Cr II	2	3.35	5.64	−2.29	−0.09	0.05
Mn	Mn I	4	2.60	5.43	−2.83	−0.63	synth
Co	Co I	2	2.68	4.99	−2.31	−0.11	synth
Ni	Ni I	3	4.70	6.22	−1.52	0.68	0.04
Zn	Zn I	2	2.37	4.56	−2.19	0.01	0.05
Sr	Sr II	2	0.75	2.87	−2.12	0.08	synth
Ba	Ba II	2	0.25	2.18	−1.93	0.27	synth

σ indicates the random error.

TABLE 4.4: Elemental Abundance Determinations for SDSS J064655.6+411620.5 .

Elements	Species	N_{lines}	A(X)	Solar	[X/H]	[X/Fe]	σ
Li	LiI	1	0.95				
C	CH	...	6.00	8.43	−2.43	−0.53	synth
O	O I	...	7.30	8.69	−1.39	0.51	synth
Na	Na I	2	4.75	6.24	−1.49	0.41	synth
Mg	Mg I	4	5.91	7.60	−1.69	0.21	synth
Al	Al I	1	4.92	6.45	−1.53	0.37	synth
Ca	Ca I	8	4.67	6.34	−1.67	0.23	0.09
Sc	Sc II	5	1.72	3.15	−1.43	0.47	synth
Ti	Ti I	7	3.47	4.95	−-1.47	0.43	0.08
	Ti II	6	3.57	4.95	−1.38	0.52	0.06
Cr	Cr I	3	3.80	5.64	−1.84	0.06	0.09
	Cr II	2	4.06	5.64	−1.58	0.32	0.08
Mn	Mn I	4	3.24	5.43	−2.19	−0.29	synth
Co	Co I	2	2.62	4.99	−2.37	−0.47	synth
Ni	Ni I	3	4.56	6.22	−1.66	0.24	0.07
Zn	Zn I	2	2.89	4.56	−1.67	0.23	0.06
Sr	Sr II	2	1.25	2.87	−1.62	0.28	synth
Ba	Ba II	2	0.75	2.18	−1.43	0.47	synth

σ indicates random error.

TABLE 4.5: Elemental Abundance Determinations for SDSS J225641.25+395145.9 .

Elements	Species	N_{lines}	A(X)	Solar	[X/H]	[X/Fe]	σ
Na	Na I	2	5.68	6.24	−0.56	1.74	synth
Mg	Mg I	4	4.90	7.60	−2.70	−0.40	synth
Al	Al I	1	4.50	6.45	−1.95	0.35	synth
Ca	Ca I	8	4.40	6.34	−2.94	−0.64	0.12
Sc	Sc II	5	1.40	3.15	−1.75	0.55	synth
Ti	Ti I	7	3.10	4.95	−1.85	0.55	0.10
	Ti II	6	2.95	4.95	−2.00	0.30	0.08
Cr	Cr I	3	4.00	5.64	−1.64	0.66	0.09
	Cr II	2	3.60	5.64	−2.04	0.26	0.13
Mn	Mn I	4	3.29	5.43	−2.14	0.16	synth
Co	Co I	2	3.00	4.99	−1.99	0.31	synth
Ni	Ni I	3	4.40	6.22	−1.82	0.48	0.08
Sr	Sr II	2	0.50	2.87	−2.37	−0.07	synth
Ba	Ba II	2	0.00	2.18	−2.18	0.12	synth

σ indicates the random error.

4.4 Results and discussion

4.4.1 Light element anti-correlations

All the three stars SDSS J193712.01+502455.50 ,SDSS J064655.6+411620.5 ,SDSS J225641.25+395145.9 show enhancement in [Na/Fe] and [Al/Fe] in comparison to the other Halo stars of similar metallicity. They also show under-abundance of [C/Fe] with enhancement in [O/Fe] which is compatible with the yields for a second generation globular cluster star. [Mg/Fe] is also found to be depleted in SDSS J193712.01+502455.50 and SDSS J064655.6+411620.5 but with the expected value for [Ca/Fe] around +0.4 dex which is compatible with the extreme globular cluster abundances. Since the elements like C, O, Mg could be significantly altered during the quiescent burning in the proton fusion reactions (Gratton *et al.* 2004), we have restricted Ca as the best representative of α elements for comparison with halo star abundances. However, SDSS J225641.25+395145.9 shows a strong depletion of both [Mg/Fe] and [Ca/Fe] which might be due to significantly lower impact of supernovae type II on the parent cluster or it might have migrated from satellite galaxies (Kirby *et al.* 2009). We have conducted a comparative study of these three stars with the Halo population and globular cluster abundances using light elemental abundances as shown in Figure 2. The panels a and b display the enhancement in [Na/Fe] and [Al/Fe] with respect to [Fe/H] in globular clusters as compared to the Halo stars. To clearly separate the GC population from the halo stars we have plotted [(Na+Al)/Fe] vs [Fe/H]. All the three program stars clearly fall in the domain of GC abundances in these plots. To strengthen the argument, we have also tried to look for the Na-O and Mg-Al anti-correlations in the panels d and e. Though we could not detect O in SDSS J225641.25+395145.9 and could only get an upper limit for SDSS J064655.6+411620.5 (marked with an arrow) the abundances fit better with the globular cluster population. Apart from globular clusters, the origin of such peculiar abundance pattern could be mass transfer from

a binary component. Such stars could be polluted by the winds of an AGB companion which would then show enhancement in [C/Fe] and slow neutron capture elements(ref). Any remaining Li would also be destroyed. However, the presence of Li in SDSS J193712.01+502455.50 and SDSS J064655.6+411620.5 along with a depleted value of [C/Fe] indicates such a scenario to be extremely unlikely(few references) in these stars. In the case of SDSS J225641.25+395145.9 , the low value of [Sr/Fe]$= -0.1$ constrains such a possibility.

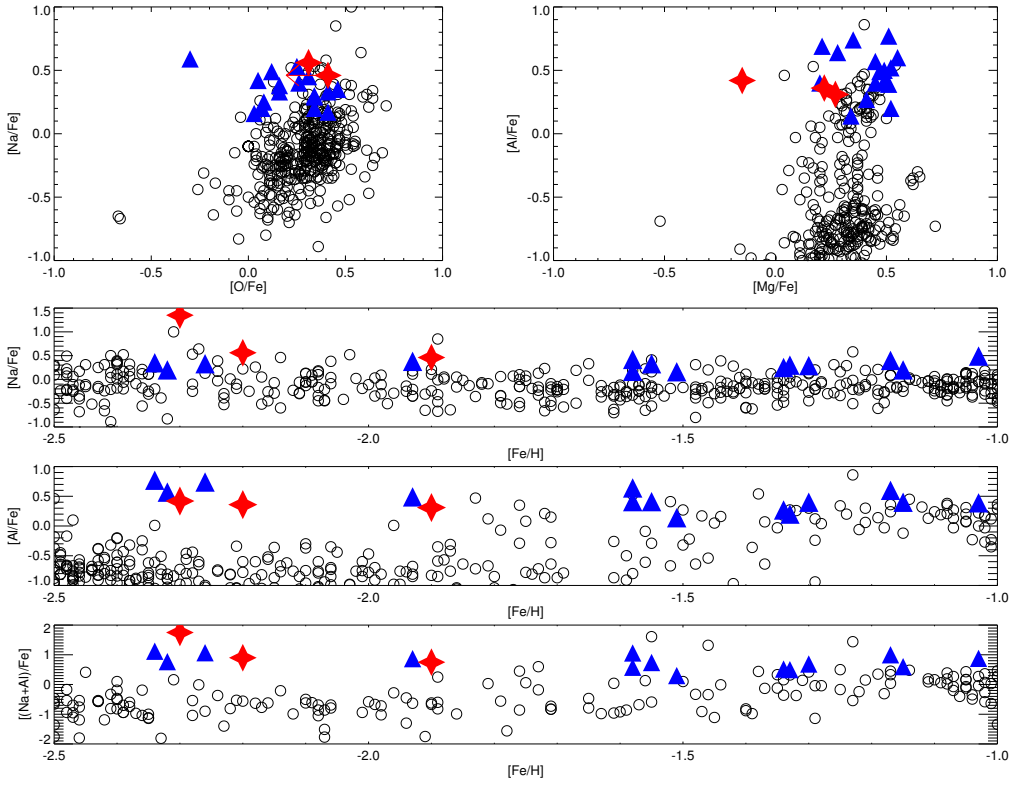

FIGURE 4.2: A comparative study on the light element abundances for globular clusters and Halo stars. The blue upwards triangles mark the mean globular cluster abundances whereas the open circles indicate the halo stars. The three stars discussed here are marked in red filled stars. The top two panels study the Na-O and Mg-Al anticorrelations whereas the lower three panels show the distribution of the key elements with the metallicity. Our program stars consistently fall in the domain of GC abundances in all the plots. The data for GCs are taken from (Carretta *et al.* 2009a) and the abundances for halo stars are taken from the SAGA database.

4.4.2 Nature of original polluters of GCs

We have also done a comparative study using the heavy elements as they remain unaltered during the proton burning stages and thus provide an opportunity to study the chemical enrichment at their epoch of formation. Absence of any enhancement in C also indicates r-process to be the chief mechanism for the production of the n-capture elements in these stars. Following Tsujimoto and Shigeyama (2014a,b) heavier r-process is produced by NS−NS mergers alone((e.g., Thielemann *et al.* 2017) whereas light r-process could be produced by both NS−NS mergers and CCSNe. The nucleosynthesis products of these two sources are mixed to different amounts within the sub-haloes due to the differences in their wind speeds and a vari- ations of sub-halo masses (Prantzos and Charbonnel 2006; Ishimaru *et al.* 2015). The high ratios of [light r-process/heavier r-process] is argued to be produced by massive sub-haloes and a lower ratio is produced in low mass sub-haloes. In Figure 3 we have used barium as a representative element for heavier r-process elements, and strontium to represent lighter r-process elements (Susmitha Rani *et al.* 2016) The red dots mark the α poor halo stars and the upward triangles mark the mean globular cluster abundances from literature. Two distinct populations could be identified. A lower value of [Sr/Ba] indicates maximum contribution from NS−NS whereas a higher value of [Sr/Ba] indicates a higher contribution from core collapse supernovae. All the three globular cluster escapees along with majority of the other Globular clusters being placed towards the bottom indicate NS−NS mergers to be the chief contributor(e.g., Hotokezaka *et al.* 2015; Wallner *et al.* 2015; Drout *et al.* 2017; Shappee *et al.* 2017b) which is expected from the denser environment compared to the Galactic halo. In this figure, the X-axis does not represent the formation epoch as the globular clusters were formed at the same epoch as the EMP stars but have migrated from their original position towards the current position as shown in the plot due to self-enrichment over the evolutionary time scale. We have also plotted the well

studied r-process enhanced satellite dwarf spheroidal galaxy Reticulum II in upward red triangles which also shows a similar trend. We shall revisit the paradigm at the end of chapter 5.

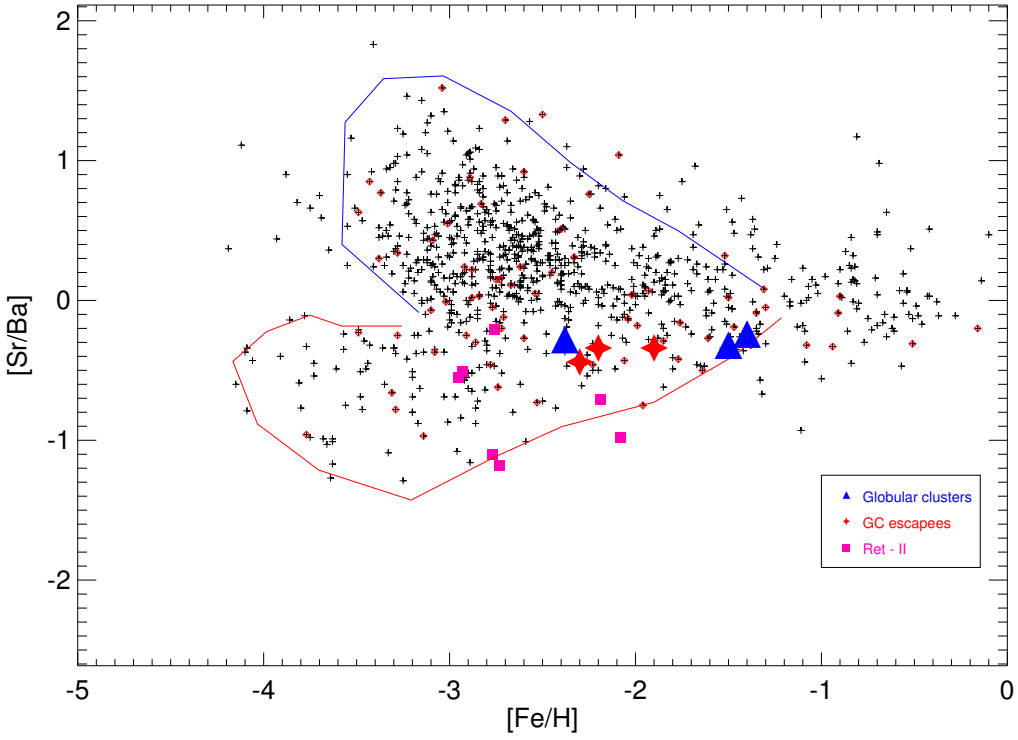

FIGURE 4.3: Exploring the origin of Halo and globular clusters. The red line marks the contributions for NS-NS mergers whereas blue line marks the contribution from core collapse supernova. The halo stars from literature are marked in black dots while the data for globular cluster stars from this study are marked in red diamonds. The GCs from literature are shown in blue upward triangles.

4.4.3 Blue Straggler

SDSS J225641.25+395145.9 is found to be a blue straggler. It occupies a position to the left of the turn off in the HR diagram. The chemical anomalies as expected in globular cluster stars like an enhancement in [Na/Fe] is much more pronounced in SDSS J225641.25+395145.9 . This could either be the actual unmixed abundances that could hardly be observed in evolved stars in their giant phases or it could

be resulting from binary mass transfer which might have led to the formation of the blue straggler. In the case of the unmixed scenario discovery of such blue stragglers could be used as a smoking gun to study the true composition of the progenitor population. However, no detection of Li makes it unlikely to be unmixed or undiluted and is consistent with the previous studies on Halo blue stragglers (e.g Ryan *et al.* (2001)) which explains such stars on the basis of binary mass transfer. It would make an extremely interesting problem for future studies to test for the signatures of mass transfer and demarcate between the two scenarios.

4.5 Conclusion

A large sample of stars (60) in the domain of GC metallicity with a weak carbon molecular g-band from the low resolution fits have been studied in high resolution to find signatures of the second generation stars of globular clusters. Out of the sample, only 3 were found to be consistent with all the expected light element anomalies. This study was an attempt to understand the progenitor population of globular cluster stars and to address the question regarding why the GC stars are so unique. Rare classes of stars like r-process rich stars, CEMP-no stars have been discovered in the halo but till date not a single bonafide halo star has been discovered with similar anomalies to GC star. So the stars studied here could be GC escapees or they could be the first detection of bonafide Halo members with massive star progenitors that resulted in similar abundance pattern. Binarity studies and proper motion studies could help shed some light on this aspect.

Chapter 5

R-process rich stars from the HESP-GOMPA Survey

5.1 Introduction

Detection and measurement of the abundances of the rare elements in metal poor stars provide a wealth of information regarding their formation history and the prevalent astrophysical conditions in the early stages of the Galaxy (Beers and Christlieb 2005; Frebel and Norris 2015a,b). The low iron content in these stars already indicates that the natal clouds had received contributions from very few stars which in certain cases could be a single star(e.g. Placco *et al.* 2014). The category of rare elements that are most important to trace the nature of the first stars and the early galaxies are the ones that are formed by the rapid neutron capture process (e.g., Sneden *et al.* 1996; Christlieb *et al.* 2004; Frebel *et al.* 2007; Roederer *et al.* 2014; Placco *et al.* 2017; Hansen *et al.* 2018; Holmbeck *et al.* 2018; Sneden *et al.* 1996).

The enhancements in the n-capture elements in the low mass, old metal poor stars in the Halo could be produced by either *s*-process or *r*-process. The enhancement in *s*-process is attributed to mass transfer from its relatively massive binary companion in its AGB phase usually comes when the binary component transfers the mass. Lucatello *et al.* (2006) has shown that most of the stars with *s*-process enhancements actually have an unseen binary component. On the other hand, enhancements in *r*-process is intrinsic to a star. Such nuclides could be produced under very exotic conditions and require extreme fine tuning of several physical parameters like temperature, mass, entropy, neutron flux, etc (Argast *et al.* 2004). The primary site for the production of *r*-process elements is still being debated. The main contenders are core-collapse supernovae, magneto-rotationally jet-driven supernovae and neutron star mergers (e.g., Lattimer and Schramm 1974; Rosswog *et al.* 2014; Lippuner *et al.* 2017) and neutron star-black hole mergers. It requires the order of a few seconds to produce these enrichments in the gas during such violent events.

The pattern of *r*-process enhancement is universal and robust. All the stars with chemical imprints of enriched *r*-process show the same patterns as the scaled solar abundance pattern. However, this universal nature of *r*-process pattern holds good for Ba and higher elements. In the lighter elements certain discrepancies have been noted (Barklem *et al.* 2005; Honda *et al.* 2006; Roederer *et al.* 2010; Hansen 2012; Yong *et al.* 2013). The current understanding states that the overall *r*-process enhancement in the stars could be a composite event rather than a single event. A weak *r*-process (also known as limited *r*-process) could be responsible for the production of the lighter elements but lacked sufficient neutron flux to produce the heavier elements (Truran *et al.* 2002; Frebel 2018) whereas the main *r*-process could be responsible for the production of the second peak elements and beyond. A mechanism called "Lighter Element Primary Process" or LEPP was also proposed by Travaglio *et al.* (2004) which preferentially produces the lighter elements in the

TABLE 5.1: Observation details for the reported objects observed through HESP at R 30000.

Object	obs.time	frames	SNR	Vmag	Rad.vel
SDSS J0043+1948	1800s	6	130.2	9.90	−196.5
SDSS J0648+3231	2400s	3	117.8	9.92	135.5
SDSS J0652+4105	2700s	3	68.0	11.36	98.5
SDSS J0921+5034	2400s	6	50.9	11.75	−130.5
SDSS J1730+4143	2400s	3	58.7	12.03	−133.0
SDSS J1930+6926	2400s	3	40.4	12.33	126.0
SDSS J2319+1917	2700s	3	77.0	11.60	−250.5

early galaxy.

The r-process enhanced stars are the ideal candidates to constrain and provide detailed information about sites and mechanisms of r-process enhancements at the earliest epochs.

5.2 Observations and analysis

The details of the observation of the newly detected $r-$process rich stars are listed in Table 5.1. The radial velocities are computed by cross-correlating the observed spectrum with the synthetic template. Stellar parameters are determined by the same methods as described in Chapter 2. The adopted stellar parameters are listed in Table 5.2. The elemental abundances for each star are given in Table 5.3 to 5.9

TABLE 5.2: Adopted stellar parameters for the stars

Object	Eff.temp(K)	log(g)	ξ	[Fe/H]
SDSS J0043+1948	4500	1.50	1.80	−2.25
SDSS J0648+3231	4800	1.70	1.50	−2.35
SDSS J0652+4105	5000	2.50	1.50	−2.56
SDSS J0921+5034	4800	1.75	1.50	−2.65
SDSS J1730+4143	4900	2.50	1.75	−2.85
SDSS J1930+6926	4600	2.10	1.50	−3.00
SDSS J2319+1917	4500	1.25	1.50	−2.10

5.3 Abundance

5.3.1 Light and Fe-peak elements

Abundances for carbon have been derived from the molecular band (known as g-band) around the 4313 Å region by using the method of spectrum synthesis. The spectral sitting for the g-band region is shown for three of the stars in Figure 5.1. The coloured lines indicate the synthetic spectra whereas the dots denote the observed spectrum. The best fit for each target star is marked in red. Nitrogen could be measured in only one of the stars. The CN molecular band at 3883 Å is used to derive the abundances of N by iteratively changing the N abundances while keeping the C abundances constant as derived from g-band synthesis. Due to the poor S/N towards the blue end of the spectrum. Measurement and detection from the CN band region are difficult using HESP spectra owing to the poor signal-to-noise at that region.

Among the light elements, abundances for Na, Mg, Al and Ca could be derived for all the stars. A mixture of equivalent width analysis and spectral synthesis were

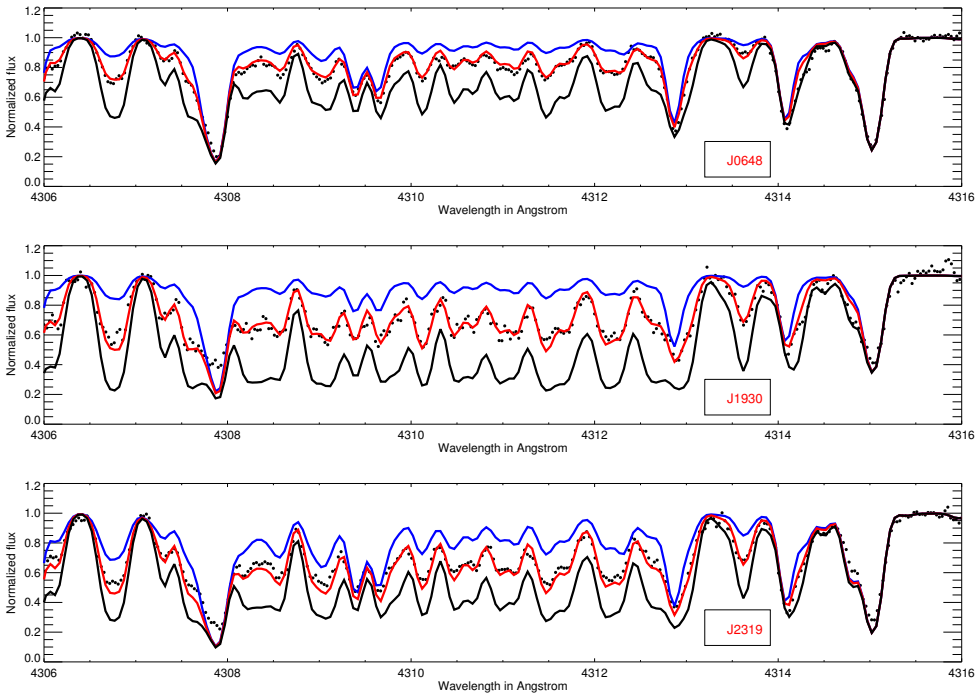

FIGURE 5.1: The fits for carbon molecular band for three of the $r-$process enhanced stars. Red marks the best spectral fit.

used for measuring the abundances. Spectrum synthesis was primarily used for the weaker lines whereas the method equivalent width measurement was employed for the relatively stronger and clean lines. The NLTE corrections were applied on a case to case basis for Na and Al as discussed by Baumueller and Gehren (1997); Andrievsky *et al.* (2008, 2007). The enhancement in α elements of about 0.4 dex as expected for typical halo stars was noted for all the objects except for SDSS J231923.85+191715.4 which indicates that it might have undergone a different star formation history in the sub-halo and the birth cloud have not received sufficient contribution from type-II supernovae.

Abundances could be derived for the Fe-peak elements like Sc, Cr, Mn, Co and Ni by the method of equivalent width analysis. Additionally, Cu and Zn could also be measured for a few of the target stars. The derived abundances are similar to the other normal stars of similar metallicity. They tend to track the Fe content of the star in a similar manner as described in Chapter 4.

5.3.2 Neutron capture elements

For the seven stars studied here, we could obtain abundances for up to 11 neutron-capture elements. The factors that primarily prohibit from measuring a larger number of n-capture elements in these stars are the following.

- Most of the target stars have relatively higher metallicity as seen in table 2 and hence show relatively stronger metal lines compared to the EMP or UMP stars. These lines cause blending which creates difficulty in measuring the weak n-capture elements.
- The poor signal-to-noise ratios at the blue end of the spectrum. The bulk of the spectral lines of the key n-capture elements fall around the 4000 Å region where the quality of signal gets degraded and no meaningful abundances could be derived.

The abundances for the elements Sr, Y, Zr, Ba, Ce, Nd, Sm, Eu, Dy and Th were measured using spectral synthesis which accounts for hyperfine transitions as well as blending of the absorption features. Sr is usually measured from two lines - 4077 Å and 4215 Å. The 4077 Å line is in some cases too strong for reliable measurement and in those cases only one line at 4215 Å is used to derive the abundance. Abundances for Ba is derived using four lines - 4554 Å, 4915 Å , 5853 Å and 6141 Å. NLTE corrections have also been taken into account for the strong 4554 Å, 4077 Å and 4215 Å lines following Short and Hauschildt (2006) which found only a small offset of +0.14 in case of Ba and even smaller offsets for Sr. Eu abundances could also be derived for all the stars; two lines at 4129 Å and 4205 Å were used to derive the Eu abundances. The spectral synthesis for three of the most important elements to classify *r*-process rich stars - Eu, Sr and Ba are shown in the top, middle and bottom panels of Figure 5.2.

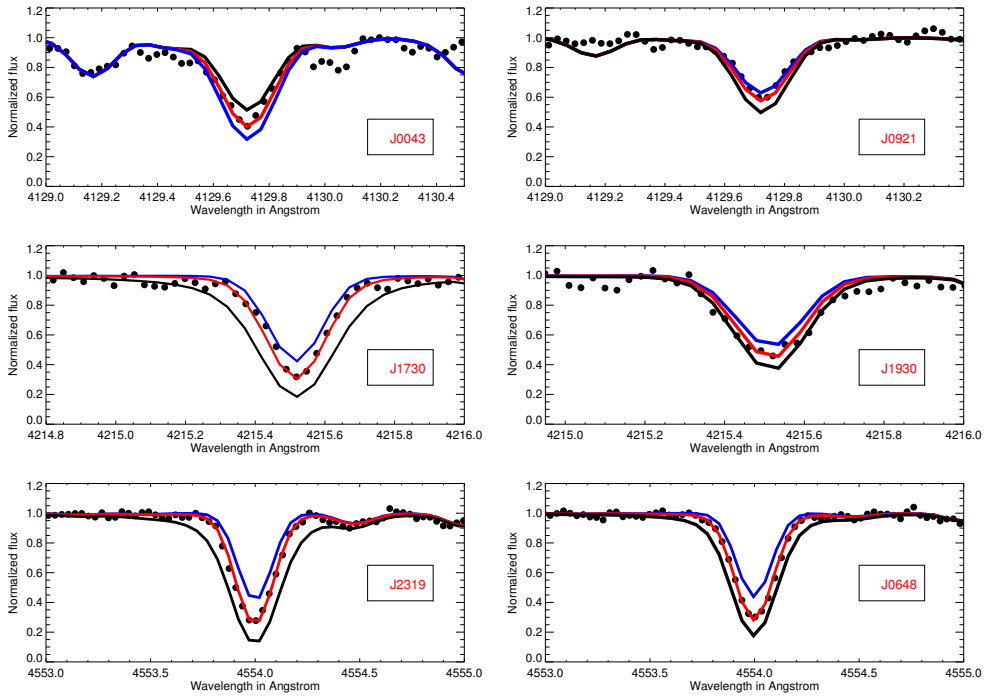

FIGURE 5.2: Spectral fitting for the key $r-$process elements Eu, Sr and Ba. Red is used to show the best fit spectra.

The elements like Sm, Dy and Th could be detected in very few of the targets depending upon brightness, [Fe/H], S/N and enhancement of the particular r-process elements. Syntheses for some of the other key r-process elements like Th, Nd, Ce, La, Zr and Y are shown for different stars in Figure 5.3.

5.3.3 Globular clusters

The Sr and Ba abundances were derived for the globular cluster NGC 1851. The photometric colors were obtained from Anderson *et al.* (2008) by cross-matching the coordinates of the stars from ESO. Then, the stellar parameters were derived by the standard isochrone fitting. The isochrones were obtained from Marigo *et al.* (2008); Girardi *et al.* (2000). Cluster metallicity was assumed for all the stars and the spectrum synthesis was done using TURBOSPECTRUM for different abundances of Sr and Ba. Examples of best fit spectra are shown in Figure 5.4.

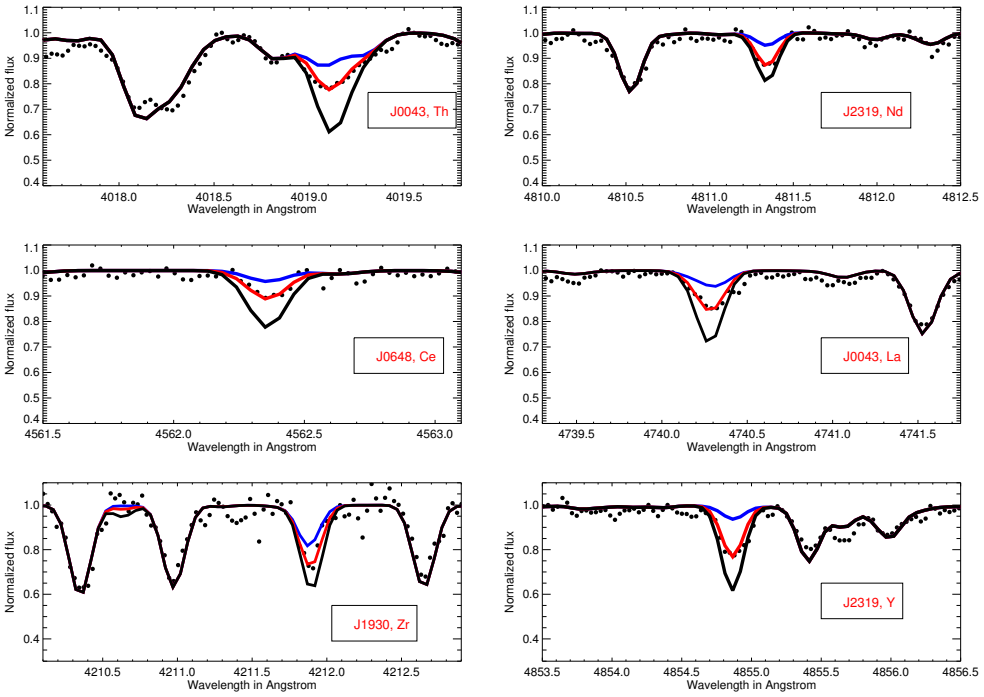

FIGURE 5.3: Spectral fits for some of the important $r-$process elements for different stars. Black indicates the observed spectra and red lines mark the best fit.

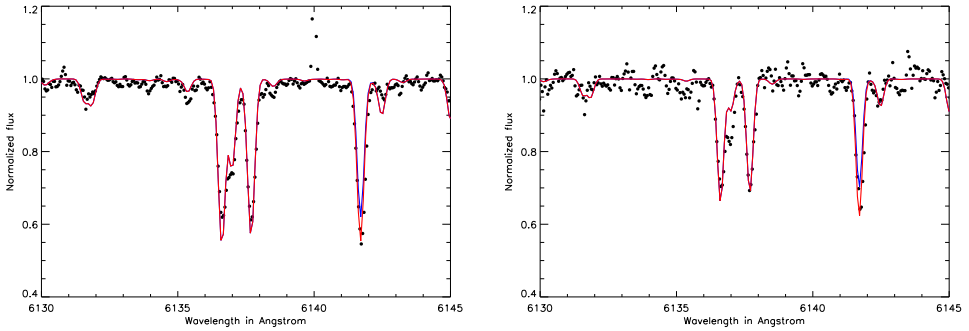

FIGURE 5.4: The fits for Ba lines using FLAMES-GIRAFFE data. Black represents the observations while red is used for synthetic spectrum.

TABLE 5.3: Elemental Abundance Determinations for SDSS J004305.27+194859.20 .

Elements	Species	N_{lines}	A(X)	Solar	[X/H]	[X/Fe]	σ
C	CH		5.25	8.43	−3.18	−0.93	synth
Na	Na I	2	4.0	6.24	−2.24	0.01	synth
Mg	Mg I	5	5.50	7.60	−2.10	0.15	synth
Al	Al I	1	2.96	6.45	−3.49	−1.24	0.09
Ca	Ca I	11	4.5	6.34	−1.84	0.41	0.06
Sc	Sc II	3	1.10	3.15	−2.15	0.10	0.11
Ti	Ti I	4	3.2	4.95	−1.75	0.50	0.13
	Ti II	13	3.1	4.95	−1.85	0.40	0.12
Cr	Cr I	6	3.10	5.64	−2.54	−0.29	0.08
	Cr II	1	3.85	5.64	−1.81	0.44	0.09
Mn	Mn I	5	2.7	5.43	−2.73	−0.48	0.14
Co	Co I	2	2.60	4.99	−2.39	−0.14	0.08
Ni	Ni I	4	3.80	6.22	−2.42	−0.17	synth
Zn	Zn I	1	2.60	4.56	−1.96	0.29	synth
Sr	Sr II	2	0.75	2.87	−2.12	0.13	synth
Y	Y II	2	0.00	2.21	−2.21	0.04	synth
Zr	Zr II	3	0.75	2.58	−1.68	0.57	synth
Ba	Ba II	2	0.50	2.18	−1.68	0.57	synth
La	La II	3	−0.60	1.11	−1.71	0.54	synth
Ce	Ce II	3	−0.30	1.58	−1.88	0.37	synth
Nd	Nd II	2	−0.25	1.42	−1.67	0.58	synth
Sm	Sm II	2	−0.69	0.96	−1.65	0.60	synth
Eu	Eu II	1	−0.75	0.52	−1.27	0.98	synth
Dy	Dy II	2	−0.50	1.10	−1.60	0.65	synth
Th	Th II	1	−0.95	0.02	−0.97	1.28	synth

σ indicates the random error.

TABLE 5.4: Elemental Abundance Determinations for SDSS J064813.33+323105.2 .

Elements	Species	N_{lines}	A(X)	Solar	[X/H]	[X/Fe]	σ
C	CH		5.50	8.43	−2.93	−0.58	synth
Na	Na I	2	4.11	6.21	−2.10	0.25	synth
Mg	Mg I	5	5.60	7.59	−1.99	0.36	synth
Al	Al I	1	2.41	6.43	−4.02	−1.67	0.12
Ca	Ca I	11	4.43	6.32	−1.89	0.46	0.09
Sc	Sc II	3	0.89	3.15	−2.26	0.09	0.08
Ti	Ti I	4	3.07	4.93	−1.86	0.49	0.10
	Ti II	13	2.90	4.93	−2.03	0.32	0.06
Cr	Cr I	6	3.32	5.62	−2.30	0.05	0.06
	Cr II	1	3.54	5.62	−2.08	0.27	0.09
Mn	Mn I	5	2.77	5.42	−2.65	−0.30	0.13
Co	Co I	2	2.68	4.93	−2.25	0.10	0.09
Ni	Ni I	4	4.32	6.20	−1.88	0.47	synth
Cu	Cu I	2	1.03	4.19	−3.16	0.81	synth
Zn	Zn I	1	2.44	4.56	−2.12	0.23	synth
Sr	Sr II	2	0.75	2.83	−2.08	0.27	synth
Y	Y II	2	0.00	2.21	−2.21	0.14	synth
Zr	Zr II	3	0.75	2.59	−1.84	0.51	synth
Ba	Ba II	2	0.25	2.25	−2.00	0.35	synth
Ce	Ce II	3	−0.46	1.58	−2.04	0.31	synth
Nd	Nd II	2	−0.39	1.42	−1.81	0.54	synth
Sm	Sm II	2	−0.81	0.96	−1.77	0.58	synth
Eu	Eu II	1	−1.15	0.52	−1.67	0.68	synth

σ indicates the random error.

TABLE 5.5: Elemental Abundance Determinations for SDSS J065252.76+410506 .

Elements	Species	N_{lines}	A(X)	Solar	[X/H]	[X/Fe]	σ
Li	Li I	1	1.60				synth
C	CH		5.75	8.43	−2.68	−0.13	synth
Na	Na I	2	4.23	6.21	−1.98	0.57	synth
Mg	Mg I	5	5.62	7.59	−1.97	0.58	synth
Al	Al I	1	1.96	6.43	−4.47	−1.92	0.18
Ca	Ca I	11	4.14	6.32	−2.18	0.37	0.08
Sc	Sc II	5	1.00	3.15	−2.15	0.40	0.10
Ti	Ti I	4	2.94	4.93	−1.99	0.56	0.15
	Ti II	13	2.78	4.93	−2.15	0.40	0.11
Cr	Cr I	6	3.04	5.62	−2.58	−0.03	0.16
	Cr II	1	3.79	5.62	−1.83	0.75	0.09
Mn	Mn I	5	2.71	5.42	−2.71	−0.16	0.12
Co	Co I	2	2.39	4.93	−2.54	0.01	0.08
Ni	Ni I	4	3.82	6.20	−2.38	0.17	synth
Zn	Zn I	1	2.57	4.56	−1.99	0.56	synth
Sr	Sr II	2	1.00	2.83	−1.83	0.72	synth
Y	Y II	2	0.25	2.21	−1.96	0.59	synth
Zr	Zr II	3	0.75	2.59	−1.84	0.71	synth
Ba	Ba II	2	0.50	2.25	−1.75	0.80	synth
La	La II	2	−0.87	1.11	−1.98	0.57	synth
Nd	Nd II	2	0.0	1.42	−1.42	1.13	synth
Eu	Eu II	1	−1.0	0.52	−1.52	1.03	synth

σ indicates the random error.

TABLE 5.6: Elemental Abundance Determinations for SDSS J092157.27+503404.7 .

Elements	Species	N_{lines}	A(X)	Solar	[X/H]	[X/Fe]	σ
C	CH		5.50	8.43	−2.93	−0.28	synth
Na	Na I	2	4.08	6.21	−2.13	0.52	synth
Mg	Mg I	5	5.38	7.59	−2.21	0.44	synth
Al	Al I	1	2.39	6.443	−4.04	−1.39	0.21
Ca	Ca I	11	4.13	6.32	−2.19	0.46	0.08
Sc	Sc II	3	0.28	3.15	−2.87	−0.22	0.06
Ti	Ti I	4	2.42	4.93	−2.51	0.14	0.14
	Ti II	13	2.65	4.93	−2.28	0.37	0.08
Cr	Cr I	6	2.95	5.62	−2.67	−0.02	0.13
	Cr II	1	3.57	5.62	−2.05	0.60	0.10
Mn	Mn I	5	2.04	5.42	−3.38	−0.73	0.15
Co	Co I	2	2.06	4.99	−2.87	−0.22	0.05
Ni	Ni I	4	4.18	6.20	−2.02	0.63	synth
Zn	Zn I	1	2.44	4.56	−2.12	0.53	synth
Sr	Sr II	2	0.50	2.83	−2.33	032	synth
Y	Y II	2	0.0	2.21	−2.21	0.44	synth
Zr	Zr II	3	0.30	2.59	−2.29	0.36	synth
Ba	Ba II	2	0.0	2.25	−2.25	0.40	synth
La	La II	3	−0.65	1.11	−1.76	0.89	synth
Ce	Ce II	3	0.15	1.58	−1.43	1.22	synth
Nd	Nd II	2	−0.45	1.42	−1.87	0.78	synth
Sm	Sm II	2	−1.00	0.96	−1.96	0.69	synth
Eu	Eu II	1	−0.90	0.52	−1.42	1.23	synth
Dy	Dy II	2	−0.80	1.10	−1.90	0.75	synth

σ indicates the random error.

TABLE 5.7: Elemental Abundance Determinations for SDSS J173025.57+414334.7 .

Elements	Species	N_{lines}	A(X)	Solar	[X/H]	[X/Fe]	σ
C	CH		5.50	8.43	−2.93	−0.08	synth
N	CN		6.00	7.83	−1.83	1.02	synth
Na	Na I	2	3.50	6.21	−2.71	0.14	synth
Mg	Mg I	5	5.30	7.59	−2.29	0.56	synth
Al	Al I	1	2.55	6.43	−3.88	−1.03	0.16
Ca	Ca I	11	3.84	6.32	−2.48	0.37	0.09
Sc	Sc II	3	0.30	3.15	−2.85	0.00	0.07
Ti	Ti I	4	2.70	4.93	−2.23	0.62	0.09
	Ti II	13	2.80	4.93	−2.13	0.72	0.06
Cr	Cr I	6	2.80	5.62	−2.82	0.03	0.12
	Cr II	1	3.00	5.62	−2.62	0.23	0.11
Mn	Mn I	5	2.10	5.42	−3.32	−0.47	0.18
Co	Co I	2	2.15	4.93	−2.78	0.07	0.14
Ni	Ni I	4	3.6	6.22	−2.62	0.23	synth
Sr	Sr II	2	0.50	2.83	−2.33	0.52	synth
Y	Y II	2	0.00	2.21	−2.21	0.64	synth
Zr	Zr II	3	0.50	2.58	−2.08	0.77	synth
Ba	Ba II	2	0.00	2.25	−2.25	0.60	synth
Eu	Eu II	1	−1.25	0.52	−1.77	1.08	synth

σ indicates the random error.

TABLE 5.8: Elemental Abundance Determinations for SDSS J193018.91+692636.1 .

Elements	Species	N_{lines}	A(X)	Solar	[X/H]	[X/Fe]	σ
C	CH		5.25	8.43	−3.18	−0.18	synth
Na	Na I	2	3.10	6.21	−2.11	−0.11	synth
Mg	Mg I	5	5.24	7.59	−2.35	0.65	synth
Al	Al I	1	1.74	6.43	−4.69	−1.69	0.14
Ca	Ca I	11	3.88	6.32	−2.44	0.56	0.11
Sc	Sc II	3	−0.42	3.15	−3.57	0.67	0.07
Ti	Ti I	4	2.60	4.93	−2.33	0.57	0.10
	Ti II	13	1.78	4.93	−3.15	0.15	0.08
Cr	Cr I	6	2.59	5.62	−3.03	−0.03	0.11
	Cr II	1	3.50	5.64	−2.14	0.86	0.06
Mn	Mn I	5	2.94	5.42	−2.48	0.42	0.18
Co	Co I	2	1.12	4.93	−3.81	−0.81	0.14
Ni	Ni I	4	3.10	6.20	−3.10	−0.10	synth
Sr	Sr II	2	−0.50	2.83	−3.33	−0.33	synth
Y	Y II	2	−0.10	2.21	−2.31	0.69	synth
Zr	Zr II	3	0.50	2.59	−2.09	0.91	synth
Ba	Ba II	2	−0.75	2.25	−3.00	0.00	synth
Ce	Ce II	3	−0.30	1.58	−1.88	1.12	synth
Eu	Eu II	1	−1.50	0.52	−2.02	0.98	synth

σ indicates the random error.

TABLE 5.9: Elemental Abundance Determinations for SDSS J231923.85+191715.4 .

Elements	Species	N_{lines}	A(X)	Solar	[X/H]	[X/Fe]	σ
C	CH		5.75	8.43	−2.68	−0.58	synth
Na	Na I	2	4.12	6.21	−2.09	0.01	synth
Mg	Mg I	5	5.58	7.59	−2.01	0.09	synth
Al	Al I	1	2.42	6.43	−4.01	−1.91	0.17
Ca	Ca I	11	4.17	6.32	−2.15	−0.05	0.08
Sc	Sc II	3	0.82	3.15	−2.33	−0.23	0.09
Ti	Ti I	4	2.89	4.93	−2.04	0.06	0.15
	Ti II	13	2.63	4.93	−2.30	−0.20	0.11
Cr	Cr I	6	3.35	5.62	−2.27	−0.17	0.06
	Cr II	1	3.5	5.62	−2.12	−0.02	0.04
Mn	Mn I	5	3.80	5.42	−1.62	0.48	0.19
Co	Co I	2	3.15	4.93	−1.78	0.32	0.12
Ni	Ni I	4	4.45	6.20	−1.75	0.35	synth
Zn	Zn I	1	2.27	4.56	−2.29	−0.19	synth
Sr	Sr II	2	0.75	2.83	−2.08	0.02	synth
Y	Y II	2	0.00	2.21	−2.21	−0.11	synth
Zr	Zr II	3	0.50	2.59	−2.09	0.01	synth
Ba	Ba II	2	0.00	2.25	−2.25	−0.15	synth
La	La II	3	−1.20	1.11	−2.31	−0.21	synth
Ce	Ce II	3	−0.75	1.58	−2.33	−0.23	synth
Nd	Nd II	2	−0.43	1.42	−1.85	0.25	synth
Eu	Eu II	1	−1.15	0.52	−1.67	0.43	synth

σ indicates random error.

5.4 Discussion

5.4.1 New identifications of *r*-process enhanced stars

In this study, we have identified 7 new stars in the Halo with moderate to high enhancement in *r*-process abundances. Following the standard definition laid down by Beers and Christlieb (2005), three of them are r-II stars ([Eu/Fe] $> +1.0$ and [Ba/Eu] < 0.0) while the other four are r-I stars ($1.0 >$ [Eu/Fe] > 0.3 and [Ba/Eu] < 0.0) as shown in Table 5.10. The distribution over metallicity of the objects range from [Fe/H] $= -2.95$ to [Fe/H] $= -2.10$ and thus spanning a range of 0.85 dex. This metal poor end is more suited to find such stars as the *r*-process signatures are not wiped out or diluted by subsequent chemical evolution. At higher metallicities, stars with the strongest *r*-process signatures (r-II stars) could be detected (e.g 18024226-4404426 at [Fe/H] $= -1.55$). The moderate spread in [Eu/Fe] in our sample of 0.80 dex could be attributed to the contributions from several *r*-process events (Sneden *et al.* 2000; Travaglio *et al.* 2004; Hansen *et al.* 2018). The spread of our sample is shown in Figure 5.5 with all the program stars marked in red diamonds, The data for reference has been compiled from the first data release of *r*-process alliance and few other well known *r*-process rich stars. The dashed marks the different levels of enhancements demarcating between r-I, r-II and limited-r stars.

5.4.2 The sub populations

As we have discussed earlier, enhancement in n-capture elements in a metal poor star could be caused by both *r*-process and *s*-process. The best way to determine the contribution of one process relative to the other is by measuring the abundance of an element which could be produced by only one process with respect to

TABLE 5.10: Classification of the stars

Object	[Fe/H]	[C/Fe]	[Sr/Fe]	[Ba/Fe]	[Eu/Fe]	[Ba/Eu]	[Sr/Ba]	class
J0043	−2.25	−0.93	0.13	0.57	0.98	−0.41	−0.44	r-I
J0648	−2.35	−0.58	0.27	0.35	0.68	−0.33	−0.08	r-I
J0652	−2.57	−0.13	0.72	0.80	1.03	−0.23	−0.08	r-II
J0921	−2.65	−0.28	0.32	0.40	1.23	−0.83	−0.08	r-II
J1730	−2.85	−0.08	0.52	0.60	1.08	−0.48	−0.08	r-II
J1930	−3.00	−0.18	−0.33	0.00	0.98	−0.98	−0.33	r-I
J2319	−2.10	−0.58	0.02	−0.15	0.43	−0.58	0.17	r-I

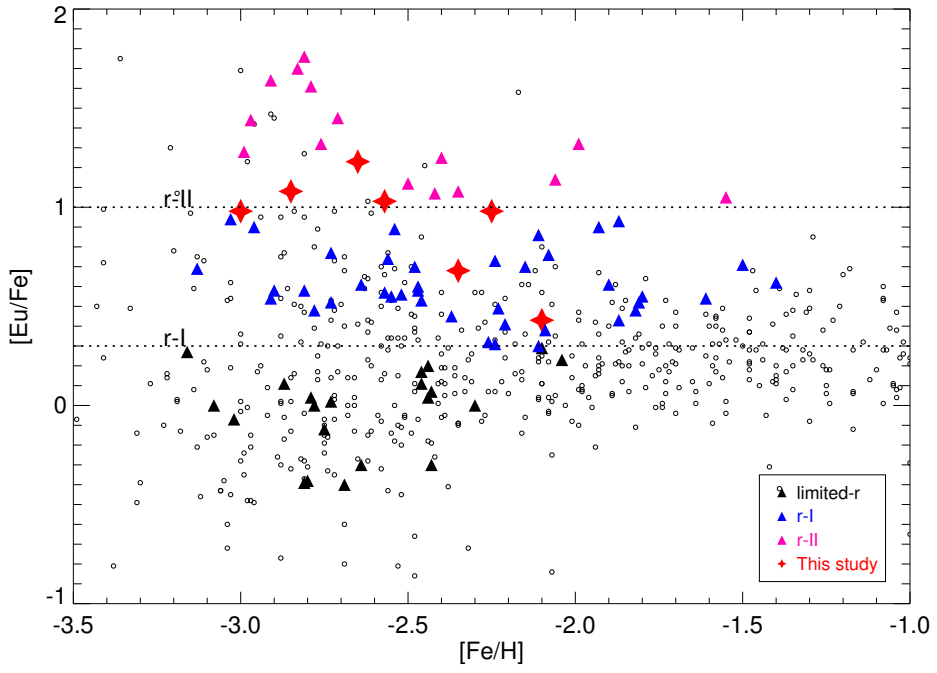

FIGURE 5.5: Distribution of [Eu/Fe] for the program stars as a function of [Fe/H] and are marked in filled red diamonds. The r-I (blue triangles),r-II (pink triangles) and limited-r (black triangles) are marked for comparison and are compiled from the *r*-process alliance (Hansen *et al.* 2018; Holmbeck *et al.* 2018; Placco *et al.* 2017; Cain *et al.* 2018). The open circles are the ones with measured Eu abundances and are taken from SAGA database. The dashed lines are marked to distinguish the different classes of *r*-process enhanced stars at [Eu/Fe] = +0.3 and [Eu/Fe] = +1.0.

another element which could be produced by both the process. Eu is a representative of pure r-process element (Simmerer *et al.* 2004) at low metallicities whereas Ba is predominantly produced by s-process but r-process also contributes at low metallicities. Pb is the end product after completion of s-process and could be the best indicator but we were unable to detect Pb in any of our spectra. Thus, [Eu/Ba] could be used as a standard yardstick to probe the relative contribution of one process to the other (Barklem *et al.* 2005; Frebel and Norris 2015b).

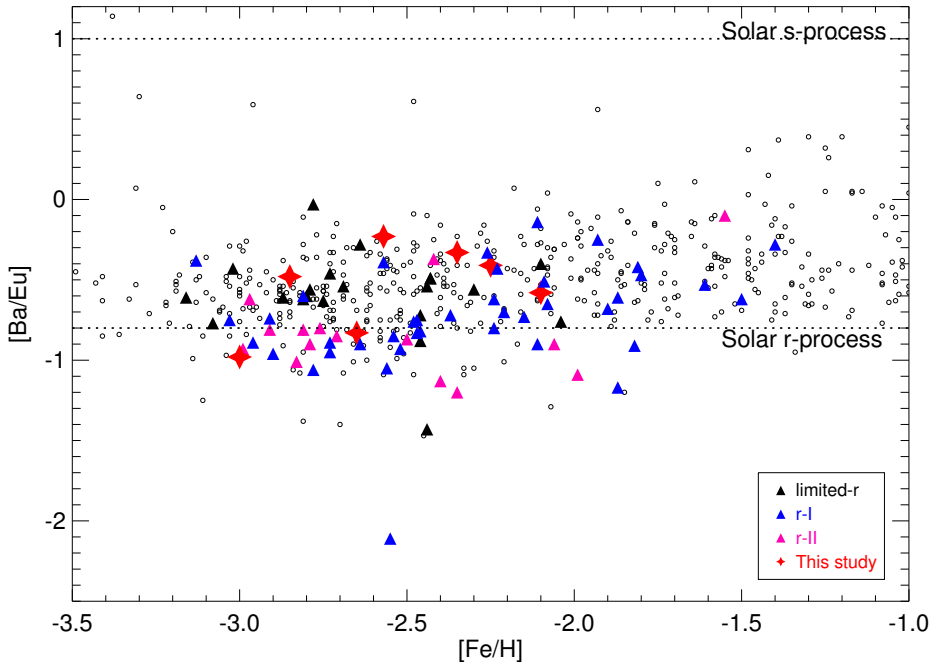

FIGURE 5.6: Distribution of [Ba/Eu] for the program stars as a function of [Fe/H] and are marked in filled red diamonds. The r-I (blue triangles), r-II (pink triangles) and limited-r (black triangles) are marked for comparison and are compiled from the r-process alliance Hansen *et al.* (2018), Holmbeck *et al.* (2018), Placco *et al.* (2017), Cain *et al.* (2018). The open circles are the ones with measured Eu abundances and are taken from SAGA database. The dashed lines represent the solar system r-process fraction at [Ba/Eu] = −0.80 and solar system s-process fraction at [Ba/Eu] = 1.0 Simmerer *et al.* (2004)

[Ba/Eu] is often used as an indicator of the degree of relative enhancements from r-process and s-process contributions. Following Simmerer *et al.* (2004), [Ba/Eu] < -0.80 implies a pure r-process origin whereas [Ba/Eu] > 1.0 marks the solar s-process. As expected, all the known r-process enhanced stars show [Ba/Eu] $<$

0.0, indicating a higher contribution from r-process in comparison to s-process. However, only a few of those lies in the paradigm of the pure r-process origin with [Ba/Eu] < -0.80. Among our sample, only two of the stars (one r-I and one r-II) represent a pure r-process origin as shown in Figure 5.6.

A few of the r-process enhanced stars show deviations from the scaled solar patterns for the lighter elements and are known as limited r-process enhanced stars as we have discussed earlier. The reason is attributed to a separate weak r-process event that preferentially produces the lighter elements. In Figure 5.7, the ratio of [Sr/Ba] has been plotted against [Eu/Fe]. The limited-r stars marked in black occupies the top left corner of the plot. None of our sample of stars is found to belong to this category. The ratio of [Sr/Ba] declines steadily as [Eu/Fe] increases which again suggests different sites and mechanisms for the production of the lighter elements. Many studies suggested that high entropy neutrino winds from a core collapse supernovae could be responsible for the limited-r stars (Woosley and Hoffman 1992; Kratz *et al.* 2007; Arcones and Montes 2011; Wanajo 2013). 2013)

5.4.3 A case of actinide boost

The abundance pattern of the light and Fe-peak elements in SDSS J004305.27+194859.20 is very similar to a typical metal poor Halo star. Among the light n-capture elements Sr, Y and Zr could be measured and they show a spread which could be attributed to a limited or weak r-process (Wanajo and Ishimaru 2006), (Hansen 2012) ; (Frebel 2018)) and has a distinct history of production from the $2^n d$ and $3^r d$ r-process peaks. The lower values of the first r-process peak elements indicate a marginal contribution from the limited r-process.

The heavy n-capture elements show a lower degree of scatter and compare well with the scaled solar abundances and the other r-process rich stars from literature.

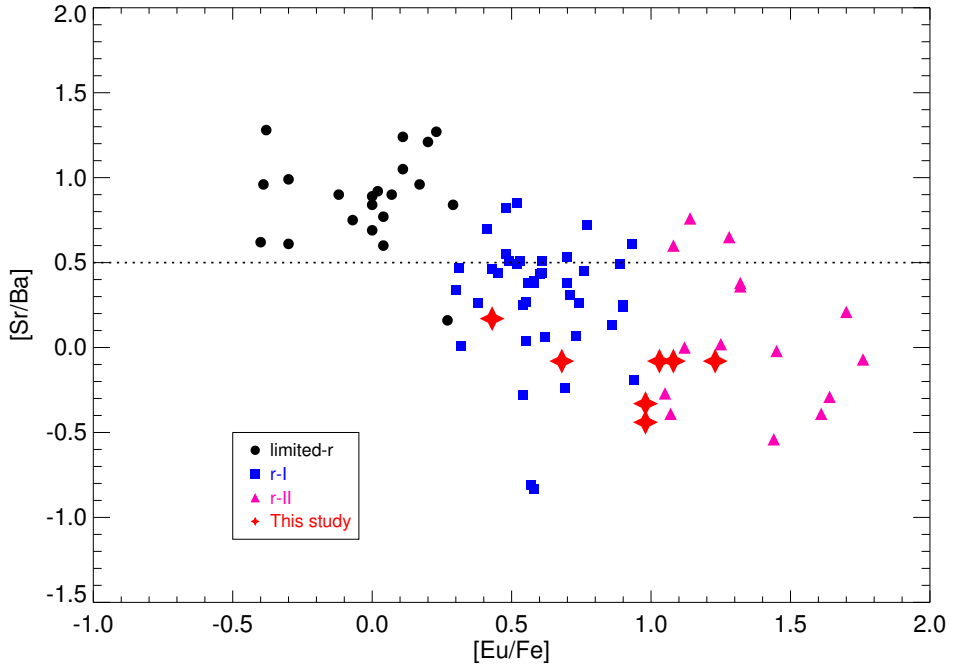

FIGURE 5.7: Distribution of [Sr/Ba] for the program stars as a function of [Eu/Fe] and are marked in filled red diamonds. The r-I (blue squares), r-II (pink triangles) and limited-r (black circles) plotted for comparison were compiled from the *r*-process alliance (Hansen *et al.* 2018), Holmbeck *et al.* (2018), Placco *et al.* (2017), Cain *et al.* (2018).

Unfortunately due to the poor signal-to-noise ratio towards the blue end of the spectrum, we could get abundances for only Ba, La, Ce, Nd, Sm, Eu and Dy out of the second *r*-process peak elements. They show a consistent level of elevation as seen in Table 5.3 which is expected in the main *r*-process.

Th is one of the more difficult elements to measure in a spectrum. We could measure the abundances for Th II line at 4019 Å and calculated the value of [Th/Fe]= 1.28. The synthesis for Th II line is shown in Figure 2. The measured [Th/Eu]= 0.30 shows a high actinide-to-lanthanide ratio and shows an actinide boost for SDSS J004305.27+194859.20 . The log ϵ(Th/Eu) = -0.20 is higher than the non-actinide boost stars which typically show a value around -0.50 (e.g. Holmbeck *et al.* 2018). The comparison of SDSS J004305.27+194859.20 with other *r*-process enhanced stars with measured Th abundances are shown in Figure 3.

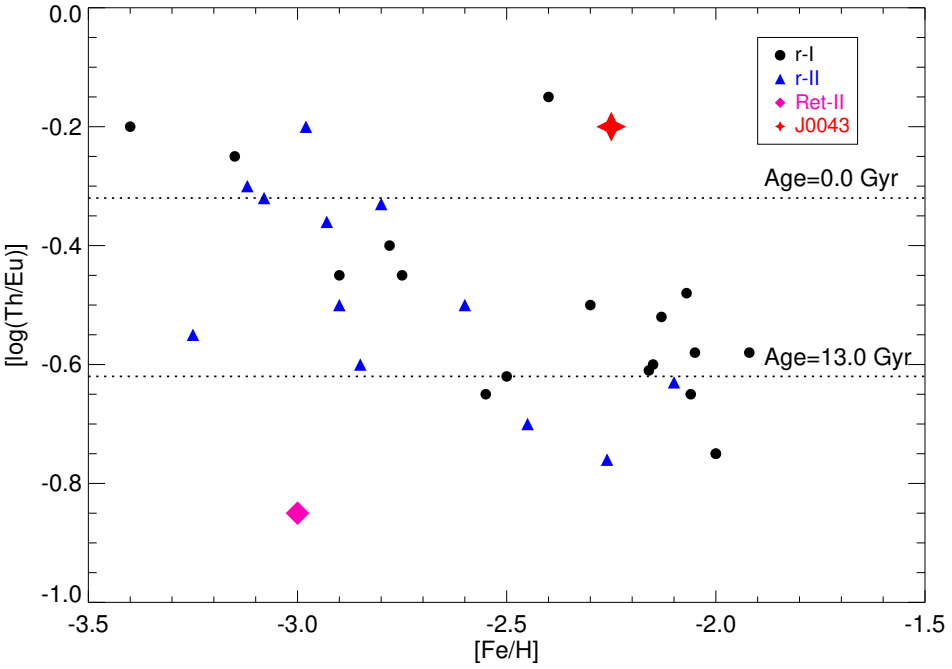

FIGURE 5.8: Distribution of logϵ[Th/Eu] for stars with detection of Th as a function of [Eu/Fe]. The program star in this study is marked in filled red diamond s. The r-I (black filled circles), r-II (blue triangles) are plotted for comparison were compiled from the *r*-process Alliance-II (Sakari *et al.* 2018),Holmbeck *et al.* (2018), Roederer *et al.* (2014), Hill *et al.* (2017), and Placco *et al.* (2017). The pink square shows the bright r-II star in Reticulum II galaxy. The dashed lines mark the corresponding ages. The stars with a high degree of actinide boost occupy the top region of the diagram with un-physical ages from [Th/Eu] ratios.

The presence of actinide boost in a significant number of stars demonstrates the variation in the production of actinides although it might be difficult to decouple them from the main *r*-process production sites (Holmbeck *et al.* 2018).

Detection and measurement of actinides also help in the determination of age using the technique of radioactive decay dating (Placco *et al.* 2017). Since U could not be measured Th/Eu chronometer could be used using the production ratios from (Schatz *et al.* 2002). However, in the case of actinide boosts using the ratio of Th/Eu leads to unphysical values as the measured values tend to be higher than the theoretically obtained initial production ratios. The existing models of *r*-process nucleosynthesis fail to successfully derive the yields of actinide-boost stars.

Thus, despite having measurements for Th and Eu, age could not be determined in case of SDSS J004305.27+194859.20 . Measurement of U could help to use the Th/U chronometer and derive the stellar age as both the elements are likely to be affected by the actinide boost proportionately.

5.4.4 *r*-process abundances in Globular cluster stars

Abundances of the key elements are also derived from archival data for NGC 1851. Earlier works have mainly concentrated on multiple generations of stars in the cluster and the difference in elemental abundances of these populations. The key criteria used for such classification are the chemical anti-correlations like O-Na and Mg-Al. The second generation stars are found to be enhanced in sodium and aluminium and depleted in magnesium and oxygen. For our analysis, we have classified the stars into first generation (FG) and second generation (SG) following Gratton *et al.* (2012b).

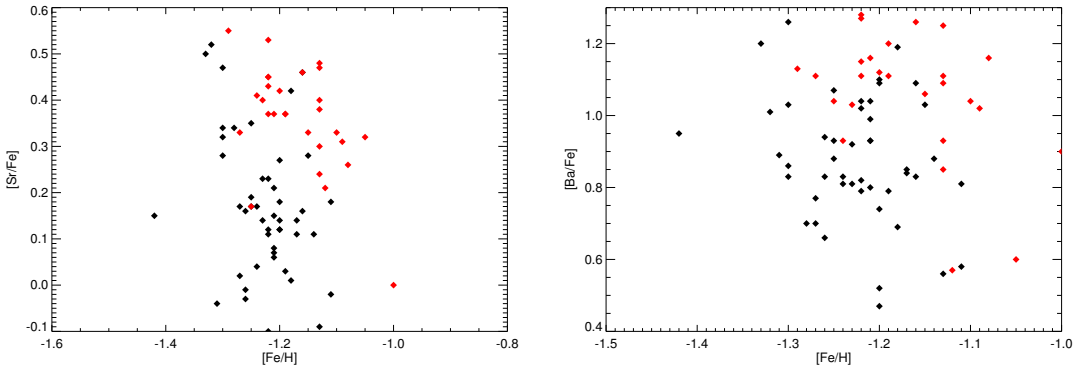

FIGURE 5.9: The distribution for [Sr/Fe] and [Ba/Fe] as a function of [Fe/H]. Red points indicate the stars of the faint SGB associated to the older population whereas black points mark the blue SGB associated with the younger population.

The distribution of neutron capture elements is explored in Figures 5.9 and 5.10. Ba and Sr are found to be comparatively enhanced in the first generation stars.

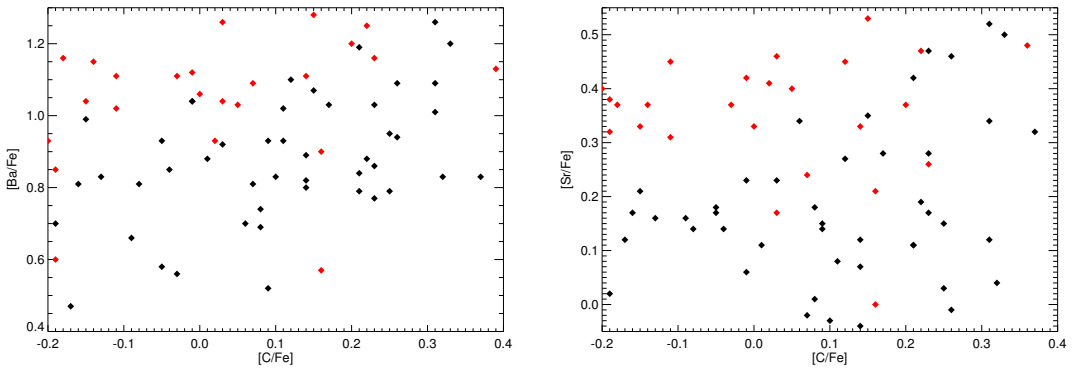

FIGURE 5.10: Trends for [Sr/Fe] and [Ba/Fe] with [C/Fe] for the two populations.

The origin of the excess could be *s*-process as well as *r*-process. A good tool to quantify *s*-process contamination could be carbon. If *s*-process rich material is transferred from an AGB star to its component then carbon is also expected to be transferred with the same. In Figure 5.10, we have shown the distribution of strontium and barium with carbon for both the populations. Though a trend is seen, large overall scatter is found to exist. The FG stars are found to be elevated in n-capture elements with respect to C which indicates that they were most likely to be polluted by an event prior to the formation of the SG stars. This indicates towards an $r-$process origin of the relative enhancement of these elements.

5.4.5 Origin of *r*-process

Strontium is the surrogate for light *r*-process elements and could be produced by both core collapse supernovae as well as neutron star-neutron star mergers whereas barium being the representative element for heavy *r*-process could be produced by neutron star-neutron star mergers alone as described in Chapter 3. Figure 5.11 shows the distribution of the FG stars of NGC 1851 and all the program stars with $r-$process enhancement. The red line at the bottom marks the paradigm of NS-NS mergers while the blue curve indicates CCSNE contributions. NGC 1851 and

other globular clusters are found to occupy the bottom of the plot showing NS-NS mergers to be the primary contributor for the enhancement in $r-$process which is expected due to the dense environment compared to the Galactic halo. The RPE stars are found to be distributed evenly in the plot indicating contributions from both the sources. In this plot, X-axis does not represent the formation epoch as the globular clusters might have formed at the same epoch as the EMP stars of the Halo but have migrated from their original position towards the current location as shown in the plot due to the process of enrichment over the evolutionary time scale. We have also plotted the very well known r-process enhanced satellite dwarf spheroidal galaxy reticulum II which also demonstrates that the primary origin of these dense systems now in the Halo is NS-NS merger.

All the globular clusters being placed slightly towards the lower side indicates maximum NS mergers. Mean abundances of a few of the well studied globular clusters have also been shown in blue upward triangles which also fall along the bottom curve. The GC escapees as shown in Chapter 3 have also been marked in pink diamonds.

Figure 5.11 also indicates that the halo $r-$process rich population might have received contributions from type-II supernova and NS-NS merger irrespective of their classification (r-I, r-II etc) as they are apparently mixed in the diagram. Search for the signatures of unmixed Ba which is taken to be of $r-$process origin is probed in figure 5.12. The $r-$process rich stars expectedly segregate towards the right with a higher abundance of [Ba/H] but again they are mixed which makes it difficult to interpret the results.

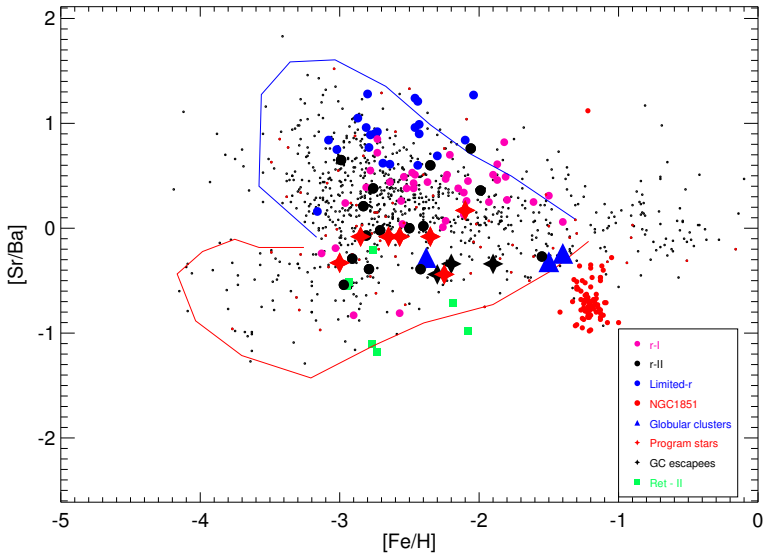

FIGURE 5.11: Probing the origin of $r-$process. The red line indicates NS-NS merger to be dominant while the blue curve represents dominance of CCSNe. The different $r-$process enhanced halo populations are marked in the figure. NGC 1851 is marked in filled red circles.

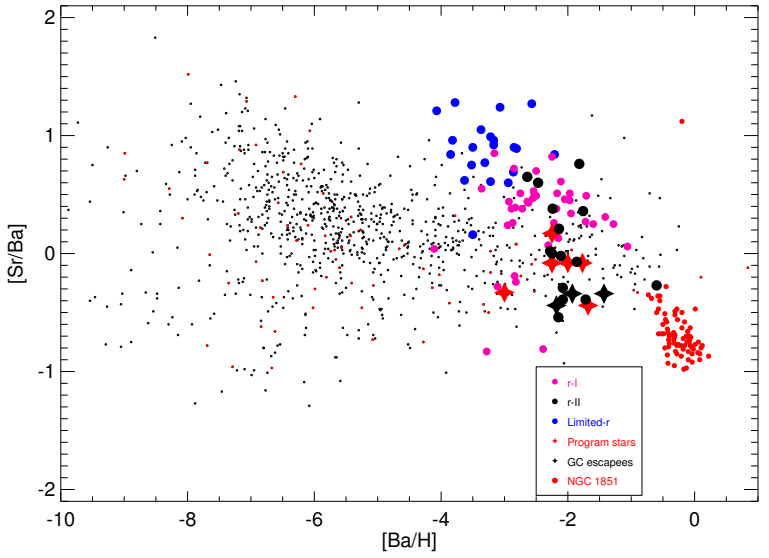

FIGURE 5.12: Distribution of the $r-$process enhanced population in [Ba/H]vs[Sr/Ba] plane. The $r-$process population is found to contain the expected higher content of [Ba/H].

5.5 Conclusion

Theoretical and observational studies have shown that robust r-process production is possible among a limited number of sites. The r-process rich stars show direct observational evidence of such rare events and the elemental abundance ratios are likely to be unaltered by mixing and dilution inside the star as well as by the primordial gas cloud. These objects help with the theoretical modelling and understanding of the physical conditions of r-process production and provide very valuable information. In this work, we have identified seven new r-process rich stars that are very bright. These are ideal candidates for detailed isotopic abundance estimation with larger 8-10m class telescopes. One of the r-process rich star with Thorium detection is the brightest known star of its kind. This offers unique possibility for detection of several key n-capture elements using larger telescopes. We also studied r-process enhancement among Globular cluster stars and found that the FG stars in the Globular cluster NGC 1851 show higher n-capture elements compared to the SG stars of the cluster. We show that the n-capture elements are likely r-process in origin, due to the no associated strong carbon enhancement among them. Finally, in this work, we compared the abundances ratios of light and heavy r-process element of stars in different environments (e.g. Halo, Globular clusters, Satellite galaxies, r-process rich and normal-EMP stars). Since NS-NS mergers are considered as potential site for the production of heavy r-process elements, the enhancement of these elements marks the time of such event and serve as a good chronometer and help probe the star formation history. In the case of Globular clusters, diagnosis of heavy and light r-process elements can also help to understand the origin of multiple stellar populations. Future large dedicated spectroscopic surveys will provide the evolution r-process abundance ratios among a wide range of stellar systems.

Chapter 6

Li distribution and new VMP stars from HESP-GOMPA survey

6.1 Introduction

The discovery of a large number of metal poor stars has provided great opportunities to study the pristine conditions that existed in the early universe when these old stellar objects were formed. Among the many studies that could be conducted on these stars, detection and measurement of Li carries a great importance. Li is the only element in the periodic table that owes its origin to the big-bang nucleosynthesis. All other elements can be cooked up in stellar interiors or other exotic stellar events.

Li is also a very fragile element which easily gets destroyed when exposed higher temperatures. A consistent depletion is seen in Li content as a star ascends the giant branch and the stellar surface is exposed to the hot tenuous matter from the stellar interior due to the convective channels that are formed this phase. This is

called evolutionary mixing which largely depletes A(Li).

Spite and Spite (1982) did a pioneering study on the abundance of Li in the unevolved older population of stars in the halo and disk. A constant abundance of Li of A(Li) = 2.2 was obtained and was subsequently termed as the "Li plateau" which was much lower than the cosmological predictions. Since then there have been many studies and efforts to understand the Li plateau and solve the Li problem (e.g. Pinsonneault *et al.* 1999; Bonifacio *et al.* 2007b; Korn *et al.* 2006 among many others). The most metal poor stars were found to have a Li abundance lower than the Spite plateau (e.g. Bonifacio *et al.* 2015) causing the "breakdown of Spite plateau" (Aoki *et al.* 2009) and a small slope of Li plateau was also discovered (Ryan *et al.* 1999) as more stars with Li detection were studied.

Apart from Li, the abundances of other important elements in the Very Metal Poor (VMP) stars are of considerable interest to the astronomers to constrain the nature of pollution received by the natal gas clouds during the formation epoch of these VMP stars. They also provide valuable constraints for improvements in the models of nucleosynthesis. More discoveries of stars of [Fe/H]<-2.0 with or without anomaly is crucial for better understanding about the events in the early universe.

6.2 Observations

The observations of the VMP stars were carried out over a total period of two years. The details of the observation of the sample are given in Chapter 2. The interesting candidates were observed for several indicates to build a good signal-to-noise ratio. The stellar parameters for the observed stars were determined using the same methodology as discussed in Chapter 2. The adopted stellar parameters

TABLE 6.1: Adopted stellar parameters for the stars

Object	Eff.temp(K)	log(g)	ξ	[Fe/H]	A(Li)
SDSS J1937+5024	4800	1.50	1.50	−2.20	1.0
SDSS J0646+4116	5150	2.25	1.50	−1.90	1.0
SDSS J1725+4202	5400	3.50	1.20	−2.50	1.80
SDSS J1146+2343	5100	3.00	1.00	−2.60	1.20
SDSS J0315+2123	5400	4.50	1.00	−2.30	1.80
SDSS J1938+4515	5500	4.00	1.50	−1.20	2.05
SDSS J0652+4105	5000	2.50	1.50	−2.56	1.62
SDSS J1953+4222	6000	4.00	1.75	−2.25	2.00
SDSS J0643+5934	4900	2.50	1.50	−2.90	1.0
SDSS J1024+4151	4800	2.50	1.50	−2.25	1.0
SDSS J0024+3203	5700	3.75	1.50	−2.45	2.00
SDSS J1933+4524	5800	4.50	1.80	−1.80	2.30
SDSS J1341+4741	5450	2.50	1.80	−3.20	1.95

of the stars with detection of Li in the HESP-GOMPA survey are listed in Table 6.1.

6.3 Abundance analysis

6.3.1 Lithium

Li abundances have been derived from the strong absorption features at 6707.76 Å and 6707.98 Å by using the method of spectrum synthesis. The continuum level for the observed spectra is estimated locally around the Li doublet. The observed spectra were fitted iteratively with the synthetic spectra for different values of Li

abundance and the best fit was adopted for each star. Li abundances were kept as the only free parameter in the synthesis spectra. Examples of spectrum synthesis for Li are shown in Figure 6.1.

The errors in the abundance analysis of Li primarily originates from uncertainties in estimates of temperature. A difference of $\tilde{1}$00K is found to alter the Li abundance by 0.10 dex on an average. For determination of abundances of neutral species like Li, uncertainties in surface gravity play a minimal role and can be ignored.

6.3.2 Heavier elements

The abundances of the heavier elements have been derived in the same manner as described in the previous chapters. In this case (e.g.[X/Fe]) the errors due to temperature and gravity if very small as they tend to cancel out while computing the ratios (Cayrel *et al.* 2004; Bonifacio *et al.* 2009; Spite, M. *et al.* 2015). Random error is the main source of error in this case and has been tabulated for each star in the respective tables. Some examples of spectral for the VMP stars are shown in Figures 6.1 to 6.4. The complete abundance tables for the individual VMP stars are listed in Tables 6.2 to Table 6.13.

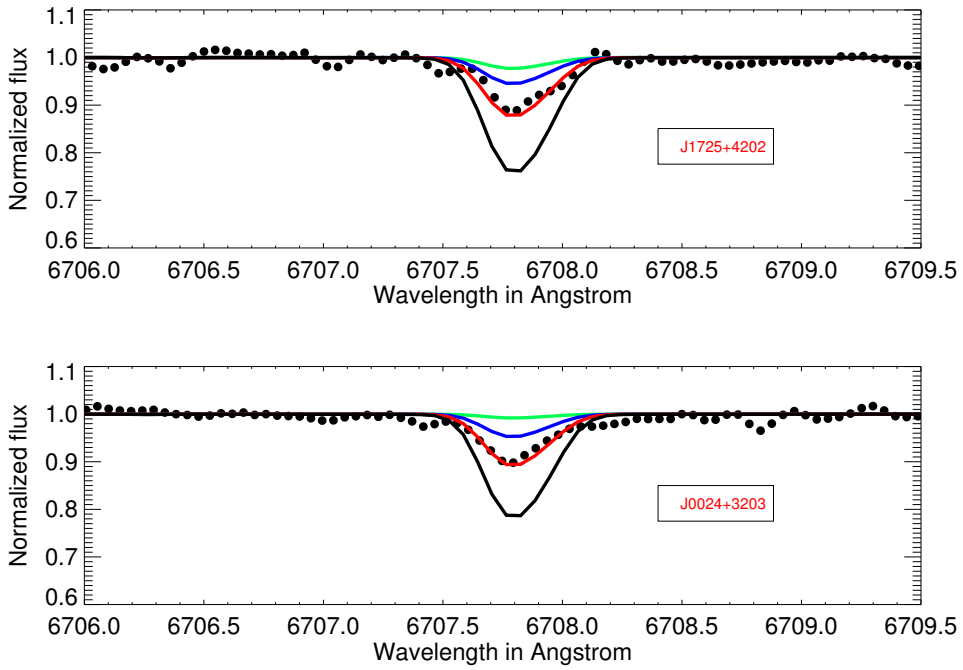

FIGURE 6.1: The spectral synthesis for Li for two of the VMP stars. Red line marks the best fit spectrum.

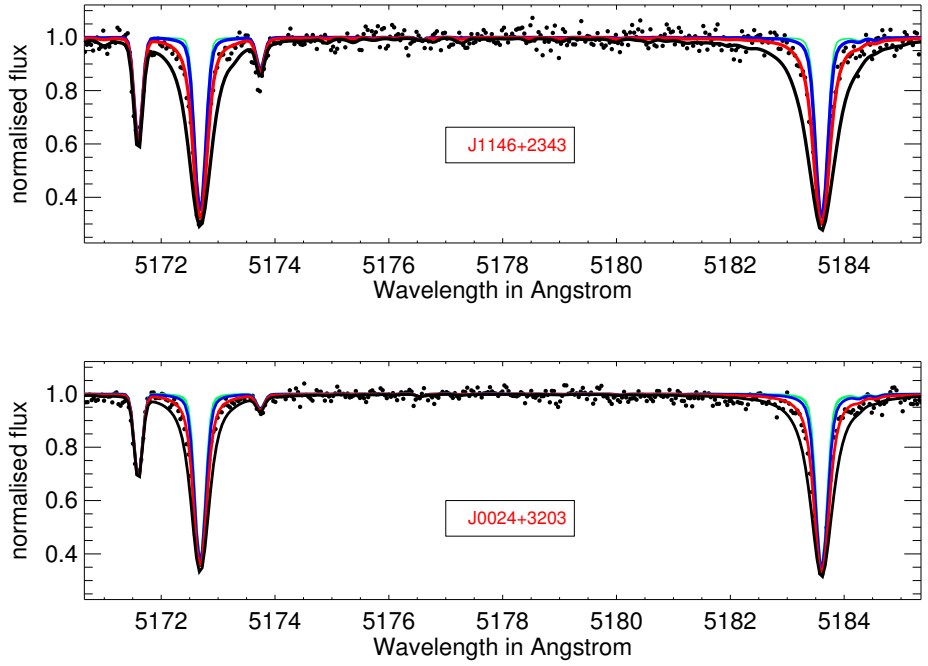

FIGURE 6.2: Spectral synthesis for MgI triplet region at 5172, Å for the VMP stars. Red denotes the best fit.

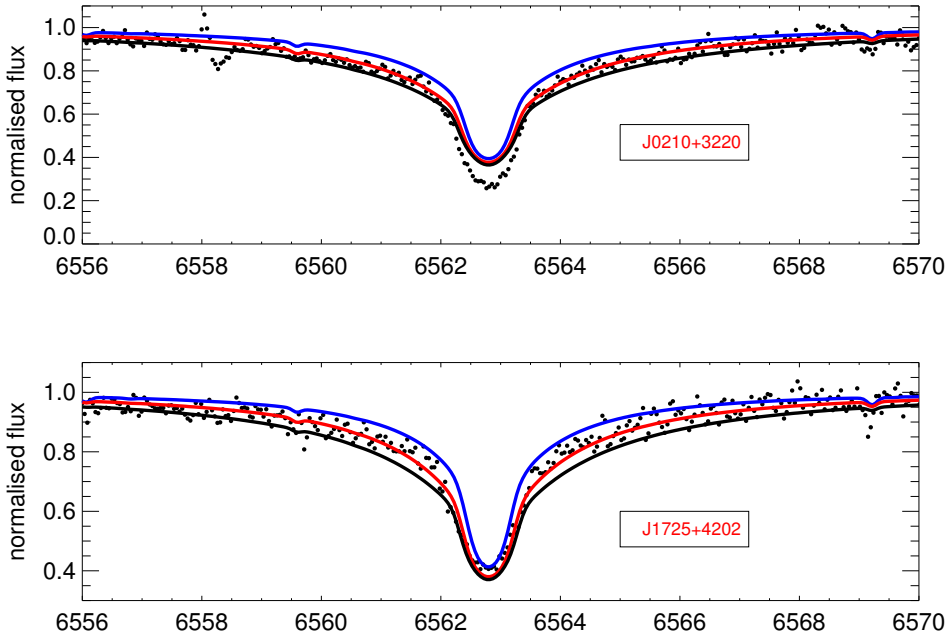

FIGURE 6.3: Spectral synthesis for Hα line for the VMP stars. Red is used for the best fit.

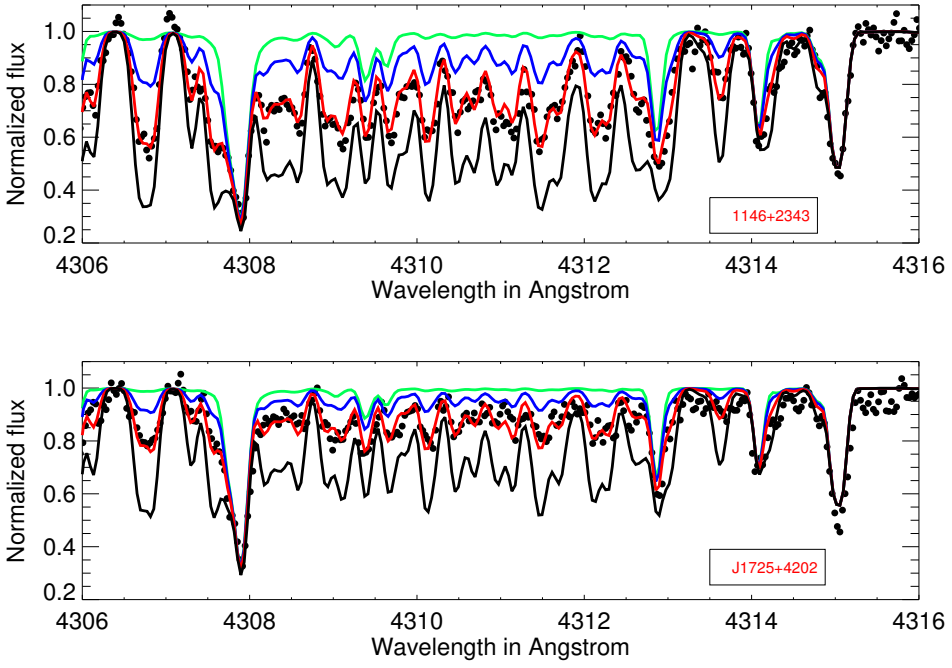

FIGURE 6.4: The spectrum synthesis for the carbon molecular g-band region. Red indicates the best fit

TABLE 6.2: Elemental Abundance Determinations for J1146+2343

Elements	Species	N_{lines}	A(X)	Solar	[X/H]	[X/Fe]	σ
Li	Li I	1	1.20				
C	CH	...	6.00	8.43	−2.43	−0.17	0.04
Na	Na I	2	3.67	6.21	−2.64	−0.04	0.01
Mg	Mg I	4	5.39	7.59	−2.00	0.60	0.01
Al	Al I	1	1.90	6.43	−4.53	−1.93	0.02
Ca	Ca I	8	4.10	6.32	−2.22	0.38	0.06
Sc	Sc II	5	−0.73	3.15	−2.42	0.18	0.01
Ti	Ti I	7	2.83	4.93	−2.10	0.50	0.03
	Ti II	6	2.62	4.93	−2.31	0.29	0.04
Cr	Cr I	3	2.97	5.62	−2.65	−0.05	0.05
	Cr II	2	3.49	5.62	−2.13	0.47	0.05
Mn	Mn I	4	2.84	5.42	−2.58	−0.02	0.02
Co	Co I	2	2.36	4.93	−2.57	0.03	0.01
Ni	Ni I	3	4.31	6.20	−1.89	0.71	0.04
Zn	Zn I	2	2.57	4.56	−1.99	0.61	0.05
Sr	Sr II	2	0.75	2.83	−2.08	0.52	0.01
Ba	Ba II	2	0.25	2.25	−2.00	0.60	0.01

σ indicates the random error.

TABLE 6.3: Elemental Abundance Determinations for J0210+3220

Elements	Species	N_{lines}	A(X)	Solar	[X/H]	[X/Fe]	σ
C	CH	...	6.00	8.43	−2.43	0.02	synth
Na	Na I	2	3.94	6.21	−2.27	0.18	synth
Mg	Mg I	4	5.23	7.59	−2.36	0.09	synth
Si	Si I	1	6.02	7.51	−1.49	0.96	
Ca	Ca I	8	4.16	6.32	−2.16	0.29	0.0
Sc	Sc II	5	0.84	3.15	−2.31	0.14	0.11
Ti	Ti I	7	3.10	4.93	−1.83	0.62	0.09
	Ti II	6	2.91	4.93	−2.02	0.43	0.07
Cr	Cr I	3	3.06	5.62	−2.56	−0.11	0.08
	Cr II	2	4.15	5.62	−2.47	−0.02	0.06
Mn	Mn I	4	1.60	5.42	−2.92	−0.47	0.12
Co	Co I	2	1.99	4.93	−2.94	−0.49	0.09
Ni	Ni I	3	4.35	6.20	−1.85	0.60	0synth
Cu	Cu I	1	1.59	4.19	−2.60	−0.15	synth
Zn	Zn I	2	2.76	4.56	−1.80	0.65	synth
Sr	Sr II	2	0.75	2.83	−2.08	0.37	synth
Ba	Ba II	2	0.0	2.25	−2.25	0.20	synth

σ indicates the random error.

TABLE 6.4: Elemental Abundance Determinations for J0315+2123

Elements	Species	N_{lines}	A(X)	Solar	[X/H]	[X/Fe]	σ
Li	Li I	1	1.80				
C	CH	...	6.10	8.43	−2.33	−0.03	synth
Na	Na I	2	3.74	6.21	−2.47	−0.17	synth
Mg	Mg I	4	5.85	7.59	−1.74	0.56	synth
Si	Si I	1	5.77	7.51	−1.74	0.56	synth
Ca	Ca I	8	4.24	6.34	−2.10	0.20	0.08
Sc	Sc II	5	−1.04	3.15	−2.11	0.19	0.04
Ti	Ti I	7	3.11	4.93	−1.82	0.48	0.09
	Ti II	6	2.98	4.93	−1.95	0.35	0.13
Cr	Cr I	3	3.08	5.62	−2.54	−0.22	0.08
	Cr II	2	3.19	5.62	−2.43	−0.13	0.09
Mn	Mn I	4	2.60	5.42	−2.82	−0.52	0.12
Co	Co I	2	2.70	4.93	−2.23	0.07	0.06
Ni	Ni I	3	4.44	6.20	−1.76	0.54	0.08
Cu	Cu I	2	2.32	4.19	−1.87	0.43	
Zn	Zn I	2	3.09	4.56	−1.47	0.83	synth
Sr	Sr II	2	0.40	2.83	−2.43	−0.03	synth
Ba	Ba II	2	0.25	2.25	−2.00	−0.30	synth

σ indicates the random error.

TABLE 6.5: Elemental Abundance Determinations for J0753+4908

Elements	Species	N_{lines}	A(X)	Solar	[X/H]	[X/Fe]	σ
C	CH	...	6.50	8.43	−1.93	0.07	synth
Na	Na I	2	4.16	6.21	−2.05	−0.05	synth
Mg	Mg I	4	5.77	7.59	−1.82	0.18	synth
Al	Al I	1	2.28	6.43	−4.15	−2.15	synth
Ca	Ca I	8	4.30	6.32	−2.02	−0.02	0.10
Sc	Sc II	5	1.58	3.15	−1.57	0.43	0.06
Ti	Ti I	7	3.36	4.93	−1.57	0.43	0.08
	Ti II	6	3.37	4.93	−1.56	0.44	0.07
Cr	Cr I	3	2.93	5.62	−2.69	−0.69	0.13
	Cr II	2	4.64	5.62	−0.98	1.02	0.11
Mn	Mn I	4	3.11	5.42	−2.31	−0.31	0.14
Co	Co I	2	2.46	4.93	−2.47	−0.47	0.07
Ni	Ni I	3	4.43	6.20	−1.77	0.23	0.04
Cu	Cu I	2	2.65	4.19	−1.54	−0.46	synth
Zn	Zn I	2	3.50	4.56	−1.06	0.94	synth
Sr	Sr II	2	1.00	2.83	−1.83	0.17	synth
Ba	Ba II	2	0.50	2.25	−1.75	0.25	synth

σ indicates the random error.

TABLE 6.6: Elemental Abundance Determinations for J1521+3647

Elements	Species	N_{lines}	A(X)	Solar	[X/H]	[X/Fe]	σ
C	CH	...	6.50	8.43	−1.93	0.22	synth
Na	Na I	2	4.19	6.21	−2.02	0.13	synth
Mg	Mg I	4	5.77	7.59	−1.82	0.33	synth
Al	Al I	1	1.94	6.43	−4.49	−2.34	synth
Ca	Ca I	8	4.40	6.32	−1.92	0.23	0.11
Ti	Ti I	7	3.63	4.93	−-1.30	0.85	0.08
	Ti II	6	3.23	4.93	−1.70	0.45	0.09
Cr	Cr I	3	3.36	5.62	−2.26	−0.11	0.07
	Cr II	2	4.00	5.62	−1.62	0.53	0.06
Co	Co I	2	2.70	4.93	−2.23	−0.08	0.08
Ni	Ni I	3	4.06	6.20	−2.14	0.01	0.09
Cu	Cu I	2	2.33	4.19	−1.86	0.29	synth
Zn	Zn I	2	3.05	4.56	−1.51	0.64	synth
Sr	Sr II	2	0.50	2.83	−2.33	−0.18	synth
Ba	Ba II	2	0.25	2.25	−2.00	0.15	synth

σ indicates the random error.

TABLE 6.7: Elemental Abundance Determinations for J1725+4202

Elements	Species	N_{lines}	A(X)	Solar	[X/H]	[X/Fe]	σ
Li	Li I	1	1.80				
C	CH	...	6.00	8.43	−2.43	0.07	synth
Na	Na I	2	3.92	6.21	−2.29	0.21	synth
Mg	Mg I	4	5.53	7.59	−2.06	0.44	synth
Al	Al I	1	2.37	6.43	−4.06	−1.56	synth
Ca	Ca I	8	4.28	6.32	−2.02	0.48	0.08
Sc	Sc II	5	0.63	3.15	−2.52	−0.02	0.09
Ti	Ti I	7	2.88	4.93	−2.05	0.45	0.08
	Ti II	6	2.87	4.93	−2.06	0.44	0.04
Cr	Cr I	3	3.03	5.62	−2.59	−0.09	0.07
	Cr II	2	3.46	5.62	−2.16	0.34	0.11
Mn	Mn I	4	2.60	5.42	−2.92	−0.32	0.15
Co	Co I	2	2.54	4.93	−2.39	0.11	0.09
Ni	Ni I	3	4.26	6.20	−1.94	0.56	0.08
Zn	Zn I	2	2.71	4.56	−1.85	0.65	synth
Sr	Sr II	2	0.75	2.83	−2.08	0.42	synth
Ba	Ba II	2	0.00	2.25	−2.25	0.25	synth

σ indicates the random error.

TABLE 6.8: Elemental Abundance Determinations for j0643+5934

Elements	Species	N_{lines}	A(X)	Solar	[X/H]	[X/Fe]	σ
C	CH	...	5.75	8.43	−2.68	0.22	synth
Na	Na I	2	3.54	6.21	−2.67	0.23	synth
Mg	Mg I	4	5.03	7.59	−2.56	0.34	synth
Al	Al I	1	1.70	6.43	−4.73	−1.83	0.09
Ca	Ca I	8	3.61	6.32	−2.71	0.19	0.06
Sc	Sc II	5	0.47	3.15	−2.68	0.22	0.11
Ti	Ti I	7	2.42	4.93	−2.51	0.39	0.10
	Ti II	6	2.36	4.93	−2.57	0.33	0.07
Cr	Cr I	3	2.44	5.62	−3.18	−0.28	0.08
	Cr II	2	3.12	5.62	−2.40	0.50	0.08
Mn	Mn I	4	1.52	5.42	−3.90	−1.00	0.12
Co	Co I	2	2.32	4.93	−2.61	0.29	0.11
Ni	Ni I	3	3.78	6.20	−2.42	0.48	0.09
Zn	Zn I	2	1.86	4.56	−2.70	0.20	0.06
Sr	Sr II	2	0.00	2.83	−2.83	0.07	synth
Ba	Ba II	2	−0.50	2.25	−2.75	0.15	synth

σ indicates the random error.

TABLE 6.9: Elemental Abundance Determinations for J2320+1742

Elements	Species	N_{lines}	A(X)	Solar	[X/H]	[X/Fe]	σ
C	CH	...	6.00	8.43	−2.43	−0.08	synth
Na	Na I	2	3.75	6.21	−2.46	−0.11	synth
Mg	Mg I	4	5.52	7.59	−2.07	0.27	synth
Al	Al I	1	1.77	6.43	−4.66	−2.31	synth
Ca	Ca I	8	4.00	6.32	−2.32	0.03	0.13
Sc	Sc II	5	0.06	3.15	−3.09	−0.74	0.14
Ti	Ti I	7	3.08	4.93	−1.85	0.50	0.09
	Ti II	6	2.54	4.93	−2.39	−0.04	0.05
Cr	Cr I	3	2.86	5.62	−2.76	−0.41	0.09
	Cr II	2	3.62	5.62	−2.00	0.35	0.07
Mn	Mn I	4	2.54	5.42	−2.88	−0.53	0.15
Co	Co I	2	1.88	4.93	−3.05	−0.70	0.14
Ni	Ni I	3	4.29	6.20	−1.91	0.44	0.09
Zn	Zn I	2	2.36	4.56	−2.20	0.15	0.08
Sr	Sr II	2	0.50	2.83	−2.33	0.02	synth
Ba	Ba II	2	0.00	2.25	−2.25	0.10	synth

σ indicates the random error.

TABLE 6.10: Elemental Abundance Determinations for J0447+5434

Elements	Species	N_{lines}	A(X)	Solar	[X/H]	[X/Fe]	σ
C	CH	...	6.00	8.43	−2.43	0.07	synth
Na	Na I	2	3.60	6.21	−2.61	−0.11	synth
Mg	Mg I	4	5.24	7.59	−2.35	0.15	synth
Al	Al I	1	1.90	6.43	−4.53	−2.03	synth
Ca	Ca I	8	4.04	6.32	−2.28	0.22	0.10
Sc	Sc II	5	0.17	3.15	−2.98	−0.48	0.09
Ti	Ti I	7	2.79	4.93	−2.14	0.36	0.12
	Ti II	6	2.85	4.93	−2.08	0.42	0.07
Cr	Cr I	3	2.90	5.62	−2.72	−0.22	0.13
	Cr II	2	3.30	5.62	−2.32	0.18	0.09
Mn	Mn I	4	2.72	5.42	−2.70	−0.20	0.08
Co	Co I	2	2.17	4.93	−2.76	−0.26	0.03
Ni	Ni I	3	3.73	6.20	−2.47	0.03	0.05
Cu	Cu I	2	1.71	4.19	−2.48	synth	
Zn	Zn I	2	2.10	4.56	−2.46	0.04	synth
Sr	Sr II	2	0.25	2.83	−2.58	−0.08	synth
Ba	Ba II	2	0.00	2.25	−2.25	0.25	synth

σ indicates the random error.

TABLE 6.11: Elemental Abundance Determinations for J1024+4151

Elements	Species	N_{lines}	A(X)	Solar	[X/H]	[X/Fe]	σ
Li	Li I	1	1.00				
C	CH	...	6.00	8.43	−2.43	−0.18	synth
Na	Na I	2	3.90	6.21	−2.31	−0.06	synth
Mg	Mg I	4	5.76	7.59	−2.03	0.22	synth
Al	Al I	1	1.99	6.43	−4.44	−2.19	synth
Ca	Ca I	8	3.68	6.32	−2.64	0.46	0.09
Si	Si I	2	5.22	7.51	−2.29	−0.04	
Sc	Sc II	5	1.08	3.15	−2.23	0.12	0.08
Ti	Ti I	7	3.52	4.93	−1.41	0.84	0.12
	Ti II	6	3.01	4.93	−1.92	0.33	0.09
Cr	Cr I	3	3.25	5.62	−2.37	−0.12	0.13
	Cr II	2	3.50	5.62	−2.12	0.13	0.09
Mn	Mn I	4	2.51	5.42	−2.91	−0.66	0.10
Co	Co I	2	2.46	4.93	−2.47	−0.22	0.06
Ni	Ni I	3	4.47	6.20	−1.73	0.52	0.09
Cu	Cu I	1	2.89	4.56	−1.67	0.58	synth
Zn	Zn I	2	2.89	4.56	−1.67	0.58	0.11
Sr	Sr II	2	0.75	2.83	−2.08	0.17	synth
Ba	Ba II	2	0.50	2.25	−1.75	0.50	synth

σ indicates the random error.

TABLE 6.12: Elemental Abundance Determinations for J0024+3203

Elements	Species	N_{lines}	A(X)	Solar	[X/H]	[X/Fe]	σ
Li	Li I	1	2.00				
C	CH	...	6.00	8.43	−2.43	0.02	synth
Na	Na I	2	4.22	6.21	−1.99	0.46	synth
Mg	Mg I	4	5.64	7.59	−1.95	0.50	synth
Al	Al I	1	3.00	6.43	−3.43	−0.98	synth
Si	Si I	2	5.46	7.51	−2.05	0.40	0.09
Ca	Ca I	8	4.37	6.32	−1.95	0.50	0.06
Sc	Sc II	5	1.03	3.15	−2.12	0.33	0.06
Ti	Ti I	7	3.14	4.93	−1.79	0.66	0.09
	Ti II	6	3.03	4.93	−1.90	0.55	0.05
Cr	Cr I	3	3.21	5.62	−2.41	0.04	0.12
	Cr II	2	3.52	5.62	−2.10	0.35	0.07
Mn	Mn I	4	2.62	5.42	−2.80	−0.35	0.11
Co	Co I	2	2.73	4.93	−2.20	0.25	0.06
Ni	Ni I	3	4.42	6.20	−1.88	0.57	synth
Zn	Zn I	2	2.71	4.56	−1.85	0.60	0.07
Sr	Sr II	2	1.00	2.83	−1.83	0.62	synth
Ba	Ba II	2	0.25	2.25	−2.00	0.45	synth

σ indicates the random error.

6.4 Discussion

6.4.1 Li distribution in the metal poor regime

The detection of lithium indicates that a star unlikely to have experienced AGB binary mass transfer or direct winds from a massive star and has preserved the signatures of the primordial nucleosynthesis events in its surface. Mass transfer from a low-mass AGB would produce large amounts of carbon and deplete lithium, along with the production of *s*-process enhanced material. A (4-7$M_{\odot}$) AGB star that had experienced hot bottom burning produces large nitrogen and very low carbon. There are some models in which AGB stars could produce lithium through the Cameron-Fowler mechanism (Cameron and Fowler 1971). It is unclear if an AGB with mass 3-4$M_{\odot}$ could explain the observed star-to-star C, N, low *s*-process elements and lithium.

The distribution of the abundance of Li has been plotted with temperature for different stellar families in Figure 6.5. The stars have been further categorized into giants and dwarfs for each class of objects. The literature data is compiled from SAGA database and the program stars with detection of Li are marked in red diamonds. As noted by several studies on Li abundances in metal poor stars (Spite, Bonifacio, etc) the plateau is observed for warmer dwarf stars with T_{eff} ¿ 5800. However, the scatter tends to increase as temperature decreases from 6500 to 5700. The slope could also be seen. The different stellar families, particularly CEMP-no and EMP stars are believed to have different progenitor populations and have undergone different star formation history. The identical distribution of Li indicates the ISM to be well mixed during the epochs of their formation. Hence, Li could not be used as a yardstick to differentiate between the different stellar populations. Only three of our sample stars with Li are the main sequence turn off stars which is not a good number to test the consistency of the slope for our

sample. Black and blue are used for the literature sample to differentiate between giants and dwarfs. The CEMP-s star SDSS J1953+4722 falls on the edge of the Li desert (Aguilera-Gómez *et al.* 2018). Evolutionary mixing inside the star in its sub-giant phase tends to deplete the original lithium abundance of the star-forming cloud. As seen in Figure 6.5 the depletion of Li as the star ascends the giant branch could be understood.

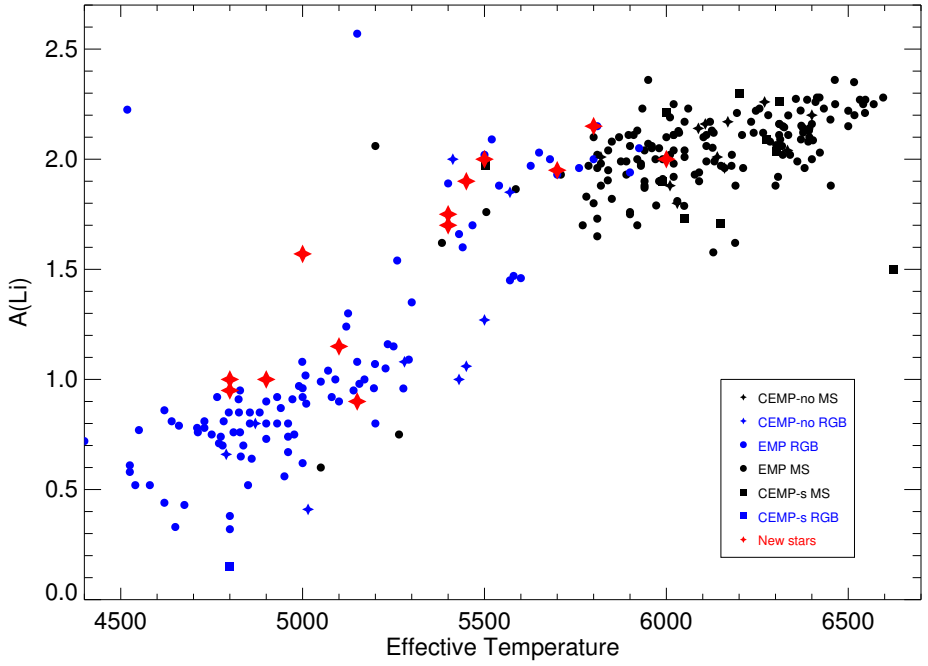

FIGURE 6.5: The distribution of A(Li) as a function of T_eff for the different stellar families. The program stars are marked by large red diamonds.

The significant large scatter in the Li abundance in the Spite plateau region could also be due to the adoption of different T-eff scales for the stars compiled from SAGA database for the comparison. As stated by Bonifacio *et al.* (2007a) the Spite plateau appears very different for different temperature scales (e.g. V-K produces no slope with large scatter whereas Hα shows a small slope with less scatter). For the stars in our sample, we have adopted the temperature from the ionization equilibrium using Fe lines which is consistent with the Hα based temperature (with a difference up to 100 K). Using photometric colors (V-K)

for determination of temperature (Ramírez and Meléndez 2005) leads to slightly warmer temperatures and consequently higher Li abundances.

The trend of Li abundance with metallicity is shown in Figure 6.6. The cosmological value of Li and the observed value of Spite plateau is shown in black lines. The small slope could be seen and the scatter tends to increase for MS stars as metallicity decreases. The lowest metallicity stars have a lower value of Li abundance which reaches the Spite plateau at [Fe/H] ¿ -3.50 albeit with large scatter. Our sample being small in size could not yield significant results but detection of Li in more number of stars would provide us better opportunities to understand the evolution and (possible) depletion of Li in the early universe.

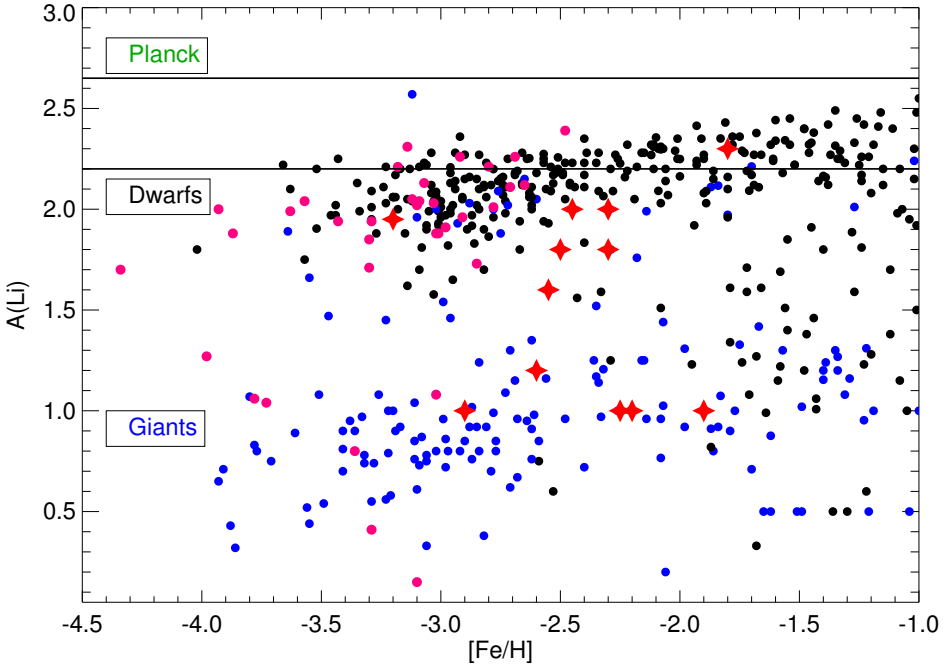

FIGURE 6.6: The distribution of A(Li) as a function of [Fe/H]. The predictions from Planck mission and the Spite plateau abundances are shown by black solid lines. The dwarf stars are marked in black while giant stars are marked in blue. CEMP-no stars are shown in red dots. The program stars with Li detection in this study are shown by filled red diamonds.

6.4.2 Trends with other elements

Pasquini *et al.* (2005) found a trend for Li abundances with other elements like Na, O and N for the TO stars in NGC 6752. A(Li) was found to correlate with [O/Fe] and anti-correlate with [Na/Fe] and [N/Fe]. Bonifacio *et al.* (2007a) also confirmed the A(Li)-[Na/Fe] anti-correlations in 47 Tucanae. However, no such trends could be noticed among the Halo stars. In Figure 6.7, the halo stars have been divided into giants (blue dots) and dwarfs (black dots). The depletion of A(Li) due to evolutionary mixing can be seen in all the four panels. No trends could be seen for A[Li] with [Na/Fe] (as reported in few GCs), [Ca/Fe] (representative of α abundance), [Cr/Fe] (Fe-peak element) and [Ba/Fe] (n-capture element). We have also marked the abundances of the GC escapees and CEMP-no star in coloured diamonds in each of the panels.

6.4.3 CEMP stars

Matsuno *et al.* (2017) has proposed a novel way of classifying the CEMP stars using the abundances of Li. Since CEMP-s stars have undergone mass transfer they are more likely to show a depleted Li abundance whereas the CEMP-no stars are most likely preserve the primordial Li till it reaches the subgiant phase. However, this criterion could not be universal as there exist a few CEMP-s stars in the literature with high abundances of Li. SDSS J1953+4722 , one of the CEMP-s stars in this study also shows a very high value of A(Li)=2.40. These stars have mostly received contributions from a Li rich ejecta from the companion star during its AGB phase which could produce Li by the Cameron Fowler mechanism.

According to the analysis of Meynet *et al.* (2010) and Masseron *et al.* (2012), the stars falling at the edge of Li-depleted stars (A(Li) = 2.00 are adopted as

the separation between Li-normal and Li-depleted metal-poor stars). A slight depletion from the Spite Plateau value could be attributed to internal mixing of the star, or the observed value of lithium for SDSS J1341+4741 and J0024 may be the result of several concurrent phenomena.

- The ejected material from the progenitor SN will have depleted lithium abundance along with other nucleosynthetic elements and enhanced carbon (for the case of SDSS J1341+4741) that is mixed with the primordial cloud. Depending upon the dilution factor in the natal cloud, it may be possible to achieve the necessary lithium value Piau *et al.* (2006); Meynet *et al.* (2010); Maeder *et al.* (2015).

- A Spite Plateau value of Li was present in the natal cloud of SDSS J1341+4741 , and it is depleted by thermohaline mixing or meridional circulation (Masseron *et al.* 2012) in the star. If we consider the current evolutionary state of the star to be in the RGB phase, this could be a viable mechanism.

- Enhanced rotationally-induced mixing in the RGB phase (following Denissenkov and Herwig 2004) can lead to formation of lithium in the star, following depletion of all the primordial lithium. It is very difficult to differentiate between an AGB or a massive rotating star as the precursor using Li as the sole yardstick, as both result in almost the same nucleosynthetic yield of Li (Meynet *et al.* 2006; Masseron *et al.* 2012).

6.4.4 VMP stars

Several new VMP stars have been identified in this study as seen in Tables 6.2 to 6.12. The stars show the expected features like signatures of odd-even nucleosynthesis for the light elements, standard α enhancement of [α/Fe] $\tilde{0}$.40, abundances

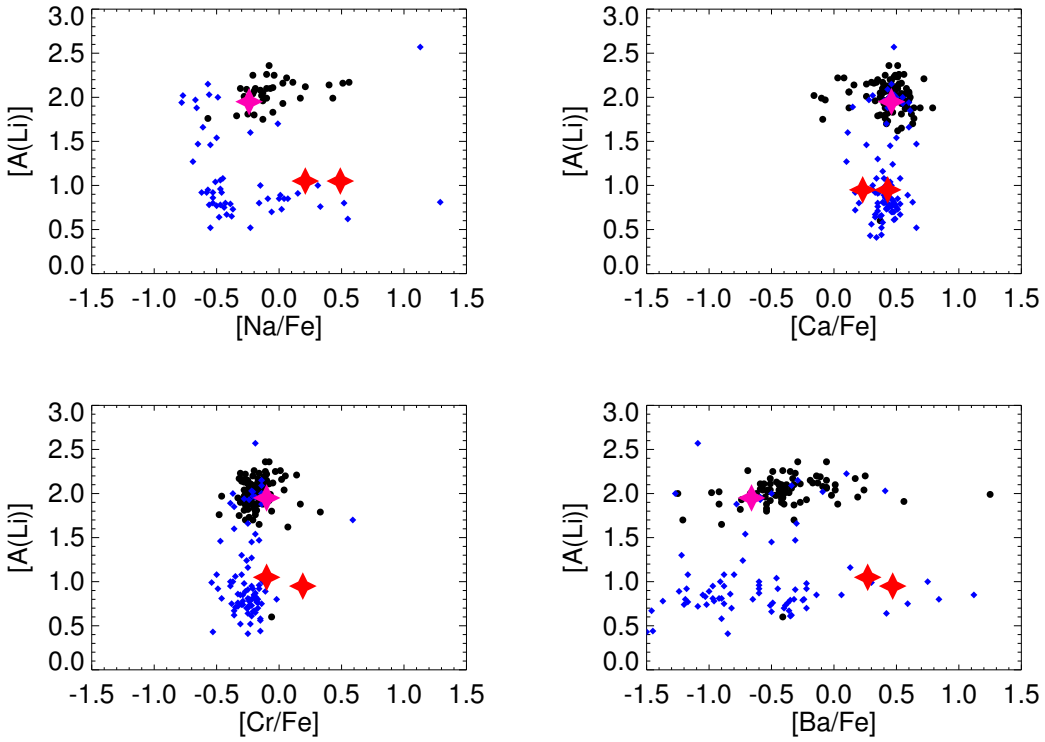

FIGURE 6.7: The Li abundance for VMP and EMP stars with detection of Li. The black dots mark the dwarf stars while blue dots represent the giant. The GC escapees from this study are marked in red diamonds whereas the CEMP-no star is marked in pink diamond.

of Fe-peak elements scaled to Fe abundances and the expected production of n-capture elements of the neutron capture elements. The trends for the abundances of light and n-capture elements are shown in Figures 6.8 and 6.9. The program stars have not been separately highlighted to keep the plots neat.

As seen in Figure 6.8, RGB and MS stars follow a similar trend for light elements. [Na/Fe] tends to increase with an increase in [Fe/H] whereas it is mostly a scatter with no singular trend for [Mg/Fe] and [Al/Fe] at the lowest metallicities for VMP stars. Figure 6.9 tries to find the trends for the n-capture elements in VMP stars. CEMP stars have also been separately marked in red as they tend to dominate at lowest metallicities and play a key role in the production of n-capture elements. [Ba/Fe] tends to rise as [Fe/H] increases. This might indicate the onset of the dominance of *s*-process at higher metallicity (Wallerstein *et al.* 1997). However, a

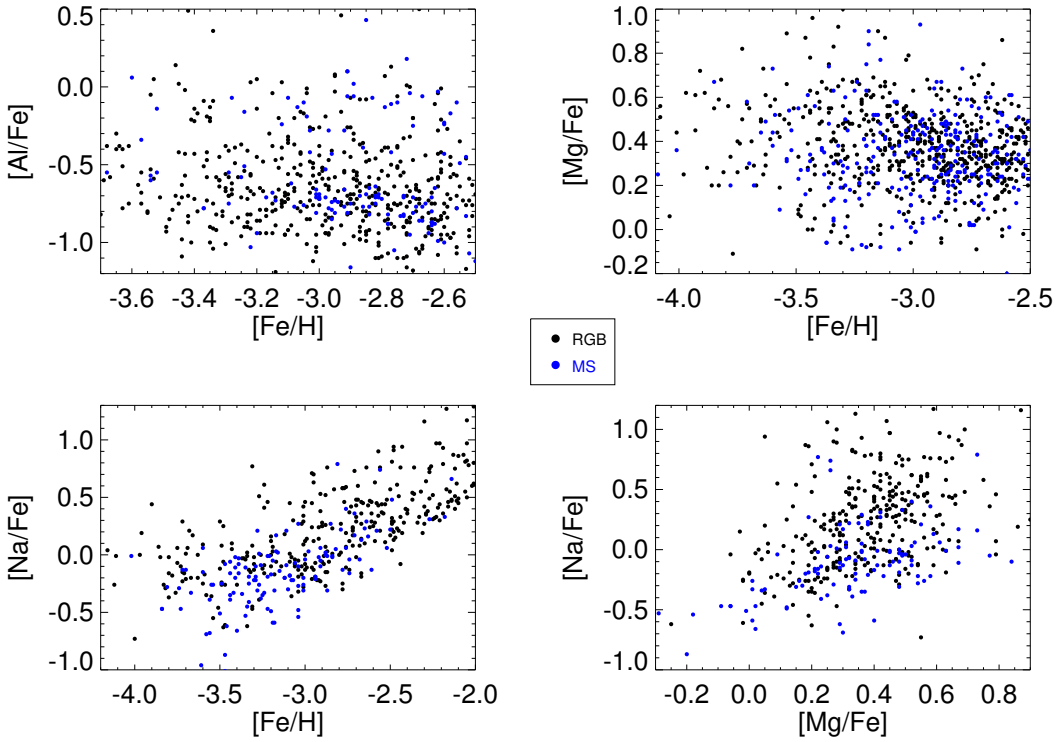

FIGURE 6.8: Distribution of light elements for the VMP stars in the Galactic halo, taken from the SAGA database. The EMP giants are marked by black points, whereas dwarfs are marked by blue points.

similar increase in [Sr/Fe] is also expected which is not observed. This results in a marginal decrease in [Sr/Ba] as metallicity increases. The histogram in the last panel confirms a similar distribution of VMP and CEMP stars.

6.5 Conclusion

We studied Lithium abundance among metal poor stars that have solar abundance ratio, CEMP-no stars, r-process rich stars and GC escapees. Lithium is in general depleted in CEMP-s stars, however, the CEMP-no stars show very similar Li distribution as the EMP stars. The giants and dwarfs among them show similar Li abundances in CEMP-no and EMP stars. This indicates that the enhanced

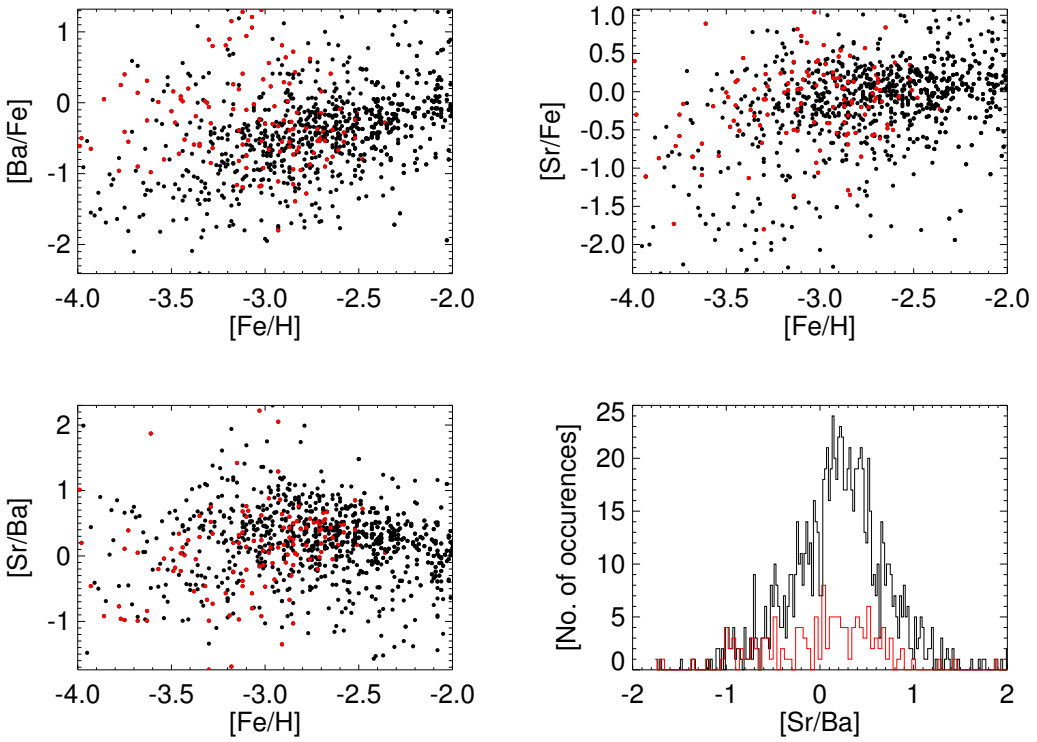

FIGURE 6.9: Trends of Sr and Ba for VMP stars in the Galactic halo. CEMP-no stars have also been separately marked in red dots. The distribution for both the classes of stars follow a similar pattern as shown in the last panel.

carbon in CEMP-no is likely from its star forming cloud and hence a massive star origin for carbon. There are few CEMP-s stars that show enhanced Lithium abundance compared to other typical CEMP-s stars. These objects might have an i-process origin for their n-capture elements and will be interesting for further investigation.

Chapter 7

Conclusions and Future Work

7.1 Conclusions

This study has reported high resolution spectra of several classes of stars in the very metal poor domain. Some of them have shown remarkable characteristics like over-abundance of carbon, strong enhancement of r-process, and widespread abundance of lithium.

We have also been able to tag a few stars of globular cluster origin using nucleosynthetic signatures out of which one is speculated to be a blue straggler, an extremely rare object to be found in the Halo.

Comparative study between the families of stars was also carried out and an offset between CEMP-no and EMP stars was noted for the trend in Cr abundance against metallicity. This could point to a different chemical evolutionary history of these two populations. One of the CEMP-no stars was also found to be in a binary system but the detection of undepleted Li indicates that no mass transfer has

taken place.

We report the detection of Thorium in one of the $r-$process rich stars and it was found to have a high degree of actinide boost. Cosmochronometry using [Th/Eu] yielded unphysical ages. The reported sample of r-I and r-II stars were found to have the expected signatures of strong contributions from an r-process rich source during their epoch of formation in the early universe.

The evolution of the Halo is intricately linked with globular clusters evolution and mass loss. The low [Sr/Ba] for NGC 1851 studied in this work indicate towards primary contribution from $NS - NS$ mergers towards Galactic chemical enrichment as compared to type II SNe. Few GCs from the literature were also found to display similar abundance pattern. This study also indicates that due to a closed environment GC stars have chemically evolved at a much rapid pace compared to ordinary Halo stars despite being born at the same epoch which is expected due to high retention of matter by the cluster potential. The stars of globular cluster origin discovered in the Halo are also found to lie in close proximity to the globular clusters in the [Sr/Ba] vs [Fe/H] plane showing a greater contribution from NS-NS mergers and is thus consistent with theoretical predictions.

7.2 Future Work

Abundances of key elements neutron capture elements like Sr and Ba are obtained for five metal poor globular clusters M2, M3, M13, M15 AND M71. Earlier abundance studies in the literature have concentrated on multiple generations of stars in the cluster and the difference in elemental abundances of these populations. The key criteria used for such classification are the chemical anti-correlations like

O-Na and Mg-Al. The second generation stars are found to be enhanced in sodium and aluminium while at the same time being depleted in magnesium and oxygen as discussed earlier.

In the future, we want to undertake a study on the origin of neutron capture elements in GCs. In the current study used the data of NGC 1851 from the archival data of ESO and derived the Sr and Ba abundances which were consistent with the values abundances of Gratton which validated our methods. The grids for the key elements Sr and Ba are already in place as discussed earlier in chapter 2. We have also downloaded the spectra for several metal poor GCs covering the wavelength ranges for Sr and Ba. The goal is to derive the abundances for these GCs and probe the *r*-process enrichment history.

The grids were initially used for the low resolution archival data of SDSS for the five GCs M2, M3, M13, M15 and M91. Though the resolution is very low we were still able to detect Sr and Ba in few of the stars in these clusters. The distribution of [Sr/Fe] and []Ba/Fe] as a function of [C/Fe] for the four clusters from SDSS data is shown in figure 7.1 and 7.2. They show a scatter and no trends with [C/Fe] could be deduced. When overplotted with the halo stars and NGC 1851 they all occupy the lower region of the plot favouring the NS-NS merger scenario as seen in figure 7.3. However, to confirm these results we need to study the GCs at a higher resolution. It would be very important to verify the results with a larger sample and better quality of data. Hence our plan to undertake such studies with ESO archival data would be helpful to understand the nature of the primary polluters of the GCs.

Apart from the archival data of GCs, we also plan to use LAMOST data for future observations using the 2-m class and larger telescopes. We plan to fit the low resolution data from LAMOST and find interesting targets for observation. The primary aim would be to choose stars of the lowest metallicity with a good

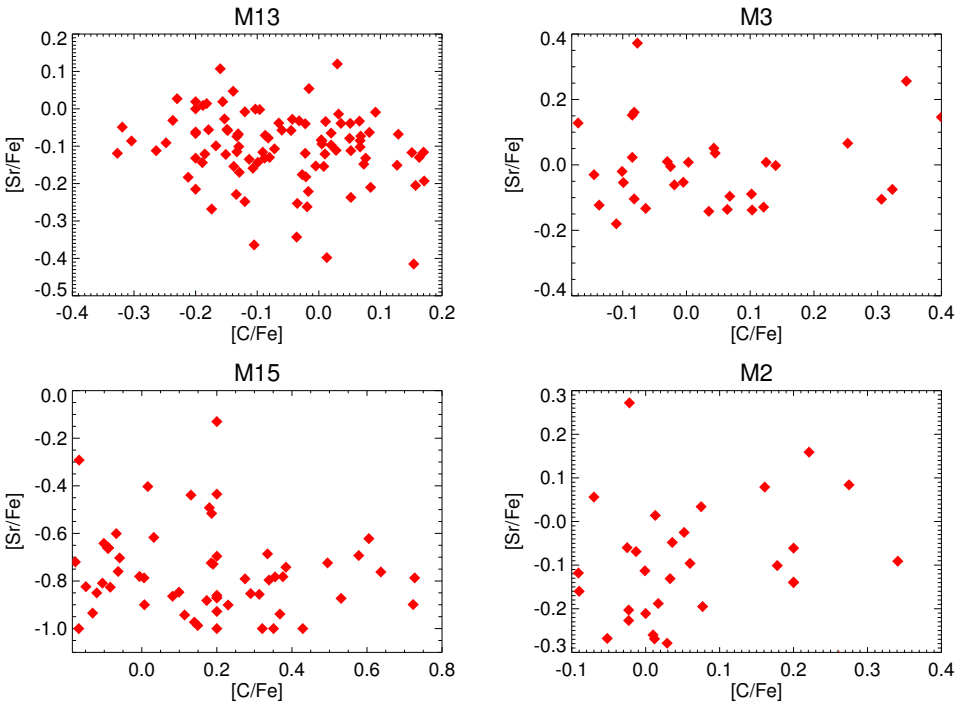

FIGURE 7.1: The distribution of [Sr/Fe] as a function of [C/Fe] for the four GCs from SDSS. No trend could be observed.

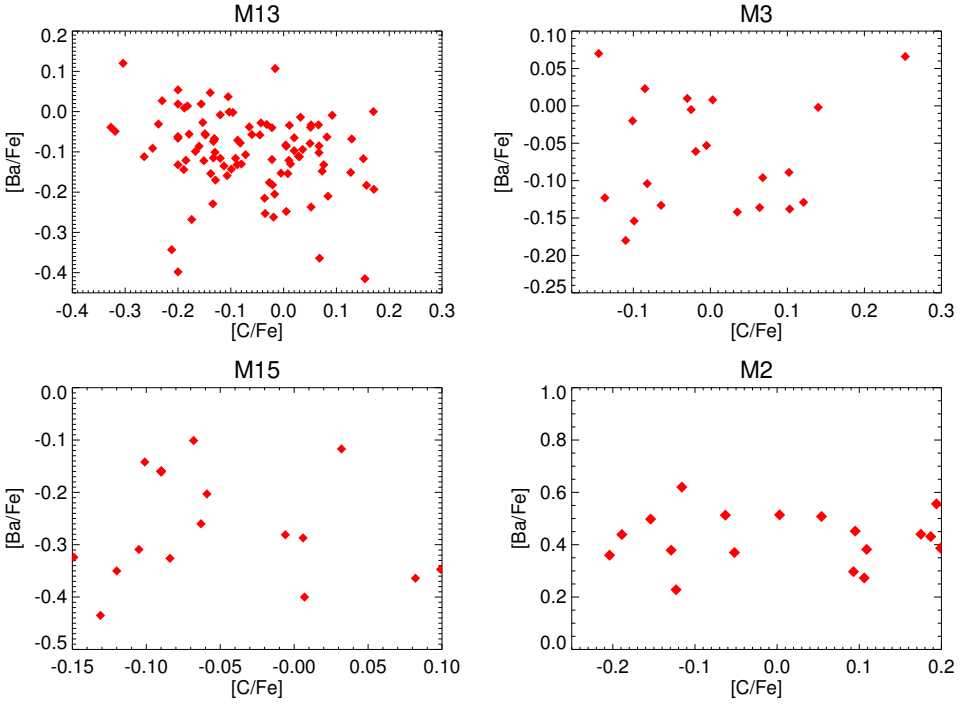

FIGURE 7.2: The distribution of [Ba/Fe] as a function of [C/Fe] for the four GCs from SDSS. No trend could be noticed.

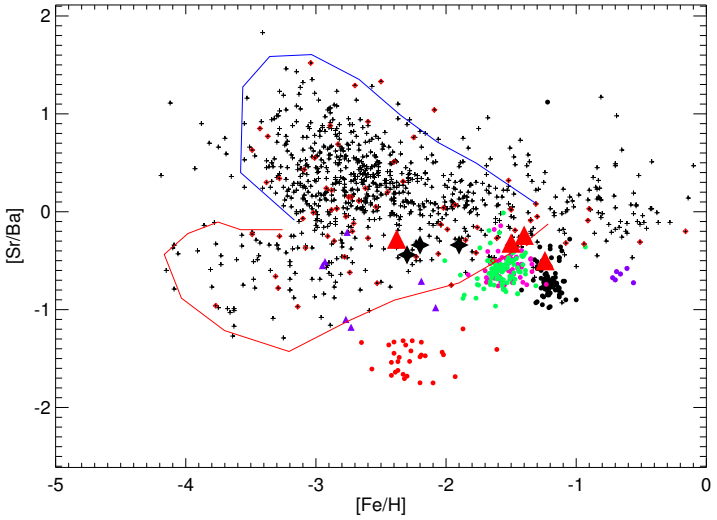

FIGURE 7.3: Comparison of halo stars and GCs in the [Sr/Ba] vs [Fe/H] plane. The coloured filled circles represent the GCs from the SDSS data. Red triangles indicate GCs from literature while the black diamonds are the GC escapees discovered in this study. The black filled circles are the abundances derived for the stars in NGC 1851 from GIRAFFE spectra.

fit showing considerable S/N ratios. We hope to add many more interesting stars with chemical peculiarities to the HESP-GOMPA survey and turn it to one of the leading high resolution spectroscopic surveys currently being pursued.

Bibliography

Aguilera-Gómez, Claudia, Ramírez, Iván and Chanamé, Julio, 2018, "Lithium abundance patterns of late-F stars: an in-depth analysis of the lithium desert", *Astron. Astrophys.*, **614**, A55. [DOI], [ADS], [arXiv:1803.05922 [astro-ph.SR]]

Alonso, A., Arribas, S. and Martinez-Roger, C., 1996, "The empirical scale of temperatures of the low main sequence (F0V-K5V).", *Astron. Astrophys.*, **313**, 873–890. [ADS]

Alonso, A., Arribas, S. and Martínez-Roger, C., 1999, "The effective temperature scale of giant stars (F0-K5). II. Empirical calibration of T_{eff} versus colours and [Fe/H]", *Astron. Astrophys. Suppl.*, **140**, 261–277. [DOI], [ADS]

Alpher, R. A., Bethe, H. and Gamow, G., 1948, "The Origin of Chemical Elements", *Physical Review*, **73**, 803–804. [DOI], [ADS]

Alvarez, R. and Plez, B., 1998a, "Near-infrared narrow-band photometry of M-giant and Mira stars: models meet observations", *Astron. Astrophys.*, **330**, 1109–1119. [ADS], [astro-ph/9710157]

Alvarez, R. and Plez, B., 1998b, "Near-infrared narrow-band photometry of M-giant and Mira stars: models meet observations", *Astron. Astrophys.*, **330**, 1109–1119. [ADS], [astro-ph/9710157]

Anders, F., Chiappini, C., Santiago, B. X., Rocha-Pinto, H. J., Girardi, L., da Costa, L. N., Maia, M. A. G., Steinmetz, M., Minchev, I., Schultheis, M.,

Boeche, C., Miglio, A., Montalbán, J., Schneider, D. P., Beers, T. C., Cunha, K., Allende Prieto, C., Balbinot, E., Bizyaev, D., Brauer, D. E., Brinkmann, J., Frinchaboy, P. M., García Pérez, A. E., Hayden, M. R., Hearty, F. R., Holtzman, J., Johnson, J. A., Kinemuchi, K., Majewski, S. R., Malanushenko, E., Malanushenko, V., Nidever, D. L., O'Connell, R. W., Pan, K., Robin, A. C., Schiavon, R. P., Shetrone, M., Skrutskie, M. F., Smith, V. V., Stassun, K. and Zasowski, G., 2014, "Chemodynamics of the Milky Way. I. The first year of APOGEE data", *Astron. Astrophys.*, **564**, A115. [DOI], [ADS], [arXiv:1311.4549 [astro-ph.GA]]

Anderson, J., Sarajedini, A., Bedin, L. R., King, I. R., Piotto, G., Reid, I. N., Siegel, M., Majewski, S. R., Paust, N. E. Q., Aparicio, A., Milone, A. P., Chaboyer, B. and Rosenberg, A., 2008, "The Acs Survey of Globular Clusters. V. Generating a Comprehensive Star Catalog for each Cluster", *Astron. J.*, **135**, 2055–2073. [DOI], [ADS], [arXiv:0804.2025]

Anderson, L., Aubourg, É., Bailey, S., Beutler, F., Bhardwaj, V., Blanton, M., Bolton, A. S., Brinkmann, J., Brownstein, J. R., Burden, A., Chuang, C.-H., Cuesta, A. J., Dawson, K. S., Eisenstein, D. J., Escoffier, S., Gunn, J. E., Guo, H., Ho, S., Honscheid, K., Howlett, C., Kirkby, D., Lupton, R. H., Manera, M., Maraston, C., McBride, C. K., Mena, O., Montesano, F., Nichol, R. C., Nuza, S. E., Olmstead, M. D., Padmanabhan, N., Palanque-Delabrouille, N., Parejko, J., Percival, W. J., Petitjean, P., Prada, F., Price-Whelan, A. M., Reid, B., Roe, N. A., Ross, A. J., Ross, N. P., Sabiu, C. G., Saito, S., Samushia, L., Sánchez, A. G., Schlegel, D. J., Schneider, D. P., Scoccola, C. G., Seo, H.-J., Skibba, R. A., Strauss, M. A., Swanson, M. E. C., Thomas, D., Tinker, J. L., Tojeiro, R., Magaña, M. V., Verde, L., Wake, D. A., Weaver, B. A., Weinberg, D. H., White, M., Xu, X., Yèche, C., Zehavi, I. and Zhao, G.-B., 2014, "The clustering of galaxies in the SDSS-III Baryon Oscillation Spectroscopic Survey: baryon acoustic oscillations in the Data Releases 10 and 11 Galaxy samples", *Mon. Not. Roy. Astron. Soc.*, **441**, 24–62. [DOI], [ADS], [arXiv:1312.4877]

Andrievsky, S. M., Spite, M., Korotin, S. A., Spite, F., Bonifacio, P., Cayrel, R., Hill, V. and François, P., 2007, "NLTE determination of the sodium abundance in a homogeneous sample of extremely metal-poor stars", *Astron. Astrophys.*, **464**(3), 1081–1087. [DOI], [ADS], [arXiv:astro-ph/0701199 [astro-ph]]

Andrievsky, S. M., Spite, M., Korotin, S. A., Spite, F., Bonifacio, P., Cayrel, R., Hill, V. and François, P., 2008, "NLTE determination of the aluminium abundance in a homogeneous sample of extremely metal-poor stars", *Astron. Astrophys.*, **481**(2), 481–487. [DOI], [ADS], [arXiv:0802.1519 [astro-ph]]

Aoki, W., Beers, T. C., Christlieb, N., Norris, J. E., Ryan, S. G. and Tsangarides, S., 2007, "Carbon-enhanced Metal-poor Stars. I. Chemical Compositions of 26 Stars", *Astrophys. J.*, **655**, 492–521. [DOI], [ADS], [astro-ph/0609702]

Aoki, W., Barklem, P. S., Beers, T. C., Christlieb, N., Inoue, S., García Pérez, A. E., Norris, J. E. and Carollo, D., 2009, "Lithium Abundances of Extremely Metal-Poor Turnoff Stars", *Astrophys. J.*, **698**, 1803–1812. [DOI], [ADS], [arXiv:0904.1448 [astro-ph.SR]]

Aoki, W., Beers, T. C., Lee, Y. S., Honda, S., Ito, H., Takada-Hidai, M., Frebel, A., Suda, T., Fujimoto, M. Y., Carollo, D. and Sivarani, T., 2013, "High-resolution Spectroscopy of Extremely Metal-poor Stars from SDSS/SEGUE. I. Atmospheric Parameters and Chemical Compositions", *Astron. J.*, **145**, 13. [DOI], [ADS], [arXiv:1210.1946 [astro-ph.SR]]

Arcones, A. and Montes, F., 2011, "Production of Light-element Primary Process Nuclei in Neutrino-driven Winds", *Astrophys. J.*, **731**, 5. [DOI], [ADS], [arXiv:1007.1275 [astro-ph.GA]]

Argast, D., Samland, M., Thielemann, F.-K. and Qian, Y.-Z., 2004, "Neutron star mergers versus core-collapse supernovae as dominant r-process sites in the early Galaxy", *Astron. Astrophys.*, **416**, 997–1011. [DOI], [ADS], [astro-ph/0309237]

Armandroff, T. E., Da Costa, G. S. and Zinn, R., 1992, "Metallicities for the outer-halo globular clusters PAL 3, 4, and 14", *Astron. J.*, **104**, 164–177. [DOI], [ADS]

Armosky, B. J., Sneden, C., Langer, G. E. and Kraft, R. P., 1994, "Abundance trends among neutron capture elements in giants of globular clusters M5, M3, M13, M92, and M15", *Astron. J.*, **108**, 1364–1374. [DOI], [ADS]

Arnett, W. D., 1971, "Galactic Evolution and Nucleosynthesis", *Astrophys. J.*, **166**, 153. [DOI], [ADS]

Ashman, K. M. and Carr, B. J., 1988, "Pre-galactic cooling flows and baryonic dark matter", *Mon. Not. Roy. Astron. Soc.*, **234**, 219–240. [DOI], [ADS]

Ashman, K. M. and Zepf, S. E., 1992, "Globular Clusters, Mergers, and Galaxy Evolution", in *American Astronomical Society Meeting Abstracts*, Bulletin of the American Astronomical Society, 24, [ADS]

Asplund, M., 2005, "Uncertainties in Stellar Abundance Analyses", *Highlights of Astronomy*, **13**, 542. [ADS]

Asplund, M., Grevesse, N., Sauval, A. J. and Scott, P., 2009, "The Chemical Composition of the Sun", *Ann. Rev. Astron. Astrophys.*, **47**, 481–522. [DOI], [ADS], [arXiv:0909.0948 [astro-ph.SR]]

Audouze, J. and Silk, J., 1995, "The First Generation of Stars: First Steps toward Chemical Evolution of Galaxies", *Astrophys. J. Lett.*, **451**, L49. [DOI], [ADS], [astro-ph/9508040]

Balbinot, Eduardo and Gieles, Mark, 2018, "The devil is in the tails: the role of globular cluster mass evolution on stream properties", *Mon. Not. Roy. Astron. Soc.*, **474**(2), 2479–2492. [DOI], [ADS], [arXiv:1702.02543 [astro-ph.GA]]

Bandyopadhyay, Avrajit, Sivarani, Thirupathi, Susmitha, Antony, Beers, Timothy C., Giridhar, Sunetra, Surya, Arun and Masseron, Thomas, 2018, "Chemical

Composition of Two Bright, Extremely Metal-poor Stars from the SDSS MARVELS Pre-survey", *Astrophys. J.*, **859**(2), 114. [DOI], [ADS], [arXiv:1805.02280 [astro-ph.SR]]

Barklem, P. S., Christlieb, N., Beers, T. C., Hill, V., Bessell, M. S., Holmberg, J., Marsteller, B., Rossi, S., Zickgraf, F.-J. and Reimers, D., 2005, "The Hamburg/ESO R-process enhanced star survey (HERES). II. Spectroscopic analysis of the survey sample", *Astron. Astrophys.*, **439**, 129–151. [DOI], [ADS], [astro-ph/0505050]

Battaglia, G., North, P., Jablonka, P., Shetrone, M., Minniti, D., Díaz, M., Starkenburg, E. and Savoy, M., 2017, "What is the Milky Way outer halo made of?. High resolution spectroscopy of distant red giants", *Astron. Astrophys.*, **608**, A145. [DOI], [ADS], [arXiv:1710.01320 [astro-ph.GA]]

Baumueller, D. and Gehren, T., 1997, "Aluminium in metal-poor stars.", *Astron. Astrophys.*, **325**, 1088–1098. [ADS]

Bayo, A., Rodrigo, C., Barrado Y Navascués, D., Solano, E., Gutiérrez, R., Morales-Calderón, M. and Allard, F., 2008, "VOSA: virtual observatory SED analyzer. An application to the Collinder 69 open cluster", *Astron. Astrophys.*, **492**, 277–287. [DOI], [ADS], [arXiv:0808.0270]

Bedin, L. R., Piotto, G., Anderson, J., King, I. R., Cassisi, S. and Momany, Y., 2004, "The double main sequence of Omega Centauri", *Memorie della Societa Astronomica Italiana Supplementi*, **5**, 105. [ADS], [astro-ph/0406076]

Beers, T. C. and Christlieb, N., 2005, "The Discovery and Analysis of Very Metal-Poor Stars in the Galaxy", *Ann. Rev. Astron. Astrophys.*, **43**, 531–580. [DOI], [ADS]

Beers, T. C., Preston, G. W. and Shectman, S. A., 1985, "A search for stars of very low metal abundance. I", *Astron. J.*, **90**, 2089–2102. [DOI], [ADS]

Beers, T. C., Preston, G. W. and Shectman, S. A., 1992, "A search for stars of very low metal abundance. II", *Astron. J.*, **103**, 1987–2034. [DOI], [ADS]

Beers, T. C., Placco, V. M., Carollo, D., Rossi, S., Lee, Y. S., Frebel, A., Norris, J. E., Dietz, S. and Masseron, T., 2017, "Bright Metal-Poor Stars from the Hamburg/ESO Survey. II. A Chemodynamical Analysis", *Astrophys. J.*, **835**, 81. [DOI], [ADS], [arXiv:1611.03762 [astro-ph.SR]]

Bergemann, M. and Cescutti, G., 2010, "Chromium: NLTE abundances in metal-poor stars and nucleosynthesis in the Galaxy", *Astron. Astrophys.*, **522**, A9. [DOI], [ADS], [arXiv:1006.0243 [astro-ph.SR]]

Bergemann, M. and Gehren, T., 2008, "NLTE abundances of Mn in a sample of metal-poor stars", *Astron. Astrophys.*, **492**(3), 823–831. [DOI], [ADS], [arXiv:0811.0681 [astro-ph]]

Bergemann, Maria, Pickering, Juliet C. and Gehren, Thomas, 2010, "NLTE analysis of CoI/CoII lines in spectra of cool stars with new laboratory hyperfine splitting constants", *Mon. Not. Roy. Astron. Soc.*, **401**(2), 1334–1346. [DOI], [ADS], [arXiv:0909.2178 [astro-ph.SR]]

Bloecker, T. and Schoenberner, D., 1991, "A 7-solar-mass AGB model sequence not complying with the core mass-luminosity relation", *Astron. Astrophys.*, **244**, L43–L46. [ADS]

Bonifacio, P., Molaro, P., Sivarani, T., Cayrel, R., Spite, M., Spite, F., Plez, B., Andersen, J., Barbuy, B., Beers, T. C., Depagne, E., Hill, V., François, P., Nordström, B. and Primas, F., 2007a, "First stars VII - Lithium in extremely metal poor dwarfs", *Astron. Astrophys.*, **462**, 851–864. [DOI], [ADS], [astro-ph/0610245]

Bonifacio, P., Molaro, P., Sivarani, T., Cayrel, R., Spite, M., Spite, F., Plez, B., Andersen, J., Barbuy, B., Beers, T. C., Depagne, E., Hill, V., François, P., Nordström, B. and Primas, F., 2007b, "First stars VII - Lithium in extremely metal poor dwarfs", *Astron. Astrophys.*, **462**, 851–864. [DOI], [ADS], [astro-ph/0610245]

Bonifacio, P., Spite, M., Cayrel, R., Hill, V., Spite, F., François, P., Plez, B., Ludwig, H.-G., Caffau, E., Molaro, P., Depagne, E., Andersen, J., Barbuy, B., Beers, T. C., Nordström, B. and Primas, F., 2009, "First stars XII. Abundances in extremely metal-poor turnoff stars, and comparison with the giants", *Astron. Astrophys.*, **501**, 519–530. [DOI], [ADS], [arXiv:0903.4174]

Bonifacio, P., Caffau, E., Spite, M., Limongi, M., Chieffi, A., Klessen, R. S., François, P., Molaro, P., Ludwig, H.-G., Zaggia, S., Spite, F., Plez, B., Cayrel, R., Christlieb, N., Clark, P. C., Glover, S. C. O., Hammer, F., Koch, A., Monaco, L., Sbordone, L. and Steffen, M., 2015, "TOPoS . II. On the bimodality of carbon abundance in CEMP stars Implications on the early chemical evolution of galaxies", *Astron. Astrophys.*, **579**, A28. [DOI], [ADS], [arXiv:1504.05963]

Boothroyd, A. I. and Sackmann, I.-J., 1992, "Breakdown of the core mass-luminosity relation at high luminosities on the asymptotic giant branch", *Astrophys. J. Lett.*, **393**, L21–L24. [DOI], [ADS]

Bragaglia, A., Carretta, E., Gratton, R. G., Lucatello, S., Milone, A., Piotto, G., D'Orazi, V., Cassisi, S., Sneden, C. and Bedin, L. R., 2010, "X-shooter Observations of Main-sequence Stars in the Globular Cluster NGC 2808: First Chemical Tagging of a He-normal and a He-rich Dwarf", *Astrophys. J. Lett.*, **720**, L41–L45. [DOI], [ADS], [arXiv:1007.5299]

Bragaglia, A., Carretta, E., Sollima, A., Donati, P., D'Orazi, V., Gratton, R. G., Lucatello, S. and Sneden, C., 2015, "NGC 6139: a normal massive globular cluster, or a first-generation dominated cluster? Clues from the light elements", *Astron. Astrophys.*, **583**, A69. [DOI], [ADS], [arXiv:1507.07562 [astro-ph.SR]]

Bragaglia, A., Carretta, E., D'Orazi, V., Sollima, A., Donati, P., Gratton, R. G. and Lucatello, S., 2017, "NGC 6535: the lowest mass Milky Way globular cluster with a Na-O anti-correlation? Cluster mass and age in the multiple population context", *Astron. Astrophys.*, **607**, A44. [DOI], [ADS], [arXiv:1708.07705 [astro-ph.SR]]

Briley, M. M., Smith, V. V., Suntzeff, N. B., Lambert, D. L., Bell, R. A. and Hesser, J. E., 1996, "Sodium abundance variations in main-sequence stars of the globular cluster 47 Tucanae", *Nature*, **383**, 604–606. [DOI], [ADS]

Bromm, V., Yoshida, N., Hernquist, L. and McKee, C. F., 2009, "The formation of the first stars and galaxies", *Nature*, **459**, 49–54. [DOI], [ADS], [arXiv:0905.0929]

Burkert, A., Truran, J. W. and Hensler, G., 1992, "The collapse of our Galaxy and the formation of the Galactic disk", *Astrophys. J.*, **391**, 651–658. [DOI], [ADS]

Cain, M., Frebel, A., Gull, M., Ji, A. P., Placco, V. M., Beers, T. C., Meléndez, J., Ezzeddine, R., Casey, A. R., Hansen, T. T., Roederer, I. U. and Sakari, C., 2018, "The R-Process Alliance: Chemical Abundances for a Trio of r-process-enhanced Stars–One Strong, One Moderate, and One Mild", *Astrophys. J.*, **864**, 43. [DOI], [ADS], [arXiv:1807.03734 [astro-ph.SR]]

Cameron, A. G. W. and Fowler, W. A., 1971, "Lithium and the s-PROCESS in Red-Giant Stars", *Astrophys. J.*, **164**, 111. [DOI], [ADS]

Capaccioli, M., Ortolani, S. and Piotto, G., 1991, "Empirical correlations between globular cluster parameters and mass function morphology", *Astron. Astrophys.*, **244**, 298–302. [ADS]

Capaccioli, M., Piotto, G. and Stiavelli, M., 1993, "Disc Shocking and the Mass Function of Galactic Globular Clusters", *Mon. Not. Roy. Astron. Soc.*, **261**, 819. [DOI], [ADS]

Carollo, D., Beers, T. C., Lee, Y. S., Chiba, M., Norris, J. E., Wilhelm, R., Sivarani, T., Marsteller, B., Munn, J. A., Bailer-Jones, C. A. L., Fiorentin, P. R. and York, D. G., 2007, "Two stellar components in the halo of the Milky Way", *Nature*, **450**, 1020–1025. [DOI], [ADS], [arXiv:0706.3005]

Carr, B. J. and Rees, M. J., 1984, "How large were the first pregalactic objects?", *Mon. Not. Roy. Astron. Soc.*, **206**, 315–325. [DOI], [ADS]

Carretta, E., Gratton, R., Cohen, J. G., Beers, T. C. and Christlieb, N., 2002, "Stellar Archaeology: A Keck Pilot Program on Extremely Metal-poor Stars from the Hamburg/ESO Survey. II. Abundance Analysis", *Astron. J.*, **124**, 481–506. [DOI], [ADS], [astro-ph/0204083]

Carretta, E., Bragaglia, A., Gratton, R. and Lucatello, S., 2009a, "Na-O anticorrelation and HB. VIII. Proton-capture elements and metallicities in 17 globular clusters from UVES spectra", *Astron. Astrophys.*, **505**, 139–155. [DOI], [ADS], [arXiv:0909.2941]

Carretta, E., Bragaglia, A., Gratton, R. G., Lucatello, S., Catanzaro, G., Leone, F., Bellazzini, M., Claudi, R., D'Orazi, V., Momany, Y., Ortolani, S., Pancino, E., Piotto, G., Recio-Blanco, A. and Sabbi, E., 2009b, "Na-O anticorrelation and HB. VII. The chemical composition of first and second-generation stars in 15 globular clusters from GIRAFFE spectra", *Astron. Astrophys.*, **505**, 117–138. [DOI], [ADS], [arXiv:0909.2938]

Carretta, E., Bragaglia, A., D'Orazi, V., Lucatello, S. and Gratton, R. G., 2010a, "The radial distribution of stars of different stellar generations in the globular cluster NGC 3201", *Astron. Astrophys.*, **519**, A71. [DOI], [ADS], [arXiv:1006.5867]

Carretta, E., Bragaglia, A., Gratton, R. G., Recio-Blanco, A., Lucatello, S., D'Orazi, V. and Cassisi, S., 2010b, "Properties of stellar generations in globular clusters and relations with global parameters", *Astron. Astrophys.*, **516**, A55. [DOI], [ADS], [arXiv:1003.1723]

Carretta, E., Bragaglia, A., Lucatello, S., D'Orazi, V., Gratton, R. G., Donati, P., Sollima, A. and Sneden, C., 2017, "Chemical characterisation of the globular cluster NGC 5634 associated to the Sagittarius dwarf spheroidal galaxy", *Astron. Astrophys.*, **600**, A118. [DOI], [ADS], [arXiv:1701.03116 [astro-ph.SR]]

Castelli, F. and Kurucz, R. L., 2004, "New Grids of ATLAS9 Model Atmospheres", *ArXiv Astrophysics e-prints*. [ADS], [astro-ph/0405087]

Cayrel, R., Depagne, E., Spite, M., Hill, V., Spite, F., François, P., Plez, B., Beers, T., Primas, F., Andersen, J., Barbuy, B., Bonifacio, P., Molaro, P. and Nordström, B., 2004, "First stars V - Abundance patterns from C to Zn and supernova yields in the early Galaxy", *Astron. Astrophys.*, **416**, 1117–1138. [DOI], [ADS], [astro-ph/0311082]

Chiappini, C., 2013, "First stars and reionization: Spinstars", *Astronomische Nachrichten*, **334**, 595–604. [DOI], [ADS]

Choplin, A., Maeder, A., Meynet, G. and Chiappini, C., 2016, "Constraints on CEMP-no progenitors from nuclear astrophysics", *Astron. Astrophys.*, **593**, A36. [DOI], [ADS], [arXiv:1606.02752 [astro-ph.SR]]

Christlieb, N., 2003, "Finding the Most Metal-poor Stars of the Galactic Halo with the Hamburg/ESO Objective-prism Survey (With 6 Figures)", in *Reviews in Modern Astronomy*, (Ed.) Schielicke, R. E., Reviews in Modern Astronomy, 16, [DOI], [ADS], [astro-ph/0308016]

Christlieb, N., Beers, T. C., Barklem, P. S., Bessell, M., Hill, V., Holmberg, J., Korn, A. J., Marsteller, B., Mashonkina, L., Qian, Y.-Z., Rossi, S., Wasserburg, G. J., Zickgraf, F.-J., Kratz, K.-L., Nordström, B., Pfeiffer, B., Rhee, J. and Ryan, S. G., 2004, "The Hamburg/ESO R-process Enhanced Star survey (HERES). I. Project description, and discovery of two stars with strong enhancements of neutron-capture elements", *Astron. Astrophys.*, **428**, 1027–1037. [DOI], [ADS], [astro-ph/0408389]

Coelho, P., Percival, S. M. and Salaris, M., 2011, "Chemical Abundance Anticorrelations in Globular Cluster Stars: The Effect on Cluster Integrated Spectra", *Astrophys. J.*, **734**, 72. [DOI], [ADS], [arXiv:1104.1618]

Cohen, J. G., 1978, "Abundances in globular cluster red giants. I - M3 and M13", *Astrophys. J.*, **223**, 487–508. [DOI], [ADS]

Cooke, Ryan J. and Madau, Piero, 2014, "Carbon-enhanced Metal-poor Stars: Relics from the Dark Ages", *The Astrophysical Journal*, **791**(2), 116URL: http://stacks.iop.org/0004-637X/791/i=2/a=116

Cowan, J. J. and Rose, W. K., 1977, "Production of C-14 and neutrons in red giants", *Astrophys. J.*, **212**, 149–158. [DOI], [ADS]

Cristallo, S., Straniero, O., Piersanti, L. and Gobrecht, D., 2015, "Evolution, Nucleosynthesis, and Yields of AGB Stars at Different Metallicities. III. Intermediate-mass Models, Revised Low-mass Models, and the ph-FRUITY Interface", *The Astrophysical Journal Supplement Series*, **219**(2), 40. [DOI], [ADS], [arXiv:1507.07338 [astro-ph.SR]]

Dalal, Neal, Lithwick, Yoram and Kuhlen, Michael, 2010, "The Origin of Dark Matter Halo Profiles", *arXiv e-prints*, arXiv:1010.2539. [ADS], [arXiv:1010.2539 [astro-ph.CO]]

Dawson, K. S., Schlegel, D. J., Ahn, C. P., Anderson, S. F., Aubourg, É., Bailey, S., Barkhouser, R. H., Bautista, J. E., Beifiori, A., Berlind, A. A., Bhardwaj, V., Bizyaev, D., Blake, C. H., Blanton, M. R., Blomqvist, M., Bolton, A. S., Borde, A., Bovy, J., Brandt, W. N., Brewington, H., Brinkmann, J., Brown, P. J., Brownstein, J. R., Bundy, K., Busca, N. G., Carithers, W., Carnero, A. R., Carr, M. A., Chen, Y., Comparat, J., Connolly, N., Cope, F., Croft, R. A. C., Cuesta, A. J., da Costa, L. N., Davenport, J. R. A., Delubac, T., de Putter, R., Dhital, S., Ealet, A., Ebelke, G. L., Eisenstein, D. J., Escoffier, S., Fan, X., Filiz Ak, N., Finley, H., Font-Ribera, A., Génova-Santos, R., Gunn, J. E., Guo, H., Haggard, D., Hall, P. B., Hamilton, J.-C., Harris, B., Harris, D. W., Ho, S., Hogg, D. W., Holder, D., Honscheid, K., Huehnerhoff, J., Jordan, B., Jordan, W. P., Kauffmann, G., Kazin, E. A., Kirkby, D., Klaene, M. A., Kneib, J.-P., Le Goff, J.-M., Lee, K.-G., Long, D. C., Loomis, C. P., Lundgren, B., Lupton, R. H., Maia, M. A. G., Makler, M., Malanushenko, E., Malanushenko, V., Mandelbaum, R., Manera, M., Maraston, C., Margala, D., Masters, K. L., McBride, C. K., McDonald, P., McGreer, I. D., McMahon,

R. G., Mena, O., Miralda-Escudé, J., Montero-Dorta, A. D., Montesano, F., Muna, D., Myers, A. D., Naugle, T., Nichol, R. C., Noterdaeme, P., Nuza, S. E., Olmstead, M. D., Oravetz, A., Oravetz, D. J., Owen, R., Padmanabhan, N., Palanque-Delabrouille, N., Pan, K., Parejko, J. K., Pâris, I., Percival, W. J., Pérez-Fournon, I., Pérez-Ràfols, I., Petitjean, P., Pfaffenberger, R., Pforr, J., Pieri, M. M., Prada, F., Price-Whelan, A. M., Raddick, M. J., Rebolo, R., Rich, J., Richards, G. T., Rockosi, C. M., Roe, N. A., Ross, A. J., Ross, N. P., Rossi, G., Rubiño-Martin, J. A., Samushia, L., Sánchez, A. G., Sayres, C., Schmidt, S. J., Schneider, D. P., Scóccola, C. G., Seo, H.-J., Shelden, A., Sheldon, E., Shen, Y., Shu, Y., Slosar, A., Smee, S. A., Snedden, S. A., Stauffer, F., Steele, O., Strauss, M. A., Streblyanska, A., Suzuki, N., Swanson, M. E. C., Tal, T., Tanaka, M., Thomas, D., Tinker, J. L., Tojeiro, R., Tremonti, C. A., Vargas Magaña, M., Verde, L., Viel, M., Wake, D. A., Watson, M., Weaver, B. A., Weinberg, D. H., Weiner, B. J., West, A. A., White, M., Wood-Vasey, W. M., Yeche, C., Zehavi, I., Zhao, G.-B. and Zheng, Z., 2013, "The Baryon Oscillation Spectroscopic Survey of SDSS-III", *Astron. J.*, **145**, 10. [DOI], [ADS], [arXiv:1208.0022]

Decressin, T. and Charbonnel, C., 2007, "The Impacts of Rotation on Nucleosynthesis in Metal-Poor AGB Stars", in *Why Galaxies Care About AGB Stars: Their Importance as Actors and Probes*, (Eds.) Kerschbaum, F., Charbonnel, C., Wing, R. F., Astronomical Society of the Pacific Conference Series, 378, [ADS]

Denissenkov, P. A. and Herwig, F., 2003, "The Abundance Evolution of Oxygen, Sodium, and Magnesium in Extremely Metal Poor Intermediate-Mass Stars: Implications for the Self-Pollution Scenario in Globular Clusters", *Astrophys. J. Lett.*, **590**, L99–L102. [DOI], [ADS], [astro-ph/0305494]

Denissenkov, P. A. and Herwig, F., 2004, "Enhanced Extra Mixing in Low-Mass Red Giants: Lithium Production and Thermal Stability", *Astrophys. J.*, **612**, 1081–1091. [DOI], [ADS]

Denissenkov, P. A. and VandenBerg, D. A., 2003a, "Thermal Stability of Rotating Low-Mass Subgiants and Red Giants", *Astrophys. J.*, **598**, 1246–1254. [DOI], [ADS]

Denissenkov, P. A. and VandenBerg, D. A., 2003b, "Canonical Extra Mixing in Low-Mass Red Giants", *Astrophys. J.*, **593**, 509–523. [DOI], [ADS]

Denissenkov, P. A. and Weiss, A., 1996, "Deep diffusive mixing in globular-cluster red giants.", *Astron. Astrophys.*, **308**, 773–784. [ADS]

Denissenkov, P. A., Weiss, A. and Wagenhuber, J., 1997, "Could intermediate-mass AGB stars produce star-to-star abundance variations in globular-cluster red giants?", *Astron. Astrophys.*, **320**, 115–124. [ADS]

Djorgovski, S., Piotto, G. and Capaccioli, M., 1993, "What determines the stellar mass functions in globular clusters?", *Astron. J.*, **105**, 2148–2157. [DOI], [ADS]

Drout, M. R., Piro, A. L., Shappee, B. J., Kilpatrick, C. D., Simon, J. D., Contreras, C., Coulter, D. A., Foley, R. J., Siebert, M. R., Morrell, N., Boutsia, K., Di Mille, F., Holoien, T. W.-S., Kasen, D., Kollmeier, J. A., Madore, B. F., Monson, A. J., Murguia-Berthier, A., Pan, Y.-C., Prochaska, J. X., Ramirez-Ruiz, E., Rest, A., Adams, C., Alatalo, K., Bañados, E., Baughman, J., Beers, T. C., Bernstein, R. A., Bitsakis, T., Campillay, A., Hansen, T. T., Higgs, C. R., Ji, A. P., Maravelias, G., Marshall, J. L., Bidin, C. M., Prieto, J. L., Rasmussen, K. C., Rojas-Bravo, C., Strom, A. L., Ulloa, N., Vargas-González, J., Wan, Z. and Whitten, D. D., 2017, "Light curves of the neutron star merger GW170817/SSS17a: Implications for r-process nucleosynthesis", *Science*, **358**, 1570–1574. [DOI], [ADS], [arXiv:1710.05443 [astro-ph.HE]]

Eggen, O. J., Lynden-Bell, D. and Sandage, A. R., 1962, "Evidence from the motions of old stars that the Galaxy collapsed.", *Astrophys. J.*, **136**, 748. [DOI], [ADS]

Eisenstein, D. J., Annis, J., Gunn, J. E., Szalay, A. S., Connolly, A. J., Nichol, R. C., Bahcall, N. A., Bernardi, M., Burles, S., Castander, F. J., Fukugita,

M., Hogg, D. W., Ivezić, Ž., Knapp, G. R., Lupton, R. H., Narayanan, V., Postman, M., Reichart, D. E., Richmond, M., Schneider, D. P., Schlegel, D. J., Strauss, M. A., SubbaRao, M., Tucker, D. L., Vanden Berk, D., Vogeley, M. S., Weinberg, D. H. and Yanny, B., 2001, "Spectroscopic Target Selection for the Sloan Digital Sky Survey: The Luminous Red Galaxy Sample", *Astron. J.*, **122**, 2267–2280. [DOI], [ADS], [astro-ph/0108153]

Eisenstein, D. J., Weinberg, D. H., Agol, E., Aihara, H., Allende Prieto, C., Anderson, S. F., Arns, J. A., Aubourg, É., Bailey, S., Balbinot, E. and et al., 2011, "SDSS-III: Massive Spectroscopic Surveys of the Distant Universe, the Milky Way, and Extra-Solar Planetary Systems", *Astron. J.*, **142**, 72. [DOI], [ADS], [arXiv:1101.1529 [astro-ph.IM]]

Fall, S. M. and Rees, M. J., 1985, "A theory for the origin of globular clusters", *Astrophys. J.*, **298**, 18–26. [DOI], [ADS]

Fall, S. M. and Rees, M. J., 1988, "The origin of globular clusters", in *The Harlow-Shapley Symposium on Globular Cluster Systems in Galaxies*, (Eds.) Grindlay, J. E., Philip, A. G. D., IAU Symposium, 126, [ADS]

Fall, S. M. and Zhang, Q., 2001, "Dynamical Evolution of the Mass Function of Globular Star Clusters", *Astrophys. J.*, **561**, 751–765. [DOI], [ADS], [astro-ph/0107298]

Forbes, Duncan A., Bastian, Nate, Gieles, Mark, Crain, Robert A., Kruijssen, J. M. Diederik, Larsen, Søren S., Ploeckinger, Sylvia, Agertz, Oscar, Trenti, Michele, Ferguson, Annette M. N., Pfeffer, Joel and Gnedin, Oleg Y., 2018, "Globular cluster formation and evolution in the context of cosmological galaxy assembly: open questions", *Proceedings of the Royal Society of London Series A*, **474**(2210), 20170616. [DOI], [ADS], [arXiv:1801.05818 [astro-ph.GA]]

Forestini, M. and Charbonnel, C., 1997, "Nucleosynthesis of light elements inside thermally pulsing AGB stars: I. The case of intermediate-mass stars", *Astron. Astrophys. Suppl.*, **123**, 241–272. [DOI], [ADS], [astro-ph/9608153]

Frebel, A. and Norris, J. E., 2015a, "Near-Field Cosmology with Extremely Metal-Poor Stars", *Ann. Rev. Astron. Astrophys.*, **53**, 631–688. [DOI], [ADS], [arXiv:1501.06921 [astro-ph.SR]]

Frebel, A., Christlieb, N., Norris, J. E., Beers, T. C., Bessell, M. S., Rhee, J., Fechner, C., Marsteller, B., Rossi, S., Thom, C., Wisotzki, L. and Reimers, D., 2006, "Bright Metal-poor Stars from the Hamburg/ESO Survey. I. Selection and Follow-up Observations from 329 Fields", *Astrophys. J.*, **652**, 1585–1603. [DOI], [ADS], [astro-ph/0608332]

Frebel, A., Christlieb, N., Norris, J. E., Thom, C., Beers, T. C. and Rhee, J., 2007, "Discovery of HE 1523-0901, a Strongly r-Process-enhanced Metal-poor Star with Detected Uranium", *Astrophys. J. Lett.*, **660**, L117–L120. [DOI], [ADS], [astro-ph/0703414]

Frebel, Anna, 2018, "From Nuclei to the Cosmos: Tracing Heavy-Element Production with the Oldest Stars", *Annual Review of Nuclear and Particle Science*, **68**(1), 237–269. [DOI], [ADS], [arXiv:1806.08955 [astro-ph.SR]]

Frebel, Anna and Norris, John E., 2015b, "Near-Field Cosmology with Extremely Metal-Poor Stars", *Annual Review of Astronomy and Astrophysics*, **53**, 631–688. [DOI], [ADS], [arXiv:1501.06921 [astro-ph.SR]]

Freeman, K. and Bland-Hawthorn, J., 2002, "The New Galaxy: Signatures of Its Formation", *Ann. Rev. Astron. Astrophys.*, **40**, 487–537. [DOI], [ADS], [astro-ph/0208106]

Fulbright, J. P., Wyse, R. F. G., Ruchti, G. R., Gilmore, G. F., Grebel, E., Bienaymé, O., Binney, J., Bland-Hawthorn, J., Campbell, R., Freeman, K. C., Gibson, B. K., Helmi, A., Munari, U., Navarro, J. F., Parker, Q. A., Reid, W., Seabroke, G. M., Siebert, A., Siviero, A., Steinmetz, M., Watson, F. G., Williams, M. and Zwitter, T., 2010, "The RAVE Survey: Rich in Very Metal-poor Stars", *Astrophys. J. Lett.*, **724**, L104–L108. [DOI], [ADS], [arXiv:1010.4491 [astro-ph.SR]]

Fulbright, Jon. P., McWilliam, Andrew and Rich, R. Michael, 2006, "Abundances of Baade's Window Giants from Keck HIRES Spectra. I. Stellar Parameters and [Fe/H] Values", *Astrophys. J.*, **636**(2), 821–841. [DOI], [ADS], [arXiv:astro-ph/0510408 [astro-ph]]

García-Hernández, D. A., Zamora, O., Yagüe, A., Uttenthaler, S., Karakas, A. I., Lugaro, M., Ventura, P. and Lambert, D. L., 2013, "Hot bottom burning and s-process nucleosynthesis in massive AGB stars at the beginning of the thermally-pulsing phase", *Astron. Astrophys.*, **555**, L3. [DOI], [ADS], [arXiv:1306.2134 [astro-ph.SR]]

García Pérez, A. E., Cunha, K., Shetrone, M., Majewski, S. R., Johnson, J. A., Smith, V. V., Schiavon, R. P., Holtzman, J., Nidever, D., Zasowski, G., Allende Prieto, C., Beers, T. C., Bizyaev, D., Ebelke, G., Eisenstein, D. J., Frinchaboy, P. M., Girardi, L., Hearty, F. R., Malanushenko, E., Malanushenko, V., Meszaros, S., O'Connell, R. W., Oravetz, D., Pan, K., Robin, A. C., Schneider, D. P., Schultheis, M., Skrutskie, M. F., Simmonsand, A. and Wilson, J. C., 2013, "Very Metal-poor Stars in the Outer Galactic Bulge Found by the APOGEE Survey", *Astrophys. J. Lett.*, **767**, L9. [DOI], [ADS], [arXiv:1301.1367 [astro-ph.SR]]

Ge, J., Thomas, N. B., Li, R., Senan Seieroe Grieves, N., Ma, B., de Lee, N. M., Lee, B. C., Liu, J., Bolton, A. S., Thakar, A. R., Weaver, B. and SDSS-Iii Marvels Team, 2015, "The SDSS-III DR12 MARVELS radial velocity data release: the first data release from the multiple object Doppler exoplanet survey", in *American Astronomical Society Meeting Abstracts #225*, American Astronomical Society Meeting Abstracts, 225, [ADS]

Girardi, L., Bressan, A., Bertelli, G. and Chiosi, C., 2000, "Evolutionary tracks and isochrones for low- and intermediate-mass stars: From 0.15 to 7 M_{sun}, and from Z=0.0004 to 0.03", *Astron. Astrophys. Suppl.*, **141**, 371–383. [DOI], [ADS], [astro-ph/9910164]

Gnedin, O. Y. and Ostriker, J. P., 1997, "Destruction of the Galactic Globular Cluster System", *Astrophys. J.*, **474**, 223–255. [DOI], [ADS], [astro-ph/9603042]

Gratton, R., Sneden, C. and Carretta, E., 2004, "Abundance Variations Within Globular Clusters", *Ann. Rev. Astron. Astrophys.*, **42**, 385–440. [DOI], [ADS]

Gratton, R. G., Bonifacio, P., Bragaglia, A., Carretta, E., Castellani, V., Centurion, M., Chieffi, A., Claudi, R., Clementini, G., D'Antona, F., Desidera, S., François, P., Grundahl, F., Lucatello, S., Molaro, P., Pasquini, L., Sneden, C., Spite, F. and Straniero, O., 2001, "The O-Na and Mg-Al anticorrelations in turn-off and early subgiants in globular clusters", *Astron. Astrophys.*, **369**, 87–98. [DOI], [ADS], [astro-ph/0012457]

Gratton, R. G., Carretta, E. and Bragaglia, A., 2012a, "Multiple populations in globular clusters. Lessons learned from the Milky Way globular clusters", *Astron. Astrophys. Rev.*, **20**, 50. [DOI], [ADS], [arXiv:1201.6526 [astro-ph.SR]]

Gratton, R. G., Villanova, S., Lucatello, S., Sollima, A., Geisler, D., Carretta, E., Cassisi, S. and Bragaglia, A., 2012b, "Spectroscopic analysis of the two subgiant branches of the globular cluster NGC 1851", *Astron. Astrophys.*, **544**, A12. [DOI], [ADS], [arXiv:1205.5719 [astro-ph.SR]]

Grevesse, N., Scott, P., Asplund, M. and Sauval, A. J., 2015, "The elemental composition of the Sun. III. The heavy elements Cu to Th", *Astron. Astrophys.*, **573**, A27. [DOI], [ADS], [arXiv:1405.0288 [astro-ph.SR]]

Gunn, J. E., 1980, "The dynamics of galaxies and the 'missing mass' problem", *Philosophical Transactions of the Royal Society of London Series A*, **296**, 313–318. [DOI], [ADS]

Gunn, J. E., 1982, "The evolution of galaxies", in *Astrophysical Cosmology Proceedings*, (Eds.) Brueck, H. A., Coyne, G. V., Longair, M. S., [ADS]

Gunn, J. E., Carr, M., Rockosi, C., Sekiguchi, M., Berry, K., Elms, B., de Haas, E., Ivezić, Ž., Knapp, G., Lupton, R., Pauls, G., Simcoe, R., Hirsch, R., Sanford,

D., Wang, S., York, D., Harris, F., Annis, J., Bartozek, L., Boroski, W., Bakken, J., Haldeman, M., Kent, S., Holm, S., Holmgren, D., Petravick, D., Prosapio, A., Rechenmacher, R., Doi, M., Fukugita, M., Shimasaku, K., Okada, N., Hull, C., Siegmund, W., Mannery, E., Blouke, M., Heidtman, D., Schneider, D., Lucinio, R. and Brinkman, J., 1998, "The Sloan Digital Sky Survey Photometric Camera", *Astron. J.*, **116**, 3040–3081. [DOI], [ADS], [astro-ph/9809085]

Gunn, J. E., Siegmund, W. A., Mannery, E. J., Owen, R. E., Hull, C. L., Leger, R. F., Carey, L. N., Knapp, G. R., York, D. G., Boroski, W. N., Kent, S. M., Lupton, R. H., Rockosi, C. M., Evans, M. L., Waddell, P., Anderson, J. E., Annis, J., Barentine, J. C., Bartoszek, L. M., Bastian, S., Bracker, S. B., Brewington, H. J., Briegel, C. I., Brinkmann, J., Brown, Y. J., Carr, M. A., Czarapata, P. C., Drennan, C. C., Dombeck, T., Federwitz, G. R., Gillespie, B. A., Gonzales, C., Hansen, S. U., Harvanek, M., Hayes, J., Jordan, W., Kinney, E., Klaene, M., Kleinman, S. J., Kron, R. G., Kresinski, J., Lee, G., Limmongkol, S., Lindenmeyer, C. W., Long, D. C., Loomis, C. L., McGehee, P. M., Mantsch, P. M., Neilsen, Jr., E. H., Neswold, R. M., Newman, P. R., Nitta, A., Peoples, Jr., J., Pier, J. R., Prieto, P. S., Prosapio, A., Rivetta, C., Schneider, D. P., Snedden, S. and Wang, S.-i., 2006, "The 2.5 m Telescope of the Sloan Digital Sky Survey", *Astron. J.*, **131**, 2332–2359. [DOI], [ADS], [astro-ph/0602326]

Gustafsson, B., Edvardsson, B., Eriksson, K., Jørgensen, U. G., Nordlund, Å. and Plez, B., 2008, "A grid of MARCS model atmospheres for late-type stars. I. Methods and general properties", *Astron. Astrophys.*, **486**, 951–970. [DOI], [ADS], [arXiv:0805.0554]

Hampel, M., Stancliffe, R. J., Lugaro, M. and Meyer, B. S., 2016, "The Intermediate Neutron-capture Process and Carbon-enhanced Metal-poor Stars", *Astrophys. J.*, **831**, 171. [DOI], [ADS], [arXiv:1608.08634 [astro-ph.SR]]

Hansen, C. J., 2012, "A near field cosmology study of heavy elements in very metal-poor stars", in *American Institute of Physics Conference Series*, (Eds.)

Umemura, M., Omukai, K., American Institute of Physics Conference Series, 1480, [DOI], [ADS], [arXiv:1211.6117 [astro-ph.SR]]

Hansen, T. T., Andersen, J., Nordström, B., Beers, T. C., Placco, V. M., Yoon, J. and Buchhave, L. A., 2016a, "The role of binaries in the enrichment of the early Galactic halo. III. Carbon-enhanced metal-poor stars - CEMP-s stars", *Astron. Astrophys.*, **588**, A3. [DOI], [ADS], [arXiv:1601.03385 [astro-ph.SR]]

Hansen, T. T., Andersen, J., Nordström, B., Beers, T. C., Placco, V. M., Yoon, J. and Buchhave, L. A., 2016b, "The role of binaries in the enrichment of the early Galactic halo. II. Carbon-enhanced metal-poor stars: CEMP-no stars", *Astron. Astrophys.*, **586**, A160. [DOI], [ADS], [arXiv:1511.08197 [astro-ph.SR]]

Hansen, T. T., Holmbeck, E. M., Beers, T. C., Placco, V. M., Roederer, I. U., Frebel, A., Sakari, C. M., Simon, J. D. and Thompson, I. B., 2018, "The R-process Alliance: First Release from the Southern Search for R-process-enhanced Stars in the Galactic Halo", *Astrophys. J.*, **858**, 92. [DOI], [ADS], [arXiv:1804.03114 [astro-ph.SR]]

Harbeck, D., Smith, G. H. and Grebel, E. K., 2003, "CN Abundance Variations on the Main Sequence of 47 Tucanae", *Astron. J.*, **125**, 197–207. [DOI], [ADS], [astro-ph/0210364]

Heger, A. and Woosley, S. E., 2002, "The Nucleosynthetic Signature of Population III", *Astrophys. J.*, **567**, 532–543. [DOI], [ADS], [astro-ph/0107037]

Heger, A. and Woosley, S. E., 2010, "Nucleosynthesis and Evolution of Massive Metal-free Stars", *Astrophys. J.*, **724**, 341–373. [DOI], [ADS], [arXiv:0803.3161]

Heiter, U. and Eriksson, K., 2006, "Geometry of giant star model atmospheres: a consistency test", *Astron. Astrophys.*, **452**, 1039–1048. [DOI], [ADS], [astro-ph/0603273]

Helmi, A., Babusiaux, C., Koppelman, H. H., Massari, D., Veljanoski, J. and Brown, A. G. A., 2018, "The merger that led to the formation of the Milky

Way's inner stellar halo and thick disk", *Nature*, **563**, 85–88. [DOI], [ADS], [arXiv:1806.06038]

Herwig, Falk, 2005, "Evolution of Asymptotic Giant Branch Stars", *Annual Review of Astronomy and Astrophysics*, **43**(1), 435–479. [DOI], [https://doi.org/10.1146/annurev.astro.43.072103.150600]URL: `https://doi.org/10.1146/annurev.astro.43.072103.150600`

Hill, V., Christlieb, N., Beers, T. C., Barklem, P. S., Kratz, K.-L., Nordström, B., Pfeiffer, B. and Farouqi, K., 2017, "The Hamburg/ESO R-process Enhanced Star survey (HERES). XI. The highly r-process-enhanced star CS 29497-004", *Astron. Astrophys.*, **607**, A91. [DOI], [ADS], [arXiv:1608.07463]

Holmbeck, E. M., Beers, T. C., Roederer, I. U., Placco, V. M., Hansen, T. T., Sakari, C. M., Sneden, C., Liu, C., Lee, Y. S., Cowan, J. J. and Frebel, A., 2018, "The R-Process Alliance: 2MASS J09544277+5246414, the Most Actinide-enhanced R-II Star Known", *Astrophys. J. Lett.*, **859**, L24. [DOI], [ADS], [arXiv:1805.11925 [astro-ph.SR]]

Honda, S., Aoki, W., Ishimaru, Y., Wanajo, S. and Ryan, S. G., 2006, "Neutron-Capture Elements in the Very Metal Poor Star HD 122563", *Astrophys. J.*, **643**, 1180–1189. [DOI], [ADS], [astro-ph/0602107]

Hotokezaka, K., Piran, T. and Paul, M., 2015, "Short-lived ^{244}Pu points to compact binary mergers as sites for heavy r-process nucleosynthesis", *Nature Physics*, **11**, 1042. [DOI], [ADS], [arXiv:1510.00711 [astro-ph.HE]]

Iben, Jr., I., 1976, "Further adventures of a thermally pulsing star", *Astrophys. J.*, **208**, 165–176. [DOI], [ADS]

Iben, Jr., I. and Renzini, A., 1982, "On the formation of carbon star characteristics and the production of neutron-rich isotopes in asymptotic giant branch stars of small core mass", *Astrophys. J. Lett.*, **263**, L23–L27. [DOI], [ADS]

Ishimaru, Yuhri, Wanajo, Shinya and Prantzos, Nikos, 2015, "Neutron Star Mergers as the Origin of r-process Elements in the Galactic Halo Based on the Sub-halo Clustering Scenario", *Astrophys. J.*, **804**(2), L35. [DOI], [ADS], [arXiv:1504.04559 [astro-ph.GA]]

Ivans, I. I., Kraft, R. P., Sneden, C., Smith, G. H., Rich, R. M. and Shetrone, M., 2001, "New Analyses of Star-to-Star Abundance Variations among Bright Giants in the Mildly Metal-poor Globular Cluster M5", *Astron. J.*, **122**, 1438–1463. [DOI], [ADS], [astro-ph/0106249]

Ivezić, Ž., Beers, T. C. and Jurić, M., 2012, "Galactic Stellar Populations in the Era of the Sloan Digital Sky Survey and Other Large Surveys", *Ann. Rev. Astron. Astrophys.*, **50**, 251–304. [DOI], [ADS], [arXiv:1308.6386]

Jofré, P. and Weiss, A., 2011, "The age of the Milky Way halo stars from the Sloan Digital Sky Survey", *Astron. Astrophys.*, **533**, A59. [DOI], [ADS], [arXiv:1105.2022 [astro-ph.GA]]

Johnson, J. A., Herwig, F., Beers, T. C. and Christlieb, N., 2007, "A Search for Nitrogen-enhanced Metal-poor Stars", *Astrophys. J.*, **658**, 1203–1216. [DOI], [ADS], [astro-ph/0608666]

Karakas, A. I. and Lattanzio, J. C., 2003, "Production of Aluminium and the Heavy Magnesium Isotopes in Asymptotic Giant Branch Stars", *Publications of the Astronomical Society of Australia*, **20**, 279–293. [DOI], [ADS]

Kayser, A., Hilker, M., Grebel, E. K. and Willemsen, P. G., 2008, "Comparing CN and CH line strengths in a homogeneous spectroscopic sample of 8 Galactic globular clusters", *Astron. Astrophys.*, **486**, 437–452. [DOI], [ADS], [arXiv:0805.1067]

Keller, S. C., Bessell, M. S., Frebel, A., Casey, A. R., Asplund, M., Jacobson, H. R., Lind, K., Norris, J. E., Yong, D., Heger, A., Magic, Z., da Costa, G. S., Schmidt, B. P. and Tisserand, P., 2014, "A single low-energy, iron-poor supernova as the source of metals in the star SMSS J031300.36-670839.3", *Nature*, **506**, 463–466. [DOI], [ADS], [arXiv:1402.1517 [astro-ph.SR]]

Kilpatrick, C. D., Foley, R. J., Kasen, D., Murguia-Berthier, A., Ramirez-Ruiz, E., Coulter, D. A., Drout, M. R., Piro, A. L., Shappee, B. J., Boutsia, K., Contreras, C., Di Mille, F., Madore, B. F., Morrell, N., Pan, Y.-C., Prochaska, J. X., Rest, A., Rojas-Bravo, C., Siebert, M. R., Simon, J. D. and Ulloa, N., 2017, "Electromagnetic evidence that SSS17a is the result of a binary neutron star merger", *Science*, **358**, 1583–1587. [DOI], [ADS], [arXiv:1710.05434 [astro-ph.HE]]

King, I., Gilmore, G. and van der Kruit, P. C. (Eds.), 1990, *The Milky Way As Galaxy*. [ADS]

Kirby, E. N., Guhathakurta, P., Bolte, M., Sneden, C. and Geha, M. C., 2009, "Multi-element Abundance Measurements from Medium-resolution Spectra. I. The Sculptor Dwarf Spheroidal Galaxy", *Astrophys. J.*, **705**, 328–346. [DOI], [ADS], [arXiv:0909.3092]

Korn, A. J., Grundahl, F., Richard, O., Barklem, P. S., Mashonkina, L., Collet, R., Piskunov, N. and Gustafsson, B., 2006, "A probable stellar solution to the cosmological lithium discrepancy", *Nature*, **442**, 657–659. [DOI], [ADS], [astro-ph/0608201]

Kraft, R. P., 1979, "On the nonhomogeneity of metal abundances in stars of globular clusters and satellite subsystems of the Galaxy", *Ann. Rev. Astron. Astrophys.*, **17**, 309–343. [DOI], [ADS]

Kraft, R. P., Trefzger, C. F. and Suntzeff, N., 1979, "Is there a composition gradient in the halo", in *The Large-Scale Characteristics of the Galaxy*, (Ed.) Burton, W. B., IAU Symposium, 84, [ADS]

Kraft, R. P., Sneden, C., Smith, G. H., Shetrone, M. D., Langer, G. E. and Pilachowski, C. A., 1997, "Proton Capture Chains in Globular Cluster Stars.II.Oxygen, Sodium, Magnesium, and Aluminum Abundances in M13 Giants Brighter Than the Horizontal Branch", *Astron. J.*, **113**, 279. [DOI], [ADS]

Kratz, K.-L., Farouqi, K., Pfeiffer, B., Truran, J. W., Sneden, C. and Cowan, J. J., 2007, "Explorations of the r-Processes: Comparisons between Calculations and Observations of Low-Metallicity Stars", *Astrophys. J.*, **662**, 39–52. [DOI], [ADS], [astro-ph/0703091]

Kruijssen, J. M. Diederik, 2014a, "Globular cluster formation in the context of galaxy formation and evolution", *Classical and Quantum Gravity*, **31**(24), 244006. [DOI], [ADS], [arXiv:1407.2953 [astro-ph.GA]]

Kruijssen, J. M. Diederik, 2014b, "Globular cluster formation in the context of galaxy formation and evolution", *Classical and Quantum Gravity*, **31**(24), 244006. [DOI], [ADS], [arXiv:1407.2953 [astro-ph.GA]]

Kurucz, R., 1993, "ATLAS9 Stellar Atmosphere Programs and 2 km/s grid.", *ATLAS9 Stellar Atmosphere Programs and 2 km/s grid. Kurucz CD-ROM No. 13. Cambridge, Mass.: Smithsonian Astrophysical Observatory, 1993.*, **13**. [ADS]

Lai, D. K., Bolte, M., Johnson, J. A., Lucatello, S., Heger, A. and Woosley, S. E., 2008, "Detailed Abundances for 28 Metal-poor Stars: Stellar Relics in the Milky Way", *Astrophys. J.*, **681**, 1524-1556. [DOI], [ADS], [arXiv:0804.1370]

Langer, G. E., Hoffman, R. and Sneden, C., 1993, "Sodium-oxygen abundance anticorrelations and deep-mixing scenarios for globular-cluster giants", *Pub. Astron. Soc. Pac.*, **105**, 301–307. [DOI], [ADS]

Langer, N., Heger, A., Wellstein, S. and Herwig, F., 1999, "Mixing and nucleosynthesis in rotating TP-AGB stars", *Astron. Astrophys.*, **346**, L37–L40. [ADS], [astro-ph/9904257]

Lattanzio, J. and Forestini, M., 1999, "Nucleosynthesis in AGB Stars", in *Asymptotic Giant Branch Stars*, (Eds.) Le Bertre, T., Lebre, A., Waelkens, C., IAU Symposium, 191, [ADS]

Lattimer, J. M. and Schramm, D. N., 1974, "Black-hole-neutron-star collisions", *Astrophys. J. Lett.*, **192**, L145–L147. [DOI], [ADS]

Lau, H. H. B., Stancliffe, R. J. and Tout, C. A., 2007, "Carbon-rich extremely metal poor stars: signatures of Population III asymptotic giant branch stars in binary systems", *Mon. Not. Roy. Astron. Soc.*, **378**, 563–568. [DOI], [ADS], [astro-ph/0703685]

Lee, J.-W., 2010, "Variations in the Na-O anticorrelation in globular clusters: evidence for a deep mixing episode in red giant branch stars", *Mon. Not. Roy. Astron. Soc.*, **405**, L36–L40. [DOI], [ADS], [arXiv:1003.3516]

Lee, Y. S., Beers, T. C., Masseron, T., Plez, B., Rockosi, C. M., Sobeck, J., Yanny, B., Lucatello, S., Sivarani, T., Placco, V. M. and Carollo, D., 2013, "Carbon-enhanced Metal-poor Stars in SDSS/SEGUE. I. Carbon Abundance Estimation and Frequency of CEMP Stars", *Astron. J.*, **146**, 132. [DOI], [ADS], [arXiv:1310.3276 [astro-ph.SR]]

Lee, Y. S., Beers, T. C., Kim, Y. K., Placco, V., Yoon, J., Carollo, D., Masseron, T. and Jung, J., 2017, "Chemical Cartography. I. A Carbonicity Map of the Galactic Halo", *Astrophys. J.*, **836**, 91. [DOI], [ADS], [arXiv:1702.00195]

Li, H.-N., Zhao, G., Christlieb, N., Wang, L., Wang, W., Zhang, Y., Hou, Y. and Yuan, H., 2015, "Spectroscopic Analysis of Metal-poor Stars from LAMOST: Early Results", *Astrophys. J.*, **798**, 110. [DOI], [ADS], [arXiv:1501.03062 [astro-ph.SR]]

Lind, K., Koposov, S. E., Battistini, C., Marino, A. F., Ruchti, G., Serenelli, A., Worley, C. C., Alves-Brito, A., Asplund, M., Barklem, P. S., Bensby, T., Bergemann, M., Blanco-Cuaresma, S., Bragaglia, A., Edvardsson, B., Feltzing, S., Gruyters, P., Heiter, U., Jofre, P., Korn, A. J., Nordlander, T., Ryde, N., Soubiran, C., Gilmore, G., Randich, S., Ferguson, A. M. N., Jeffries, R. D., Vallenari, A., Allende Prieto, C., Pancino, E., Recio-Blanco, A., Romano, D., Smiljanic, R., Bellazzini, M., Damiani, F., Hill, V., de Laverny, P., Jackson,

R. J., Lardo, C. and Zaggia, S., 2015, "The Gaia-ESO Survey: A globular cluster escapee in the Galactic halo", *Astron. Astrophys.*, **575**, L12. [DOI], [ADS], [arXiv:1502.03934 [astro-ph.SR]]

Lippuner, J., Fernández, R., Roberts, L. F., Foucart, F., Kasen, D., Metzger, B. D. and Ott, C. D., 2017, "Signatures of hypermassive neutron star lifetimes on r-process nucleosynthesis in the disc ejecta from neutron star mergers", *Mon. Not. Roy. Astron. Soc.*, **472**, 904–918. [DOI], [ADS], [arXiv:1703.06216 [astro-ph.HE]]

Lucatello, S., Beers, T. C., Christlieb, N., Barklem, P. S., Rossi, S., Marsteller, B., Sivarani, T. and Lee, Y. S., 2006, "The Frequency of Carbon-enhanced Metal-poor Stars in the Galaxy from the HERES Sample", *Astrophys. J. Lett.*, **652**, L37–L40. [DOI], [ADS], [astro-ph/0609730]

Lucatello, Sara, Tsangarides, Stelios, Beers, Timothy C., Carretta, Eugenio, Gratton, Raffaele G. and Ryan, Sean G., 2005, "The Binary Frequency Among Carbon-enhanced, s-Process-rich, Metal-poor Stars", *The Astrophysical Journal*, **625**(2), 825URL: `http://stacks.iop.org/0004-637X/625/i=2/a=825`

Madriz Aguilar, José Edgar, Zamarripa, J., Peraza, A. and Licea, J. A., 2017, "Λ(t) CDM and the present accelerating expansion of the universe from 5D scalar vacuum", *Physics of the Dark Universe*, **18**, 11–16. [DOI], [ADS], [arXiv:1706.08886 [gr-qc]]

Maeda, K. and Nomoto, K., 2003, "Bipolar Supernova Explosions: Nucleosynthesis and Implications for Abundances in Extremely Metal-Poor Stars", *Astrophys. J.*, **598**, 1163–1200. [DOI], [ADS], [astro-ph/0304172]

Maeder, A. and Meynet, G., 2015, "The first stars: a classification of CEMP-no stars", *Astron. Astrophys.*, **580**, A32. [DOI], [ADS], [arXiv:1506.04508 [astro-ph.SR]]

Maeder, A., Meynet, G. and Chiappini, C., 2015, "The first stars: CEMP-no stars and signatures of spinstars", *Astron. Astrophys.*, **576**, A56. [DOI], [ADS], [arXiv:1412.5754 [astro-ph.SR]]

Majewski, Steven R., Schiavon, Ricardo P., Frinchaboy, Peter M., Allende Prieto, Carlos, Barkhouser, Robert, Bizyaev, Dmitry, Blank, Basil, Brunner, Sophia, Burton, Adam, Carrera, Ricardo, Chojnowski, S. Drew, Cunha, Kátia, Epstein, Courtney, Fitzgerald, Greg, García Pérez, Ana E., Hearty, Fred R., Henderson, Chuck, Holtzman, Jon A., Johnson, Jennifer A., Lam, Charles R., Lawler, James E., Maseman, Paul, Mészáros, Szabolcs, Nelson, Matthew, Nguyen, Duy Coung, Nidever, David L., Pinsonneault, Marc, Shetrone, Matthew, Smee, Stephen, Smith, Verne V., Stolberg, Todd, Skrutskie, Michael F., Walker, Eric, Wilson, John C., Zasowski, Gail, Anders, Friedrich, Basu, Sarbani, Beland, Stephane, Blanton, Michael R., Bovy, Jo, Brownstein, Joel R., Carlberg, Joleen, Chaplin, William, Chiappini, Cristina, Eisenstein, Daniel J., Elsworth, Yvonne, Feuillet, Diane, Fleming, Scott W., Galbraith-Frew, Jessica, García, Rafael A., García-Hernández, D. Aníbal, Gillespie, Bruce A., Girardi, Léo, Gunn, James E., Hasselquist, Sten, Hayden, Michael R., Hekker, Saskia, Ivans, Inese, Kinemuchi, Karen, Klaene, Mark, Mahadevan, Suvrath, Mathur, Savita, Mosser, Benoît, Muna, Demitri, Munn, Jeffrey A., Nichol, Robert C., O'Connell, Robert W., Parejko, John K., Robin, A. C., Rocha-Pinto, Helio, Schultheis, Matthias, Serenelli, Aldo M., Shane, Neville, Silva Aguirre, Victor, Sobeck, Jennifer S., Thompson, Benjamin, Troup, Nicholas W., Weinberg, David H. and Zamora, Olga, 2017, "The Apache Point Observatory Galactic Evolution Experiment (APOGEE)", *Astron. J.*, **154**(3), 94. [DOI], [ADS], [arXiv:1509.05420 [astro-ph.IM]]

Marigo, P., Bressan, A. and Chiosi, C., 1998, "TP-AGB stars with envelope burning", *Astron. Astrophys.*, **331**, 564–580. [ADS], [astro-ph/9710093]

Marigo, P., Girardi, L., Bressan, A., Groenewegen, M. A. T., Silva, L. and Granato, G. L., 2008, "Evolution of asymptotic giant branch stars. II. Optical

to far-infrared isochrones with improved TP-AGB models", *Astron. Astrophys.*, **482**, 883–905. [DOI], [ADS], [arXiv:0711.4922]

Martell, S. L., 2011, "Light-element abundance variations in globular clusters", *Astronomische Nachrichten*, **332**, 467. [DOI], [ADS], [arXiv:1105.5010 [astro-ph.GA]]

Martell, S. L. and Grebel, E. K., 2010, "Light-element abundance variations in the Milky Way halo", *Astron. Astrophys.*, **519**, A14. [DOI], [ADS], [arXiv:1005.4070]

Martell, S. L., Smolinski, J. P., Beers, T. C. and Grebel, E. K., 2011, "Building the Galactic halo from globular clusters: evidence from chemically unusual red giants", *Astron. Astrophys.*, **534**, A136. [DOI], [ADS], [arXiv:1109.3916]

Martell, S. L., Shetrone, M. D., Lucatello, S., Schiavon, R. P., Mészáros, S., Allende Prieto, C., García-Hernández, D. A., Beers, T. C. and Nidever, D. L., 2016, "Chemical Tagging in the SDSS-III/APOGEE Survey: New Identifications of Halo Stars with Globular Cluster Origins", *Astrophys. J.*, **825**, 146. [DOI], [ADS], [arXiv:1605.05792]

Martell, Sarah L., 2018, "Rediscovering the origins of the stellar halo with chemical tagging", in *Rediscovering Our Galaxy*, (Eds.) Chiappini, Cristina, Minchev, Ivan, Starkenburg, Else, Valentini, Marica, IAU Symposium, 334, [DOI], [ADS], [arXiv:1710.03858 [astro-ph.GA]]

Masseron, T., van Eck, S., Famaey, B., Goriely, S., Plez, B., Siess, L., Beers, T. C., Primas, F. and Jorissen, A., 2006, "CS 30322-023: an ultra metal-poor TP-AGB star?", *Astron. Astrophys.*, **455**, 1059–1072. [DOI], [ADS], [astro-ph/0605658]

Masseron, T., Johnson, J. A., Lucatello, S., Karakas, A., Plez, B., Beers, T. C. and Christlieb, N., 2012, "Lithium Abundances in Carbon-enhanced Metal-poor Stars", *Astrophys. J.*, **751**, 14. [DOI], [ADS], [arXiv:1203.3295 [astro-ph.SR]]

Matsuno, T., Aoki, W., Beers, T. C., Lee, Y. S. and Honda, S., 2017, "High-resolution Spectroscopy of Extremely Metal-poor Stars from SDSS/SEGUE.

III. Unevolved Stars with [Fe/H] $\lesssim$ -3.5", *Astron. J.*, **154**, 52. [DOI], [ADS], [arXiv:1706.04712 [astro-ph.SR]]

McWilliam, A., 1998, "Barium Abundances in Extremely Metal-poor Stars", *Astron. J.*, **115**, 1640–1647. [DOI], [ADS]

McWilliam, A., Preston, G. W., Sneden, C. and Searle, L., 1995, "Spectroscopic Analysis of 33 of the Most Metal Poor Stars. II.", *Astron. J.*, **109**, 2757. [DOI], [ADS]

Mészáros, S., Martell, S. L., Shetrone, M., Lucatello, S., Troup, N. W., Bovy, J., Cunha, K., García-Hernández, D. A., Overbeek, J. C., Allende Prieto, C., Beers, T. C., Frinchaboy, P. M., García Pérez, A. E., Hearty, F. R., Holtzman, J., Majewski, S. R., Nidever, D. L., Schiavon, R. P., Schneider, D. P., Sobeck, J. S., Smith, V. V., Zamora, O. and Zasowski, G., 2015, "Exploring Anticorrelations and Light Element Variations in Northern Globular Clusters Observed by the APOGEE Survey", *Astron. J.*, **149**, 153. [DOI], [ADS], [arXiv:1501.05127 [astro-ph.SR]]

Meynet, G., Ekström, S. and Maeder, A., 2006, "The early star generations: the dominant effect of rotation on the CNO yields", *Astron. Astrophys.*, **447**, 623–639. [DOI], [ADS], [astro-ph/0510560]

Meynet, G., Hirschi, R., Ekstrom, S., Maeder, A., Georgy, C., Eggenberger, P. and Chiappini, C., 2010, "Are C-rich ultra iron-poor stars also He-rich?", *Astron. Astrophys.*, **521**, A30. [DOI], [ADS], [arXiv:1004.5024 [astro-ph.SR]]

Milone, A. P., Marino, A. F., Piotto, G., Bedin, L. R., Anderson, J., Aparicio, A., Cassisi, S. and Rich, R. M., 2012, "A Double Main Sequence in the Globular Cluster NGC 6397", *Astrophys. J.*, **745**, 27. [DOI], [ADS], [arXiv:1110.1077 [astro-ph.SR]]

Murray, S. D. and Lin, D. N. C., 1992, "Globular cluster formation - The fossil record", *Astrophys. J.*, **400**, 265–272. [DOI], [ADS]

Nakamura, T., Umeda, H., Nomoto, K., Thielemann, F.-K. and Burrows, A., 1999, "Nucleosynthesis in Type II Supernovae and the Abundances in Metal-poor Stars", *Astrophys. J.*, **517**, 193–208. [DOI], [ADS], [astro-ph/9809307]

Nishimura, N., Takiwaki, T. and Thielemann, F.-K., 2015, "The r-process Nucleosynthesis in the Various Jet-like Explosions of Magnetorotational Core-collapse Supernovae", *Astrophys. J.*, **810**, 109. [DOI], [ADS], [arXiv:1501.06567 [astro-ph.SR]]

Nomoto, K., Kobayashi, C. and Tominaga, N., 2013, "Nucleosynthesis in Stars and the Chemical Enrichment of Galaxies", *Ann. Rev. Astron. Astrophys.*, **51**, 457–509. [DOI], [ADS]

Nordlander, T. and Lind, K., 2017, "Non-LTE aluminium abundances in late-type stars", *Astron. Astrophys.*, **607**, A75. [DOI], [ADS], [arXiv:1708.01949 [astro-ph.SR]]

Norris, J. and Freeman, K. C., 1979, "The cyanogen distribution of the giants in 47 Tucanae", *Astrophys. J. Lett.*, **230**, L179–L182. [DOI], [ADS]

Norris, J., Cottrell, P. L., Freeman, K. C. and Da Costa, G. S., 1981, "The abundance spread in the giants of NGC 6752", *Astrophys. J.*, **244**, 205–220. [DOI], [ADS]

Odenkirchen, M., Grebel, E. K., Rockosi, C. M., Dehnen, W., Ibata, R., Rix, H.-W., Stolte, A., Wolf, C., Anderson, Jr., J. E., Bahcall, N. A., Brinkmann, J., Csabai, I., Hennessy, G., Hindsley, R. B., Ivezić, Ž., Lupton, R. H., Munn, J. A., Pier, J. R., Stoughton, C. and York, D. G., 2001, "Detection of Massive Tidal Tails around the Globular Cluster Palomar 5 with Sloan Digital Sky Survey Commissioning Data", *Astrophys. J. Lett.*, **548**, L165–L169. [DOI], [ADS], [astro-ph/0012311]

Paegert, M., Stassun, K. G., De Lee, N., Pepper, J., Fleming, S. W., Sivarani, T., Mahadevan, S., Mack, III, C. E., Dhital, S., Hebb, L. and Ge, J., 2015,

"Target Selection for the SDSS-III MARVELS Survey", *Astron. J.*, **149**, 186. [DOI], [ADS], [arXiv:1505.04708 [astro-ph.SR]]

Pasquini, L., Bonifacio, P., Molaro, P., Francois, P., Spite, F., Gratton, R. G., Carretta, E. and Wolff, B., 2005, "Li in NGC 6752 and the formation of globular clusters", *Astron. Astrophys.*, **441**(2), 549–553. [DOI], [ADS], [arXiv:astro-ph/0506651 [astro-ph]]

Peebles, P. J. E. and Dicke, R. H., 1968, "Origin of the Globular Star Clusters", *Astrophys. J.*, **154**, 891. [DOI], [ADS]

Peterson, R. C., 1976, "Constraints on nucleosynthesis imposed by extremely metal-poor stars", *Astrophys. J.*, **206**, 800–808. [DOI], [ADS]

Peterson, R. C., 1980, "Evidence from sodium-abundance variations among red giants of M13 for inhomogeneities in the protocluster gas", *Astrophys. J. Lett.*, **237**, L87–L91. [DOI], [ADS]

Piau, L., Beers, T. C., Balsara, D. S., Sivarani, T., Truran, J. W. and Ferguson, J. W., 2006, "From First Stars to the Spite Plateau: A Possible Reconciliation of Halo Stars Observations with Predictions from Big Bang Nucleosynthesis", *Astrophys. J.*, **653**, 300–315. [DOI], [ADS], [astro-ph/0603553]

Pinsonneault, M. H., Walker, T. P., Steigman, G. and Narayanan, V. K., 1999, "Halo Star Lithium Depletion", *Astrophys. J.*, **527**, 180–198. [DOI], [ADS], [astro-ph/9803073]

Piotto, G., 1991, "Properties of the Globular Cluster Mass Functions", in *The Formation and Evolution of Star Clusters*, (Ed.) Janes, K., Astronomical Society of the Pacific Conference Series, 13, [ADS]

Piotto, G., 2009, "Observations of multiple populations in star clusters", in *The Ages of Stars*, (Eds.) Mamajek, E. E., Soderblom, D. R., Wyse, R. F. G., IAU Symposium, 258, [DOI], [ADS]

Piotto, G., Bedin, L. R., Anderson, J., King, I. R., Cassisi, S., Milone, A. P., Villanova, S., Pietrinferni, A. and Renzini, A., 2007, "A Triple Main Sequence in the Globular Cluster NGC 2808", *Astrophys. J. Lett.*, **661**, L53–L56. [DOI], [ADS], [astro-ph/0703767]

Placco, V. M., Frebel, A., Beers, T. C., Christlieb, N., Lee, Y. S., Kennedy, C. R., Rossi, S. and Santucci, R. M., 2014, "Metal-poor Stars Observed with the Magellan Telescope. II. Discovery of Four Stars with [Fe/H] $\leq$ -3.5", *Astrophys. J.*, **781**, 40. [DOI], [ADS], [arXiv:1311.5855 [astro-ph.SR]]

Placco, V. M., Frebel, A., Beers, T. C., Yoon, J., Chiti, A., Heger, A., Chan, C., Casey, A. R. and Christlieb, N., 2016, "Observational Constraints on First-Star Nucleosynthesis. II. Spectroscopy of an Ultra metal-poor CEMP-no Star", *Astrophys. J.*, **833**, 21. [DOI], [ADS], [arXiv:1609.02134 [astro-ph.SR]]

Placco, V. M., Holmbeck, E. M., Frebel, A., Beers, T. C., Surman, R. A., Ji, A. P., Ezzeddine, R., Points, S. D., Kaleida, C. C., Hansen, T. T., Sakari, C. M. and Casey, A. R., 2017, "RAVE J203843.2-002333: The First Highly R-process-enhanced Star Identified in the RAVE Survey", *Astrophys. J.*, **844**, 18. [DOI], [ADS], [arXiv:1706.02934 [astro-ph.SR]]

Plez, B., 2012, "Turbospectrum: Code for spectral synthesis", [ADS]

Plez, B. and Cohen, J. G., 2005, "Analysis of the carbon-rich very metal-poor dwarf G77-61", *Astron. Astrophys.*, **434**, 1117–1124. [DOI], [ADS], [astro-ph/0501535]

Plez, B., Brett, J. M. and Nordlund, Å., 1992, "Spherical opacity samples of model atmospheres for M giants and supergiants", in *Instabilities in Evolved Super- and Hypergiants*, (Eds.) de Jager, C., Nieuwenhuijzen, H., [ADS]

Plez, B., Smith, V. V. and Lambert, D. L., 1993, "Lithium Abundances and Other Clues to Envelope Burning in Small Magellanic Cloud Asymptotic Giant Branch Stars", *Astrophys. J.*, **418**, 812. [DOI], [ADS]

Pols, O. R., Izzard, R. G., Glebbeek, E. and Stancliffe, R. J., 2009, "The Puzzling Frequencies of CEMP and NEMP Stars", *Publications of the Astronomical Society of Australia*, **26**, 327–329. [DOI], [ADS], [arXiv:0910.1489 [astro-ph.SR]]

Pols, O. R., Izzard, R. G., Stancliffe, R. J. and Glebbeek, E., 2012, "The occurrence of nitrogen-enhanced metal-poor stars: implications for the initial mass function in the early Galactic halo", *Astron. Astrophys.*, **547**, A76. [DOI], [ADS], [arXiv:1209.6082]

Prantzos, N. and Charbonnel, C., 2006, "On the self-enrichment scenario of galactic globular clusters: constraints on the IMF", *Astron. Astrophys.*, **458**, 135–149. [DOI], [ADS], [astro-ph/0606112]

Pritzl, B. J., Venn, K. A. and Irwin, M., 2005, "A Comparison of Elemental Abundance Ratios in Globular Clusters, Field Stars, and Dwarf Spheroidal Galaxies", *Astron. J.*, **130**, 2140–2165. [DOI], [ADS], [astro-ph/0506238]

Qian, Y.-Z. and Wasserburg, G. J., 2002, "Determination of Nucleosynthetic Yields of Supernovae and Very Massive Stars from Abundances in Metal-Poor Stars", *Astrophys. J.*, **567**, 515–531. [DOI], [ADS], [astro-ph/0110532]

Ramírez, I. and Meléndez, J., 2005, "The Effective Temperature Scale of FGK Stars. II. T_{eff}:Color:[Fe/H] Calibrations", *Astrophys. J.*, **626**, 465–485. [DOI], [ADS], [astro-ph/0503110]

Ramírez, I., Meléndez, J. and Chanamé, J., 2012, "Oxygen Abundances in Low- and High-α Field Halo Stars and the Discovery of Two Field Stars Born in Globular Clusters", *Astrophys. J.*, **757**, 164. [DOI], [ADS], [arXiv:1208.3675 [astro-ph.SR]]

Ramirez, S. V. and Cohen, J. G., 2001, "Abundances in Stars from the Red Giant Branch Tip to the Near the Main Sequence Turn Off in M71: III. O, Na, Si, Ca, Ti, Cr, & Ni", *arXiv Astrophysics e-prints*. [ADS], [astro-ph/0107114]

Ramírez, S. V. and Cohen, J. G., 2002, "Abundances in Stars from the Red Giant Branch Tip to Near the Main-Sequence Turnoff in M71. III. Abundance Ratios", *Astron. J.*, **123**, 3277–3297. [DOI], [ADS], [astro-ph/0111572]

Ramírez, S. V., Cohen, J. G., Buss, J. and Briley, M. M., 2001, "Abundances in Stars from the Red Giant Branch Tip to Near the Main-Sequence Turnoff in M71. II. Iron Abundance", *Astron. J.*, **122**, 1429–1437. [DOI], [ADS], [astro-ph/0103494]

Richards, G. T., Fan, X., Newberg, H. J., Strauss, M. A., Vanden Berk, D. E., Schneider, D. P., Yanny, B., Boucher, A., Burles, S., Frieman, J. A., Gunn, J. E., Hall, P. B., Ivezić, Ž., Kent, S., Loveday, J., Lupton, R. H., Rockosi, C. M., Schlegel, D. J., Stoughton, C., SubbaRao, M. and York, D. G., 2002, "Spectroscopic Target Selection in the Sloan Digital Sky Survey: The Quasar Sample", *Astron. J.*, **123**, 2945–2975. [DOI], [ADS], [astro-ph/0202251]

Richtler, T. and Fichtner, H., 1993, "On the Formation of Globular Clusters", in *The Globular Cluster-Galaxy Connection*, (Eds.) Smith, G. H., Brodie, J. P., Astronomical Society of the Pacific Conference Series, 48, [ADS]

Roederer, I. U., Cowan, J. J., Karakas, A. I., Kratz, K.-L., Lugaro, M., Simmerer, J., Farouqi, K. and Sneden, C., 2010, "The Ubiquity of the Rapid Neutron-capture Process", *Astrophys. J.*, **724**, 975–993. [DOI], [ADS], [arXiv:1009.4496 [astro-ph.SR]]

Roederer, I. U., Preston, G. W., Thompson, I. B., Shectman, S. A. and Sneden, C., 2014, "Neutron-capture Nucleosynthesis in the First Stars", *Astrophys. J.*, **784**, 158. [DOI], [ADS], [arXiv:1402.4144 [astro-ph.SR]]

Rosswog, S., Korobkin, O., Arcones, A., Thielemann, F.-K. and Piran, T., 2014, "The long-term evolution of neutron star merger remnants - I. The impact of r-process nucleosynthesis", *Mon. Not. Roy. Astron. Soc.*, **439**, 744–756. [DOI], [ADS], [arXiv:1307.2939 [astro-ph.HE]]

Ryan, S. G., Norris, J. E. and Beers, T. C., 1996, "Extremely Metal-poor Stars. II. Elemental Abundances and the Early Chemical Enrichment of the Galaxy", *Astrophys. J.*, **471**, 254. [DOI], [ADS]

Ryan, S. G., Norris, J. E. and Beers, T. C., 1999, "The Spite Lithium Plateau: Ultrathin but Postprimordial", *Astrophys. J.*, **523**, 654–677. [DOI], [ADS], [astro-ph/9903059]

Ryan, S. G., Beers, T. C., Kajino, T. and Rosolankova, K., 2001, "Ultra-Lithium-deficient Halo Stars and Blue Stragglers: A Common Origin?", *Astrophys. J.*, **547**, 231–239. [DOI], [ADS], [astro-ph/0010413]

Sakari, C. M., Placco, V. M., Farrell, E. M., Roederer, I. U., Wallerstein, G., Beers, T. C., Ezzeddine, R., Frebel, A., Hansen, T., Holmbeck, E. M., Sneden, C., Cowan, J. J., Venn, K. A., Davis, C. E., Matijevič, G., Wyse, R. F. G., Bland-Hawthorn, J., Chiappini, C., Freeman, K. C., Gibson, B. K., Grebel, E. K., Helmi, A., Kordopatis, G., Kunder, A., Navarro, J., Reid, W., Seabroke, G., Steinmetz, M. and Watson, F., 2018, "The R-Process Alliance: First Release from the Northern Search for r-process-enhanced Metal-poor Stars in the Galactic Halo", *Astrophys. J.*, **868**, 110. [DOI], [ADS], [arXiv:1809.09156 [astro-ph.SR]]

Salaris, M. and Weiss, A., 2002, "Homogeneous age dating of 55 Galactic globular clusters. Clues to the Galaxy formation mechanisms", *Astron. Astrophys.*, **388**, 492–503. [DOI], [ADS], [astro-ph/0204410]

Salaris, M., Cassisi, S. and Weiss, A., 2002, "Red Giant Branch Stars: The Theoretical Framework", *Pub. Astron. Soc. Pac.*, **114**, 375–402. [DOI], [ADS], [astro-ph/0201387]

Schatz, H., Toenjes, R., Pfeiffer, B., Beers, T. C., Cowan, J. J., Hill, V. and Kratz, K.-L., 2002, "Thorium and Uranium Chronometers Applied to CS 31082-001", *Astrophys. J.*, **579**, 626–638. [DOI], [ADS], [astro-ph/0104335]

Scott, P., Asplund, M., Grevesse, N., Bergemann, M. and Sauval, A. J., 2015a, "The elemental composition of the Sun. II. The iron group elements Sc to Ni", *Astron. Astrophys.*, **573**, A26. [DOI], [ADS], [arXiv:1405.0287 [astro-ph.SR]]

Scott, P., Grevesse, N., Asplund, M., Sauval, A. J., Lind, K., Takeda, Y., Collet, R., Trampedach, R. and Hayek, W., 2015b, "The elemental composition of the Sun. I. The intermediate mass elements Na to Ca", *Astron. Astrophys.*, **573**, A25. [DOI], [ADS], [arXiv:1405.0279 [astro-ph.SR]]

Searle, L. and Zinn, R., 1978, "Compositions of halo clusters and the formation of the galactic halo", *Astrophys. J.*, **225**, 357–379. [DOI], [ADS]

Shappee, B. J., Simon, J. D., Drout, M. R., Piro, A. L., Morrell, N., Prieto, J. L., Kasen, D., Holoien, T. W.-S., Kollmeier, J. A., Kelson, D. D., Coulter, D. A., Foley, R. J., Kilpatrick, C. D., Siebert, M. R., Madore, B. F., Murguia-Berthier, A., Pan, Y.-C., Prochaska, J. X., Ramirez-Ruiz, E., Rest, A., Adams, C., Alatalo, K., Bañados, E., Baughman, J., Bernstein, R. A., Bitsakis, T., Boutsia, K., Bravo, J. R., Di Mille, F., Higgs, C. R., Ji, A. P., Maravelias, G., Marshall, J. L., Placco, V. M., Prieto, G. and Wan, Z., 2017a, "Early spectra of the gravitational wave source GW170817: Evolution of a neutron star merger", *Science*, **358**, 1574–1578. [DOI], [ADS], [arXiv:1710.05432 [astro-ph.HE]]

Shappee, B. J., Simon, J. D., Drout, M. R., Piro, A. L., Morrell, N., Prieto, J. L., Kasen, D., Holoien, T. W.-S., Kollmeier, J. A., Kelson, D. D., Coulter, D. A., Foley, R. J., Kilpatrick, C. D., Siebert, M. R., Madore, B. F., Murguia-Berthier, A., Pan, Y.-C., Prochaska, J. X., Ramirez-Ruiz, E., Rest, A., Adams, C., Alatalo, K., Bañados, E., Baughman, J., Bernstein, R. A., Bitsakis, T., Boutsia, K., Bravo, J. R., Di Mille, F., Higgs, C. R., Ji, A. P., Maravelias, G., Marshall, J. L., Placco, V. M., Prieto, G. and Wan, Z., 2017b, "Early spectra of the gravitational wave source GW170817: Evolution of a neutron star merger", *Science*, **358**, 1574–1578. [DOI], [ADS], [arXiv:1710.05432 [astro-ph.HE]]

Sharma, M., Theuns, T. and Frenk, C., 2017, "CEMPlifying reionization", *ArXiv e-prints*. [ADS], [arXiv:1712.05811]

Shetrone, M. D., 1996, "MG and AL Abundances in Halo Globular Clusters", in *Formation of the Galactic Halo...Inside and Out*, (Eds.) Morrison, H. L., Sarajedini, A., Astronomical Society of the Pacific Conference Series, 92, [ADS]

Shi, J. R., Takada-Hidai, M., Takeda, Y., Tan, K. F., Hu, S. M., Zhao, G. and Cao, C., 2012, "Silicon Abundances in nearby Stars from the Si I Infrared Lines", *Astrophys. J.*, **755**, 36. [DOI], [ADS]

Short, C. I. and Hauschildt, P. H., 2006, "NLTE Strontium and Barium in Metal-poor Red Giant Stars", *Astrophys. J.*, **641**, 494–503. [DOI], [ADS], [astro-ph/0601210]

Simmerer, J., Sneden, C., Cowan, J. J., Collier, J., Woolf, V. M. and Lawler, J. E., 2004, "The Rise of the s-Process in the Galaxy", *Astrophys. J.*, **617**, 1091–1114. [DOI], [ADS], [astro-ph/0410396]

Sitnova, T. M., Mashonkina, L. I. and Ryabchikova, T. A., 2016, "A non-local thermodynamical equilibrium line formation for neutral and singly ionized titanium in model atmospheres of reference A-K stars", *Mon. Not. Roy. Astron. Soc.*, **461**(1), 1000–1011. [DOI], [ADS], [arXiv:1605.05129 [astro-ph.SR]]

Sivarani, T., Beers, T. C., Bonifacio, P., Molaro, P., Cayrel, R., Herwig, F., Spite, M., Spite, F., Plez, B., Andersen, J., Barbuy, B., Depagne, E., Hill, V., François, P., Nordström, B. and Primas, F., 2006, "First stars X. The nature of three unevolved carbon-enhanced metal-poor stars", *Astron. Astrophys.*, **459**, 125–135. [DOI], [ADS], [astro-ph/0608112]

Smith, B. D., Wise, J. H., O'Shea, B. W., Norman, M. L. and Khochfar, S., 2015, "The first Population II stars formed in externally enriched mini-haloes", *Mon. Not. Roy. Astron. Soc.*, **452**, 2822–2836. [DOI], [ADS], [arXiv:1504.07639]

Smolinski, J. P., Martell, S. L., Beers, T. C. and Lee, Y. S., 2011, "A Survey of CN and CH Variations in Galactic Globular Clusters from Sloan Digital Sky Survey Spectroscopy", *Astron. J.*, **142**, 126. [DOI], [ADS], [arXiv:1105.5378]

Sneden, C., McWilliam, A., Preston, G. W., Cowan, J. J., Burris, D. L. and Armosky, B. J., 1996, "The Ultra–Metal-poor, Neutron-Capture–rich Giant Star CS 22892-052", *Astrophys. J.*, **467**, 819. [DOI], [ADS]

Sneden, C., Cowan, J. J., Ivans, I. I., Fuller, G. M., Burles, S., Beers, T. C. and Lawler, J. E., 2000, "Evidence of Multiple R-Process Sites in the Early Galaxy: New Observations of CS 22892-052", *Astrophys. J. Lett.*, **533**, L139–L142. [DOI], [ADS], [astro-ph/0003086]

Solà, Joan and Gómez-Valent, Adrià, 2015, "The $\bar{\Lambda}CDM$ cosmology: From inflation to dark energy through running Λ", *International Journal of Modern Physics D*, **24**(4), 1541003. [DOI], [ADS], [arXiv:1501.03832 [gr-qc]]

Spite, F. and Spite, M., 1982, "Abundance of lithium in unevolved halo stars and old disk stars - Interpretation and consequences", *Astron. Astrophys.*, **115**, 357–366. [ADS]

Spite, M., Cayrel, R., Plez, B., Hill, V., Spite, F., Depagne, E., François, P., Bonifacio, P., Barbuy, B., Beers, T., Andersen, J., Molaro, P., Nordström, B. and Primas, F., 2005, "First stars VI - Abundances of C, N, O, Li, and mixing in extremely metal-poor giants. Galactic evolution of the light elements", *Astron. Astrophys.*, **430**, 655–668. [DOI], [ADS], [astro-ph/0409536]

Spite, M., Cayrel, R., Hill, V., Spite, F., François, P., Plez, B., Bonifacio, P., Molaro, P., Depagne, E., Andersen, J., Barbuy, B., Beers, T. C., Nordström, B. and Primas, F., 2006, "First stars IX - Mixing in extremely metal-poor giants. Variation of the $^{12}C/^{13}C$, [Na/Mg] and [Al/Mg] ratios", *Astron. Astrophys.*, **455**, 291–301. [DOI], [ADS], [astro-ph/0605056]

Spite, M., Caffau, E., Bonifacio, P., Spite, F., Ludwig, H.-G., Plez, B. and Christlieb, N., 2013, "Carbon-enhanced metal-poor stars: the most pristine objects?", *Astron. Astrophys.*, **552**, A107. [DOI], [ADS], [arXiv:1303.1791]

Spite, M., Spite, F., Caffau, E. and Bonifacio, P., 2015, "Lithium abundance in a turnoff halo star on an extreme orbit", *A&A*, **582**, A74. [DOI]URL: `https://doi.org/10.1051/0004-6361/201526878`

Starkenburg, E., Shetrone, M. D., McConnachie, A. W. and Venn, K. A., 2014, "Binarity in carbon-enhanced metal-poor stars", *Mon. Not. Roy. Astron. Soc.*, **441**, 1217–1229. [DOI], [ADS], [arXiv:1404.0385 [astro-ph.SR]]

Steigman, G., 2005, "Neutrinos and Big Bang Nucleosynthesis", *Physica Scripta Volume T*, **121**, 142–146. [DOI], [ADS], [hep-ph/0501100]

Strauss, M. A., Weinberg, D. H., Lupton, R. H., Narayanan, V. K., Annis, J., Bernardi, M., Blanton, M., Burles, S., Connolly, A. J., Dalcanton, J., Doi, M., Eisenstein, D., Frieman, J. A., Fukugita, M., Gunn, J. E., Ivezić, Ž., Kent, S., Kim, R. S. J., Knapp, G. R., Kron, R. G., Munn, J. A., Newberg, H. J., Nichol, R. C., Okamura, S., Quinn, T. R., Richmond, M. W., Schlegel, D. J., Shimasaku, K., SubbaRao, M., Szalay, A. S., Vanden Berk, D., Vogeley, M. S., Yanny, B., Yasuda, N., York, D. G. and Zehavi, I., 2002, "Spectroscopic Target Selection in the Sloan Digital Sky Survey: The Main Galaxy Sample", *Astron. J.*, **124**, 1810–1824. [DOI], [ADS], [astro-ph/0206225]

Suda, T., Katsuta, Y., Yamada, S., Suwa, T., Ishizuka, C., Komiya, Y., Sorai, K., Aikawa, M. and Fujimoto, M. Y., 2008, "Stellar Abundances for the Galactic Archeology (SAGA) Database — Compilation of the Characteristics of Known Extremely Metal-Poor Stars", *Pub. Astron. Soc. Japan*, **60**, 1159–1171. [DOI], [ADS], [arXiv:0806.3697]

Suda, Takuma, Komiya, Yutaka, Yamada, Shimako, Katsuta, Yutaka, Aoki, W, Gil-Pons, Pilar, Doherty, Carolyn, Campbell, Simon, Wood, Peter Robert

and Fujimoto, Masayuki Y, 2012, "AGB evolution and nucleosynthesis at low-metallicity constrained by the star formation history of our galaxy", in *Proceedings of Science - XII International Symposium on Nuclei in the Cosmos*, (Eds.) Lattanzio, John, Karakas, Amanda, Dracoulis, George, Scuola Internazionale Superiore di Studi Avanzati (S I S S A)

Susmitha Rani, A., Sivarani, T., Beers, T. C., Fleming, S., Mahadevan, S. and Ge, J., 2016, "Abundance analysis of SDSS J134338.67+484426.6; an extremely metal-poor star from the MARVELS pre-survey", *Mon. Not. Roy. Astron. Soc.*, **458**, 2648–2656. [DOI], [ADS], [arXiv:1603.00480 [astro-ph.SR]]

Thielemann, F.-K., Eichler, M., Panov, I. V. and Wehmeyer, B., 2017, "Neutron Star Mergers and Nucleosynthesis of Heavy Elements", *Annual Review of Nuclear and Particle Science*, **67**, 253–274. [DOI], [ADS], [arXiv:1710.02142 [astro-ph.HE]]

Tominaga, N., Iwamoto, N. and Nomoto, K., 2014, "Abundance Profiling of Extremely Metal-poor Stars and Supernova Properties in the Early Universe", *Astrophys. J.*, **785**, 98. [DOI], [ADS], [arXiv:1309.6734 [astro-ph.SR]]

Toomre, A. and Toomre, J., 1972a, "Galactic Bridges and Tails", *Astrophys. J.*, **178**, 623–666. [DOI], [ADS]

Toomre, A. and Toomre, J., 1972b, "Model of the Encounter Between NGC 5194 and 5195.", in *Bulletin of the American Astronomical Society*, *Bulletin of the American Astronomical Society* , 4, [ADS]

Travaglio, C., Gallino, R., Arnone, E., Cowan, J., Jordan, F. and Sneden, C., 2004, "Galactic Evolution of Sr, Y, And Zr: A Multiplicity of Nucleosynthetic Processes", *Astrophys. J.*, **601**, 864–884. [DOI], [ADS], [astro-ph/0310189]

Truran, J. W. and Arnett, W. D., 1971, "Explosive Nucleosynthesis and the Composition of Metal-Poor Stars", *Astrophys. Space Sci.*, **11**, 430–442. [DOI], [ADS]

Truran, J. W., Cowan, J. J., Pilachowski, C. A. and Sneden, C., 2002, "Probing the Neutron-Capture Nucleosynthesis History of Galactic Matter", *Pub. Astron. Soc. Pac.*, **114**, 1293–1308. [DOI], [ADS], [astro-ph/0209308]

Tsujimoto, T. and Shigeyama, T., 2014a, "The Origins of Light and Heavy R-process Elements Identified by Chemical Tagging of Metal-poor Stars", *Astrophys. J. Lett.*, **795**, L18. [DOI], [ADS], [arXiv:1410.1891]

Tsujimoto, T. and Shigeyama, T., 2014b, "Enrichment history of r-process elements shaped by a merger of neutron star pairs", *Astron. Astrophys.*, **565**, L5. [DOI], [ADS], [arXiv:1405.1443]

Umeda, H. and Nomoto, K., 2003, "First-generation black-hole-forming supernovae and the metal abundance pattern of a very iron-poor star", *Nature*, **422**, 871–873. [DOI], [ADS], [astro-ph/0301315]

Umeda, H. and Nomoto, K., 2005, "Variations in the Abundance Pattern of Extremely Metal-Poor Stars and Nucleosynthesis in Population III Supernovae", *Astrophys. J.*, **619**, 427–445. [DOI], [ADS], [astro-ph/0308029]

Umeda, H., Nomoto, K. and Nakamura, T., 2000, "Evolution and Nucleosynthesis of Metal-Free Massive Stars", in *The First Stars*, (Eds.) Weiss, A., Abel, T. G., Hill, V., [DOI], [ADS], [astro-ph/9912248]

van den Bergh, S., 1994, "Radii, structure, and orbits of globular clusters", *Astron. J.*, **108**, 2145–2153. [DOI], [ADS]

Ventura, P., D'Antona, F. and Mazzitelli, I., 2002, "Yields from low metallicity, intermediate mass AGB stars:. Their role for the CNO and lithium abundances in Globular Cluster stars", *Astron. Astrophys.*, **393**, 215–223. [DOI], [ADS]

Villanova, S., Piotto, G., King, I. R., Anderson, J., Bedin, L. R., Gratton, R. G., Cassisi, S., Momany, Y., Bellini, A., Cool, A. M., Recio-Blanco, A. and Renzini, A., 2007, "The Multiplicity of the Subgiant Branch of ω Centauri: Evidence for Prolonged Star Formation", *The Astrophysical Journal*, **663**(1), 296–314.

[DOI]URL:
`https://doi.org/10.1086%2F517905`

Wallerstein, George, , Iben, , Icko, Parker, Peter, Merchant Boesgaard, Ann, M. Hale, Gerald, Champagne, A.E., A. Barnes, Charles, Kppler, Franz, Smith, V, D. Hoffman, Robert, X. Timmes, Frank, Sneden, Chris, Boyd, R, S. Meyer, Bradley and L. Lambert, David, 1997, "Synthesis of the elements in stars: Forty years of progress", *Reviews of Modern Physics*, **69**. [DOI]

Wallner, A., Bichler, M., Buczak, K., Dressler, R., Fifield, L. K., Schumann, D., Sterba, J. H., Tims, S. G., Wallner, G. and Kutschera, W., 2015, "Settling the Half-Life of ^{60}Fe: Fundamental for a Versatile Astrophysical Chronometer", *Physical Review Letters*, **114**(4), 041101. [DOI], [ADS]

Wanajo, S., 2013, "The r-process in Proto-neutron-star Wind Revisited", *Astrophys. J. Lett.*, **770**, L22. [DOI], [ADS], [arXiv:1305.0371 [astro-ph.SR]]

Wanajo, S. and Ishimaru, Y., 2006, "r-process calculations and Galactic chemical evolution", *Nuclear Physics A*, **777**, 676–699. [DOI], [ADS], [astro-ph/0511518]

Winteler, C., Käppeli, R., Perego, A., Arcones, A., Vasset, N., Nishimura, N., Liebendörfer, M. and Thielemann, F.-K., 2012, "Magnetorotationally Driven Supernovae as the Origin of Early Galaxy r-process Elements?", *Astrophys. J. Lett.*, **750**, L22. [DOI], [ADS], [arXiv:1203.0616 [astro-ph.SR]]

Woosley, S. E. and Hoffman, R. D., 1992, "The alpha -Process and the r-Process", in *American Astronomical Society Meeting Abstracts*, Bulletin of the American Astronomical Society, 24, [ADS]

Woosley, S. E. and Weaver, T. A., 1986, "The physics of supernova explosions", *Ann. Rev. Astron. Astrophys.*, **24**, 205–253. [DOI], [ADS]

Wright, J. T. and Howard, A. W., 2009, "Efficient Fitting of Multiplanet Keplerian Models to Radial Velocity and Astrometry Data", *Astrophys. J. Suppl.*, **182**, 205-215. [DOI], [ADS], [arXiv:0904.3725 [astro-ph.SR]]

Yanny, B., Rockosi, C., Newberg, H. J., Knapp, G. R., Adelman-McCarthy, J. K., Alcorn, B., Allam, S., Allende Prieto, C., An, D., Anderson, K. S. J., Anderson, S., Bailer-Jones, C. A. L., Bastian, S., Beers, T. C., Bell, E., Belokurov, V., Bizyaev, D., Blythe, N., Bochanski, J. J., Boroski, W. N., Brinchmann, J., Brinkmann, J., Brewington, H., Carey, L., Cudworth, K. M., Evans, M., Evans, N. W., Gates, E., Gänsicke, B. T., Gillespie, B., Gilmore, G., Nebot Gomez-Moran, A., Grebel, E. K., Greenwell, J., Gunn, J. E., Jordan, C., Jordan, W., Harding, P., Harris, H., Hendry, J. S., Holder, D., Ivans, I. I., Ivezič, Ž., Jester, S., Johnson, J. A., Kent, S. M., Kleinman, S., Kniazev, A., Krzesinski, J., Kron, R., Kuropatkin, N., Lebedeva, S., Lee, Y. S., French Leger, R., Lépine, S., Levine, S., Lin, H., Long, D. C., Loomis, C., Lupton, R., Malanushenko, O., Malanushenko, V., Margon, B., Martinez-Delgado, D., McGehee, P., Monet, D., Morrison, H. L., Munn, J. A., Neilsen, Jr., E. H., Nitta, A., Norris, J. E., Oravetz, D., Owen, R., Padmanabhan, N., Pan, K., Peterson, R. S., Pier, J. R., Platson, J., Re Fiorentin, P., Richards, G. T., Rix, H.-W., Schlegel, D. J., Schneider, D. P., Schreiber, M. R., Schwope, A., Sibley, V., Simmons, A., Snedden, S. A., Allyn Smith, J., Stark, L., Stauffer, F., Steinmetz, M., Stoughton, C., SubbaRao, M., Szalay, A., Szkody, P., Thakar, A. R., Sivarani, T., Tucker, D., Uomoto, A., Vanden Berk, D., Vidrih, S., Wadadekar, Y., Watters, S., Wilhelm, R., Wyse, R. F. G., Yarger, J. and Zucker, D., 2009, "SEGUE: A Spectroscopic Survey of 240,000 Stars with g = 14-20", *Astron. J.*, **137**, 4377–4399. [DOI], [ADS], [arXiv:0902.1781 [astro-ph.GA]]

Yong, D., Norris, J. E., Bessell, M. S., Christlieb, N., Asplund, M., Beers, T. C., Barklem, P. S., Frebel, A. and Ryan, S. G., 2013, "The Most Metal-poor Stars. II. Chemical Abundances of 190 Metal-poor Stars Including 10 New Stars with [Fe/H] $\leq$ -3.5", *Astrophys. J.*, **762**, 26. [DOI], [ADS], [arXiv:1208.3003]

Yoon, J., Beers, T. C., Placco, V. M., Rasmussen, K. C., Carollo, D., He, S., Hansen, T. T., Roederer, I. U. and Zeanah, J., 2016, "Observational Constraints

on First-star Nucleosynthesis. I. Evidence for Multiple Progenitors of CEMP-No Stars", *Astrophys. J.*, **833**, 20. [DOI], [ADS], [arXiv:1607.06336 [astro-ph.SR]]

York, D. G., Adelman, J., Anderson, Jr., J. E., Anderson, S. F., Annis, J., Bahcall, N. A., Bakken, J. A., Barkhouser, R., Bastian, S., Berman, E., Boroski, W. N., Bracker, S., Briegel, C., Briggs, J. W., Brinkmann, J., Brunner, R., Burles, S., Carey, L., Carr, M. A., Castander, F. J., Chen, B., Colestock, P. L., Connolly, A. J., Crocker, J. H., Csabai, I., Czarapata, P. C., Davis, J. E., Doi, M., Dombeck, T., Eisenstein, D., Ellman, N., Elms, B. R., Evans, M. L., Fan, X., Federwitz, G. R., Fiscelli, L., Friedman, S., Frieman, J. A., Fukugita, M., Gillespie, B., Gunn, J. E., Gurbani, V. K., de Haas, E., Haldeman, M., Harris, F. H., Hayes, J., Heckman, T. M., Hennessy, G. S., Hindsley, R. B., Holm, S., Holmgren, D. J., Huang, C.-h., Hull, C., Husby, D., Ichikawa, S.-I., Ichikawa, T., Ivezić, Ž., Kent, S., Kim, R. S. J., Kinney, E., Klaene, M., Kleinman, A. N., Kleinman, S., Knapp, G. R., Korienek, J., Kron, R. G., Kunszt, P. Z., Lamb, D. Q., Lee, B., Leger, R. F., Limmongkol, S., Lindenmeyer, C., Long, D. C., Loomis, C., Loveday, J., Lucinio, R., Lupton, R. H., MacKinnon, B., Mannery, E. J., Mantsch, P. M., Margon, B., McGehee, P., McKay, T. A., Meiksin, A., Merelli, A., Monet, D. G., Munn, J. A., Narayanan, V. K., Nash, T., Neilsen, E., Neswold, R., Newberg, H. J., Nichol, R. C., Nicinski, T., Nonino, M., Okada, N., Okamura, S., Ostriker, J. P., Owen, R., Pauls, A. G., Peoples, J., Peterson, R. L., Petravick, D., Pier, J. R., Pope, A., Pordes, R., Prosapio, A., Rechenmacher, R., Quinn, T. R., Richards, G. T., Richmond, M. W., Rivetta, C. H., Rockosi, C. M., Ruthmansdorfer, K., Sandford, D., Schlegel, D. J., Schneider, D. P., Sekiguchi, M., Sergey, G., Shimasaku, K., Siegmund, W. A., Smee, S., Smith, J. A., Snedden, S., Stone, R., Stoughton, C., Strauss, M. A., Stubbs, C., SubbaRao, M., Szalay, A. S., Szapudi, I., Szokoly, G. P., Thakar, A. R., Tremonti, C., Tucker, D. L., Uomoto, A., Vanden Berk, D., Vogeley, M. S., Waddell, P., Wang, S.-i., Watanabe, M., Weinberg, D. H., Yanny, B., Yasuda, N. and SDSS Collaboration, 2000, "The Sloan Digital Sky Survey: Technical Summary", *Astron. J.*, **120**, 1579–1587. [DOI], [ADS], [astro-ph/0006396]

Zhao, G., Zhao, Y., Chu, Y., Jing, Y. and Deng, L., 2012, "LAMOST Spectral Survey", *ArXiv e-prints*. [ADS], [arXiv:1206.3569 [astro-ph.IM]]

Zinn, R., 1985, "The globular cluster system of the galaxy. IV - The halo and disk subsystems", *Astrophys. J.*, **293**, 424–444. [DOI], [ADS]